Vibration Reduction Using Command Generation in Formation Flying Satellites

A Thesis
Presented to
The Academic Faculty

by

Erika A. Ooten Biediger

In Partial Fulfillment
of the Requirements for the Degree
Doctor of Philosophy

School of Mechanical Engineering
Georgia Institute of Technology
March 16, 2005

Copyright © 2005 by Erika A. Ooten Biediger

Vibration Reduction Using Command Generation in Formation Flying Satellites

Approved by:

Professor William Singhose, Advisor
School of Mechanical Engineering
Georgia Institute of Technology

Professor Ron Arkin
College of Computing
Georgia Institute of Technology

Professor Wayne Book
School of Mechanical Engineering
Georgia Institute of Technology

Professor Dewey Hodges
School of Aerospace Engineering
Georgia Institute of Technology

Professor Aldo Ferri
School of Mechanical Engineering
Georgia Institute of Technology

Date Approved: 16 March 2005

I would like to dedicate this work to my husband,

Dan

Thank you for believing in me, for encouraging me, and for putting up with me while I finished this. You have been an inspiration to me. Without you, I would never have been able to accomplish so much.

ACKNOWLEDGEMENTS

I would like to thank my advisor Dr. William Singhose, for guiding me through this process. Your help and guidance were invaluable.

I would like to thank the NASA Goddard Space Flight Center for funding my work through a NASA Graduate Student Research Fellowship. I would like to thank the following people at Goddard for their help: Jesse Leitner, Thomas Stengle, Rich Burns, Rich Lurquette, and Mabelene Burell.

I would also like to thank the National Science Foundation for funding my research stay in Japan through a Ph.D. Dissertation Enhancement Award. I would like to thank Professor Matunaga for welcoming me into his lab and for giving me the opportunity to complete experiments using his wonderful testbed. I would also like to thank the students in his lab for making me feel welcome and for taking me to eat at *Futaba*.

I would like to thank the wonderful ladies who are part of the ARCS program in Atlanta. The sponsorship you gave me was invaluable.

I would like to thank my labmates and officemates, for being my friends. You made my workplace enjoyable. I would like to thank my family. Thank you Mom and Dad, for thinking I was crazy, but for supporting me anyways. My final thanks go to Dan, to whom I owe so much...

TABLE OF CONTENTS

LIST OF TABLES

LIST OF FIGURES

SUMMARY

The precise control of spacecraft with flexible appendages is extremely difficult. The complexity of this task is magnified many times when several flexible spacecraft must be controlled precisely and collaboratively as in formation flying. Formation flying requires a group of spacecraft to fly in a desired trajectory while maintaining both relative positions and velocities with respect to each other. This work enhances two current state-of-the-art formation flying algorithms, specifically a leader-follower and virtual-structure architecture. First, a flexible satellite model is integrated into each of these architectures. Second, input shaping is used to generate the satellites' desired trajectories, thereby enhancing the performance of the system.

Input shaping is a relatively simple technique that is used to generate system commands. When used on a flexible system, these commands allow the system to move without inducing residual vibration, limit transient deflection, and move in a fuel-efficient manner. For this case, input shaping is used to generate the desired trajectories for the formation satellites. Applying input shaping to formation flying control architectures creates several additional challenges. The input-shaping scheme, must not only eliminate vibration, it must also maintain the required formation positions and velocities. The temporal tracking and trajectory tracking are the primary performance measures evaluated.

This dissertation addresses key issues regarding the application of command generation techniques to flexible satellites controlled with formation flying control architectures. The temporal tracking and the trajectory tracking of each architecture was examined as well as the vibration characteristics of the formation satellites. Design Procedures for applying trajectory shaping for the leader-follower and virtual structure architectures were developed, and experiments performed on a flexible satellite testbed verify key simulated results.

CHAPTER I

INTRODUCTION

1.1 Formation Flying

Satellites are an important part of today's society and they complete a variety of tasks. Perhaps the most famous operational satellite is the Hubble Space Telescope. The main objective for the Hubble telescope is to "discover the constitution, physical characteristics, and dynamics of celestial bodies" [3]. In addition to performing scientific research, satellites are also used for earth remote sensing, weather, communications and global positioning [5]. Designing, building and launching a satellite is very expensive. It cost an estimated $1.5 billion to build and launch Hubble and hundreds of millions more have been spent on repairing and maintaining the instrument [3].

The overall cost of a satellite is related to its size and mass. As both of these parameters decrease, the cost of the satellite also decreases [1]. If the size of the satellite decreases, the size of its payload must also decrease. This means that the number of instruments the satellite carries is reduced, and the number of different operations it can perform is also reduced. However, if several of these small inexpensive satellites operate together, it is possible that this group, or formation, of satellites can complete the same missions previously completed by single, large, expensive satellites. It is also possible that the formation can perform missions impossible for single satellites. If one of the formation satellites does not function properly, it can be replaced. The tasks the formation can perform can be changed by simply incorporating different kinds of satellites into the formation. When a satellite no longer functions, it can be replaced and the mission can continue. This feat would be impossible to accomplish if a single large satellite malfunctioned. Therefore, utilizing a formation of smaller, cheaper satellites is more economical than building one large spacecraft.

The concept of replacing large single satellites with a group of satellites provides many

benefits including the ability to reconfigure the group to perform different missions or to optimize the current mission. Elimination of catastrophic single point failures, and increased reliability are also possible benefits. It is also possible to reduce the cost of the satellite units by utilizing mass-produced identical or semi-identical units. There also exists an opportunity to decrease the launch costs associated with a particular mission, since the smaller satellites can be more efficiently packed in the carrier vehicle's cargo capacity. Another huge benefit to utilizing formation flying satellites is that the overall performance of the cluster can be significantly improved by incorporating upgraded satellites to the cluster, or by replacing satellites that are obsolete, damaged or no longer functioning. The formation can increase the range of task missions by adding specialized micro satellites.

Today, there are many agencies, including the Department of Defense and the National Aeronautics and Space Administration (NASA) that want to use groups of smaller cheaper satellites. In order to accomplish the desired mission objectives, these fleets of satellites must work in a coordinated manner. Developing guidelines for controlling, and maneuvering the satellites, as well as developing mission protocol has been the subject of much research. In order to be an effective alternative to large single satellites, the group of satellites must be able to autonomously [73]:

- fly within specified tolerance levels
- avoid collisions
- share knowledge between satellites
- plan and schedule satellite activities

If the cluster of satellites is able to fulfill all of the above requirements, then the cluster can act as a single *virtual* satellite. The true power of formation flying satellites is the ability for observation of the same phenomena using different sensors, and platforms that are simply not available with a single large satellite. This dissertation focuses on how to coordinate activities between the satellites, specifically how to maneuver the satellites so that they move with reduced residual vibration.

1.2 Current and Future Planned Missions

There are many applications which benefit from formation flying research, and many future NASA and Air Force missions will utilize formation flying satellites. Many missions will utilize small, or micro-satellites. The mission possibilities for these groups of micro-satellites include surveillance, passive radiometry, terrain mapping, navigation and communication [6]. The key to these missions are the "off the shelf" inexpensive micro-satellites [72]. The advantage to the micro-satellites is that they are extremely inexpensive to build and launch.

1.2.1 A-Train Formation

One of the current formation flying missions is composed of several low-Earth orbiting satellites including the Aqua, CALIPSO, PARASOL, Aura, and CloudSat. This group of satellites is known as the "A-Train" Satellite Constellation [8]. The satellites in this constellation operate independently of each other. However, because they fly in similar orbits, the information an individual satellite collects can be compared to the data the other satellites collect. The satellites are spaced approximately 15 seconds to 1 minute apart, and each satellite has different earth observing instruments on board.

When a new satellite is introduced into the formation, it is only through a number of precisely timed thruster burns that keeps the new satellite from colliding with the others in the formation. Cloudsat is scheduled to launch on April 15, 2005, and will be the newest member of the "A-Train" [7].

1.2.2 TechSat 21 Formation

The Air Force Research Laboratory is exploring formation flying possibilities in a coordinated effort named TechSat 21 (Technology Satellite of the 21st Century) [6]. TechSat 21's mission objectives include performing a "distributed sparse aperture radar mission for ground-moving target indication and geolocation missions" [73]. The performance of the TechSat cluster will be compared against the performance of comparable single satellite systems. TechSat 21's missions has extremely strict requirements on the relative positions between the spacecraft. The TechSat 21 spacecraft will all be in low-Earth orbits.

1.2.3 ION-F Formation

In order for formation flying satellites to be a viable alternative to monolithic expensive satellites, the technology used by satellites in a formation must first be verified. One of the current missions that will verify many of the formation flying technologies is the ION-F mission. The mission of ION-F is to create a satellite cluster that focuses on distributed ionospheric science and distributed satellite control [15]. The University of Washington (UW) plans to build and launch the UW Dawgstar nano satellite. This satellite is hexagonal with an anticipated height of only 12.625 inches, and is only 18 inches across its largest diameter. This satellite is one of three satellites planned for the ION-F mission [15]. Each of the three small satellites is built by a different university (University of Washington, Utah State and Virginia Tech).

The leader-follower architecture will be one of the two formations attempted by the ION-F missions. The other formation will be a same-ground-track maneuver. For same-ground-track formations, the satellites are slightly staggered and are on slightly different orbital paths. However, because the earth is rotating beneath the satellites, the spacecraft are timed so that each of the spacecraft fly over the same point on the surface of the Earth.

1.2.4 Emerald Project

Another low-Earth orbit formation flying mission is the Emerald project. The main objective of this project is to promote Robust Distributed Space Systems [2]. There will be two satellites in the Emerald cluster named Beryl and Chromium. One of the expected missions for this cluster is a Navigation Control Mission. For this mission, both of the satellites will attempt to fly in formation. During this mission, the relative position between the two satellites will be controlled and closely monitored.

1.2.5 Laser Interferometer Space Antenna Mission

One of the future formation flying missions is the construction of a Laser Interferometer Space Antenna (LISA) [4, 48]. LISA is the first space based gravitational wave observatory. This cluster of satellites will house the most advanced gravitational wave measuring

instruments. The cluster is composed of three satellites configured in a triangular array. One of the difficulties for this mission is ensuring the position precision between each of the spacecraft within 10 picometers [4]. Unlike other formation flying satellite clusters, LISA will be in an earth trailing orbit.

1.2.6 Formation Applications

One type of proposed formation schemes is the interferometric wheel [22]. This formation requires four satellites, a main radar satellite and three support satellites to be positioned in a triangular configuration. The three support satellites act as receivers. The formation is required to maneuver as if turning on a wheel with the main radar satellite acting as the hub. Depending on the desired type of measurements, the three support satellites are either in front of or behind the main satellite. The primary function of this formation is interferometric studies [22].

Another proposed future formation flying application calls for the construction of a space membrane [41]. A large membrane structure can be used as a solar power satellite, a large antenna, or it could be sent off as a deep space probe. Any of these applications requires significant advances in many of the formation flying areas such as coordination and navigation, guidance and control.

1.3 Problem Statement

Much research has focused on developing control architectures for formation flying satellites, and this rich field of study has produced many different kinds of architectures. Creating a control architecture for a group of formation satellites is not trivial and there are many difficulties that arise when trying to coordinate the motion of satellites in a formation. For example, the problem of allocating the communication between the satellites, or accounting for the delay between largely spaced clusters is no small task. One of the difficulties that is usually disregarded in these architectures is the flexible nature of spacecraft. All of these architectures utilize a point mass model for the satellites. Although it can be an appropriate approximation sometimes, every satellite has some amount of flexibility. When flexible satellites are integrated into the formation architecture, excessive vibration of their

appendages is possible, especially if no attempt to mitigate this behavior has been included.

Input shaping is a simple and elegant solution that can reduce the vibration of a satellite, and its utility has been verified both theoretically and experimentally. The previous input shaping satellite research assumed that the satellites would be acting independently. There has been no research published that studies the effect of integrating input shaping with a formation flying control architecture. For some formation missions, the relative spacing between the satellites is of paramount importance, and input shaping has been shown to provide superior trajectory tracking. It is well known that input shaping introduces a delay into the system response; however, it is not well known how this delay affects the entire formation's motion.

In order for the satellite community to realize the potential for vibration reduction that comes from using input shaping, the effects it has on the formation's response must be studied. The impact of trajectory shaping on the response of flexible satellites in formation flying is the focus of this dissertation. The next section describes some of the formation flying architectures currently available.

1.4 Formation Flying Control Architectures

NASA Goddard has been a leading force in formation flying technology and has defined some of the essential formation flying parameters. A constellation is a group of two or more spacecraft in similar orbits that do not have active control over their relative positions. Formation flying, however, is defined as a group of two or more spacecraft that utilizes a control scheme in order to maintain the desired relative positions between the spacecraft [21].

The task of coordinating a group of satellites encompasses many different areas, from determining the appropriate communication rates that will keep the satellite constellation together, to determining the appropriate control architecture necessary. This dissertation focuses on the overall control architecture used to coordinate the motion of each of the satellites in the formation, and only considers spacecraft that are in a formation flying group. This work does not consider satellite constellations.

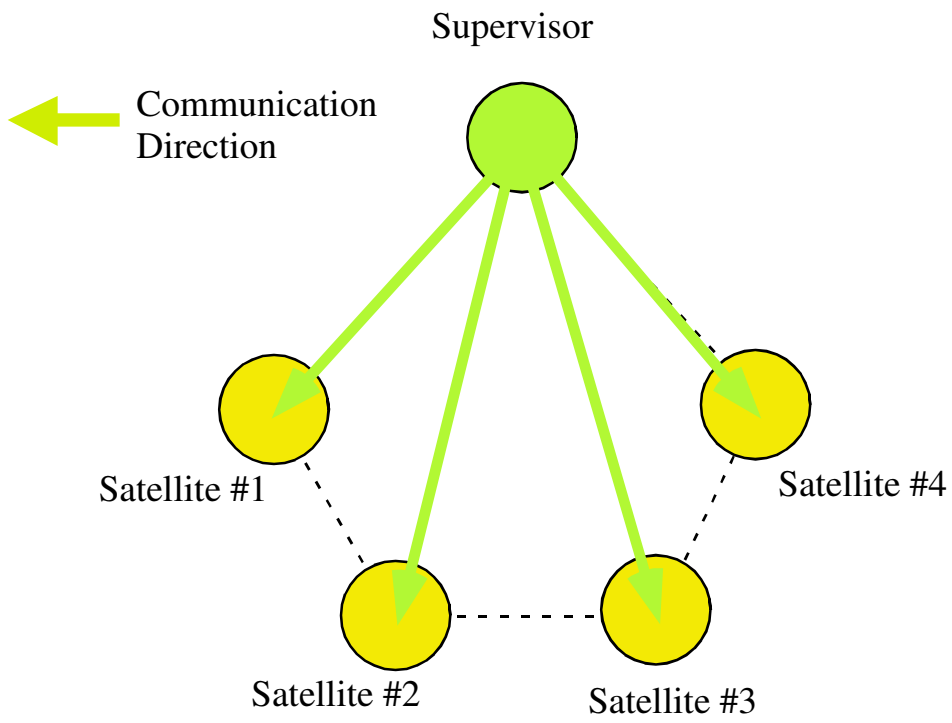

Figure 1: Centralized Formation Control.

1.4.1 Centralized Formation Control

Perhaps the earliest form of formation flying control was described by a centralized control architecture. The simplest form of centralized control is shown in Figure 1. The arrows in the picture represent the direction of satellite communication. As seen in the figure, all of the satellite communication originates from one satellite. This satellite, usually designated as the leader satellite, is responsible for maintaining the entire formation. All of the formation computations and control algorithms are generated from the leader satellite and are sent to the rest of the satellites in the formation.

In its simplest form (as shown in the figure) the other satellites in the formation do not communicate with either the leader satellite or with each other. In other words, the satellite control is centralized in one location. This form of formation control is not computation or communication intensive since only one satellite is required to communicate with the rest of the satellites in the formation. However, this can provide a single point of failure for the entire formation. If the leader satellite is disabled or destroyed, the entire formation would

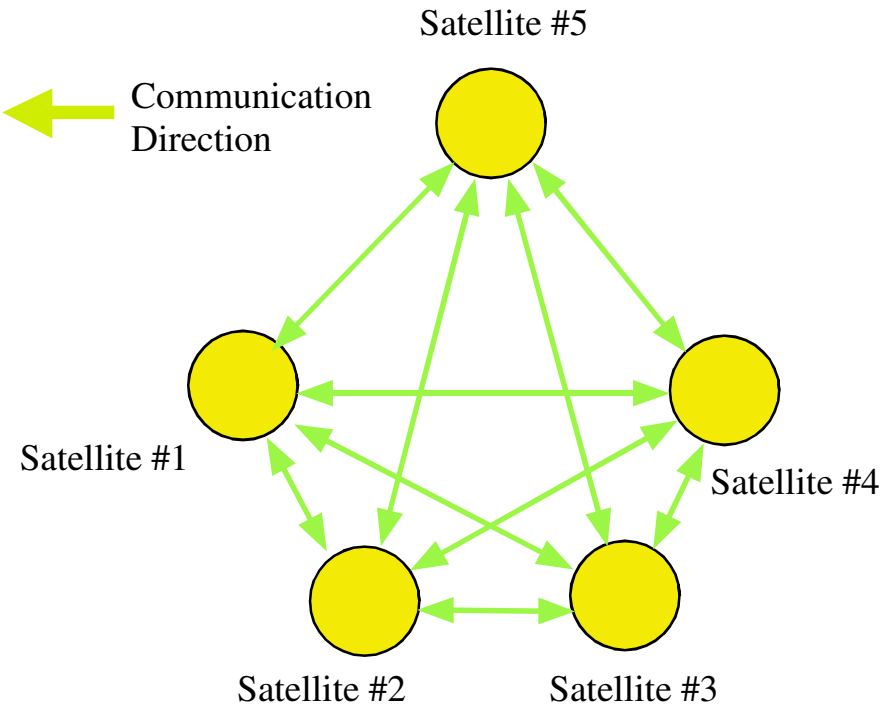

Figure 2: Decentralized Formation Control.

be unable to function. The simplest form of centralized control is not a viable candidate for space missions, since it is possible that something may happen to the leader satellite. In reality this would not be the case. Several if not all of the satellites in the formation would have the capability of acting as the leader satellite should anything happen to the current leader. It would simply be a matter of changing one of the remaining satellites in the formation to take on the supervisory role.

1.4.2 Decentralized Formation Control

Decentralized formation control is the opposite of centralized control. Figure 2 illustrates the most basic form of decentralized control. As seen in Figure 1, the arrows represent the direction of satellite communication. In decentralized control, there is no *leader* satellite. In this architecture, every satellite in the formation is responsible for communicating and maintaining the entire formation. Each of the satellites within the formation knows the relative position of every other satellite in the formation, and must broadcast its relative position

to every other satellite in the formation. As expected, decentralized formation architectures are extremely communication and computation intensive. However, they eliminate the single point failure present in centralized control.

Deciding how much communication is required to maintain the satellite formation is not a trivial task. Equally important is developing the actual formation algorithm that governs the motion of the satellites within the formation. A significant amount of research is dedicated to developing different types of control architectures. Because this is still a relatively new area of study, there is no formation flying control standard that is used for most formation flying applications.

1.4.3 Control Architectures

Although there are many different types of formation flying control architectures, the work presented in this dissertation will focus on two: Leader-Follower and a Virtual Structure Approach.

1.4.3.1 Leader-Follower

Leader-Follower is the simplest formation flying architecture. The leader-follower architecture presented here is designed from the Hill's equations representing the relative position between two spacecraft [40]. The formation consists of at least two spacecraft. For example, assume the formation is composed of two spacecraft. One of the spacecraft is designated as the *leader*, and the other is the *follower* as shown in Figure 3. In its most basic form, the leader spacecraft operates independently of the follower spacecraft employing a completely centralized control structure. The leader spacecraft follows its designated path, which in this case is a circular orbit. The follower spacecraft is completely dependent on the leader. The follower calculates the relative position between them and makes sure that it is within the desired parameters. For earth orbits, GPS systems could be used to calculate the relative position, for deep space missions, other methods such as laser interferometry must be employed. The follower spacecraft has no knowledge of the path, it only knows that it must maintain a prescribed relative distance away from the leader (for this case 1 km).

The more complicated the trajectory of the leader, the harder it is for the follower to

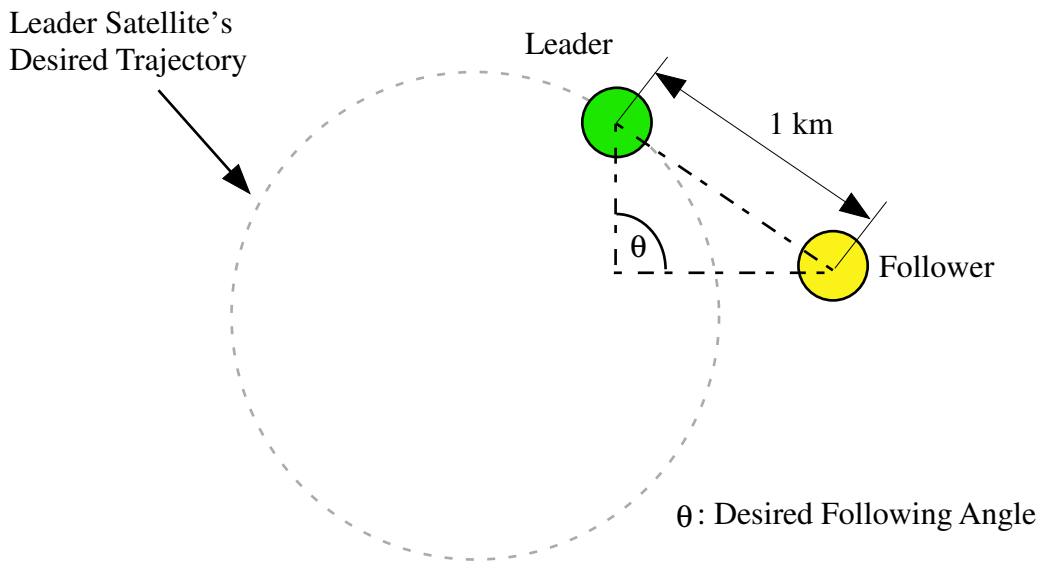

Figure 3: Basic Leader-Follower Architecture.

maintain the desired distance away. In addition, the more fuel the follower satellite must expend to maintain the desired distance. For low-Earth orbits it is possible that the fuel expenditure of the follower would be minimal and would only be needed for slight station keeping changes.

1.4.3.2 Virtual Structure

In addition to the leader-follower architecture, this work investigate the effect of input shaping on the virtual-structure architecture discussed in [12]. The architecture proposed by Beard contains elements of centralized control, decentralized control and virtual structures, and is specifically designed for deep space missions.

The formation architecture consists of two parts: the formation frame and the satellites. The formation frame is composed of a *virtual* rigid body structure and is used to generate the trajectories that the spacecraft follow. Suppose that the desired layout of the spacecraft is a triangular configuration, then the formation frame would be constructed as shown in Figure 4. The response of the formation frame is identical to a rigid body under the same conditions. The center of the virtual-structure (shown in the figure as a black dot) follows the desired trajectory.

The supervisor of the formation frame, whether it is located on a particular satellite

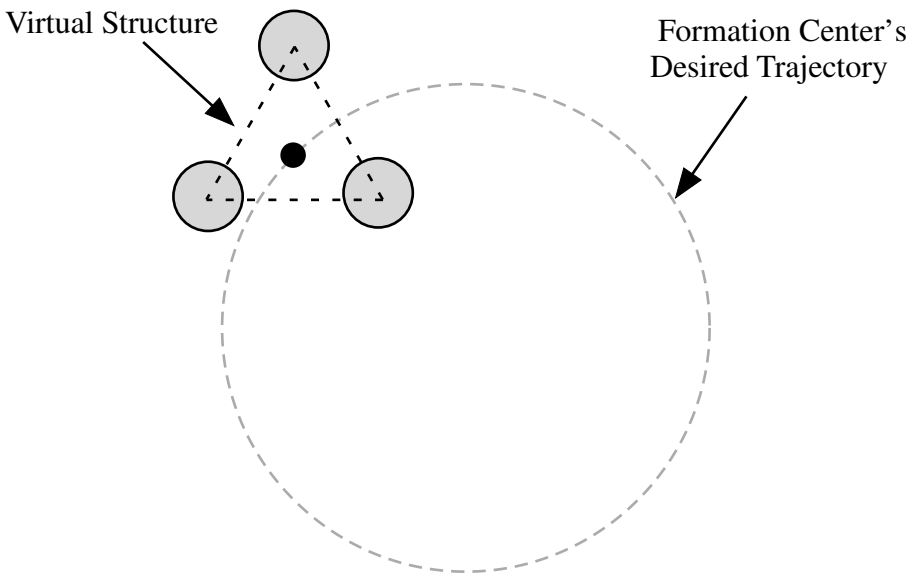

Figure 4: Virtual Structure Architecture.

or is on a ground station knows the desired trajectory and the desired configuration of the virtual structure. Because the virtual structure is assumed to be a rigid body it is simple to calculate the relative position and velocity of any point on the body. The supervisor must then transmit the desired coordinates to each of the spacecraft. The spacecraft then utilize a local control algorithm to maneuver to the desired coordinates passed by the formation supervisor. The details of the virtual structure are discussed in greater detail in Chapter 4.

1.4.4 Spacecraft Location

Much of the current formation flying research will be applied to satellites that are in orbit around the earth. Orbital formation flying is an extremely complicated task, since many different factors are involved such as differential drag, solar wind, etc. Some of the earliest work focuses on maintaining a formation of two satellites a set distance apart [40]. There has been significant amount of research in the area of circular orbital formation flying algorithms [71, 69, 50, 36]. Work has been done to ensure the stability, and minimal fuel consumption of some types of formations [28]. Some of the research has focused on utilizing adaptive learning techniques and nonlinear control algorithms in order to develop robust formation architectures [26, 46]. In addition to circular orbits, some researchers have investigated how eccentric orbits affect the development of formation flying architectures [70].

Equally important as developing the formation control architecture, is ensuring that the satellites will not collide with each other while moving from one designated position to another [31]. Other researchers develop formation architectures based on complicated lookup tables and graphical information [39].

One of the biggest difficulties in formation flying is communication failures, and research has been completed to address this [45]. There are many other things that can affect formation flying satellites, such as inter-spacecraft Coulomb forces [32].

Some of the current formation flying research focuses on developing architectures in the deep-space environment. For these applications, the magnitude of orbital effects that plague the earth orbiting formations are reduced [47, 12]. The work presented in this dissertation focuses on formation flying for deep space applications. However, the ideas presented in this dissertation are not limited to deep space applications, and the next step is to investigate how input shaping affects low-Earth orbit missions.

1.5 Earth Based Formation Flying Architectures

The previous sections discussed formation flying architectures designed specifically for space applications. The area of robotics is also a prolific area for developing formation architectures used to coordinate the motion of multiple vehicles. When the orbital dynamic effects of the spacecraft are neglected, there is little difference between architectures developed for space applications and architectures developed for terrestrial applications. How to coordinate the activities of robot formations is one of the fundamental questions addressed by many researchers. This section discusses some of these architectures.

One of the ways to coordinate multi-robot formations is by using a behavior based control algorithm. A behavior based approach was presented in [9]. In this approach, different behaviors run concurrently and the robots in the formation are able to move, keep the desired formation and avoid obstacles simultaneously. Two types of formation position determination were discussed: leader-referenced and unit-center referenced. In the unit-centered formation, the positions of the robots are determined relative to the formation center. Each of the robots is responsible for calculating the center of the formation;

therefore, each robot must be able to receive and transmit its position.

By weighting the behaviors with different values, the overall behavior of the formation is determined. For example, if the obstacle avoidance behavior is given the highest priority, it is possible that the formation's structure will dissolve when an obstacle is encountered. The robots in the formation may choose to pass the obstacle on different sides. If the behavior governing formation structure is given the highest priority, then the formation will be maintained while avoiding obstacles.

In [16], a hybrid method is presented that governs how the robots are assigned tasks. The purpose of this paper is to develop a controlling algorithm that is used to coordinate the activities of the robot formation. In this architecture, a leader-follower control is used. However, the roles of the robots are switchable depending on the situation. This means that the leader of the formation can switch to different robots depending on the situation. The focus of this paper is not on the leader-follower architecture, but on the larger controls problem of how to designate the roles for the robots. Experimentally results verify that a group of robots can accomplish a mission using this hybrid architecture.

A model predictive control used to develop formation control was presented in [18]. This approach is interesting because instead of determining specific trajectories, cost functions are minimized to compute an allowable region for each vehicle. The desired trajectory of the formation center is known in advance, but the other vehicles are not given specific locations in the formation. Collision avoidance is improved by changing the weights on some of the costs functions.

In [20] a hybrid formation control algorithm is developed that uses a leader-follower algorithm and includes a scheme for obstacle avoidance. In this control architecture, the primary vehicle follows a specified trajectory. The other vehicles in the formation switch between a leader-follower algorithm and an obstacle avoidance algorithm. This allows the formation to converge to a desired structure while maintaining collision avoidance. Communication between robots is avoided by using optimal estimation techniques.

Many different types of feedback control algorithms have been explored. In [49], a sliding mode controller was developed for a leader-follower architecture. Sliding mode control can

provide excellent tracking even in the presence of model uncertainties. It was shown that the formation is stable and that the proposed controller is robust to measurement errors and estimations of the leader satellite's velocities and orientations.

In [19], a decentralized control theory was used to control a group of autonomous robots. In order to use the theory, first it was determined wether the formation was reachable, controllable, observable and connectively stable. The stability determines the range of some of the system parameters. Two of these system parameters are interaction between vehicles and the sampling period of the communication and position feedback.

One of the tasks that these robot formations can be required to complete is a pursuit maneuver. During this maneuver, the robots in the formation may be required to pursue another vehicle in the formation. This differs from the leader-follower structure because there is no leader or follower. All of the vehicles in the formation are equal. In [37], a framework is developed so each vehicle in the formation pursues another vehicle. It was shown that the system's global behavior can be determined through appropriate controller gain selection.

1.6 Introduction: Command Generation

In order to move a satellite from one location to another, a control scheme is needed. There are many different control schemes available to accomplish this. The simplest way to maneuver a satellite, is by using a feedback control system with on-off thrusters [11].

There are many performance specifications that must be met by the desired control scheme. When the satellite is modeled as a flexible body, the complexity of control scheme must increase to meet the added system complexity. This is because of the vibration the system inherently possesses. One of the most important parameters is maneuver time. Many of the control schemes focus on moving the flexible satellite in a time optimal manner while trying to suppress the system's vibration [13, 33]. For space applications, the most important parameter in spacecraft mission planning is often fuel economy. Fuel usage dictates the life of the mission, so decreasing the amount of fuel used is paramount. There has been a lot of research completed on how to execute a desired maneuver while minimizing fuel costs

[44]. In addition to maneuvering in a time-optimal manner, the robustness to uncertainties is also a desired control characteristic. Liu combines both robustness to uncertainties and time optimality in [34].

1.6.1 Input Shaping

Input shaping is a command generation technique that is simple in concept and is generally easy to implement. An input shaper is simply an array of impulse amplitudes and their respective time locations. The earliest form of input shaping was first developed in 1957 by Smith when he formulated his Posicast control [66]. The Posicast control effort is divided into two parts. The first part of the Posicast control gives the system enough energy so that it will reach the desired setpoint within one cycle of the system's period. The second part of the control effort gives the system enough energy to counteract the vibration induced by the motion [65]. The desired setpoint is reached at the same time the velocity of the system reaches zero [66]. While this discovery proved extremely useful in theory, the technology available for implementation hindered the use of this type of control. Posicast control is extremely sensitive to modeling errors [66]. The interest in input shaping revived when digital computers became more widely available and when Singer and Seering introduced a more robust input shaper [51].

It is possible to generate an input shaper that produces no residual vibration by examining the system's response to an impulse. The simplest input shaper to derive and implement is the Zero Vibration (ZV) input shaper [51]. It is possible to generate a shaper that suppresses multiple modes, but a more complicated shaper is required [61]. The following describes how to determine the impulse amplitudes and time locations for a single-mode ZV shaper.

A linear time invariant system with one mode of vibration has the following transfer function:

$$G(s) = \frac{{\omega_n}^2}{s^2 + 2\zeta\omega_n s + {\omega_n}^2} \tag{1}$$

The response of the system show in (1) to an impulse can be found using the inverse Laplace

function as shown below:

$$y(t) = L^{-1}(G(s))$$

$$y(t) = \left[A\frac{\omega_2}{\sqrt{1-\zeta^2}}e^{-\zeta\omega_0(t-t_0)}\right]\sin\left(\omega_0\sqrt{1-\zeta^2}(t-t_0)\right) \tag{2}$$

where A is the amplitude of the impulse, ω_0 is the undamped natural frequency, ζ is the damping ratio, t is the time, and t_0 is the time of the impulse. Equation (2) is the response to a single impulse; however, because the system is linear, the system's response to multiple impulses can be found using a superposition of the system's response to each impulse. In order to simplify the response, the following trigonometric identity is used [51]:

$$B_1\sin(\alpha t+\phi_1) + B_2\sin(\alpha t+\phi_2) = A_{amp} + \sin(\alpha t+\psi) \tag{3}$$

where

$$A_{amp} = \sqrt{\left(\sum_{j=1}^{N} B_j\cos(\phi_j)\right)^2 + \left(\sum_{j=1}^{N} B_j\sin(\phi_j)\right)^2} \tag{4}$$

In order to eliminate vibration after the impulse sequence has ended, the expression for A_{amp} must equal zero at the time of the last impulse t_N. This condition can be satisfied if each of the squared terms given in (4) are both equal to zero. Satisfying this condition yields:

$$\sum_{j=1}^{N} A_j e^{-\zeta\omega(t_N-t)}\sin\left(t_j\omega\sqrt{1-\zeta^2}\right) = 0 \tag{5}$$

$$\sum_{j=1}^{N} A_j e^{-\zeta\omega(t_N-t)}\cos\left(t_j\omega\sqrt{1-\zeta^2}\right) = 0 \tag{6}$$

where A_j is the amplitude of the j^{th} impulse and t_j is the time of the j^{th} impulse.

For most input shapers, the time location of the first impulse is chosen to be zero. By setting the time location of the first impulse to zero any delay resulting from a time shift in the impulses is eliminated. In addition, in order to normalize the sequence of impulses, the sum of the impulse amplitudes is set equal to zero. The two constraint equations are:

$$t_1 = 0 \tag{7}$$

$$\sum_{j=1}^{N} A_j = 0 \tag{8}$$

Equations (5)-(8) form a set of constraint equations that are used to solve for the amplitudes and time locations of an input shaper. The ZV shaper consists of only two impulses which results in only four unknowns: A_1, A_2, t_1, and t_2. The time locations and the amplitudes of the ZV shaper are [51]:

$$\begin{bmatrix} A_j \\ t_j \end{bmatrix} = \begin{bmatrix} \frac{1}{1+K} & \frac{K}{1+K} \\ 0 & 0.5T_d \end{bmatrix} \tag{9}$$

where

$$K = e^{\frac{-\zeta\omega}{\sqrt{1-\zeta^2}}} \tag{10}$$

$$T_d = \frac{2\pi}{\omega_n\sqrt{1-\zeta^2}} \tag{11}$$

Once the impulse amplitudes and time locations are found, the impulse sequence, or input shaper, is convolved with the original reference command. As seen in (11), the input shaper amplitudes and time locations are based only on the system's natural frequency and damping ratio. Convolving any arbitrary command with a sequence of impulses designed to eliminate the residual vibration of the system will yield a command that will also eliminate the system's residual vibration. Consequently, the sequence of impulses becomes a filter for the reference command. If the sum of the amplitudes is constrained to equal one, then the shaped command will have a unity gain. This means that the system will reach the same setpoint when using either a convolved or the original command. Because the sum of the impulse amplitudes is equal to one and only positive impulses were considered, the convolved command will not exceed the maximum value of the original reference command. The difference between the two responses is that the shaped command will yield zero residual vibration. If the original command does not saturate or exceed the actuator limits, then neither will the convolved command. However, both positive and negative impulse amplitudes are possible, but additional constraint equations are required in order to make sure the actuator limits are not exceeded [59, 52, 25].

The convolution of a desired input with an input shaper can be thought of as a sequence of multiplications and additions. First, the desired input is multiplied by each of the impulse amplitudes, resulting in a series of scaled input commands. Next these scaled commands

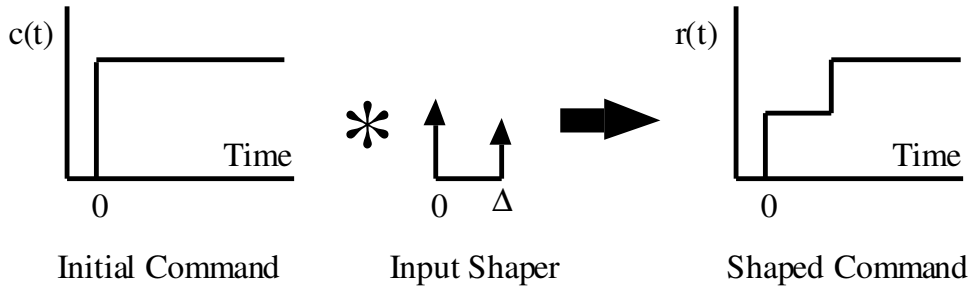

Figure 5: Convolving a Step Input.

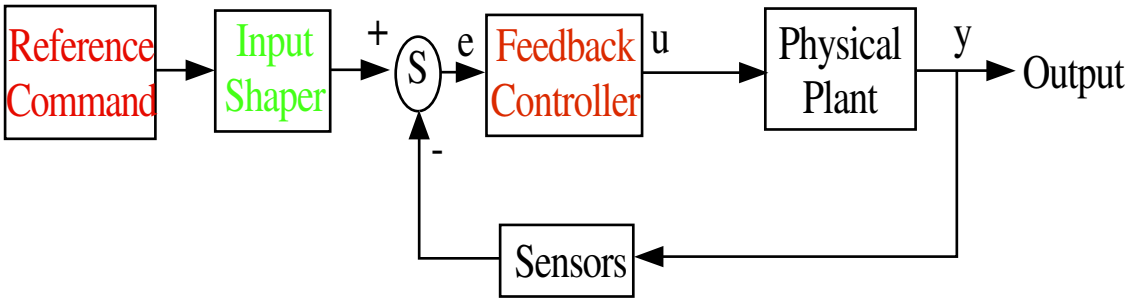

Figure 6: Generalized Control Scheme.

are shifted in time by an amount equal to the time location of the impulse. Finally, the series of time shifted, scaled inputs is added together to generate the convolved command. An example of the convolution process is shown in Figure 5. The desired input (in this case it is a step command) is convolved with an input shaper containing three impulses. The resulting convolved command is a three-step staircase command.

As stated earlier, any arbitrary command can be convolved with an input shaper, yielding a new reference command that will not produce any residual vibration. It is important to note that impulses are never sent to the systems. Instead time shifted scaled copies of the original command are sent. The system command can be a desired trajectory, desired velocity, or desired actuator effort. The shaped command is sent to the system's plant and is used as the reference command for the system. Eliminating the residual vibration from the system does not come without a cost. The price for the improved system performance is an increase in rise time equal to the duration of the input shaper.

Input shaping is analogous to a filtering technique and its normal location in the block diagram is outside the feedback loop as shown in Figure 6. Input shapers placed outside the feedback loop do not aid in disturbance rejection. However, as seen in Figure 6, the

input shaper can be used in conjunction with any feedback controller. The input shaper is designed using the natural frequency and damping ratio of the system, and the input shaper is convolved with any inputs sent to the closed-loop plant. If this is done, the response of the system to any changes in the reference command should not induce any residual vibration in the system. The disturbance rejection characteristics are based solely on the feedback controller used. It is possible to attain better performance using a feedback controller and an input shaper together rather than using either one on its own [30, 42].

However, some researchers advocate placing the input shaper inside the control loop. When placing a delay inside the control loop, it is possible for the system to go unstable. However, a lot of research has gone into investigating what is the best way to implement input shaping inside the control loop [67, 74, 29]. As long as the uncertainty in the modeled parameters is above the frequency used for the input shaper, then the system will remain stable [29].

There are many different types of input shapers. The duration of the shaper has a direct impact on the rise time of the system. One must choose between an increase in rise time versus an increase in the shaper's robustness to modeling errors. The ZV input shaper is not effective for systems with large parameter uncertainties. For systems with large uncertainties, or large changes in natural frequency or damping ratio, using a more robust input shaper ensures that the residual vibration remains below a tolerable level. Increasing the robustness of an input shaper is accomplished by adding additional constraint equations to the system of equations described by (5)-(8). In the next section, several input shapers more robust than the ZV shaper are discussed. The first shaper discussed is the Zero Vibration and Derivative (ZVD) shaper, followed by the Extra Insensitive (EI).

1.6.2 ZV and ZVD Shapers

The ZV shaper discussed in the previous section is very sensitive to modeling errors. If the system's natural frequency and damping ratio are not exactly known, then the residual vibration will not be completely eliminated. A shaper's robustness is determined by how well the shaper can eliminate the residual vibration in the presence of modeling errors. The

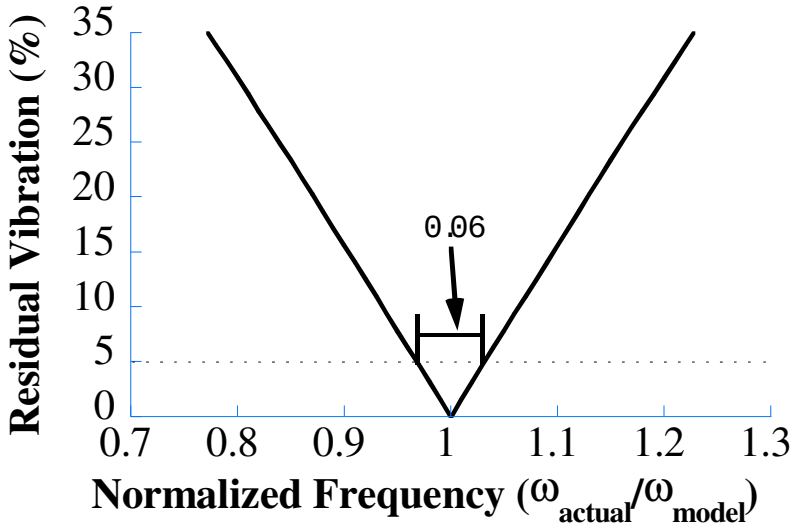

Figure 7: ZV Sensitivity Curve.

main tool used to evaluate a shaper's robustness is a sensitivity curve. The ratio of shaped vibration to unshaped vibration is designated as Percent Residual Vibration. Normalized frequency is the ratio of the system's actual natural frequency to the modeled natural frequency and is given by:

$$\text{Normalized Frequency} = \frac{\omega_{\text{actual}}}{\omega_{\text{model}}} \tag{12}$$

One way to measure the robustness of an input shaper is to calculate the width of the sensitivity curve lying below a certain level of residual vibration. The width of the curve is the shaper's *insensitivity*. Figure 7 shows the sensitivity curve for a ZV shaper. The insensitivity of a ZV shaper for a 5% residual vibration level is 0.06. Using a ZV shaper will not eliminate the residual vibration or keep the residual vibration below 5% if there is greater than a ±3% error in the natural frequency. The residual vibration will be completely eliminated only when the modeled natural frequency is perfect (normalized frequency is equal to one).

It is possible to increase the robustness of an input shaper by requiring additional constraint equations to be satisfied. One of these constraints is to set the derivative of the system's response, (4), with respect to frequency, to also be equal to zero [51]. These

additional constraints are given by:

$$\sum_{j=1}^{N} A_j t_j e^{-\zeta\omega(t_N - t_j)} \sin\left(t_j \omega \sqrt{1-\zeta^2}\right) = 0$$

$$\sum_{j=1}^{N} A_j t_j e^{-\zeta\omega(t_N - t_j)} \cos\left(t_j \omega \sqrt{1-\zeta^2}\right) = 0$$

In order to satisfy the two additional constraint equations, two more unknowns are required. Two unknowns can be added by using another impulse. Every impulse has two unknowns: the amplitude of the impulse, A_j, and the time location of the impulse t_j. By increasing the number of impulses from two to three, the additional constraint equations can be satisfied. This input shaper is known as the Zero Vibration and Derivative (ZVD) shaper. The impulse amplitudes and time locations for the ZVD shaper are:

$$\begin{bmatrix} A_j \\ t_j \end{bmatrix} = \begin{bmatrix} \frac{1}{1+2K+K^2} & \frac{2K}{1+2K+K^2} & \frac{K^2}{1+2K+K^2} \\ 0 & 0.5T_d & T_d \end{bmatrix} \tag{13}$$

where K and T are given in (11).

Changes in the shaper's robustness due to variations in the damping ratio are also important. If necessary, additional constraint equations can be introduced. For example, taking the derivative of (4) with respect to damping ratio and setting them equal to zero provides two additional constraint equations. If in addition to the other constraints, these additional constraint equations are satisfied, then the robustness to variations in damping ratio would be increased. However, it can be shown that (13) also guarantees zero derivatives with respect to damping ratio; consequently, an additional constraint is not needed [51].

The sensitivity curve for the ZV and ZVD input shapers is shown in Figure 1.6.2. Notice that the magnitude of the residual vibration and the derivative of the vibration is equal to zero when the normalized frequency is equal to one for the ZVD curve. This results from satisfying the additional constraint equations. The 5% insensitivity of the ZVD is 0.28 as opposed to the 0.06 insensitivity of the ZV shaper. Increasing the robustness, however, also increases the duration of the shaper. The ZVD shaper is twice as long as the ZV shaper; however, for many applications, this increase in rise time is outweighed by the large increase in insensitivity. It is possible to add additional constraints to the system that require the

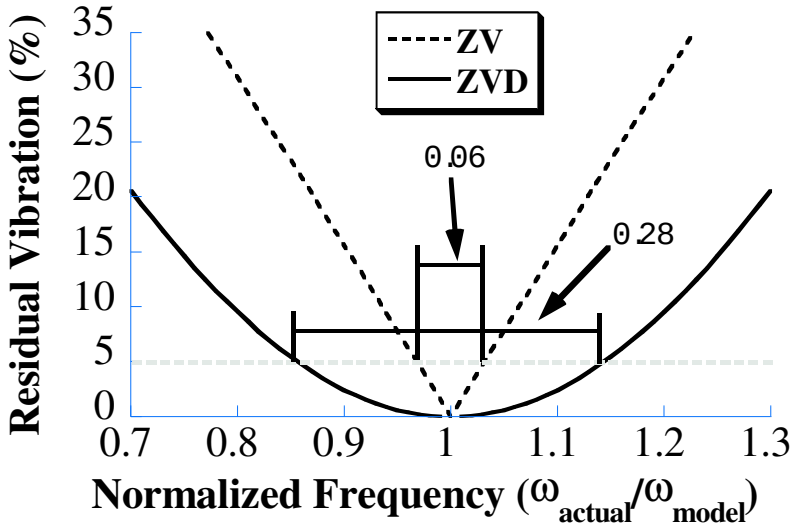

Figure 8: ZV and ZVD Sensitivity Curves.

second derivatives of the vibration with respect to the natural frequency to be equal to zero [51]. This has the effect of widening the shape of the ZVD sensitivity curve, but the shaper duration is also increased.

1.6.3 EI Shapers

It is likely that any real system will have some level of residual vibration even though an accurate model of the system exists. There will always be some modeling error, and vibration can result from disturbances in the system. Given this realization, it is possible to increase the insensitivity of an input shaper by relaxing the constraint that the vibration be equal to zero when the normalized frequency is equal to one.

An input shaper with this relaxed zero vibration constraint is known as the Extra Insensitive (EI) input shaper [58]. Although the zero vibration constraint is relaxed, the vibration is still forced to remain below a specified tolerable limit. Similar to the ZVD input shaper, the derivative of the residual vibration with respect to natural frequency must be equal to zero at the model frequency. In addition, the vibration is forced to zero on both sides of the model frequency in order to maintain symmetry in the insensitivity. Figure 1.6.3 shows the sensitivity for the single mode EI shaper. The insensitivity of the EI shaper is 0.4 which is almost double the insensitivity of the ZVD shaper. Notice that the slope of

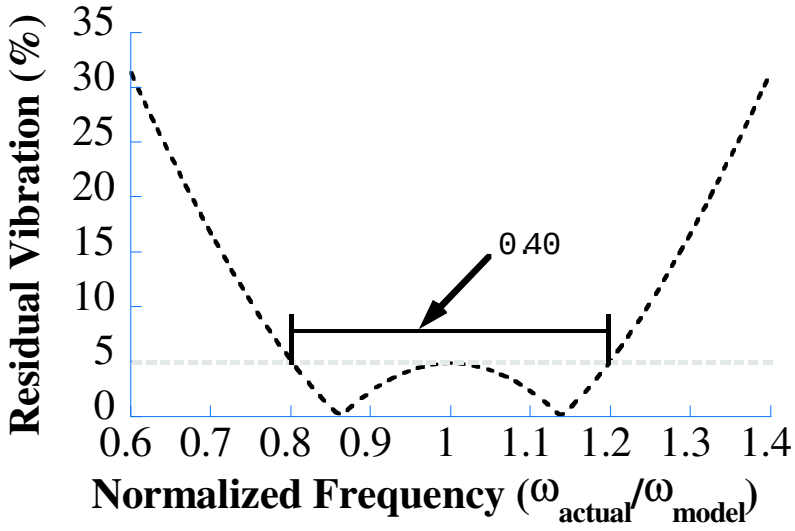

Figure 9: EI Sensitivity Curve.

the residual vibration is equal to zero when the normalized frequency equals one, and that the residual vibration equals the tolerable limit of 5% rather than zero.

The impulse amplitudes and time locations for the single-mode EI shaper for an undamped system are [58]:

$$\begin{bmatrix} A_j \\ t_j \end{bmatrix} = \begin{bmatrix} \frac{1+V_{tol}}{4} & \frac{1-V_{tol}}{2} & \frac{1+V_{tol}}{4} \\ 0 & 0.5T & T \end{bmatrix} \tag{14}$$

Figure 10 compares the sensitivity curves for the ZV, ZVD and EI shapers. As stated before, the EI's insensitivity is 0.40 as compared to 0.28 for the ZVD and 0.06 for the ZV. The EI and ZVD input shapers have the same duration, so the increase in insensitivity does not come from increasing the duration of the shaper. Instead, it results from relaxing the zero vibration constraint.

It is important to note that input shaping is not the only shaping technique that eliminates vibration in flexible systems. The Optimal Arbitrary Time-delay (OAT) filter is another technique that can be used to reduce the vibration in systems with flexibility [35]. This filtering method minimizes a cost function composed from the generalized coordinates and velocities of the system. This cost function is used to generate the filter coefficients. By adjusting the time-delay value of each filter, different levels of robustness can be achieved.

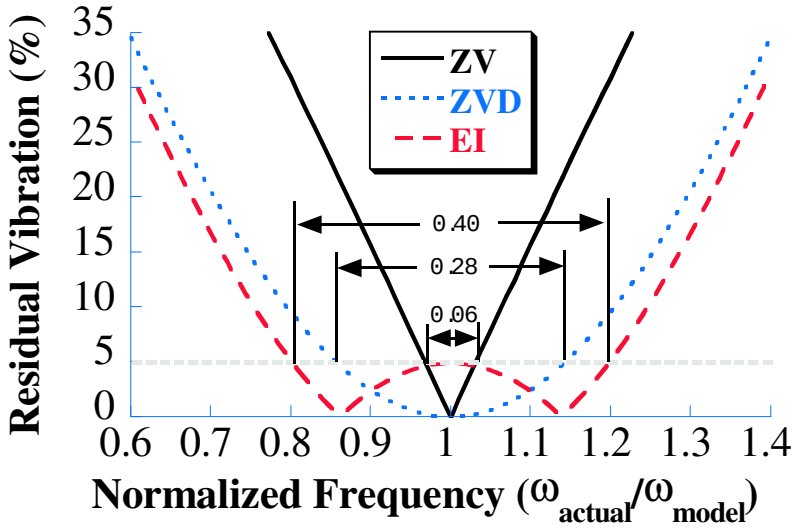

Figure 10: ZV, ZVD and EI Sensitivity Curves.

The validity of this filtering technique was experimentally verified on a two-link elastic manipulator.

1.6.4 Input Shaping for Flexible Spacecraft

There has been a lot of research that has focused on implementing command shaping on flexible space structures [56, 10, 54, 68, 60, 11, 13, 34, 44, 62, 64, 53]. Two of the most important parameters for space structures are time optimal and fuel efficient maneuvers. Fuel usage dictates the mission life which directly impacts the cost of the mission. Historically, spacecraft are maneuvered using on-off thrusters. The on-off thrusters add a degree of difficulty since they cannot produce a variable amplitude actuation force.

Many researchers have focused on developing fuel-efficient commands and time-optimal commands [64, 54, 60, 44, 13, 34, 62]. These commands are not only able to maneuver the flexible spacecraft in a fuel-efficient manner, thus increasing the mission life, but because input shaping was used to generate these commands, they reduce the amount of residual vibration in the system. It is possible to include robustness constraints thus creating a command that is insensitive to modeling errors, yet is fuel efficient. It was also found that the fuel-efficient pulse profiles produced by utilizing input shaping were comparable to the time-optimal commands for the same maneuver. For a small increase in command

length, the flexible spacecraft is able to move in a fuel-efficient manner, have limited residual vibration, and move in near time-optimal manner.

If there are large parameter uncertainties in the system, it is possible to generate extra-insensitive (EI) shapers for flexible spacecraft [55]. These input shapers are designed for increased robustness to modeling errors and for use with on-off reaction jets. The maneuvers these input shapers are designed for are rest-to-rest slewing maneuvers. These input shapers were verified through both simulation and experiment. A rotary table with a flexible steel beam was used to simulate the rotational motion of a flexible spacecraft. The results show that input shaping can be used to significantly reduce the vibration in the flexible appendage [55].

Although it is important to limit the amount of residual vibration in a system, many times it is also important to limit the amount of transient deflection. If the transient deflection during a slewing maneuver is large, it is possible to damage the structure. It is also possible that the endpoint of the space structure may deviate significantly from the intended motion. Limiting the transient deflection of a flexible space structure is a challenging task. The difficulty of this task is increased when the system is actuated using on-off thrusters. Input shaping is ideal for limiting both the transient deflection and the residual vibration [60]. In order to accomplish this dual task, additional constraint equations are needed to ensure that the input shaper satisfies the transient and endpoint vibration requirements.

In addition to maneuvering the spacecraft, thruster firings may also be required after a momentum dumping. If a satellite utilizes a momentum wheel to maintain attitude control, over time, the momentum of the wheel will build up. This results from disturbance torques that are introduced into the system. For example, the torque resulting from solar radiation pressure causes an external disturbance torque to the system. Because the momentum of the wheel is increasing with time, it is necessary to periodically dump the wheel's momentum before it reaches its maximum velocity. This task is often completed by firing the spacecraft's on-off thrusters. If the system has any flexible modes however, the thruster fire will excite these modes and lead to residual vibration. Momentum dumping is necessary for spacecraft

that utilize reaction wheels to control attitude. However, it is possible to execute the momentum dumping without exciting the residual vibration by utilizing input shaping to create the thruster command profile [10].

In reality, a space structure will have more than one mode of residual vibration. If more than one mode is dominating the response, then it may be required to eliminate two or more modes of residual vibration when slewing the structure. For flexible spacecraft requiring on-off reaction jets, it is possible to construct multi-mode input shapers [57]. These multi-mode input shapers can incorporate fuel efficient constraints [60], deflection limiting requirements [57], and robustness constraints [55]. Input shaping for more than one mode usually requires an increase in the shaper's duration.

The use of shaping has been experimentally verified. Suk demonstrated a torque shaping method tested on a flexible space structure testbed [68]. The testbed consists of a hub-appendage structure and the desired slewing maneuvers are rest-to-rest motions. The authors combine torque shaping with a Lyapunov tracking controller. The desired torque profile is shaped and the tracking controller implements the desired shaped torque profile. The experimental results confirm that torque shaping is an excellent way to slew a flexible body [68].

In the past, if the slewing maneuver is not known *a priori*, it was difficult to generate input shapers that reduced the residual vibration of space structure. However, if a closed form solution of the input shapers is known, then the slewing maneuver does not need to be known before hand. Closed-form input shaping equations are available for use with flexible structures that require on-off actuation [56]. The beauty of these closed form solutions is that optimization is not needed to solve for the appropriate input shaper. Closed-form analytic commands were experimentally verified using a flexible satellite testbed [53]. These commands were valid for undamped and lightly damped systems.

1.6.5 Effect of Input Shaping on Trajectory Following

Although input shaping can be applied to velocity and acceleration inputs, it is also possible to use input shaping with desired position inputs such as trajectory following. When input

shaping and desired trajectories are combined, the shape of the resulting trajectory differs from the original trajectory [63]. How much the shaped trajectory differs from the original trajectory depends on the shape of the original trajectory, and the type of input shaper. However, it has been experimentally shown that even with the changes to the trajectory, the shaped system is better at tracking the trajectory than the unshaped system [17].

For straight line trajectories, the difference between the shaped and unshaped trajectory is temporal in nature. Both the unshaped and shaped trajectories will begin and end with the system at the same setpoint; however, the shaped trajectory will take more time to accomplish the maneuver. This is because of the increase in rise time for the shaped trajectories. For circular trajectories, the difference between the shaped and unshaped trajectory is both temporal and spatial. Because the shaped trajectory will have a slower initial slope, the system will take longer to reach the desired position. However, the trajectory itself will also be slightly different. Input shaping has the effect of shortening the radius of the circle [63]. For example, suppose the original trajectory is a unit circle. After input shaping both the x and y trajectories, the resulting trajectory is a circle with a slightly smaller radius than unity. The more robust the input shaper, the bigger the difference between the unshaped and shaped radii. Although input shaping shortens the circle's radius, the system is better able to follow the trajectory and often has superior performance compared to the unshaped system's response [63]. This is discussed in more detail in Chapter 2.

Similar to the circle trajectories, square trajectories have both spatial and temporal differences. However, the effect of input shaping a square trajectory is the rounding of the trajectory's corners. If the unshaped trajectory is known before hand, it is possible to manipulate this trajectory so that the negative effects of shaping these trajectories are minimized [63].

1.7 Thesis Contributions

This dissertation makes several contributions to the field of formation flying. It provides several guidelines for utilizing trajectory shaping on two formation flying architectures. In addition to providing design procedures, controller gain selection is also discussed. The

primary contributions are briefly described here.

- Develop a simplified nonlinear flexible satellite model and show that trajectory shaping can still be effective at reducing the vibration of the system. Recall that the shaping is intended for linear systems, but it is shown to work on the nonlinear system developed.
- Develop a design procedure for implementing trajectory shaping on a leader-follower formation flying architecture.
- Develop a design procedure for implementing trajectory shaping on a virtual-structure formation flying architecture.
- Develop a tool for generating and evaluating the effect of combining input shaping and pulse-width modulation.
- Experimentally verify that shaping does not significantly alter the trajectory tracking of a formation flying satellite.

Because the satellites used in the current formation flying architectures are modeled as point masses, there is a need for developing a flexible satellite model that can be integrated into these architectures. *Chapter 2 presents an appropriate flexible satellite model and accompanying equations of motion.* The equations of motion for this satellite system are nonlinear, and although input shaping was developed for use on linear systems, the vibration reduction benefits extend to this nonlinear system as well. This chapter also discusses how to pick the feedback controller gains for good trajectory tracking.

The flexible model developed in Chapter 2 is integrated into both a leader-follower and virtual-structure architecture. *Chapter 3 presents the effect of shaping the leader satellite's trajectory for two types of motions, and investigates the temporal and trajectory tracking.* For some missions, temporal tracking of the formation is paramount, and it is possible to align the shaped trajectories so that temporal differences are reduced. In reality a satellite formation will not be composed of identical satellites. An investigation of multi-mode formations reveals that shaping can reduce the vibration of the satellites' flexible

appendages and improve the separation distance between the satellites. Design procedures for implementing trajectory shaping for this architecture are developed.

The benefits of shaping the formation's trajectories is not limited to a leader-follower architecture. *Chapter 4 explores the effects of shaping on a virtual-structure architecture and examines the proper location for implementing shaping.* The shaping is implemented at two levels of control: supervisor and local satellite level. Utilizing the shaping at either of these levels reduces the vibration in the flexible appendages. For multi-mode formations the benefits of shaping at either of these levels is investigated.

Although many models assume a continuous variable amplitude control effort is available, in reality it is not. *Therefore, Chapter 5 investigates the effect of combining input shaping and pulse width modulation.* In addition to theoretical results, experimental results are needed further validate the utility of input shaping on real systems. *Chapter 6 discusses the experimental results completed at the Tokyo Institute of Technology.* Experimental results validate that shaping the desired trajectory can be achieved on real systems.

This dissertation presents guidelines for integrating trajectory shaping for two types of formation architectures and demonstrates that trajectory shaping is effective at reducing the vibration while maintaining the desired formation. In addition to improving the separation distance between the satellites, the vibration of the flexible appendages is significantly reduced. In some cases, the overall maneuver time required for a particular motion is also reduced.

CHAPTER II

FLEXIBLE SPACECRAFT MODEL

In most of the current formation flying architectures, the satellites making up the formation are modeled as point masses. There are many reasons for this simplification. The primary reason for simplifying the satellite model is that it allows the research to focus on the construction of the formation architecture. Real satellites have flexibility and the flexibility can come from many different sources. It is important to study how a flexible satellite will behave when under the control of different architectures; therefore, a flexible satellite model is needed.

2.1 Equations of Motion

Satellites are complex bodies with complicated dynamics. The complexity and dynamics vary with the satellite's design and application. The purpose of this work is to investigate how combining command generation and flexible satellites affects the response and structure of the formation. Therefore, only a simple satellite model is needed. The flexible model used must meet three requirements

- the satellite must be able to translate
- the satellite must be able to rotate
- the flexible appendage must be free to oscillate

Figure 11 depicts a simple satellite model. The satellite is composed of two primary bodies: a main satellite body (m_1), and a single flexible appendage (m_2) that is pinned to the main satellite body. Although in reality the flexible appendage will have multiple modes, many times the low mode dominates the response. The command generation techniques discussed in this work can be easily extended for systems with multiple modes.

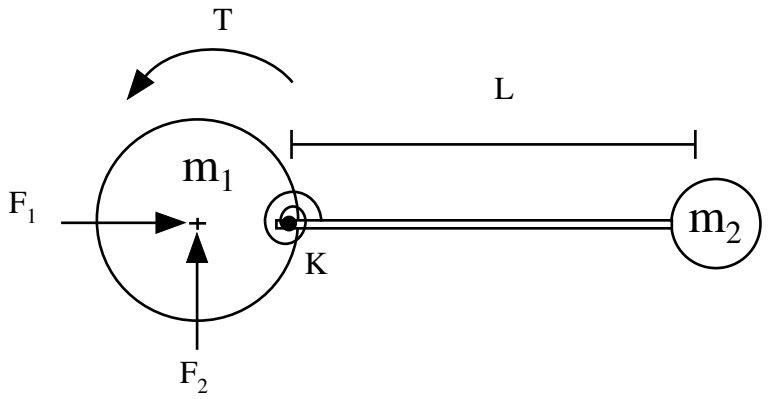

Figure 11: Simple Flexible Satellite Model.

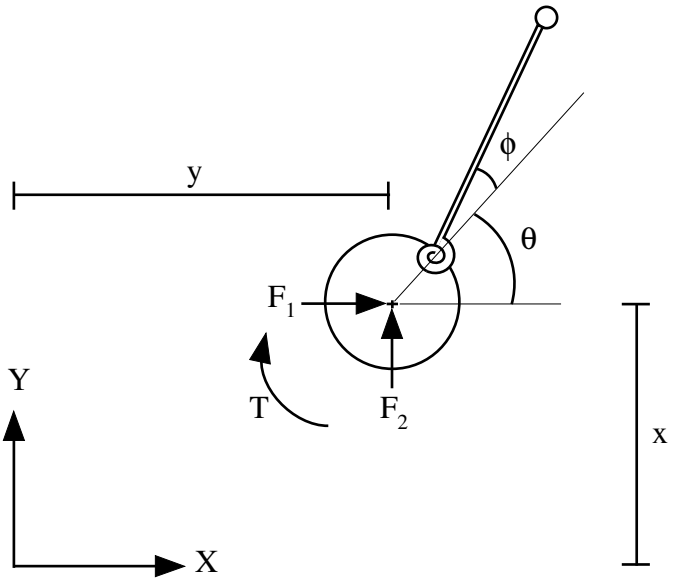

Figure 12: Flexible Satellite Generalized Coordinates.

The flexible appendage is modeled as a massless rod-point mass with a total length given by L. The flexibility of the model comes from the rotational spring which connects the main satellite body to the flexible appendage. The rotational spring represents the elasticity of a slender beam in bending. The satellite is maneuvered using two forces, F_1, and F_2 and the attitude is changed using a torque, T. The four generalized coordinates needed to fully describe the system configuration are: x, y, ϕ, and θ. These four coordinates are shown in Figure 12. The position of main satellite body, m_1, is described by spatially fixed inertial coordinates x and y. The rotation of m_1 is described by θ, and the deflection of the rotational spring is described by ϕ. The forces F_1 and F_2 are applied at the center of mass

of m_1 and are intertially fixed in the X and Y directions. The torque, T, is applied to only m_1. Because these two forces are fixed in their respective directions, they are equipollent representations of the actual thruster forces on the main satellite body. The equations of motion for the system using the inertial coordinates are:

$$\ddot{x} = \frac{F_1}{m_1} - \frac{m_2}{m_1} a_{2x} \tag{15}$$

$$\ddot{y} = \frac{F_2}{m_1} - \frac{m_2}{m_1} a_{2y} \tag{16}$$

$$\ddot{\theta} = \frac{T}{I} + \frac{K\phi}{I} + \frac{r \cdot m_2 \cdot a_{2x} \sin\theta}{I} - \frac{r \cdot m_2 \cdot a_{2y} \cos\theta}{I} \tag{17}$$

$$\ddot{\phi} = \frac{\sin(\phi+\theta)\,\ddot{x} - \cos(\theta+\phi)\,\ddot{y} - (r\cos\phi + L)\,\ddot{\theta} - r\sin\phi \cdot \dot{\phi}^2}{L} - \frac{K\phi}{m_2 L^2} \tag{18}$$

where

$$a_{2x} = \left[\ddot{x} - r\sin\theta \cdot \ddot{\theta} - \dot{\theta}^2 r\cos\theta - \left(\ddot{\theta} + \ddot{\phi}\right) L\sin(\theta+\phi) - \left(\dot{\theta} + \dot{\phi}\right)^2 L\cos(\theta+\phi)\right] \tag{19}$$

$$a_{2y} = \left[\ddot{y} + r\cos\theta \cdot \ddot{\theta} - \dot{\theta}^2 r\sin\theta + \left(\ddot{\theta} + \ddot{\phi}\right) L\cos(\theta+\phi) - \left(\dot{\theta} + \dot{\phi}\right)^2 L\sin(\theta+\phi)\right] \tag{20}$$

I is the mass moment of inertia for m_1, and K is the spring constant. The main satellite body is modeled as a disk with radius r. The mass moment of inertia is calculated as

$$I = \frac{1}{2} m r^2 \tag{21}$$

For a complete derivation of the equations of motion refer to Appendix A.

When the mass of the flexible appendage, m_2, is much smaller than the mass of the main satellite body, m_1, then the effect it has on the main satellite body is small. This can be seen in (15) and (16). When $\frac{m_2}{m_1}$ is small then the flexible satellite model can be further simplified by neglecting the effect of the m_2 on m_1. The equations of motion reduce to the following:

$$\ddot{x} = \frac{F_1}{m_1} \tag{22}$$

$$\ddot{y} = \frac{F_2}{m_2} \tag{23}$$

$$\ddot{\theta} = \frac{T + K\phi}{I} \tag{24}$$

The equations of motion for the main satellite body are now linear. The equation of motion describing ϕ remains unchanged. The flexible satellite model described above is only valid for the following conditions:

- $m_1 \gg m_2$. This model is only valid when the mass of the flexible appendage is very small when compared to the mass of the main satellite body (less than 5% of m_1). If the mass of the appendage is not small when compared to the mass of the main satellite hub, then a more complicated model is needed in order to capture the coupling effects.

- The acceleration of the main satellite body and flexible appendage tip must not deviate significantly. This condition is met when the angular acceleration of the main satellite body is small, and when the angular velocities of both the main satellite body and flexible appendage are small. For many maneuvers, aggressive motions are undesirable because they consume too much fuel and can lead to large endpoint deflections which may damage the appendage.

- L must be small. This model is only valid for small to medium length flexible appendages. For satellites that have extremely long flexible appendages, a more complicated model should be used. Long appendages have the potential for producing large accelerations at the tip of the appendage and would violate the assumption that the main satellite body and appendage tip have roughly the same acceleration. For fast maneuvers, the pin reaction forces neglected in this simple model would have a significant effect on the response of the main satellite body and should be included.

This model assumes that the effect of the flexible appendage on the main satellite body is dominated by the deformation of the spring, and that any internal deflections in the satellite are small. The spring is assumed to be a linear spring with constant K. Given that one of the equations of motion is nonlinear, it is not easy to analytically determine the natural frequency of the flexible appendage. Instead, the following linearized simplification was used to pick the value of K. Assume that the flexible appendage is attached to ground instead of a free moving body as shown in Figure 13. The natural frequency of the flexible appendage shown in Figure 13 is:

$$\omega_n = \sqrt{\frac{K}{m_2 L^2}} \tag{25}$$

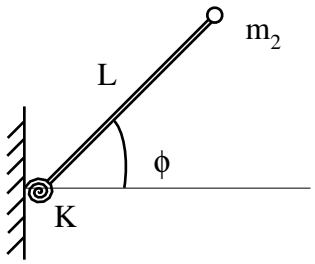

Figure 13: Linearized Simple Model.

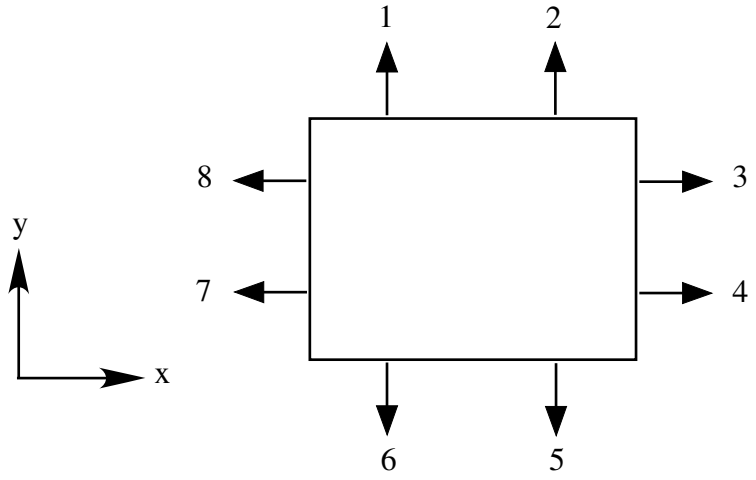

Figure 14: Satellite Thruster Configuration.

Solving for K yields

$$K = {\omega_n}^2 m_2 L^2 \tag{26}$$

where ω_n is the desired natural frequency in rad/sec. Equation (26) can be used to estimate the value of K for any desired natural frequency.

2.2 Spacecraft Control

In order to maneuver, most satellites are equipped with thrusters and reaction wheels. For two dimensional motion without using a momentum wheel, eight thrusters are needed for translation and rotation. One possible configuration of these thrusters is shown in Figure 14 [15]. In order to move the satellite in one direction, two of these thrusters must be turned on at the same time. For example to move in the positive x-direction, thrusters 7 and 8 must be turned on. Attitude maneuvers can also be completed by turning on opposite thrusters. For example, to rotate the satellite in the counter-clockwise direction, thrusters 1 and 5,

or 3 and 7 are used. A thruster map is needed so that the least number of thrusters are used in order to accomplish a particular maneuver. The thruster map is basically a look-up table that tells the satellite which set of thrusters to turn on given a desired maneuver.

The satellite model shown in Figure (12) consists of two intertially fixed thruster forces, F_1 and F_2 and a torque, T. In order to simulate the eight thrusters on a real satellite, the modeled forces and torque are equipollent representations of the thruster map.

Given the satellite's position and attitude are modeled using two intertially fixed forces and a torque, computing the necessary magnitudes of the forces and torques requires the satellite to utilize a control law. There are many different control laws available, and while some of these are simple in nature others are more complex. For the purpose of this work, a simple Proportional plus Derivative (PD) control law is utilized for each of the satellites in the formation, and has the following form:

$$\begin{aligned} F_1 &= K_p\left(x_{desired} - x\right) + K_v\left(\dot{x}_{desired} - \dot{x}\right) \\ F_2 &= K_p\left(y_{desired} - y\right) + K_v\left(\dot{y}_{desired} - \dot{y}\right) \\ T &= K_p\left(\theta_{desired} - \theta\right) + K_v\left(\dot{\theta}_{desired} - \dot{\theta}\right) \end{aligned} \tag{27}$$

where x, y and θ represent the position and orientation of m_1, and where $x_{desired}$, $y_{desired}$ and $\theta_{desired}$ represent the desired values. K_p and K_v represent the proportional and derivative controller gains. The same PD gains are used for the forces and torque.

The controller gains will be tuned so that the system responds quickly to changes in the desired trajectory, yet does not incur a large amount of overshoot. The gains will also be tuned so that the satellites have a reasonable settling time. Tuning the PD gains will be accomplished using a trial and error approach. The focus of this research is to study the effect input shaping has on formation flying architectures, not on optimizing the PD controller gains of the individual satellites.

2.3 MATLAB Simulation

The first step is to verify that the modeled system provides an accurate representation of the actual system. In order to accomplish this, a computer simulation using the equations

Table 1: Flexible Satellite Simulation Parameters.

Parameter	Value
m_1	42 Kg
m_2	1 Kg
I	5 Kg-m^2
L	1 m
r	0.5 m
K	39.5 N/rad

of motion for the flexible satellite model was developed using MATLAB. Table 1 lists the parameter values used in the MATLAB simulation. The value for K was calculated from (26) using a desired natural frequency of 1 Hz.

The following sections discuss the open and closed-loop responses of the system. Section 2.3.1 discusses the open-loop response to unshaped bang-bang commands. The closed-loop response to unshaped commands is discussed in Section 2.3.2. The response of the system to shaped commands is also discussed. For the open-loop simulations discussed in Section 2.3.3, a shaped pulse profile is used to drive the system. For the closed-loop commands discussed in Section 2.3.4, the desired step change in position or orientation is convolved with an input shaper. This shaped step change is used as the new desired setpoint for the system. For the closed-loop responses, the input shaper is outside the feedback control loop.

2.3.1 Unshaped Open Loop System Response

Figure 15 shows the open-loop response of m_1 to a simple bang-bang rotation maneuver. The satellite reaches the desired slew angle at the end of the bang-bang command. However because of the flexible appendage, there is a small amount of residual vibration in m_1. The amount of residual vibration can be better seen by looking at the response of the spring angle ϕ as seen in Figure 16. As seen from the figure, the 25° slew maneuver produces a vibration amplitude of approximately 1° in the flexible appendage. This constant amplitude appears after the transient response and does not decay because the modeled system does not have any damping. The lowest frequency is just slightly larger than 1.0 Hz (approximately 1.1 Hz), so the simple approximation of the natural frequency shown in (25) is a good

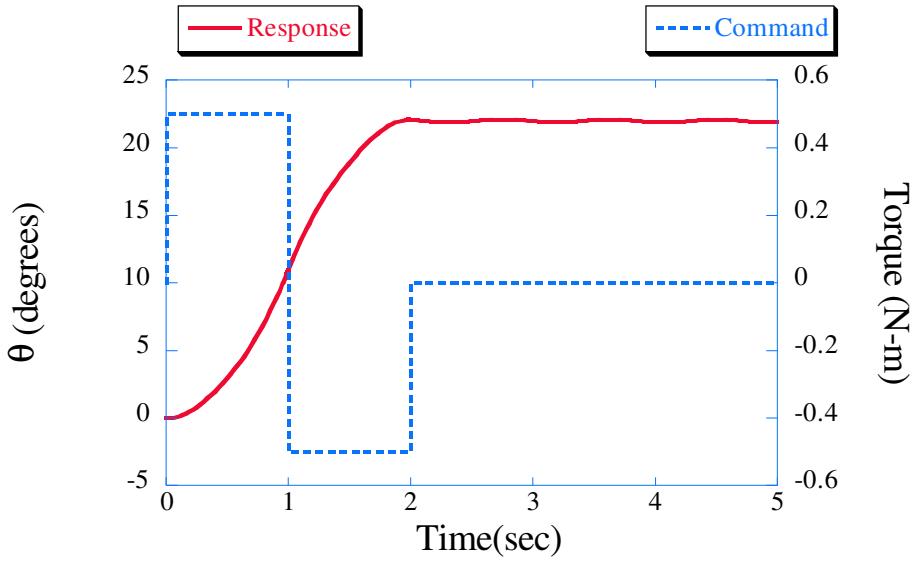

Figure 15: Satellite Response to Bang-Bang Command.

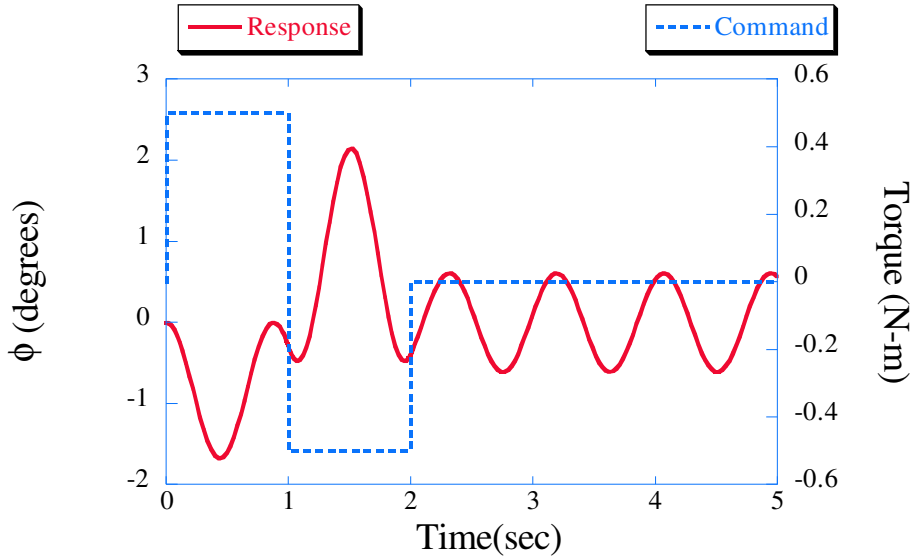

Figure 16: Spring Angle Deflection to Bang-Bang Command.

approximation.

2.3.2 Unshaped Closed Loop Response

The next step is to implement a feedback controller on the satellite model. This is accomplished by utilizing a PD controller in the feedback loop. The PD controller gains were

Table 2: Satellite PD Feedback Controller Gains.

Parameter	Value
K_p	32
K_d	8

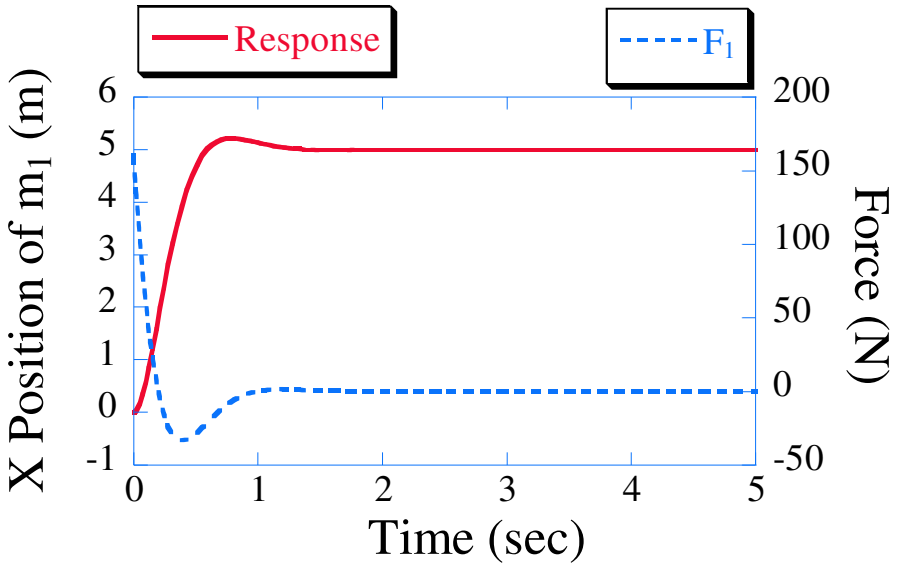

Figure 17: System Response to Step Change in X Position.

chosen so that the satellite had good trajectory tracking with minimal overshoot and minimal settling time. Table 2 shows the PD gains selected for the satellite feedback controller. The controller gains listed in Table 2 represent the controller gain divided by their respective inertia element. The following equations define what the control parameters represent.

$$\text{For } F_1 \text{ and } F_2: \quad K_p = \frac{\text{Proportional Gain}}{m_1} \tag{28}$$

$$K_d = \frac{\text{Derivative Gain}}{m_1} \tag{29}$$

$$\text{For } T: \quad K_p = \frac{\text{Proportional Gain}}{I} \tag{30}$$

$$K_d = \frac{\text{Derivative Gain}}{I} \tag{31}$$

Figure 17 shows the x position of m_1 to a step change in desired x-position. For this maneuver, θ is equal to zero. This corresponds to the flexible appendage being parallel to the x-axis. Only the F_1 force is needed to move the satellite in the intertially fixed x-direction. As seen in the figure, the step response has little peak overshoot and settles to the

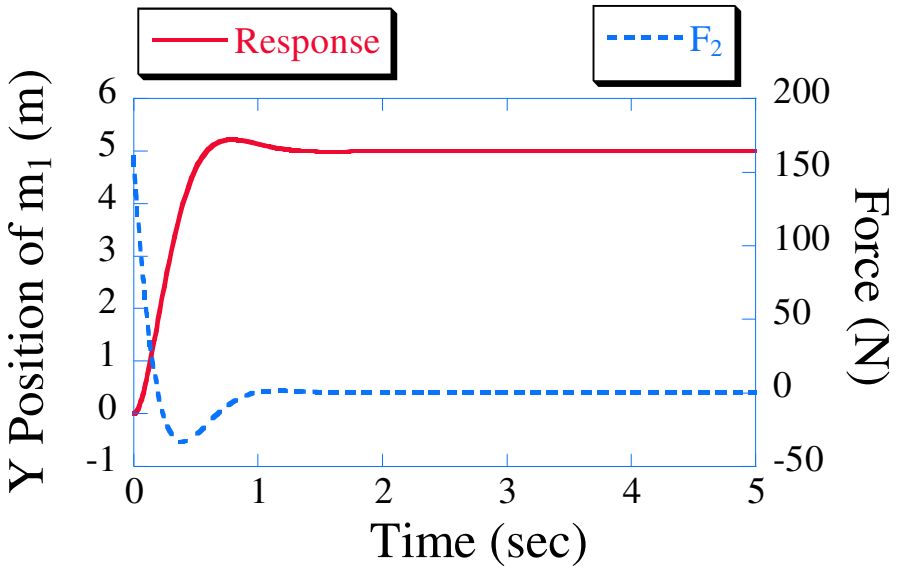

Figure 18: System Response to Step Change in Y Position.

desired location quickly. There is no residual vibration because the rotational spring is not deformed. Deformation of the rotational spring only occurs when there is a rotational change or when m_1 is moved perpendicular to the flexible appendage. For the current orientation, a perpendicular motion corresponds to a maneuver in the vertical direction (F_2). Once the orientation of m_1 changes from 0° any combination of F_1 and F_2 thruster forces that does not result in a net force parallel to the flexible appendage will cause deflection in the spring and produce residual vibration.

Figure 18 shows the y position of the m_1 to a step change in desired y-position. As in the case above, θ is equal to zero. The response to a step change in the y-direction is similar to an x-direction step change when looking at the position of m_1. m_1 reaches the desired setpoint with little overshoot and no residual vibration in the y-direction. F_2 returns to zero when m_1 reaches the desired value.

Unlike the motion in the x-direction, a maneuver in the y-direction requires a torque to compensate for the change in orientation. Figure 19 shows the attitude response of the satellite and the torque produced by the feedback controller. The desired ending value of the attitude is 0°, so the feedback controller must supply a torque in order to suppress the oscillation of the flexible appendage resulting from the motion in the y-direction. As seen in

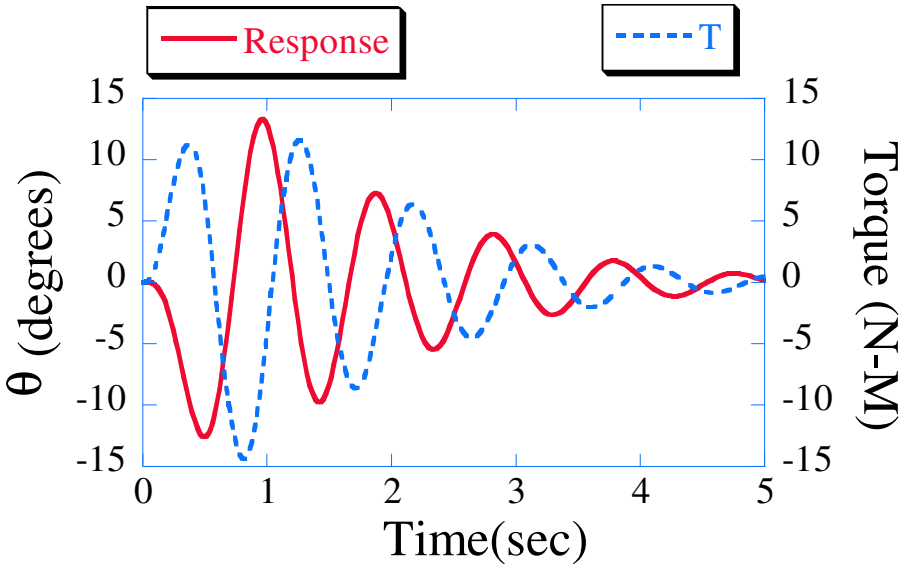

Figure 19: Attitude Response to Step Change in Y Position.

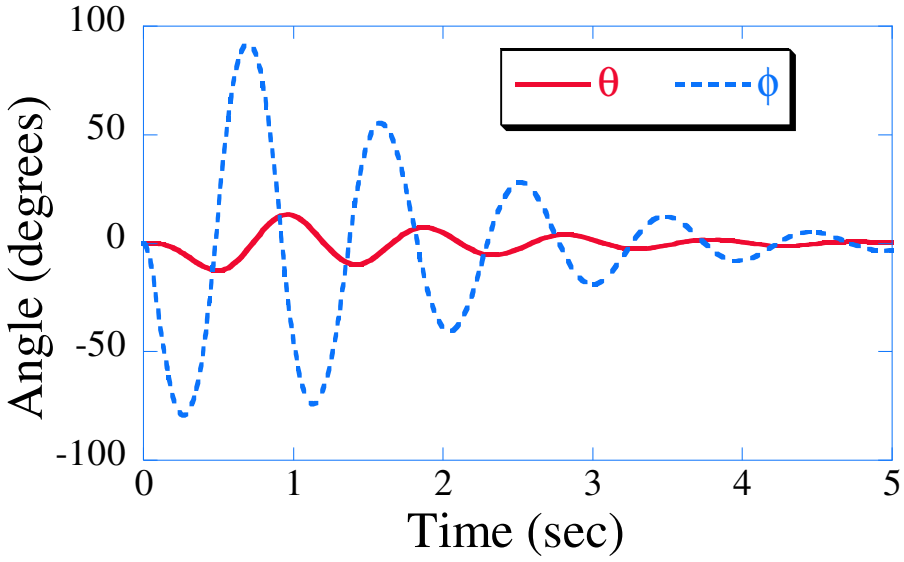

Figure 20: Attitude and Spring Angle Response to Step Change in Y Position.

the figure, with the application of the torque, the residual vibration decays exponentially. This is due to the addition of the derivative portion of the PD controller. Unlike the open loop case where the steady-state response had a constant amplitude, for the closed-loop case, the amplitude will approach zero as time approaches infinity.

Figure 20 compares the spring angle deflection, ϕ, and the attitude of the satellite, θ for a 5 unit step change in the y direction. As seen in the figure, the magnitude of ϕ is

approximately four times that of θ. Both of the oscillations eventually decay. However, the initial deflection of the spring angle is 100°. In reality, it is unlikely that any structure can withstand such a large deflection in the appendage without structural failure. Most of the satellite structures are very delicate and it is possible that such a large deflection may cause catastrophic failure.

Now that the feedback controller has been shown to provide an adequate system response to step changes in position, the next step is to make sure the PD gains allow good tracking for a given trajectory. The desired trajectory for the satellite to follow is given as a portion of a circle. The desired trajectory is described by

$$x_{desired} = \cos t \tag{32}$$

$$y_{desired} = \sin t \tag{33}$$

$$\theta_{desired} = 0 \tag{34}$$

$$\dot{x}_{desired} = 0 \tag{35}$$

$$\dot{y}_{desired} = 0 \tag{36}$$

$$\dot{\theta}_{desired} = 0 \tag{37}$$

where $0 \leq t \leq 2.6$. The starting position of the satellite is $(0, 0)$ with respect to the inertial frame. In order to test the controller's ability to quickly bring the satellite to the desired trajectory, the satellite was started off the desired trajectory. The performance of the controller can be seen in Figure 21. The simple PD controller is able to move the satellite from the initial position of $(0, 0)$ to the desired circular trajectory. Once the controller is on the desired trajectory, it does an excellent job of keeping the satellite on the desired trajectory.

Now that the feedback controller gains have been picked, it is important to investigate the tracking error of the system when the system starts at the desired initial position. Figure 22 shows the desired x and y trajectories and the response of the system. Looking at the x-components, once the system is able to reach the desired trajectory, it follows along the desired path, but with some amount of time lag. The same holds true for the

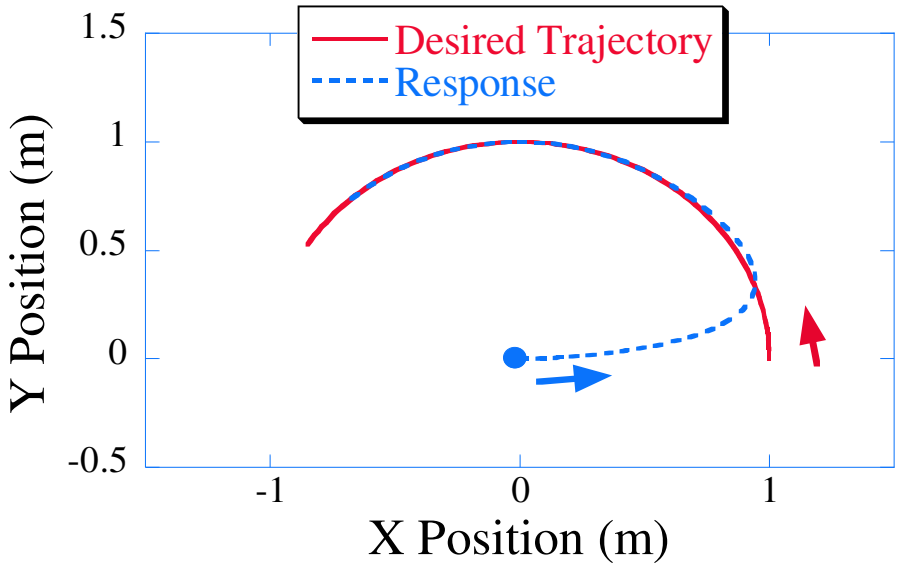

Figure 21: System Response to Circular Reference Trajectory.

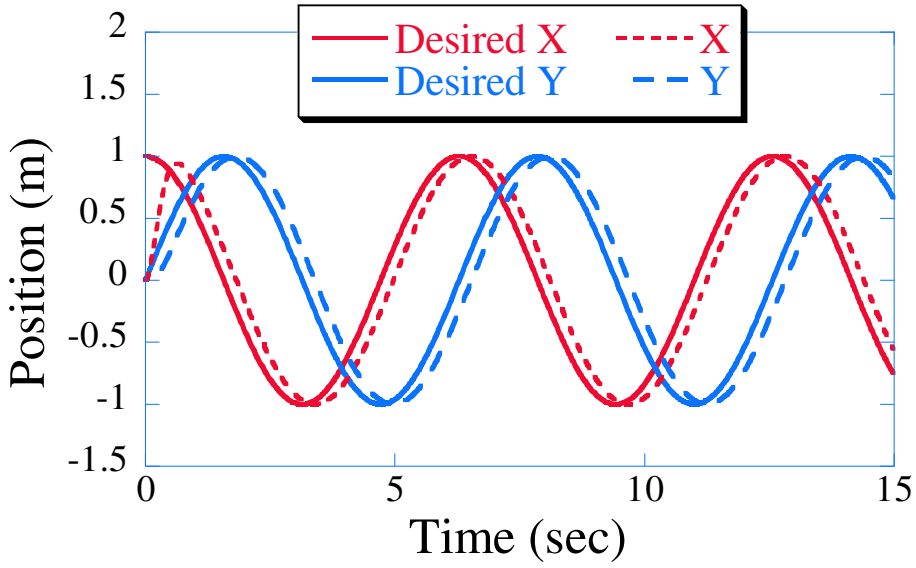

Figure 22: Time Lag of System Response to Circular Reference Trajectory.

y-components. It is reasonable to have some of amount of tracking error in the system, since it not possible to instantly change the position of any system with inertia and the trajectory is continuously varying. The amount of trajectory error can be quantified by calculating the RMS error. The RMS error for the x and y coordinates is calculated as

Table 3: RMS Error for Circular Trajectory.

Position	RMS Error
x	0.19
y	0.17

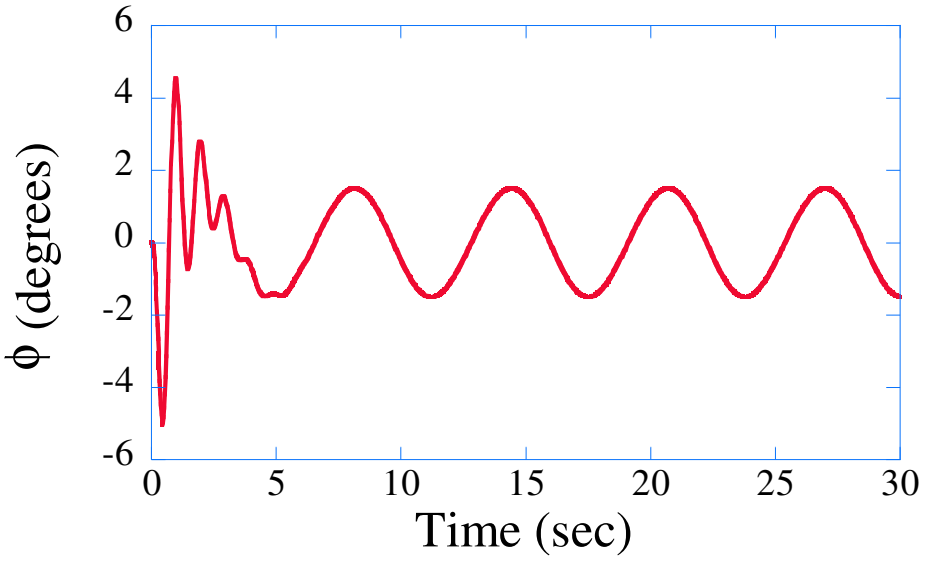

Figure 23: Spring Angle Deflection for Circular Reference Trajectory.

follows:

$$RMS_{error} = \sqrt{\frac{1}{n}\sum_{i=1}^{n}(x_{desired} - x_i)^2} \tag{38}$$

where x_i is the position of m_1 (either x or y) at time t_i, $x_{desired}$ is the desired trajectory at time t_i (either x or y), and n is the number of data points. Table 3 shows the RMS errors for the x and y position of the main satellite body when the initial position of the satellite is identical to the desired initial trajectory position ($x = 1$ and $y = 1$). The desired trajectory is calculated from (37). Notice that the RMS error is slightly larger for the x coordinate. This is due to the difference in slope between the cos and sin functions which results in a slight difference in thruster forces.

It is also important to look at the deflection of the flexible appendage when the system is commanded to follow a specified trajectory. Figure 23 shows the response of the spring angle when the system is commanded to follow the circular trajectory described by (37)

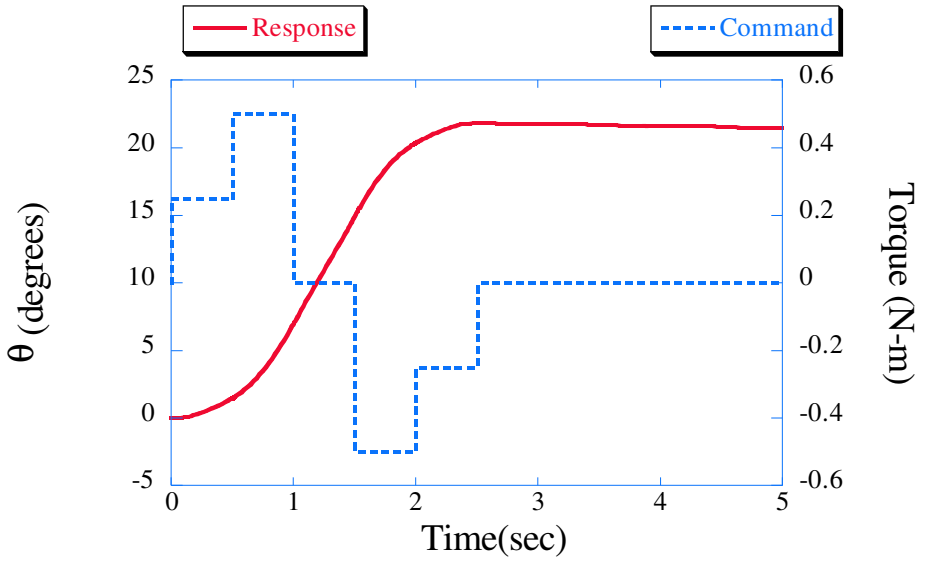

Figure 24: System Response Using 1.0 Hz ZV Input Shaping.

The steady-state peak-to-peak amplitude of vibration is approximately 3°. The steady-state response is sinusoidal because the desired trajectory is sinusoidal and the frequency of the rotation is much larger than the frequency of vibration.

2.3.3 Input Shaped Open-Loop Response

The next step is to evaluate how well input shaping affects the vibration reduction of the flexible satellite model. The first step is to use a simple open-loop bang-bang shaped profile. The input shaper is calculated based on $\omega = 1.0$ Hz and $\zeta = 0$. The amplitudes and time locations of a 1.0 Hz ZV shaper are

$$\begin{bmatrix} A \\ t \end{bmatrix} = \begin{bmatrix} 0.5 & 0.5 \\ 0 & 0.5 \end{bmatrix} \tag{39}$$

The amplitudes and time locations of a 1.0 Hz ZVD shaper are

$$\begin{bmatrix} A \\ t \end{bmatrix} = \begin{bmatrix} 0.25 & 0.5 & 0.25 \\ 0 & 0.5 & 1.0 \end{bmatrix} \tag{40}$$

Both of these shapers will be used for the open-loop and closed-loop control. Figure 24 shows the response of the flexible satellite system to a ZV shaped command. The system reaches the desired setpoint with no residual vibration. Notice that the command now has

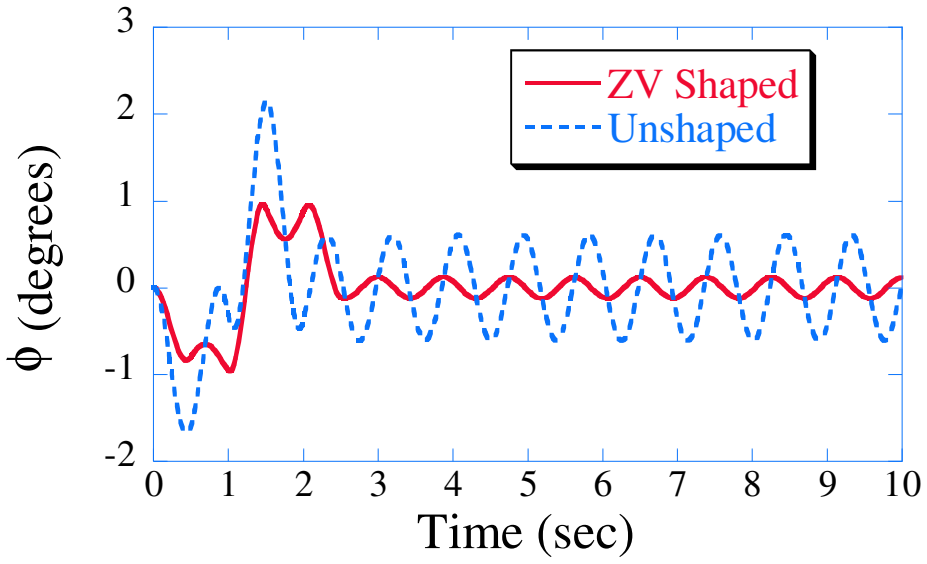

Figure 25: Spring Angle Deflection for 1.0 Hz and Unshaped Bang-Bang Commands.

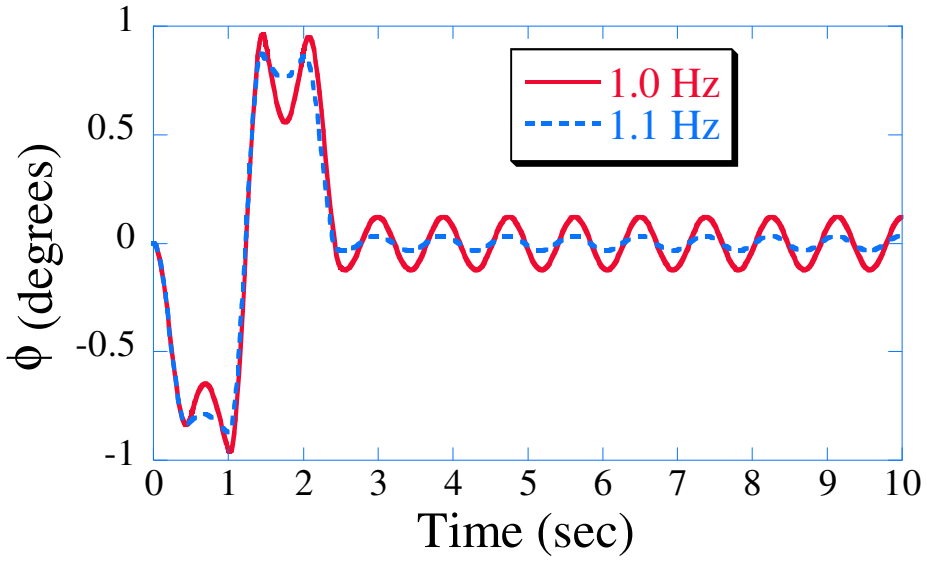

Figure 26: Spring Angle Deflection for 1.0 and 1.1 Hz ZV Shapers.

a staircase shaped profile. This results from convolving the bang-bang command used in Figure 15 with the ZV input shaper described by (40). Figure 25 shows both the unshaped and shaped spring angle deflection for the same 22° slewing maneuver. As seen in the figure, the ZV shaped case significantly reduces the residual vibration. However, it does not completely eliminate the vibration as expected. To improve the response further, the frequency of the input shaper can be changed from 1.0 Hz to 1.1 Hz. Changing the frequency

shifts the time locations slightly to the left as shown below:

$$\begin{bmatrix} A \\ t \end{bmatrix} = \begin{bmatrix} 0.5 & 0.5 \\ 0 & 0.4545 \end{bmatrix} \tag{41}$$

Figure 26 shows the spring angle deflection for the system using both the 1.0 and 1.1 Hz input shapers. These responses are for the open-loop bang-bang command. As seen in the figure, the shaper developed using the 1.1 Hz frequency eliminates more of the residual vibration. In addition, The 1.1 Hz shaper has a slightly smaller maximum deflection amplitude. However, while both of these shapers are effective at significantly reducing the residual vibration as compared to the unshaped vibration, the vibration is not completely eliminated. This is due to several different factors. First, the ZV shaper is the least robust input shaper, so any small error in estimating the natural frequency or damping ratio will lead to some level of residual vibration. The natural frequency and damping ratio for the system were based off of simplified linear model. At best, this model can only provide *estimates* of the system's natural frequency and damping ratio.

Input shaping was derived using a second order linear harmonic oscillator, so it is not designed for nonlinear systems. However, input shaping can still be effective at eliminating some of the residual vibration on nonlinear systems. The equation representing the spring angle deflection, ϕ, shown in (18), is restated below

$$\ddot{\phi} = \frac{\sin(\phi+\theta)\,\ddot{x} - \cos(\theta+\phi)\,\ddot{y} - (r\cos\phi + L)\,\ddot{\theta} - r\sin\phi\dot{\phi}^2}{L} - \frac{K\phi}{m_2 L^2} \tag{42}$$

The spring deflection is important because it represents the deflection of the flexible appendage, and it is desired to minimize this vibration. The spring angle deflection equation is composed or four nonlinear terms and one linear term. When the rotational motion of θ is small ($< 15°$), (42) is dominated by two terms: $\frac{K\phi}{m_2 L^2}$ which is a linear term, and $\frac{(r\cos\phi+L)\ddot{\phi}}{L}$ which is a nonlinear term. Therefore, even for small motions, the response of the system is generated from nonlinear equations. It may not be possible for input shaping to eliminate all of the vibration.

Figure 27 shows the satellite's response to a 1.0 Hz ZVD shaper and the ZVD shaped command. Similar to the ZV shaped commands, the system reaches the desired slewing

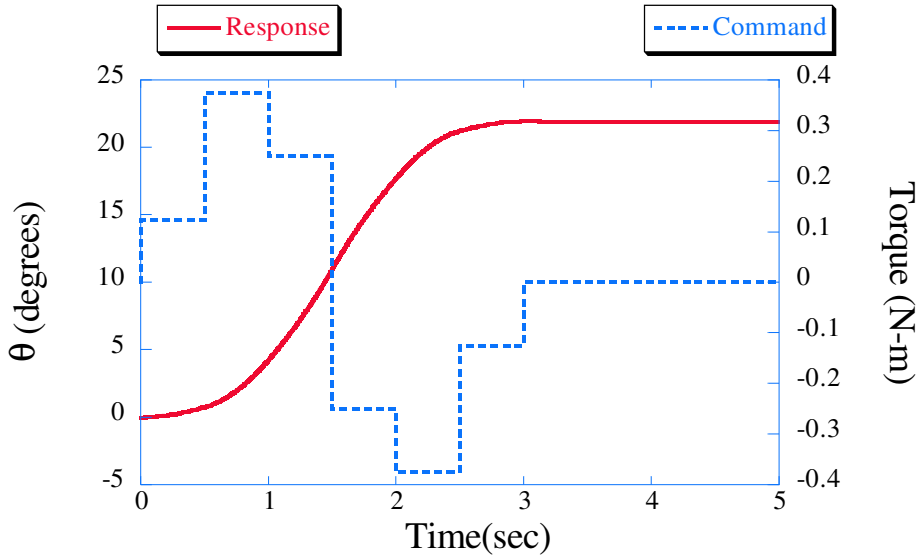

Figure 27: System Response to 1.0 Hz ZVD Shaper.

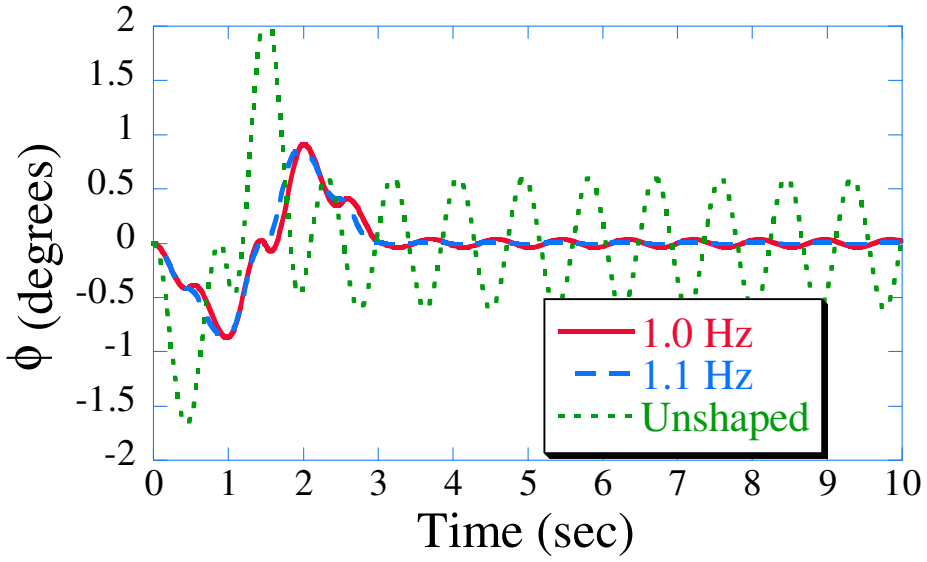

Figure 28: Spring Angle Deflection for ZVD Shaped and Unshaped Slewing Maneuvers.

angle with a negligible amount of residual vibration for m_1. Figure 28 shows the deflection of the spring angle for the unshaped, 1.0 Hz ZVD shaped, and 1.1 Hz ZVD shaped cases. The ZVD shaper clearly suppresses the residual vibration better than the unshaped case. Although the 1.0 Hz ZVD shaper does a good job at reducing the residual vibration, the 1.1 Hz ZVD shaper produces a lower level of residual vibration. As stated earlier, the ZVD input shaper is much more robust than the ZV shaper. So, it is expected that a

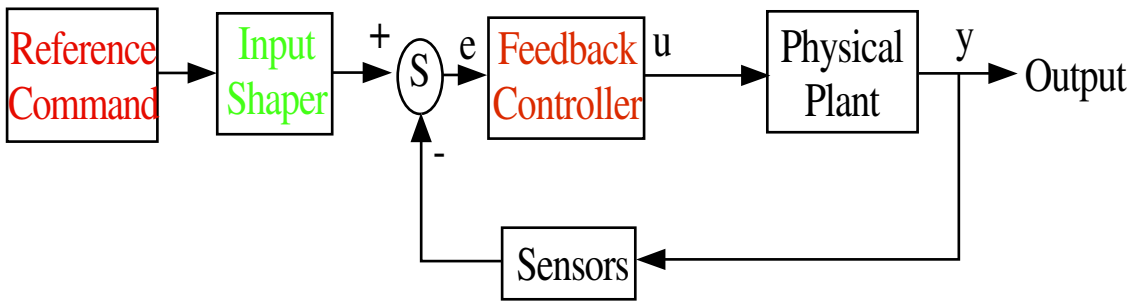

Figure 29: Closed-Loop Block Diagram

ZVD input shaper would be much more insensitive to modeling inaccuracies and perhaps to the nonlinear behavior of the system. The 1.0 Hz ZVD shaper reduces the vibration to approximately the same level as the 1.1 Hz ZV shaper. The 1.1 Hz ZVD shaper further reduces the level of residual vibration below that of the 1.1 Hz ZV input shaper.

2.3.4 Input Shaped Closed-Loop System Response

In the previous section, the open-loop response of the system to a shaped profile was examined. In this section, a feedback PD controller is added to the system. The desired trajectory is convolved with a shaper and this new trajectory is used to drive the system. The next step is to investigate the effect of input shaping on the PID feedback control. For systems with closed-loop feedback control, the input shaper is placed outside the loop as shown in Figure 29

When the satellite is oriented so that the flexible appendage is parallel to the inertial x-axis, a motion in the x-direction will not excite the flexible appendage, so adding input shaping to this motion cannot improve the residual vibration characteristics. If the satellite is not oriented with the flexible appendage parallel the x-axis, or if the maneuver does not require a motion in only the x-axis, then input shaping can help eliminate the residual vibration. Figure 30 shows the response of the flexible satellite system to a ZV shaped step change in the y-direction. It is important to note that this is the closed-loop response. The responses discussed in the previous sections were the open-loop responses. As seen in the figure, the desired change in position is no longer a single step change in position, but it is now a stair case command. The peak overshoot of the system has also been decreased, but

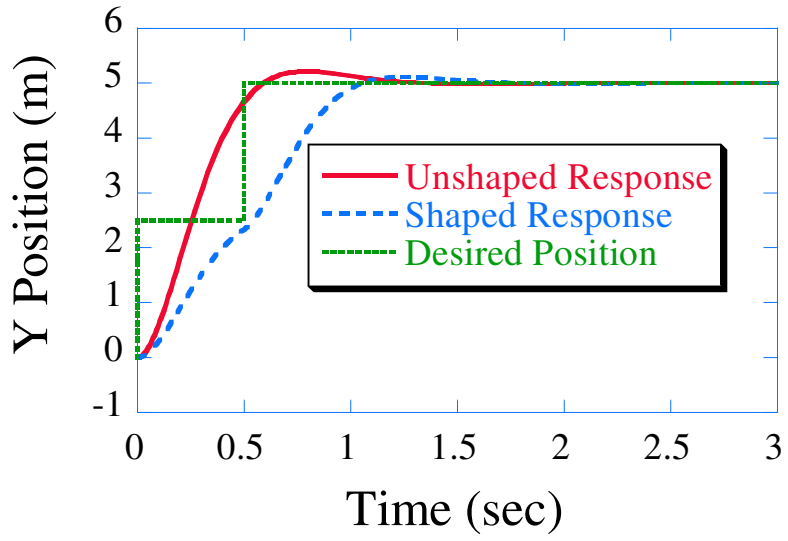

Figure 30: System Response to ZV Shaped Step Change in Y Position.

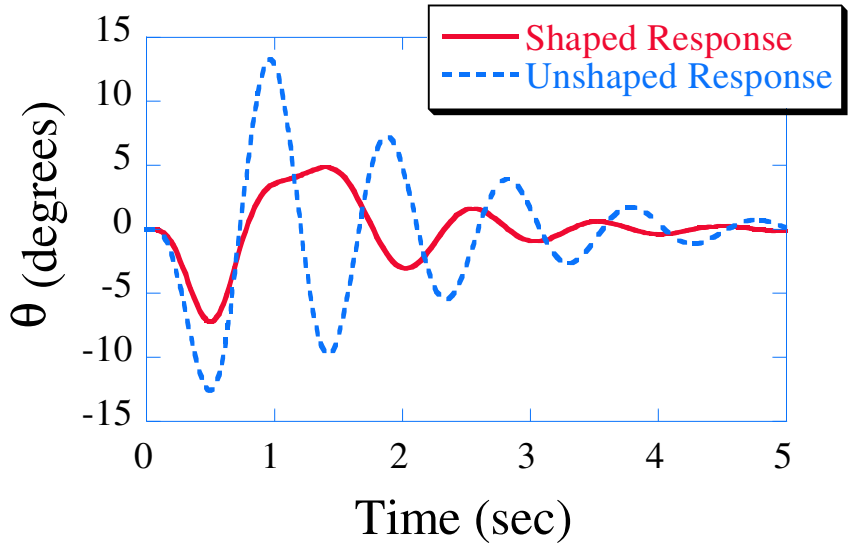

Figure 31: Attitude Response to ZV Shaped Step Change in Y Position.

the rise time of the satellite's response has been increased. The increase in rise time is equal to the duration of the 1.0 Hz ZV shaper used to shape the desired step change in position. However, the small increase in rise time is a small price to pay for the huge reduction in residual vibration.

Figure 31 shows the attitude response of the system to the unshaped and shaped step changes in y-position. Shaping the desired y position using the 1.0 Hz ZV input shaper has

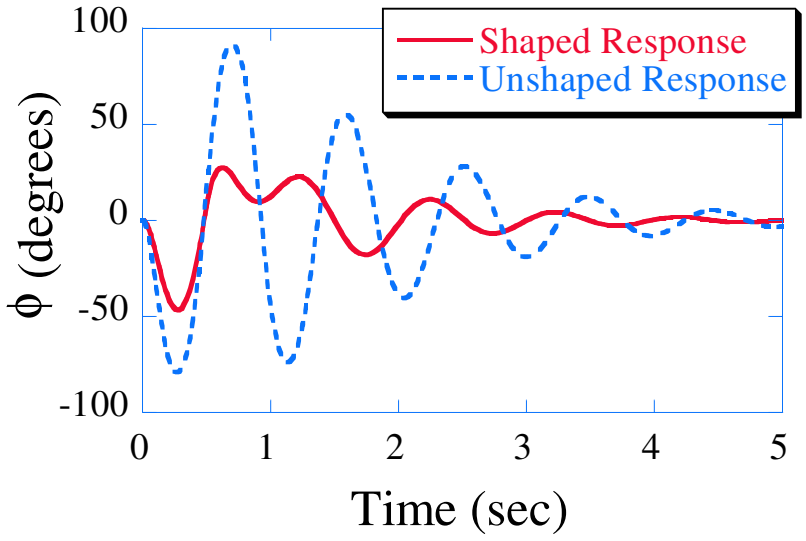

Figure 32: Spring Angle Response to ZV Shaped Step Change in Y Position.

decreased the maximum amplitude of vibration in the main satellite body to approximately $\frac{1}{3}$ of its unshaped magnitude. The setting time of the shaped m_1 response has also been reduced 27% when compared to the unshaped case.

Although the settling time and response of m_1 is important, the deflection of the flexible appendage is of primary concern. As with the unshaped case shown in Figure 32, the maximum deflection of the spring angle for the shaped case is approximately 50°. However, when compared to the unshaped response, using input shaping has significantly decreased the amount of deflection in the spring angle and the amount of residual vibration. The shaped response has a reduction of approximately 50% when compared to the level of residual vibration for the unshaped case.

Similar to the open loop case, it is possible to further reduce the amount of residual vibration in the flexible appendage by altering the frequency the input shaper is designed. For the open loop cases, a significant reduction in residual vibration was obtained by changing the frequency of the input shaper from 1.0 Hz to 1.1 Hz. Figure 33 compares the spring angle deflection for both the 1.0 and 1.1 Hz cases. Unfortunately, when using closed loop PD control, increasing the frequency from 1.0 to 1.1 does not significantly reduce the vibration reduction characteristics of the input shaper; therefore, it is appropriate to use

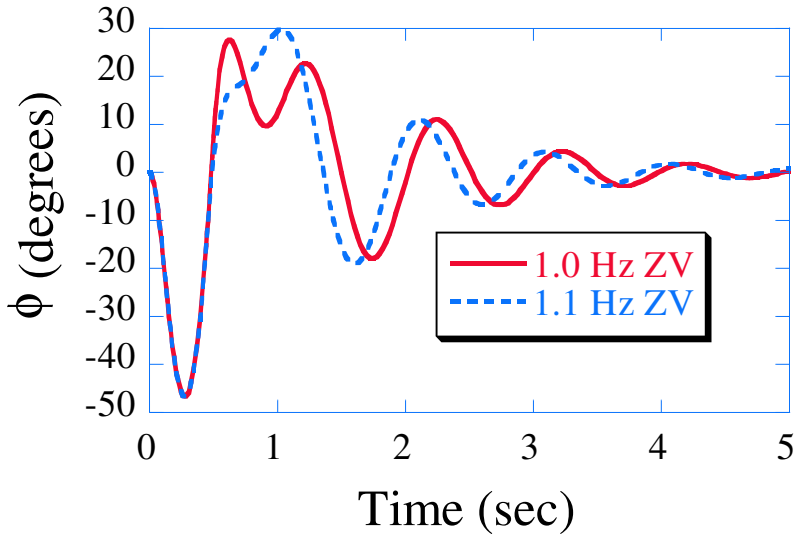

Figure 33: Spring Angle Deflection for 1.0 and 1.1 Hz ZV Shaped Frequencies.

the estimated 1.0 Hz frequency for the natural frequency of the flexible appendage. For a linear-second-order system, the addition of proportional control will increase the closed-loop undamped natural frequency of the system. The addition of derivative control does not affect the natural frequency of the system; however, it will increase the damping ratio of the system. For a linear system, it is simple to calculate the change in natural frequency and damping ratio; however, the task is much more difficult when the system is nonlinear. The addition of the PD control to a nonlinear system will also increase the closed loop undamped natural frequency and damping ratio, but its not a trivial task to calculate the effect that adding the PD gains has on the system.

However, it is possible to increase the insensitivity of the nonlinear system to both parametric changes and nonlinearities by utilizing a more robust shaper. As discussed in Section 1.6.2, the ZVD shaper is more robust then a ZV shaper. Figure 34 shows the spring angle deflection for the step change in y position. The figure compares the unshaped, ZV shaped and ZVD shaped responses. Both the ZV and ZVD shapers were formulated using the 1.0 Hz frequencies. As seen from the figure, using the ZVD shaper significantly reduces the maximum vibration amplitude and the magnitude of the residual vibration. Tables 4 and 5 show the maximum vibration amplitude and 5% settling time for the unshaped

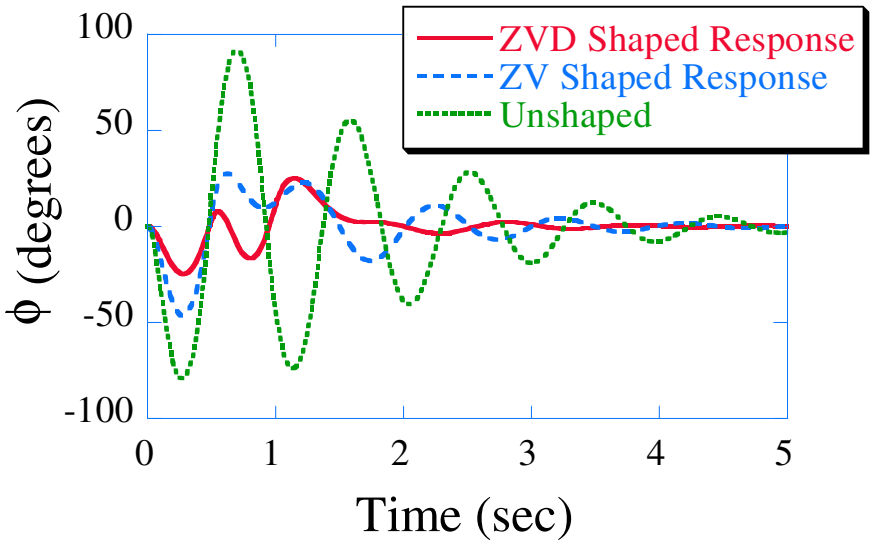

Figure 34: Spring Angle Deflection Using 1.0 Hz ZV and ZVD Shapers.

Table 4: Closed Loop System Response for θ.

Command Generation Scheme	Max Amplitude	5% Settling Time
Unshaped	13.3	5.2
ZV Shaped	7.2	4.0
ZVD Shaped	4.2	3.1

and shaped cases. Table 4 compares the responses of the main satellite body's attitude, θ. As seen from the table, the greatest reduction in both maximum vibration amplitude and settling time is achieved using the 1.0 Hz ZVD input shaper. By using the ZVD input shaper, it is possible to reduce the maximum vibration amplitude by 69%. The 5% settling time is also reduced by 42%. Table 5 compares the unshaped and shaped spring angle deflections. Again, the ZVD input shaper gives the best vibration reduction. The ZVD shaped position change decreases the maximum vibration amplitude by 73% when

Table 5: Closed Loop System Response for ϕ.

Command Generation Scheme	Max Amplitude	5% Settling Time
Unshaped	92.3	7.4
ZV Shaped	46.7	5.7
ZVD Shaped	25.0	4.8

compared to the unshaped maximum vibration. The settling time of the spring angle has also been decreased by 35%. The results shown in tables 4 and 5 are for the desired step change in y-position.

The next step is to investigate how input shaping affects the trajectory following of the flexible satellite. The trajectory used in the following simulation results is the same as described by (37). Because the trajectory is know *a priori*, it is easy to input shape the desired trajectory. The reference trajectory is convolved with the desired input shaper and the result is used as the new desired trajectory.

In order to shape the desired trajectory, it must first be normalized with respect to the initial position condition. For the circular reference trajectory, this corresponds to the following equations:

$$x_{desired} = \cos t - \cos 0 \tag{43}$$

$$y_{desired} = \sin t - \sin 0 \tag{44}$$

For these simulations, the attitude of the satellite is not required to follow a desired trajectory; therefore it is not necessary to shape it. The rest of the circular reference trajectory equations are identical to (34)-(37). After (43) and (44) are convolved with the input shaper, the initial condition is added back. This is done in order move the trajectory back to the original starting coordinates. Figure 35 shows the resulting shaped circular trajectory along with the original unshaped desired circular trajectory. It is important to note two major differences between the unshaped and shaped trajectories. First, the shaped trajectory does not have a radius equal to the unshaped circle's radius. This is because input shaping shortens the effective radius as discussed in Section 1.6.5. Table 6 shows the radii for the unshaped, ZV shaped and ZVD shaped cases. The desired trajectory radius is $1m$. The percent the shapers decrease the radius of a circular trajectory is independent of size. Table 7 shows four different desired radii and the effective radius produced by using a 1.0 Hz ZV and ZVD shaper. As seen from Table 7, using a 1.0 Hz ZV shaper reduces the radius approximately 3%, and a 1.0 Hz ZVD input shaper reduces the radius approximately 6%. The percentage the shaper reduces a circular trajectory is based only on the shaping

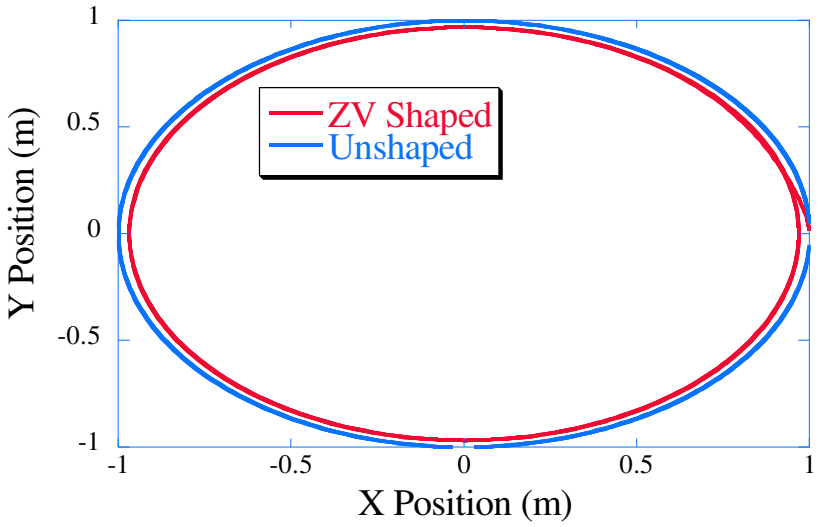

Figure 35: Unshaped and ZV Shaped Circular Trajectories.

Table 6: ZV and ZVD Shaped Trajectory Radii.

Command Generation Scheme	Circular Trajectory Radius
Unshaped	1.0
ZV Shaped	0.96
ZVD Shaped	0.94

frequency which corresponds to shaper duration. The shorter the input shaper duration, the smaller the amount the radius is reduced. Shaper duration is inversely proportional to the natural frequency. The higher the frequency used to design the input shaper, the shorter the input shaper's duration will be. For example, a 1.1 Hz ZV shaper only reduces the radius approximately 2.57%.

Using the information presented in Table 7, it is possible to modify the trajectory so that the effective radius resulting from the input shaper is closer to the original desired radius. For example, by increasing the original radius 3% (from 1.0 to 1.03), the effective radius after input shaping is 0.9980 which corresponds to only a 0.2% reduction in radius. The same technique can be used for the ZVD shaper as well. It is possible to generate the desired circle radius by pre-modifying the desired trajectory.

The second major difference between the two desired trajectories occurs at the beginning

Table 7: Effective Circular Radii Produced Using 1.0 Hz Shaped Frequency

Desired Radius (m)	ZV Radius	ZVD Radius	ZV % Reduction	ZVD % Reduction
1.0	.9689	.94	3	6
10	9.6891	9.40	3	6
100	96.8912	93.99	3	6
1000	968.9124	939.9814	3	6

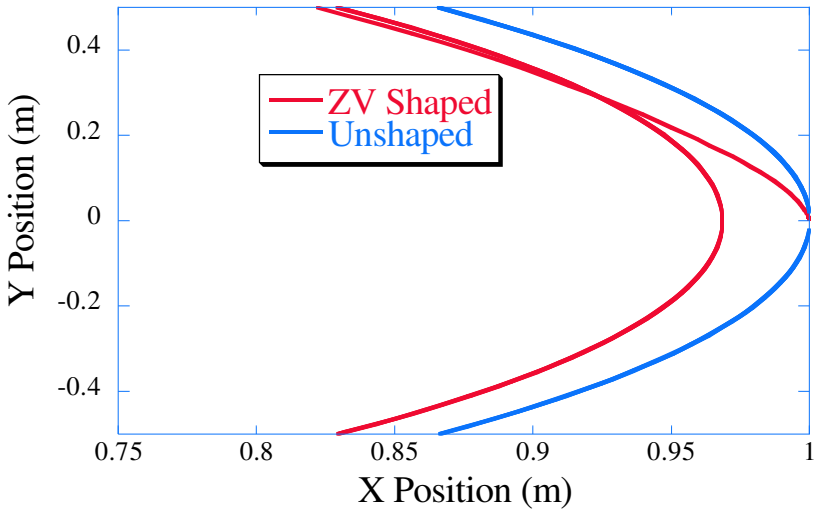

Figure 36: Unshaped and ZV Shaped Circular Trajectories.

of the trajectory. Figure 36 shows an expanded view of the unshaped and shaped circular trajectories. Notice that the shaped trajectory starts at the same point as the unshaped trajectory, but converges to the shortened shaped radius. If the difference between the unshaped radius and the shortened shaped radius is within a tolerable error band for the satellite, then the effect of the shortened radius is negligible.

Figure 37 shows the attitude response of m_1 to both the unshaped and shaped trajectories. Following the 1.0 ZV Hz reduces the maximum vibration amplitude. The steady state vibration seen in the both the unshaped and shaped responses comes from the circular trajectory. The frequency of the trajectory, which can easily be determined by examining (32) and (33), is 1 $\frac{rad}{sec}$ and the period of the circular trajectory is 2π seconds. The estimated natural frequency of the flexible appendage is 1 Hz, which corresponds to a period

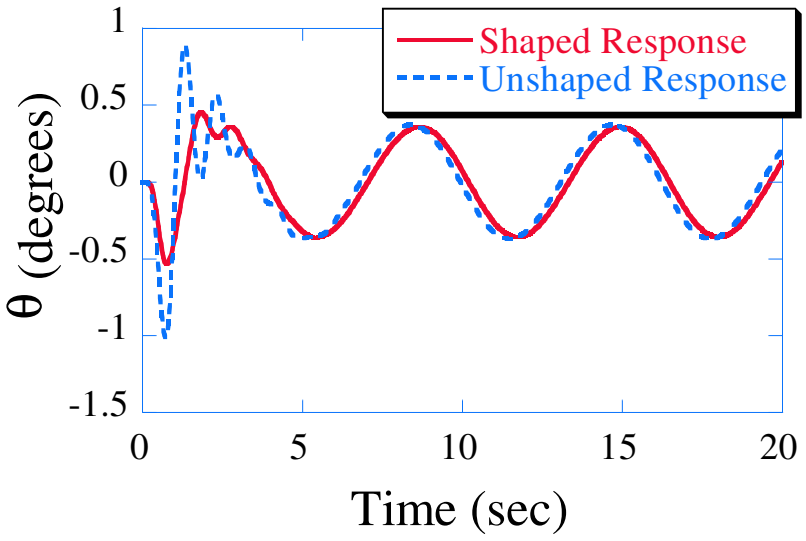

Figure 37: Attitude Response to Unshaped and Shaped Circular Trajectory.

Table 8: RMS Error for Unshaped Circular Trajectory.

Position	RMS Error
Unshaped x	0.17
ZV Shaped x	0.13
Unshaped y	0.16
ZV Shaped y	0.10

of 1 second. Therefore, the residual vibration seen in Figure 37 for both the unshaped and shaped cases, cannot come from the excitation of the flexible appendage.

As with the unshaped closed-loop case, the trajectory tracking error must be evaluated. Table 8 shows the RMS error for the unshaped and shaped cases. When calculating this RMS error, the shaped response was compared to the shaped desired reference trajectory. The RMS error is smaller for the shaped trajectories than the unshaped trajectories. This is because input shaping has reduced the amount of vibration in the system, and the satellite's thrusters do not have to produce as much torque to counteract the rotation of the main satellite body. The shaped responses have approximately 40% less tracking error.

In addition to spatial tracking error, the temporal tracking is also important for formation flying satellites. Table 9 shows the time the satellite reached the desired x trajectory positions. The desired x positions are 180° apart and correspond to the absolute maximum

Table 9: Time Lag for Circular Trajectories.

Desired x	Desired t	Unshaped t	ZV Shaped t	ZVD Shaped t
-1	3.14	3.39	3.64	3.89
1	6.3	6.53	6.78	7.04
-1	9.43	9.68	9.93	10.17
1	12.6	12.82	13.09	13.32
-1	15.7	15.96	16.21	16.42
Average Time Lag	0	.24	.50	.73

x positions. For these calculations, it was assumed that the shortened radius resulting from input shaping the trajectory had a negligible effect on the temporal tracking. The times when system reaches the absolute maximum x positions were recorded. After finding the appropriate time locations, the difference between the desired time and the actual time was calculated, and the average of these differences was calculated.

The unshaped satellite response had the shortest time lag. It reached the desired x position an average of 0.24 seconds after the desired time. The ZV shaped satellite response has a time lag of approximately double the unshaped response. The shaped satellite reached the desired x position on average 0.5 seconds after the desired time. The ZVD shaped response reached the desired x position on average 0.73 seconds after the desired time. This is three times the unshaped delay for the same desired maneuver.

Although input shaping increases the time lag in the system, there is a way to negate this effect. If the slewing maneuver must occur at a precise time, then the input shaped slewing maneuvers must be started earlier. For example, in order to decrease the time lag present in the system, the ZVD shaped slewing maneuver must be started 0.73 seconds earlier. The same idea would hold for both the ZV shaped trajectories and the unshaped trajectories. This assumes that the time lag remains constant during the entire maneuver.

2.4 Summary of Flexible Spacecraft Model

A nonlinear flexible satellite model was developed. The satellite model represents a main satellite hub with one flexible appendage extending radially outward. If more flexible appendages are required, the model can easily be changed to include additional flexible appendages. The rotational spring used to represent a flexible beam in bending does not deform for lateral movements parallel to the direction of the beam. A simple method was used in order to estimate the natural frequency of the flexible appendage. The thruster forces and torque modeled in the system represent an equipollent representation of an eight thruster satellite configuration.

A MATLAB simulation was developed in order to simulate slewing maneuvers of the flexible satellite, and to verify that input shaping is an effective way to eliminate residual vibration in the system. Open-loop control can be used for slewing maneuvers when the thruster profile is known. A PD controller is effective at both step position slewing maneuvers and trajectory following. The PD gains should be tuned so that the system responds quickly to the changing trajectory yet maintains as little overshoot as possible.

The flexible satellite model developed in this chapter is nonlinear. Input shaping was developed for linear systems. Input shaping relies on superposition, but superposition does not hold for nonlinear systems. The results discussed in this chapter show that input shaping can still greatly reduce the residual vibration for a nonlinear system. It is important to note that the frequency of this nonlinear system did not change throughout the maneuver. The effectiveness of shaping on the nonlinear response was demonstrated in two ways: for open loop control it is important to have an accurate estimate of the natural frequency, for closed-loop control a robust input shaper is more important. Both ZV and ZVD input shapers were effective at eliminating the residual vibration for both the open-loop and closed-loop control schemes.

CHAPTER III

LEADER-FOLLOWER FORMATION FLYING ARCHITECTURE

A leader-follower control architecture is perhaps the simplest formation flying architecture available. In this architecture one satellite is designated as the leader and the other satellites in the formation are designated as the followers. It is desired that the follower satellites maintain a designated distance away from the leader satellite. This chapter focuses on the effect of utilizing input shaping on a group of two satellites in a leader-follower formation. Although there are many ways to apply input shaping to this system, this work focuses on shaping the desired trajectory of the leader satellite.

It is assumed that the desired path of the leader spacecraft is completely known (i.e. desired position, velocity, attitude) in advance, and that the input shaping can be done before the motion is initiated. The control effort of the follower satellite is calculated based on the relative position and velocity between the leader and follower spacecraft. In space applications, the relative position between the satellites would be measured and the absolute position and velocity of the follower satellite would be unknown. For this work, the inertial positions and velocities of both the leader and follower satellite are used to generate the relative position and velocity. It is important to note, that the follower satellite does not have any knowledge concerning the motion of the leader satellite. It only knows that it must maintain the specified distance and velocity relative to the leader satellite.

3.1 Design Procedure for Utilizing Command Generation with Leader-Follower Formation Flying Architecture

The effect of input shaping on a leader-follower formation architecture was studied. In order to investigate what effects shaping has on the architecture, a computer simulation was developed using MATLAB. The leader-follower simulation was developed so general motion

maneuvers could be studied. The goal of investigating the leader-follower architecture is to produce a design procedure. This procedure can be used to help the controls engineer implement trajectory shaping with a leader-follower or similar formation flying architecture. The design procedure for the leader-follower architecture is as follows:

- *Select PD gains to provide excellent tracking performance.* (The detailed process for this selection is shown in Sections 2.3.2, 3.3.1, and 3.3.2.)
- *Convolve the leader's desired trajectory with a robust shaper.* (The benefit of utilizing a robust shaper will be discussed in Sections 3.3.2-3.3.5)
- *When temporal tracking is of paramount importance start the shaped maneuvers early.* (The clarification and justification of this step is given in Sections 3.3.1.1 and 3.3.1.2.)
- *Start the follower satellite as close to its designated initial position as possible.* (The reason for this step is discussed in Sections 3.3.1.2 and 3.4.)
- *For circular maneuvers, increase the desired radius before shaping.*(The justification and clarification for this step was given in Section 2.3.4.)
- *For largely spaced multi-mode formations use a multi-mode shaper.*
- *For closely spaced multi-mode formations use a robust shaper.* (The justification for this and the preceding guideline is discussed in Sections 3.4 and 3.5.)

3.2 Investigated Trajectories

Two types of trajectories are investigated: straight-line and circular trajectories. Case 1 is the straight-line motion. For this case, the leader satellite travels in a straight-line. Cases 2-5 are circular motions. The difference between cases 2-5 is the desired placement of the follower satellite.

3.2.1 Case1: Straight-Line Motion

For the straight-line trajectory shown in Figure 38, the leader follows a straight line. The follower spacecraft is not required to follow the same trajectory as the leader spacecraft, it is

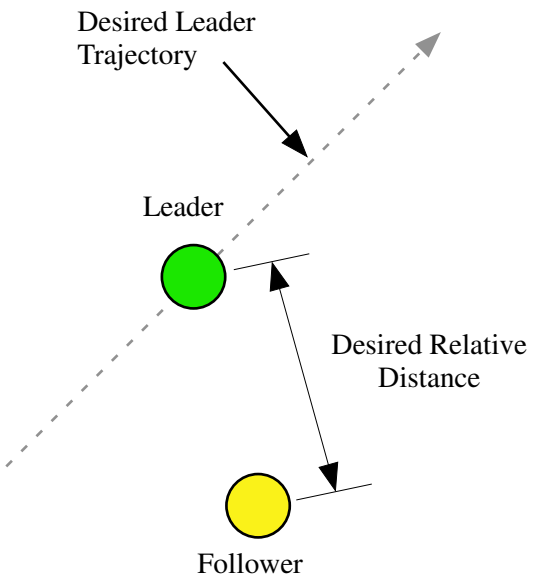

Figure 38: Leader-Follower Straight Line Trajectory for Case 1.

only required to maintain the desired relative distance away from the leader spacecraft. In addition, the relative velocity difference between the two spacecraft must also be specified. For the cases studied, the relative velocity difference between the two spacecraft was equal to zero unless otherwise specified. This means the follower spacecraft was required to match the magnitude of the leader's velocity.

3.2.2 Case 2: Same-Orbit Maneuvers

For all of the circular maneuvers (cases 2-5), the desired position of the leader satellite is:

$$x = R\cos(\omega t)$$

$$y = R\sin(\omega t) \tag{45}$$

where R is the desired radius. The desired velocity of the leader satellite is calculated by taking the derivative of (45) with respect to time. For the same-orbit maneuvers (discussed in this section), the desired trajectory for the leader satellite is a circular orbit shown in Figure 39. It is desired that the follower satellite maintain a specified distance away from the leader satellite on the same circular orbit. This is equivalent to designating a desired chord length on the circle. The follower satellite must match the magnitude of the leader's

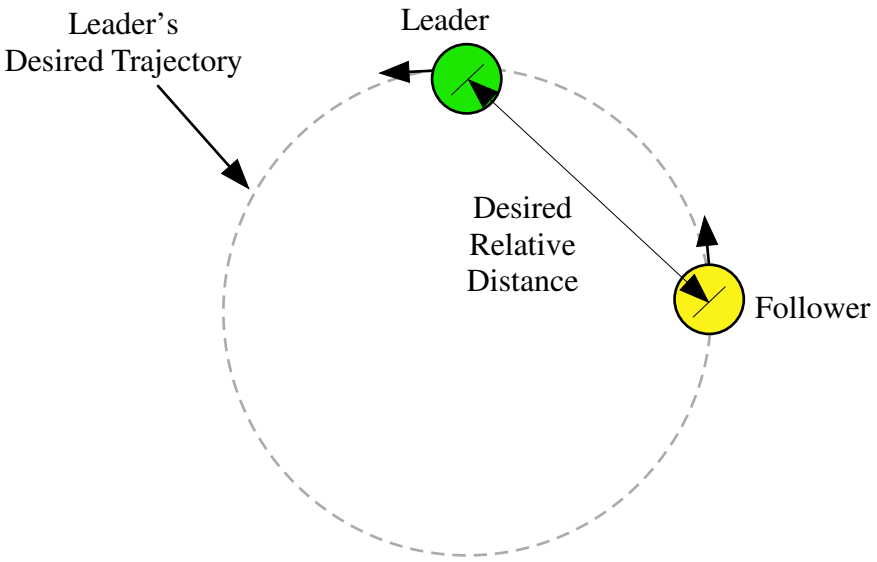

Figure 39: Case 2: Same-Orbit Trajectory.

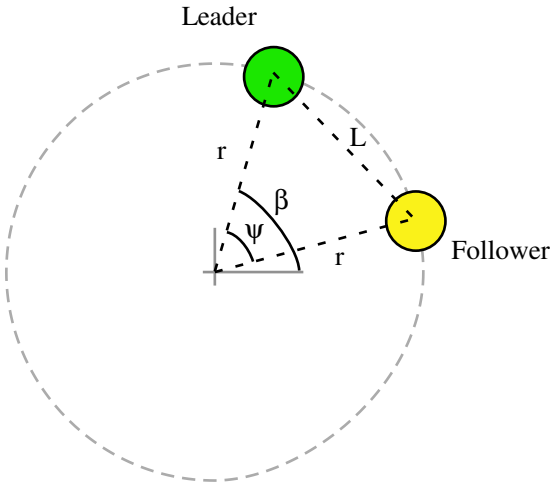

Figure 40: Leader-Follower Relationship for Same-Orbit Trajectory.

velocity at all times. Because both spacecraft are following circular paths, the direction of the velocity of each spacecraft is tangent to the orbit at all times.

The leader position (x, y) and the desired position $(x_{desired}, y_{desired})$ are known at all times. Because the leader travels in a circle, the leader spacecraft, follower spacecraft and the center of the orbit create an isosceles triangle with legs equal to the radius of the orbit, r, and the desired separation distance, l. This relationship is shown in Figure 40. In order to calculate the desired position of the follower satellite, first the interior angle of the triangle

is calculated using the bisection properties of an isosceles triangle.

$$\psi = 2 \arcsin\left(\frac{\frac{l}{2}}{r}\right) \tag{46}$$

Next, the desired follower position can be calculated using the following equations:

$$xf_{desired} = r\cos(\beta - \psi)$$

$$yf_{desired} = r\sin(\beta - \psi) \tag{47}$$

where β is calculated from the position of the leader satellite.

$$\beta = \arctan\left(\frac{y}{x}\right) \tag{48}$$

It is also possible for the leader satellite to "push" the follower satellite along (i.e. the positions of the satellites shown in Figure 39 are reversed). If this the case, then the position of the follower satellite is calculated as:

$$xf_{desired} = r\cos(\beta + \psi)$$

$$yf_{desired} = r\sin(\beta + \psi) \tag{49}$$

The follower satellite's desired velocity must match the leader's velocity in magnitude; however, the direction of the velocity will be different as shown in Figure 39. The direction of the follower's velocity can be easily calculated using the following:

$$\vec{vf}_{desired} = |\vec{v}| \cdot \vec{k} \times \vec{rf} \tag{50}$$

where v is the velocity of the leader satellite, k is the direction of positive (counter-clockwise) rotation, and rf is the position of the leader satellite calculated from (49).

This trajectory is suitable for any orbiting satellite where it is desired that the follower satellite follow the same orbit. The follower spacecraft simply lags the leader satellite in time. For earth orbiting satellites, this is not equivalent to "same ground track" orbits since the follower satellite does not cross over the same ground points as the leader satellite.

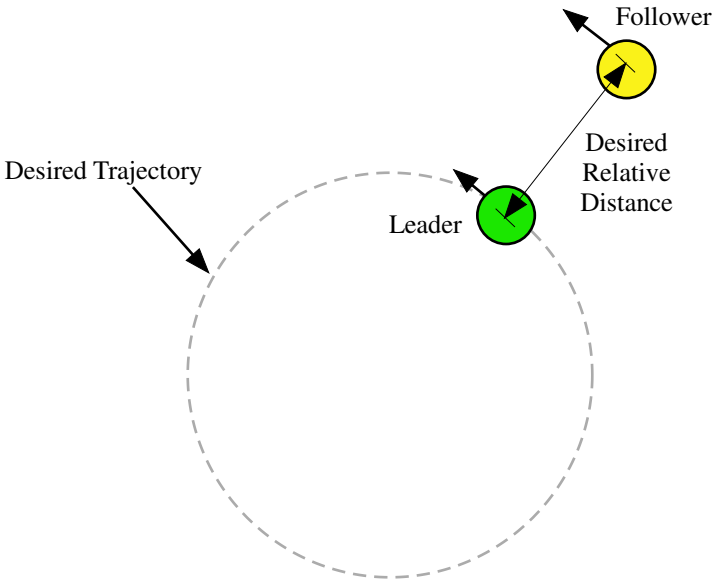

Figure 41: Case 3: Synchronized Orbit.

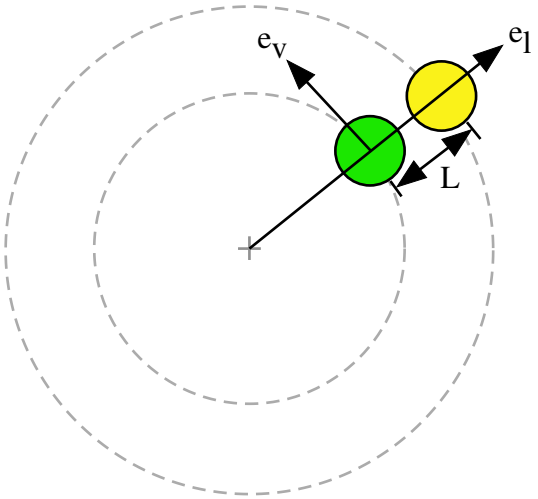

Figure 42: Synchronized Orbit: Leader Fixed Reference Frame.

3.2.3 Case 3: Synchronized Orbit Maneuvers

For the third case, the follower spacecraft is synchronized with the leader satellite as shown in Figure 41. The follower satellite maintains a specified relative radial distance away from the leader satellite. In order to calculate the desired position of the follower satellite, first a body fixed coordinate frame is attached to the leader satellite as shown in Figure 42 where e_v is a unit vector in the along track direction of the leader and e_l is a unit vector in the radial direction. The positive convention for this unit vector is such that it always points

from the leader satellite towards the follower satellite. For the case shown in Figure 42, this corresponds to a radially outward direction. If the position of the leader and follower satellites are reversed, then the e_l vector would point in towards the center of the circle.

As for the same-orbit trajectory, the position and velocity of leader satellite are known. The velocity of the leader satellite is:

$$\vec{v} = v_x\vec{i} + v_y\vec{j} \tag{51}$$

where v_x and v_y are the velocities in the inertial x and y directions. The e_v unit vector can be calculated from the velocity.

$$\vec{e_v} = \frac{v_x\vec{i} + v_y\vec{j}}{\sqrt{{v_x}^2 + {v_y}^2}} \tag{52}$$

Assuming a positive rotation for the leader, e_l can be calculated using:

$$\vec{e_l} = -\vec{k} \times \vec{e_v} \tag{53}$$

The desired position of the follower satellite is calculated as:

$$xf_{desired} = x\vec{i} + l\vec{e_l} \cdot \vec{i}$$

$$yf_{desired} = y\vec{j} + l\vec{e_l} \cdot \vec{j} \tag{54}$$

where l is the desired distance between the leader and follower satellite.

Because the rotation of leader and follower satellites must be equal for synchronized motion, the velocity of the follower spacecraft can be calculated from:

$$\vec{vf}_{desired} = \frac{|\vec{rf}_{desired}|}{|\vec{r}_{desired}|}|\vec{v}|\vec{e_v} \tag{55}$$

where $\vec{rf}_{desired}$ and $\vec{r}_{desired}$ are the desired positions of the follower and leader satellites respectively.

3.2.4 Case 4: Tangential Pursuit Maneuvers

It may be desired to have the follower satellite remain at a fixed distance away from the leader satellite, but not be radially away from the leader. Such is the motion for the tangential pursuit maneuver, and it is shown in Figure 43. For this case, the follower

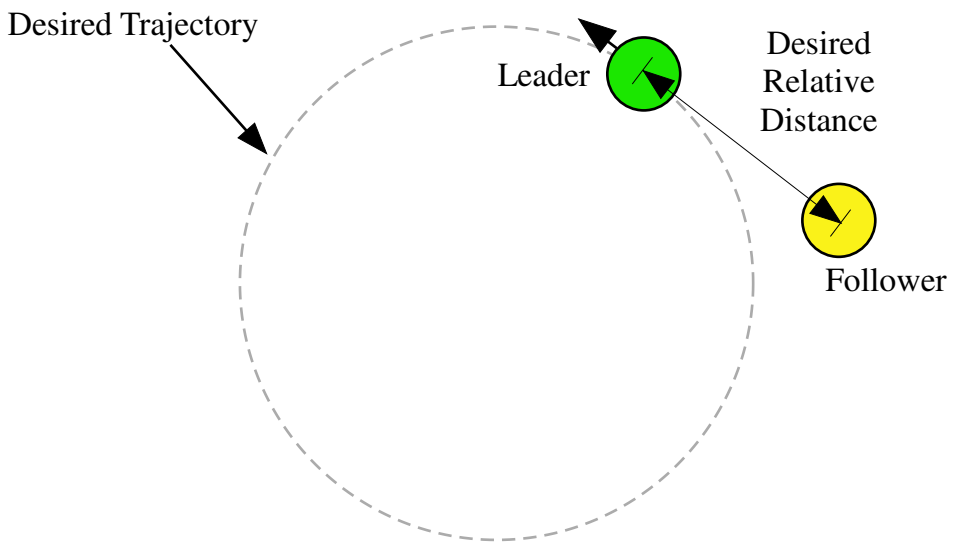

Figure 43: Case 4: Tangential Pursuit Trajectory.

satellite maintains a desired relative distance away from the leader satellite; However, the direction of the displacement is dependent on the direction of the leader's velocity.

In order to calculate the follower satellites desired position, a body fixed frame is attached to the leader satellite. This frame is identical to the frame used for case 3 (shown in Figure 42). However, instead of calculating the position of the follower using the e_l unit vector, the e_v vector is used.

$$\vec{rf}_{desired} = \vec{r} - l\vec{e}_v$$

$$xf_{desired} = x - l\vec{e_v} \cdot \vec{i}$$

$$yf_{desired} = y - l\vec{e_v} \cdot vecj \tag{56}$$

This ensures that the follower satellite is always behind the leader satellite. If the positions of the satellites are reversed (i.e. with the follower satellite in front), then the position of the follower satellite would be calculated as follows.

$$xf_{desired} = x + l\vec{e_v} \cdot \vec{i}$$

$$yf_{desired} = y + l\vec{e_v} \cdot \vec{j} \tag{57}$$

This type of circular motion, may not lend itself to useful earth orbiting applications because the path of the follower satellite is centered around a different center point. However, this application would be useful in deep space applications where it is important for

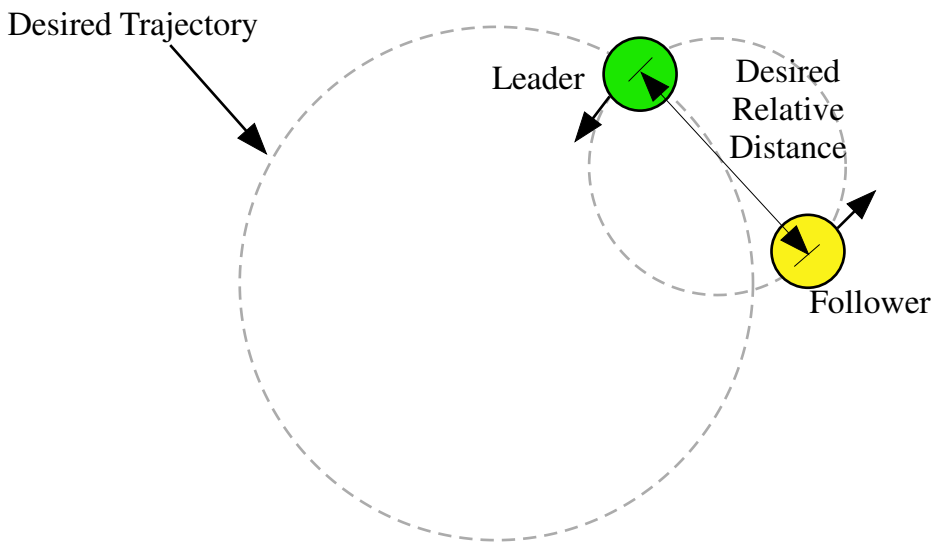

Figure 44: Case 5: Epi-Cyclic Trajectory.

the follower satellite to remain behind or in front of the leader satellite, or for servicing and rendezvous maneuvers.

3.2.5 Case 5: Epi-Cyclic Maneuvers

The last case circular trajectory case studied is the most complex motion. This trajectory mimics the path a satellite would travel when in orbit around the earth. The expected trajectory for the LISA formation is an Epi-Cyclic trajectory. For this mission, a set of three satellites will be in an earth trailing mission (the large circle in this case) while spinning about each other (the smaller circle). This path is composed of two circular paths, a small circular path and a large circular path as shown in Figure 44. The center of the smaller circle follows the perimeter of the larger circle. Both the satellites in the formation spin around each other while moving around the larger orbit. For this case, it is desired that the follower satellite remains 180° away from the leader satellite. The resulting path of both satellites is a complex combination of the two circles. The path of the leader satellite is shown in Figure 45. For this case, the frequency of the small circle was $0.2\frac{rad}{sec}$ and the frequency of the larger circle was $2\frac{rad}{sec}$.

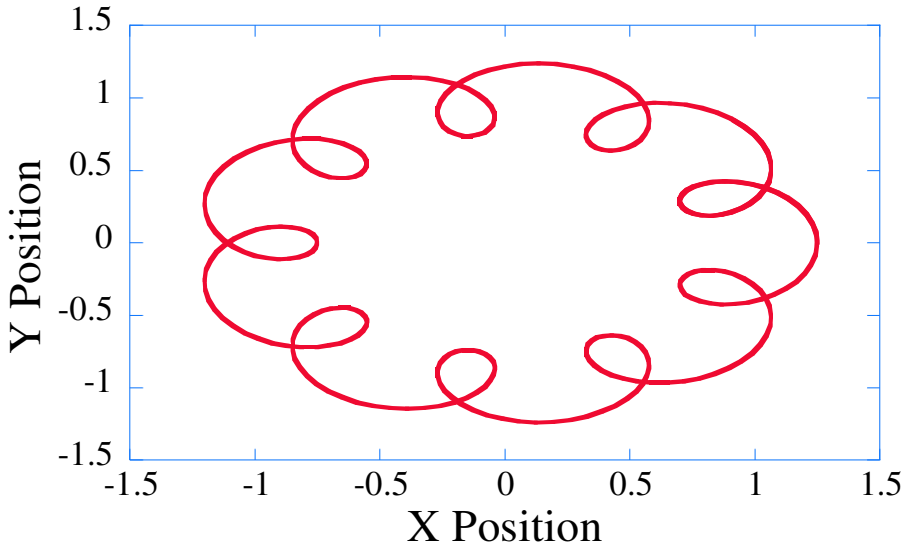

Figure 45: Case 5: Leader Satellite Path.

The desired position of the follower satellite is calculated as follows:

$$xf_{desired} = x + l\vec{e}_l \cdot \vec{i}$$
$$yf_{desired} = y + l\vec{e}_l \cdot \vec{j} \tag{58}$$

where e_l is a unit vector that points radially inward from the leader satellite to the follower satellite. The desired follower velocity is equal in magnitude to the velocity of the leader, but is in the opposite direction.

The next sections discuss the results from the MATLAB computer simulation. The goal of the simulations is to show that input shaping can be used in conjunction with a leader-follower architecture, and to develop guidelines for implementing shaping with the leader-follower architecture.

3.3 Simulation Results: Single Flexible Mode

Simulations for all five cases were run using two identical flexible satellites and identical PD gains. The flexible satellite model used in the simulations was the model discussed in Chapter 2. Both the ZV and ZVD shapers were used to shape the leader's desired trajectory. The ZV and ZVD shapers were calculated using a *1.0 Hz* frequency as discussed

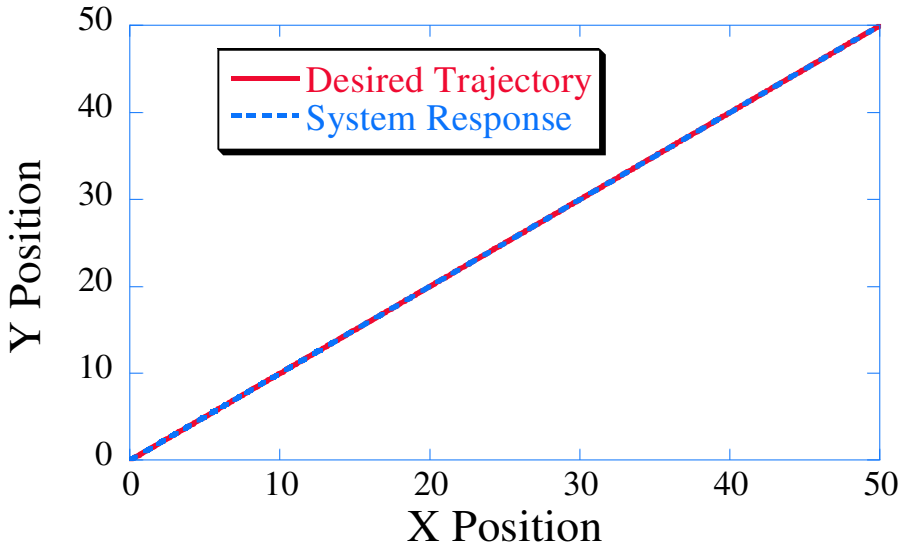

Figure 46: Leader Satellite Response to Straight-Line Trajectory.

in Chapter 2. In addition, the proportional and derivative controller gains were set to 32 and 8 respectively unless otherwise specified.

3.3.1 Case 1: Straight-Line Maneuvers

3.3.1.1 Matched Follower Satellite Initial Positions

This section discusses the effect input shaping has on the leader-follower formation performing straight-line maneuvers. The desired trajectory for the leader satellite is a straight line as shown in Figure 38. The desired position for the leader satellite is to move from left to right, starting at (0,0) and finishing at (50,50). The desired velocity of the leader satellite is the derivative of the position, and for this particular case, the desired velocity is constant and is equal to 1 $\frac{m}{sec}$.

The response of the leader's main satellite body is shown in Figure 46. As seen from the figure, spatially the leader satellite is able to follow the desired position extremely well, so the PD gains used to control the spacecraft are tuned appropriately. It is important to note that leader satellite started with an initial position that matched the desired trajectory. Since both spatial and temporal tracking are of interest, Figure 47 shows the desired trajectory and system response for the first second. From the figure, it is easy to see that the system responds quickly to the desired trajectory. At the start, the system lags the desired

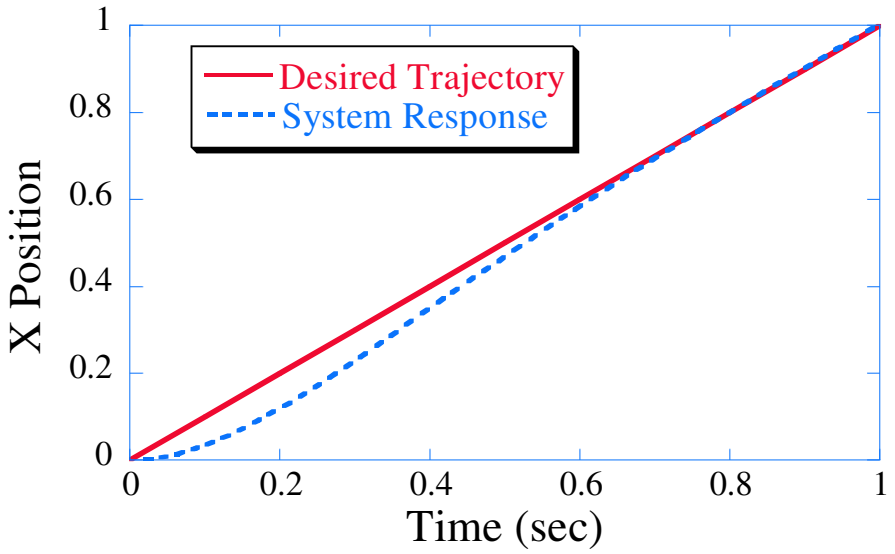

Figure 47: Leader Satellite Response to Straight-Line Trajectory.

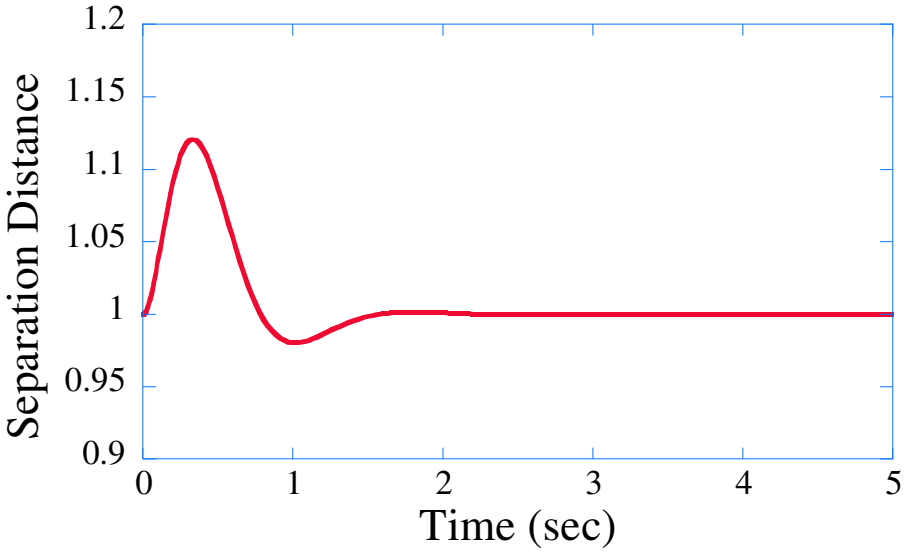

Figure 48: Follower Separation Distance for Straight-Line Maneuver.

trajectory because initially the velocity of the system is zero while the desired velocity is not zero. However, by the first second, the system's response matches the desired trajectory. The response for the y position is identical to that shown in Figure 47.

For this simulation the desired separation distance between the leader and follower was set equal to 1 m. Figure 48 shows the separation distance between the two satellites as a function of time. The separation distance was calculated as follows:

$$\text{Separation Distance} = \sqrt{(x_l - x_f)^2 + (y_l - y_f)^2} \tag{59}$$

where x_l, y_l, x_f, and y_f are the x and y positions of the leader and follower satellite respectively. For this simulation, the leader satellite started one unit away (at the desired separation distance). During the beginning of the maneuver, both the leader and follower satellite start from rest. Initially, the leader satellite is trying to catch up to the desired trajectory and the follower satellite is trying to catch up to the leader satellite and maintain the desired separation distance. As a result, the separation distance between the leader and follower satellite slightly increases. The follower satellite then overshoots the desired separation distance, but quickly settles to the desired value. After approximately 1.5 seconds, the follower satellite is able to maintain the desired separation distance of 1 m.

Although it is important that the follower satellite be able to maintain the desired separation distance, a primary concern is the motion of the flexible appendage, and how input shaping affects the formation response. In order to study this effect, the desired leader trajectory was convolved with both a ZV and ZVD input shaper. The shaped trajectory is then used as the desired trajectory for the leader satellite. The first shaper used was a 1.0 Hz ZV shaper. Figure 49 shows the spring angle responses of the leader satellite to the straight-line maneuver. Clearly the shaped case has superior performance. The input shaping reduces the maximum amplitude of the deflection, and has a shorter settling time. The shaped response settles below 0.05 degrees at 4.64 seconds, compared to the 9.32 second settling time for the unshaped case. Although the input shaped response is significantly better than the unshaped case, it is not perfect. This is due to the nonlinearities in the system as discussed in Chapter 2.

Temporal tracking is important in formation flying, and it is important to investigate how input shaping effects the formation. Input shaping delays the response of the system due to the changes in the desired trajectory. This effect is shown in Figure 50. By examining the response of the systems after $t = 0.5$ seconds, it is clear that the input shaped case is delayed by a fixed amount of time. That is, the input shaped trajectory is 0.25 seconds behind the unshaped trajectory in time. Coincidentally, 0.25 seconds is exactly $\frac{1}{2}$ the 1.0

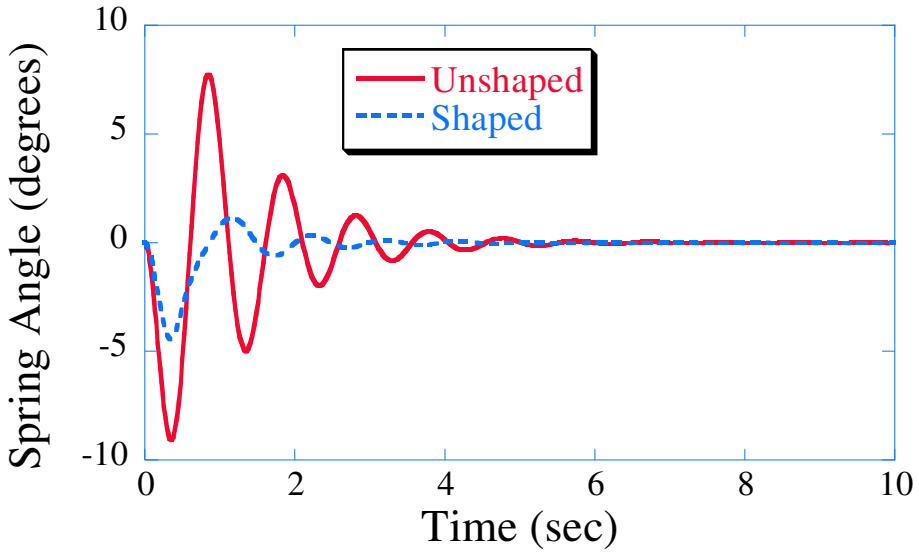

Figure 49: Leader Spring Angle Deflection During a Straight-Line Maneuver.

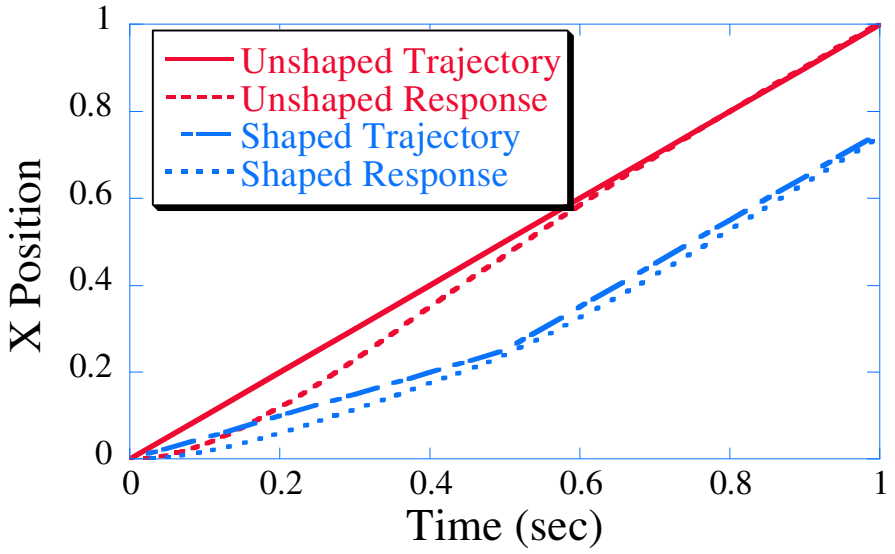

Figure 50: Leader Satellite Response to Unshaped and Shaped Straight-Line Motions.

Hz ZV shaper's duration.

Although suppression of vibration is important for the leader spacecraft, it is equally important for the follower satellite as well. This is especially true if the follower satellite has flexible modes. Unfortunately, the desired trajectory for the follower satellite is not known *a priori* as it is for the leader satellite. Fortunately, the benefits of shaping the leader satellite's desired trajectory can also be seen on the follower satellite. Figure 51 shows the

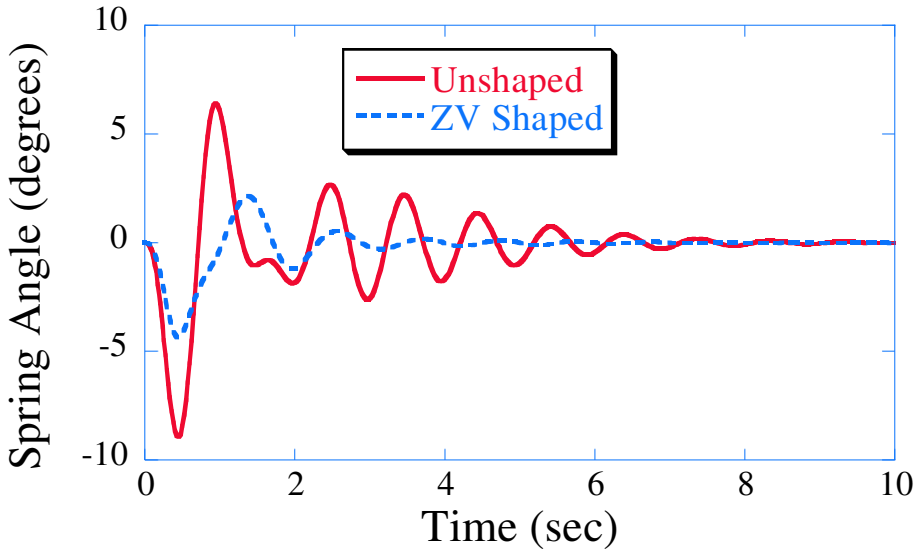

Figure 51: Follower Spring Angle Deflection During a Straight-Line Maneuver.

spring angle response for the follower satellite. As seen from the figure, input shaping the leader satellite's trajectory, reduces the maximum amplitude of residual vibration and the settling time. The time it takes for the follower's response to stay below 0.05 degrees is approximately 3.1 seconds compared to 9.3 seconds for the unshaped case.

Equally as important as reducing the vibration is maintaining the desired separation distance between the two spacecraft in the formation. Figure 52 shows the separation distance when the leader is following the ZV shaped straight-line trajectory. Shaping the leader's desired trajectory significantly decreases the maximum separation distance when compared to the unshaped case. For the unshaped case, the maximum separation distance is approximately 1.13 whereas the separation distance for the shaped case is approximately 1.06. This is approximately a 54% reduction in the maximum separation distance. It can also been seen from Figure 52 that shaping the leader's trajectory broadens the initial overshoot of the separation distance, but decreases the peak. The time it takes for the unshaped and shaped responses to settle to the desired 1m separation distance is essentially the same.

Although there are nonlinearities present in the system model, with a more robust input shaper it is possible to further eliminate the vibration present in the flexible appendage.

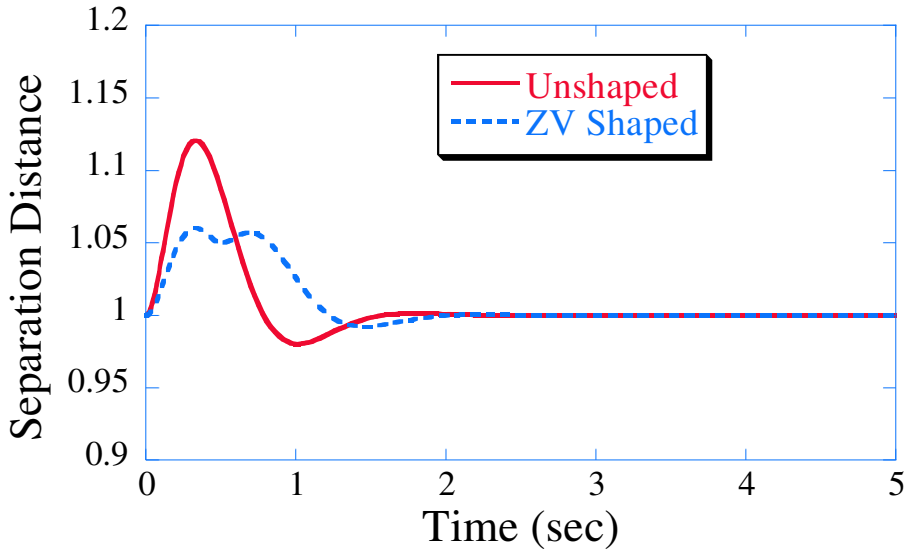

Figure 52: Separation Distance for Shaped Straight-Line Trajectory.

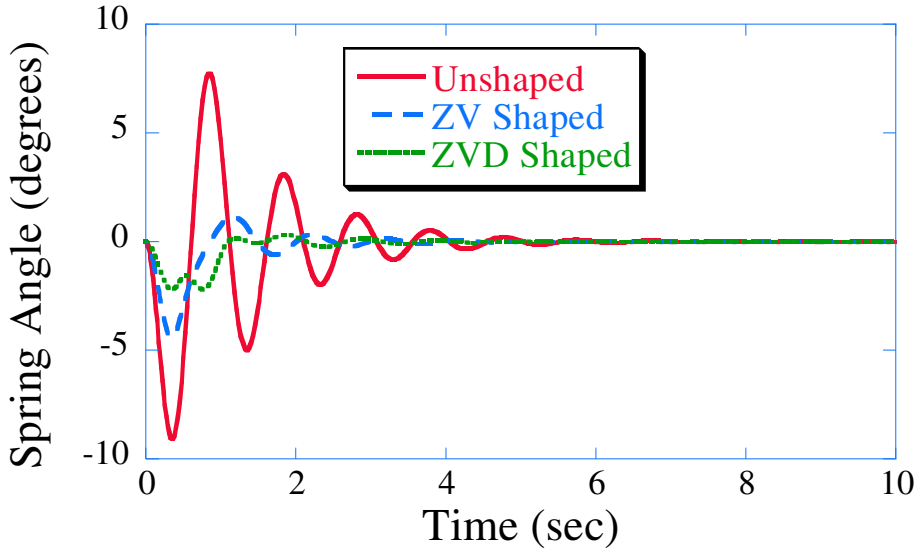

Figure 53: Leader Satellite Spring Angle Deflection for Straight-Line Maneuver.

Figure 53 shows the leader satellite's flexible appendage response to a ZVD shaped trajectory. As seen from the figure, the ZVD shaper further reduces the maximum spring angle deflection by approximately 77%. In addition, the time it takes for the response to remain below a 0.05° spring angle is also reduced. The ZVD shaped response settles below 0.05° after 2.37 seconds, compared to the 9.3 seconds for the unshaped case and 3.1 seconds for the ZV shaped case. Table 10 shows the settling times for the unshaped and shaped

Table 10: Leader Satellite's Flexible Appendage Settling Time.

	0.05° Spring Angle Settling Time
Unshaped	9.3 seconds
ZV Shaped	3.1 seconds
ZVD Shaped	2.4 seconds

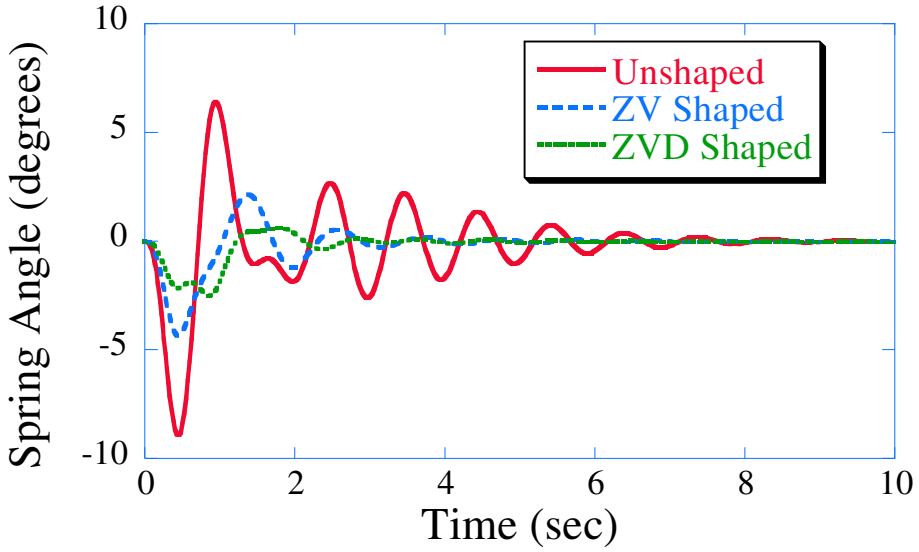

Figure 54: Follower Satellite Flexible Appendage Response for Straight-Line Maneuver.

Table 11: Follower Satellite's Flexible Appendage Settling Time.

	0.05° Spring Angle Settling Time
Unshaped	6.4 seconds
ZV Shaped	6.3 seconds
ZVD Shaped	6.0 seconds

maneuvers.

Figure 54 shows the response of the flexible appendage for the follower satellite. As seen in the figure, input shaping the leader's trajectory also affects the vibration of the flexible appendage on the follower satellite, albeit to a lesser extent. Table 11 compares the settling times for the follower satellite. The ZVD input shaped trajectory reduces the maximum spring angle deflection by approximately 71%. The time it takes for the unshaped vibration to remain below 0.05 degrees is approximately 6.4 seconds. The ZV shaped trajectory takes

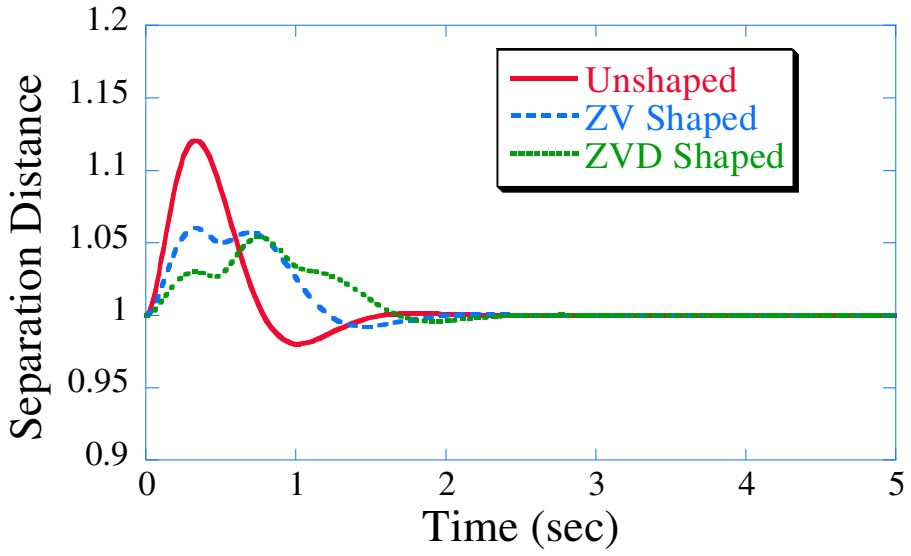

Figure 55: Separation Distance During a Straight-Line Maneuver.

approximately 6.2 seconds and the ZVD trajectory takes approximately 6.0 seconds. So input shaping the leader's trajectory has a lesser effect on the follower satellite concerning the amount of time it takes for the spring angle to remain below a particular value.

Figure 55 shows the separation distance between the two satellites for the unshaped, ZV and ZVD shaped cases. As seen from the figure, using the ZVD shaper significantly reduces the maximum separation distance compared to the unshaped case. The effect of broadening the peak can also be seen. Although the ZVD maximum amplitude is approximately equal to the ZV maximum amplitude, using the ZVD shaper provides additional robustness to modeling errors and nonlinearities present in the system.

The previous discussion focused on the case where both the leader and follower satellites' initial positions matched the desired conditions for the maneuver. However, many times in real operation, this will not be the case. Therefore, it is important to investigate what effect input shaping has on cases where the initial positions of the satellites do not match the desired initial positions. The next section investigates these effects.

3.3.1.2 Unmatched Follower Satellite Initial Positions

Figure 56 shows the responses of the main satellite bodies during the first few seconds of the desired trajectory. Notice that while the leader satellite starts at the desired initial

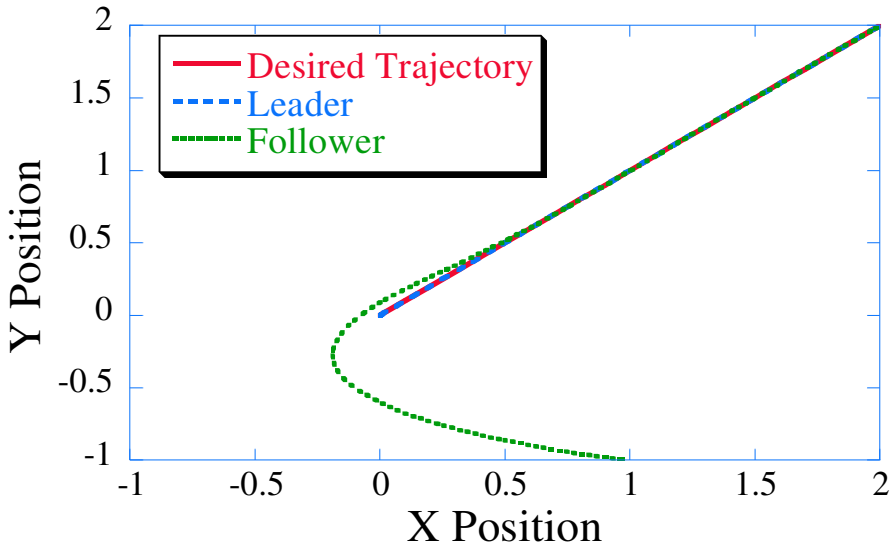

Figure 56: Formation Response to Unmatched Initial Conditions.

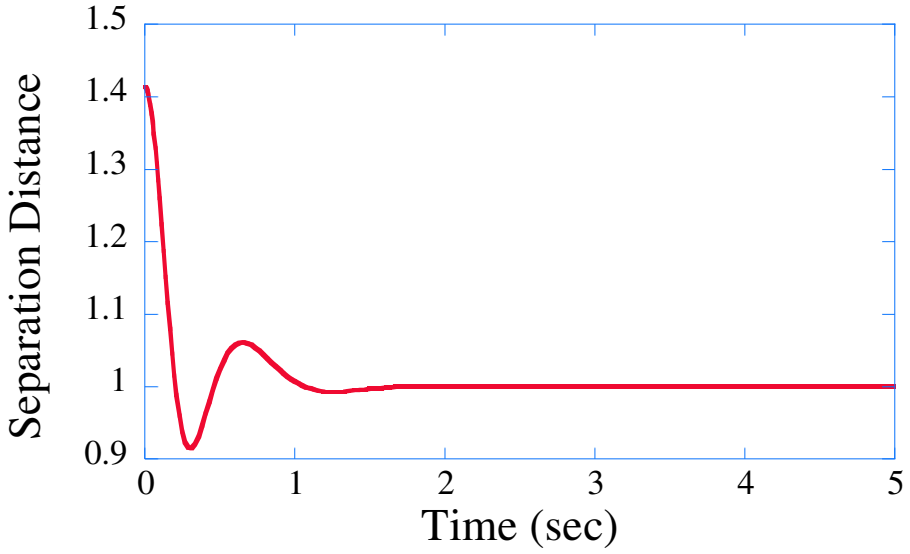

Figure 57: Separation Distance for Unmatched Straight-Line Maneuver.

conditions of (0,0), the follower satellite starts at a (-1,1) instead of the desired coordinates of (-.707,-.707). So at first, the follower satellite does not satisfy the desired separation distance of 1 m as shown in Figure 57. However, the follower satellite quickly converges onto the desired trajectory and follows the leader satellite. As seen from the figure, the initial separation distance is approximately 1.4 m, but after 2 seconds the separation distance remains very close to the desired separation distance of 1 m.

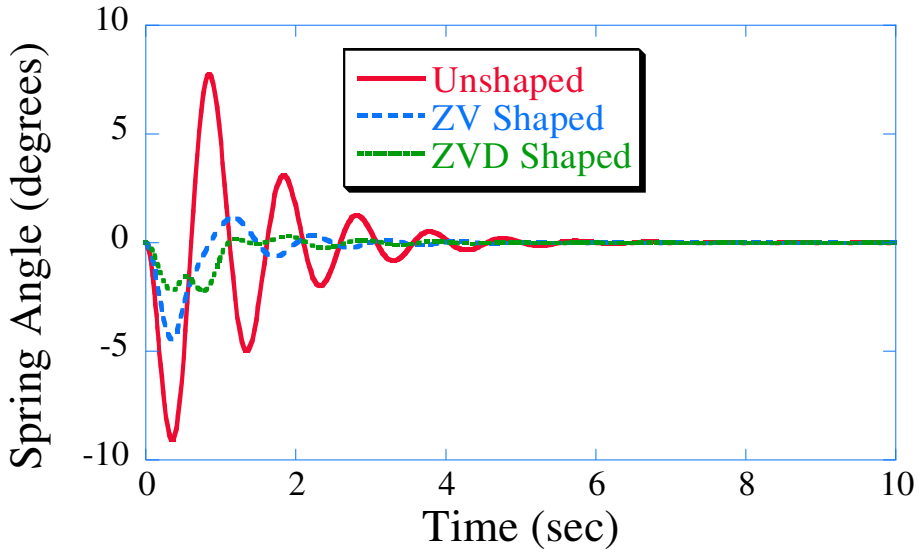

Figure 58: Leader Satellite Spring Angle Response for Unmatched Straight-Line Maneuver.

As with the previous simulation, both ZV and ZVD input shapers were convolved with the leader satellite's desired trajectory. Figure 58 shows the response of leader's flexible appendage to the different trajectories. As expected, both the ZV and ZVD shaped trajectories significantly reduce the maximum spring angle deflection of the leader satellite. The ZVD response has the smallest maximum deflection with a 77% reduction when compared to the unshaped case.

For the matched initial position case, the follower satellite was able to receive the benefits of input shaping by simply following along behind the leader satellite. For the unmatched case, it may still be possible for the follower satellite to have some vibration suppression. Figure 59 shows the spring angle response for the follower satellite. The effect of input shaping the leader satellite's desired trajectory can still be seen in the response of the follower satellite. However, the reduction in the vibration of the follower satellite is not as pronounced as it was in the matched initial position case. The smaller reduction in vibration suppression directly results from the mismatch in initial position of the follower satellite. At the beginning of the maneuver, the separation error between the two satellites is large, and the feedback controller demands a high control effort in order to reduce the distance. However, because the leader's desired trajectory is shaped, there is a slight difference in

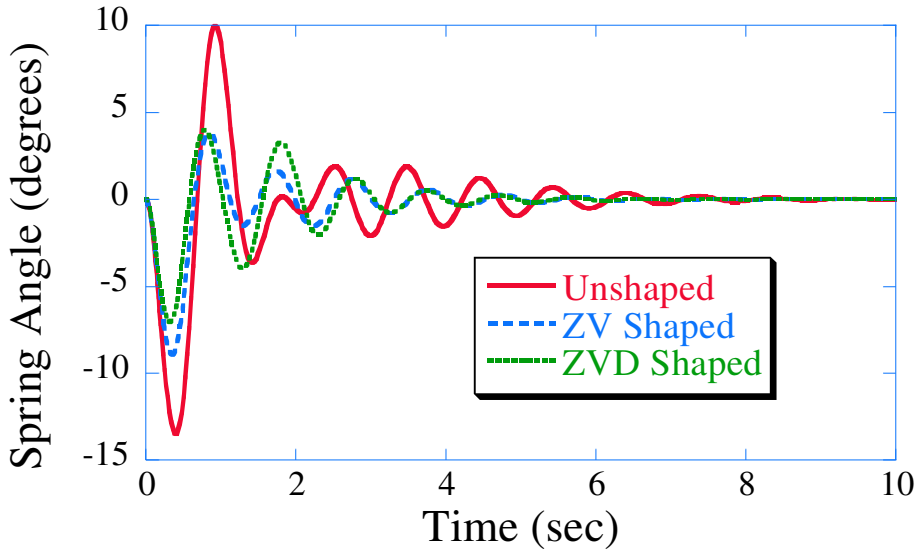

Figure 59: Follower Spring Angle Response for Unmatched Straight-Line Maneuver.

Table 12: Maximum Spring Angle Deflection.

	Maximum Spring Angle
Unshaped	13.4°
ZV Shaped	8.9°
ZVD Shaped	6.9°

the desired separation error for the unshaped and shaped cases. This results in the smaller amount of vibration seen in the follower satellite. The main benefits of input shaping can be seen in the reduction of the maximum spring angle deflection and the decreased settling time. Table 12 compares the maximum spring angle deflections. For the unshaped case, the maximum spring angle deflection is approximately 13.4°. The ZV shaped case's maximum spring angle is approximately 8.9°, and the ZVD's maximum spring angle is 6.9° which is almost a 50% reduction compared to the unshaped case.

In order to determine how the follower satellite's position influences the benefits it receives from the leader satellite's input shaping, a large array of simulations was performed In these simulations, the position of the follower satellite is displaced from the desired initial position. Its position is located on a series of concentric circles whose center is located at the desired initial position as shown in Figure 60. The radius of the circle r equals the *Distance*

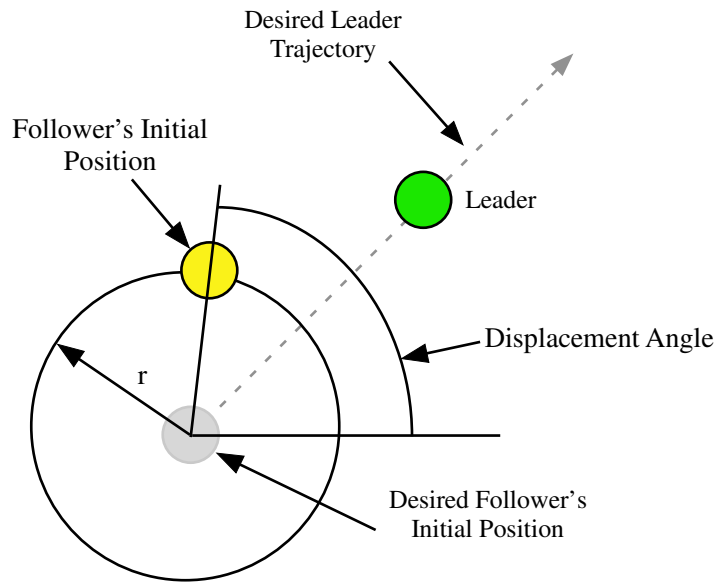

Figure 60: Initial Location of Follower Satellite.

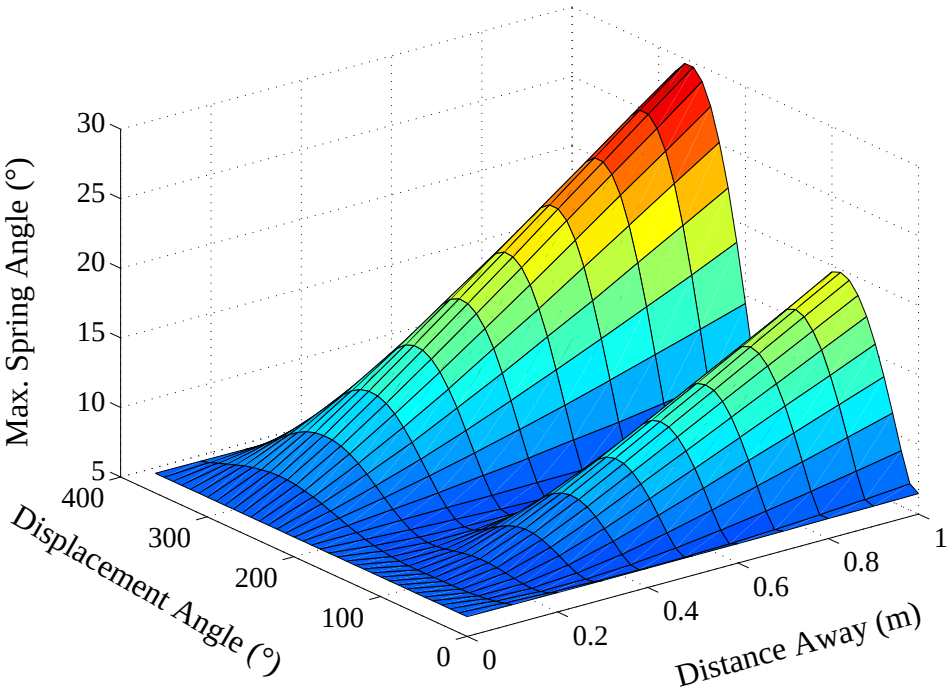

Figure 61: Follower's Maximum Spring Angle for Different Starting Positions.

Away from the desired starting location and varies from 0 to 1.0 m. The *Displacement Angle* varies from 0° to 360°. The same desired shaped leader trajectory was used for each case. Figure 61 shows the maximum deflection angle for the unshaped cases. As the

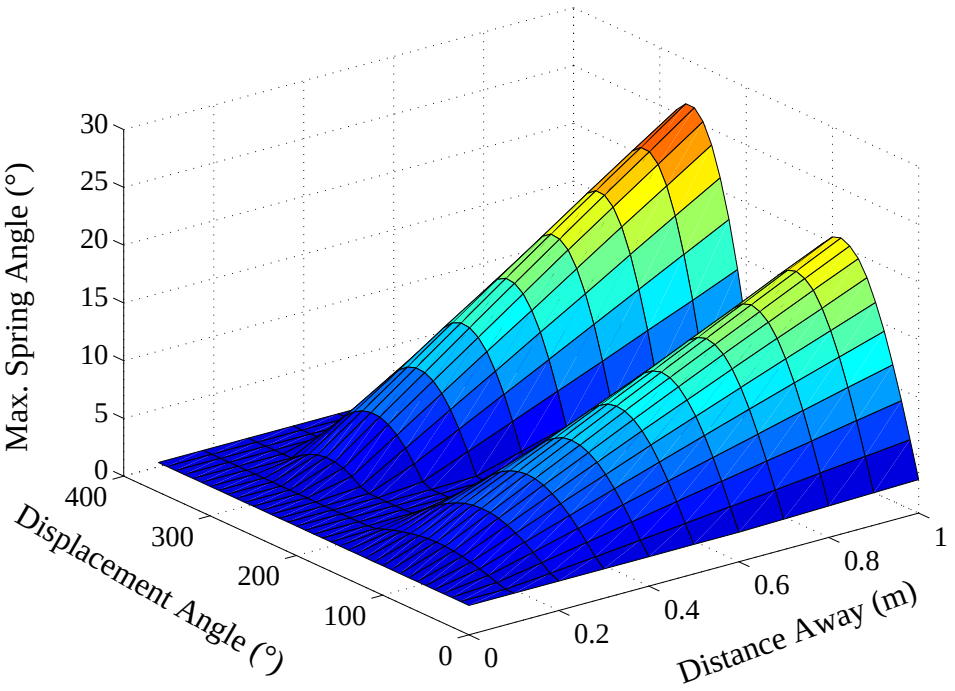

Figure 62: Follower's Maximum Spring Angle for Different Starting Locations and ZV Shaping.

distance away from the desired initial starting position increases, the maximum spring angle in the flexible appendage increases. This makes sense because the farther the satellite is away from the desired position, the greater the error seen by the feedback controller, and consequently, the greater the control force. Notice that the maximum spring angle has two humps. As the displacement angle increases above 180°, the follower satellite starts farther away from the desired initial position. Consequently once the system begins to move, the follower satellite has a larger error and an increased control effort. This results in the larger hump in the graph. When the displacement angle is $< 180°$, the follower satellite begins closer to the leader satellite.

The same array of simulations was carried out for both the ZV and ZVD shaped trajectories. Figure 62 shows the response to the ZV shaped trajectory. Notice that the maximum spring angle deflection is smaller when compared against the same unshaped starting position. For the maximum starting distance away from the desired position and for a large

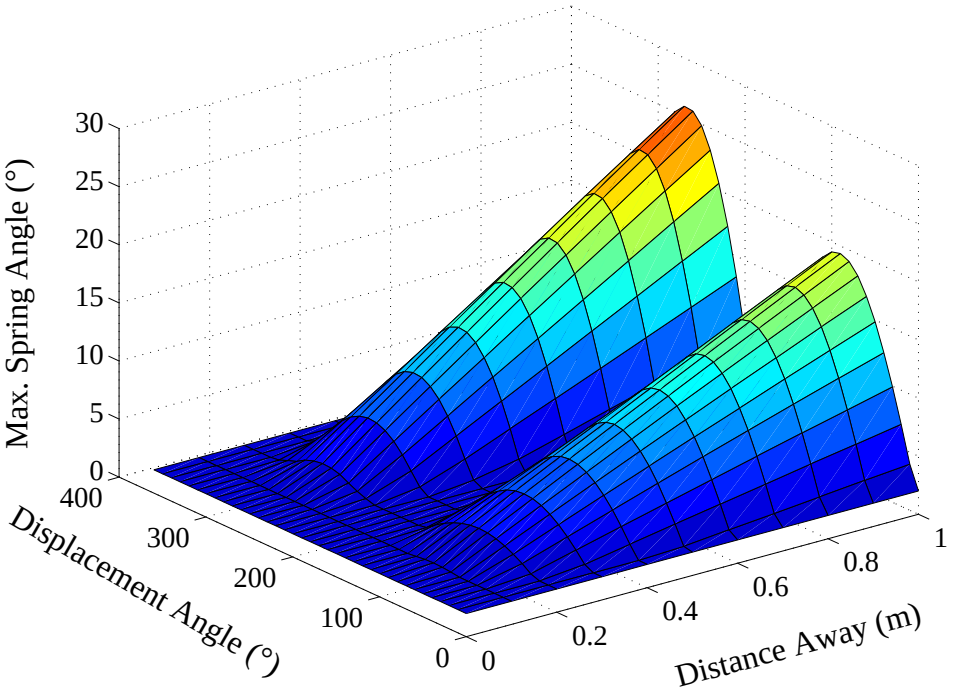

Figure 63: Follower's Max. Spring Angle for Different Starting Locations and ZVD Shaping.

displacement angle, the ZV input shaping reduces the maximum spring angle by approximately 5°. Notice that the ZV response also has two humps corresponding to the location of the follower satellite. However, both of the humps have decreased amplitudes.

Figure 63 shows the follower's maximum spring angle for the ZVD shaped trajectory. Similar to the ZV case, the ZVD cases further reduce the maximum spring angle. In fact, the ZVD shaping has the effect of lowering the entire graph. Input shaping the leader's desired trajectory can still create vibration reduction in the follower satellite. However, the extent of the vibration reduction depends on the starting position and the orientation of the follower satellite. Using a more robust input shaper helps increase the beneficial effects of the input shaping. However, as the difference between the follower's initial and desired position increases, the vibration reduction provided by shaping the leader's trajectory decreases. This is because the follower does not follow an appropriately shaped trajectory.

Input shaping the leader's desired trajectory has the effect of delaying the position of the leader. This effect is demonstrated in Figure 64. Once the duration of the input shaper

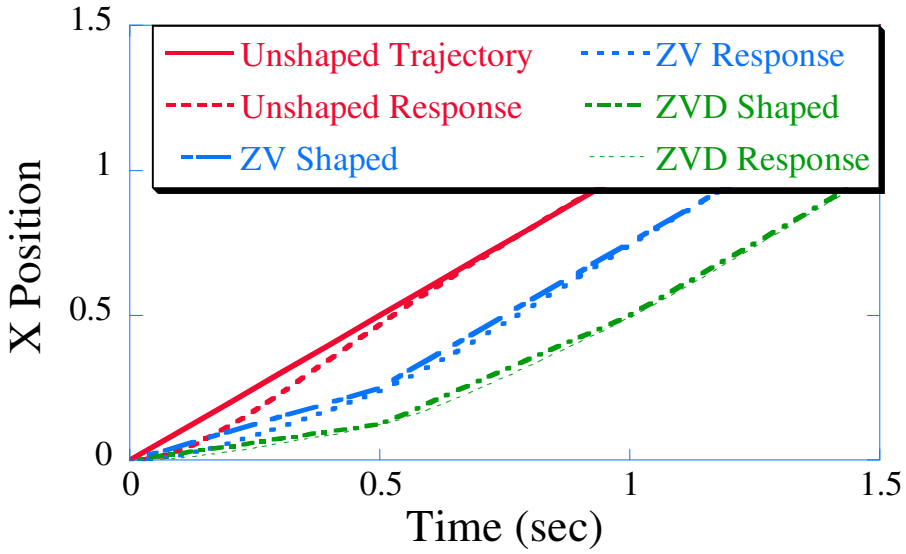

Figure 64: Initial Trajectory and Response for Straight-Line Maneuvers.

is finished, the delay of the trajectory is constant with respect to time. For the ZV shaped trajectory, after 0.5 seconds, the delay in the trajectory is 0.25 seconds which corresponds to one-half the duration of the ZV shaper. The duration of the ZVD shaper is 1.0 seconds and after 1.0 seconds, the delay in the trajectory is 0.5 seconds. This also corresponds to exactly one-half the duration of the ZVD shaper. If it desired that the leader satellite be at a precise position with respect to time, then the input shaped cases must be started early. For example, suppose it is desired that the leader satellite reach a desired position of $x = 2$ at 1 pm, the unshaped system should start moving exactly 2 seconds before 1 pm. However, the ZV shaped system must start moving exactly 2.25 seconds before 1 pm, and the ZVD shaped system must start moving 2.5 seconds before 1 pm. Provided this can be accomplished, then all three systems would reach the desired setpoint at the same time and will reach every other point along the trajectory at the same time. This is true for any point along the trajectory after the duration of the shaper has passed. For the 1.0 Hz ZV shaper this is 0.5 seconds, and for the 1.0 Hz ZVD shaper this corresponds to 1.0 seconds

3.3.1.3 Case 1: Straight-Line Motion Summary

Input shaping the leader satellite's trajectory has beneficial vibration reduction effects that are seen on both the leader satellite and the follower satellite for straight-line maneuvers.

The vibration of both satellites can be reduced by simply shaping the leader satellite's trajectory. In addition to vibration reduction of the main satellite body, the vibration of the flexible appendages is also reduced. Input shaping drastically reduces the maximum deflection for all the maneuvers. The settling time for the flexible appendages is also reduced.

The effects on the follower satellite are dependent on the follower's initial position relative to its desired initial position. For spatial tracking, input shaping tends to improve the desired separation distance between the two satellites. It has the effect of decreasing the maximum separation distance without significantly increasing the time it takes to settle to the desired separation distance. Temporally, input shaping delays the position of the satellites. However, this effect can be negated by starting the input shaped motions before the unshaped motions. After some time, the positions of the trajectories will be identical. The next section discuses the effect of input shaping on *Same-Orbit* maneuvers.

3.3.2 Case 2: Same-Orbit Maneuvers

This section discusses the effect input shaping has on both the spatial and temporal tracking for two satellites undergoing the same-orbit maneuvers shown in Figure 39. Figure 65 shows the desired trajectory and the main satellite body responses of the leader and follower satellites. For this maneuver, the leader satellite starts off at (1, 0) and the follower satellite starts at (0.5, -0.866). Both satellites travel in a counterclockwise direction along the desired trajectory.

Because the radius of the desired trajectory is also 1 m, this corresponds to the follower being 60° behind leader satellite relative to the orbit. Figure 66 shows the separation distance between the two satellites as a function of time. Although the satellites start at the desired separation distance of 1 m, throughout the maneuver, the satellites converge to a slightly higher separation distance of approximately 1.08 m. The discrepancy between the desired separation distance and the actual separation distance results directly from the PD gains of 32 and 8 used in the feedback controller. If the proportional gain is increased to 250 and the derivative gain is increased to 40, the separation distance converges to

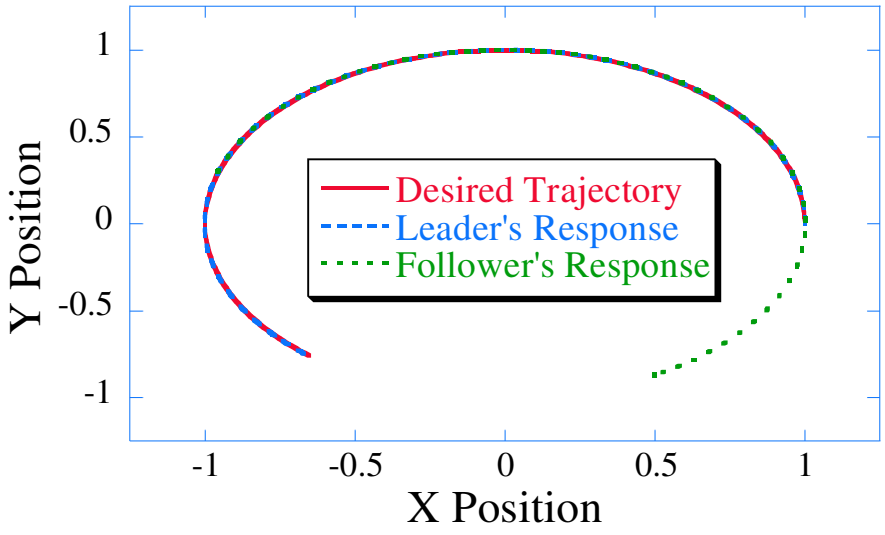

Figure 65: Formation Response to Same-Orbit Desired Trajectory.

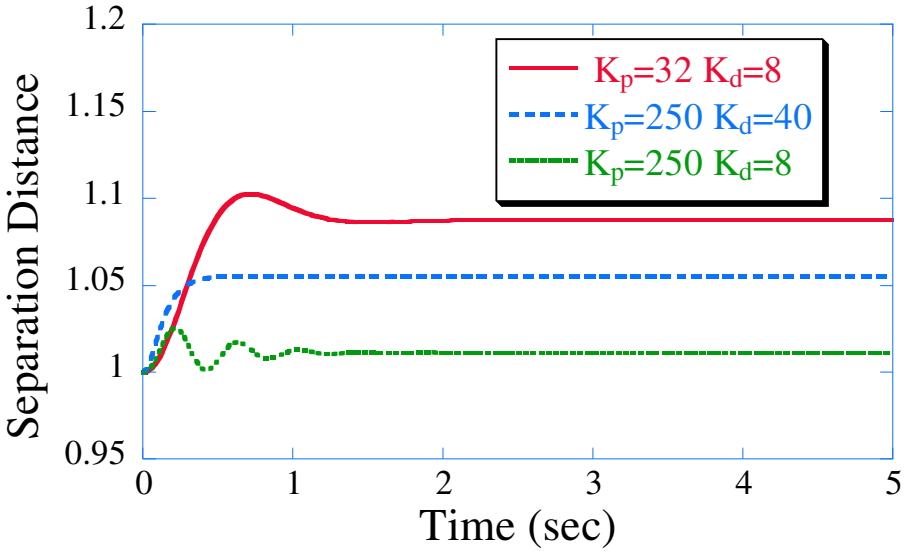

Figure 66: Same-Orbit Separation Distance.

approximately 1.05. If the proportional gain is increased from 32 to 250, but the derivative gain is kept constant at 8 then the separation distance decreases to approximately 1.01. So, for same-orbit maneuvers, increasing the proportional gain yields better separation distance convergence

Increasing the proportional gain does not come without a price. As the proportional gain increases, the vibration seen in the flexible appendage also increases. This effect is

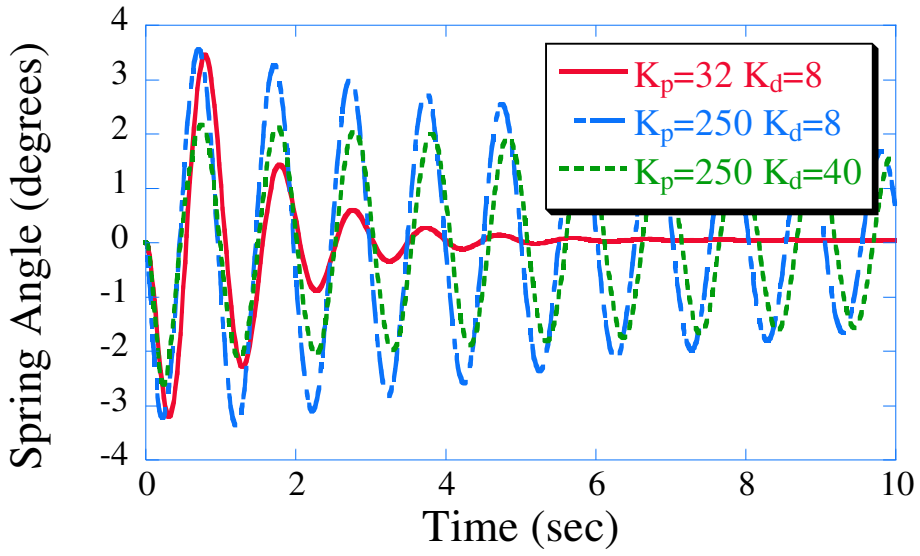

Figure 67: Spring Angle Response for Same-Orbit Maneuver.

shown in Figure 67. The two goals for the maneuver are to keep the vibration in the flexible appendage at a minimum while trying to maintain the desired separation distance; therefore the PD controller with gains of 32 and 8 respectively is the better choice. Although this controller has the largest separation distance, it has the best vibration characteristics.

Although the PD gains of 32 and 8 provide the unshaped case with the best vibration characteristics, it is possible to further reduce the spring angle vibration by using the ZV and ZVD shapers. The leader satellite's desired trajectory is convolved with the desired input shaper. Figure 68 shows the leader satellite's spring angle response for the unshaped, ZV and ZVD shaped cases. As expected, the unshaped case has the largest spring angle deflection. Both the ZV and ZVD shaped maneuvers reduce the maximum spring angle significantly. The ZV shaper reduces the maximum approximately 54% while the ZVD shaper reduces the maximum spring angle deflection approximately 77%. So if maintaining the separation distance is the top priority, then the PD gains should be increased until the desired separation distance is reached.

It was expected that applying input shaping to the leader's trajectory would generate vibration reduction for both satellites. Figure 69 shows the follower satellite's spring angle response. From this figure, it is possible to see the benefit of input shaping. The vibration

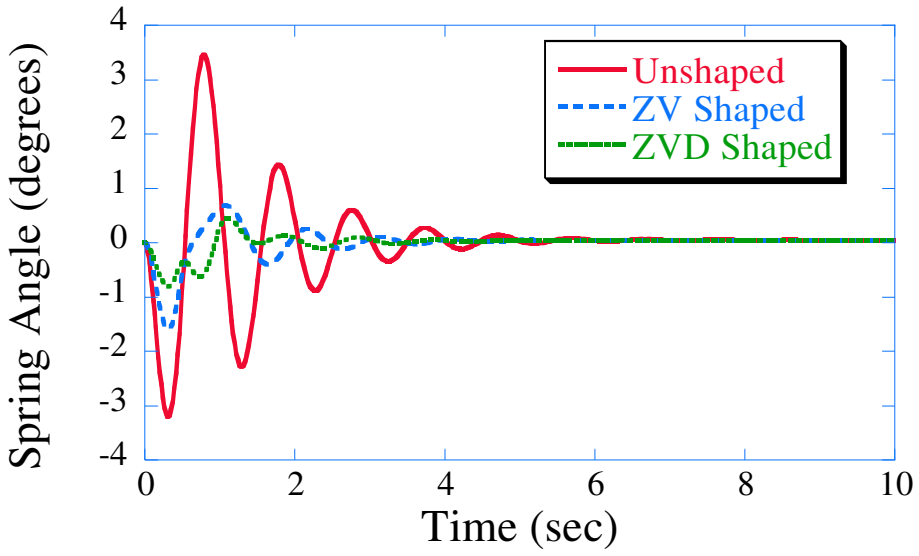

Figure 68: Leader Satellite's Spring Angle Response for Shaped Same-Orbit Maneuvers.

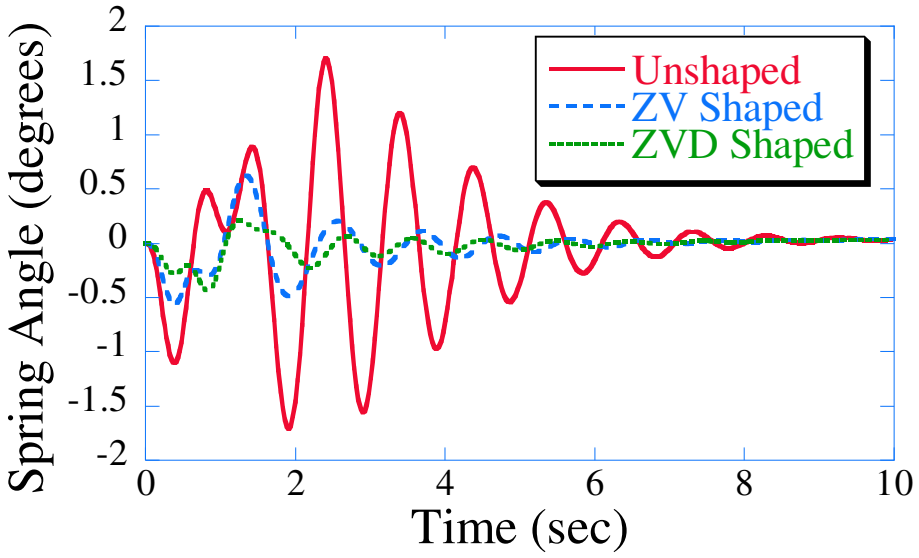

Figure 69: Follower Satellite's Spring Angle Response for Shaped Same-Orbit Maneuvers.

present in the follower satellite's spring angle is significantly reduced. Compared to the unshaped case, the ZV shaped case has a 63% vibration reduction. The ZVD shaped case as approximately 75% reduction in the vibration. As expected, both the satellites have excellent vibration suppression in the spring angle when utilizing input shaping. Both shapers provide over a 50% reduction of vibration.

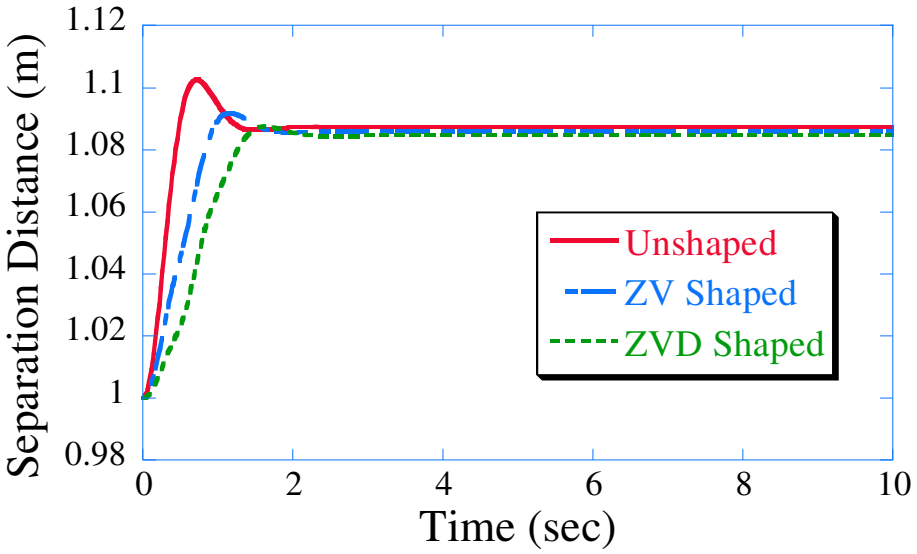

Figure 70: Separation Distance for Shaped Same-Orbit Maneuvers.

As stated earlier, one of the main goals of formation flying is to maintain desired separation distances between the satellites in the group. Figure 70 shows the effect input shaping the leader's trajectory has on the separation distance. Input shaping is not able to reduce the overall separation error. This is because the separation distance error is dominated by the controller gains. However, input shaping is able to decrease the overshoot of the error. This comes from the shape of the trajectory itself. Although input shaping does not have a direct effect on the separation error for the system, it does have a direct impact on the shape of the trajectory. As discussed in Section 2.3.4, input shaping circular trajectories reduces the effective radius of the trajectory, but it is possible to eliminate this effect by pre-modifying the command.

For the simulation discussed above, the follower satellite was approximately 60° behind the leader satellite on the same orbit. There maybe times when the follower satellite is actually ahead of the leader satellite in the orbit. Such is the simulation discussed below. For this simulation, the follower satellite is 60° ahead of the leader satellite. For this scenario, the leader satellite is "pushing" the follower satellite instead of "pulling" it.

Figure 71 shows the follower satellite's spring angle deflection. Comparing Figure 69 and Figure 71, the effect of input shaping on the vibration reduction is extremely similar;

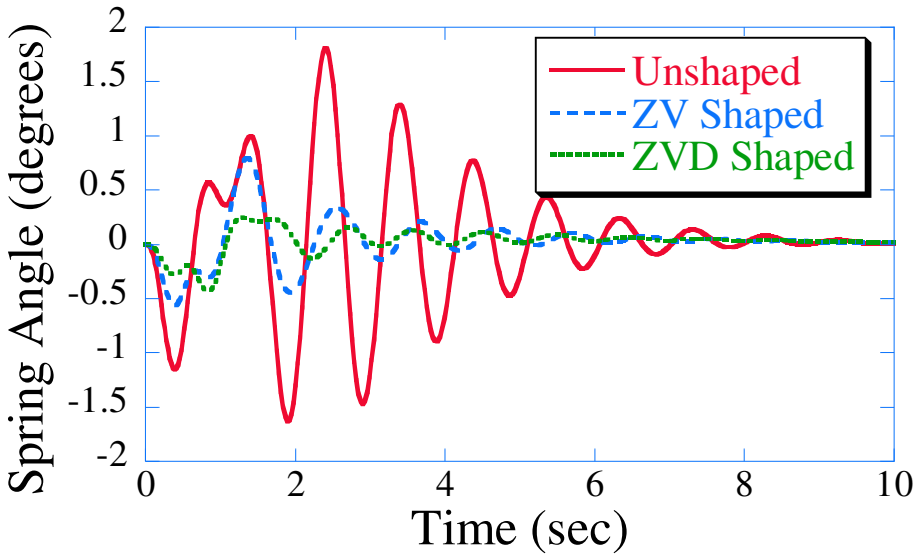

Figure 71: Follower Satellite's Spring Angle Response for Pushing-Same-Orbit Maneuver.

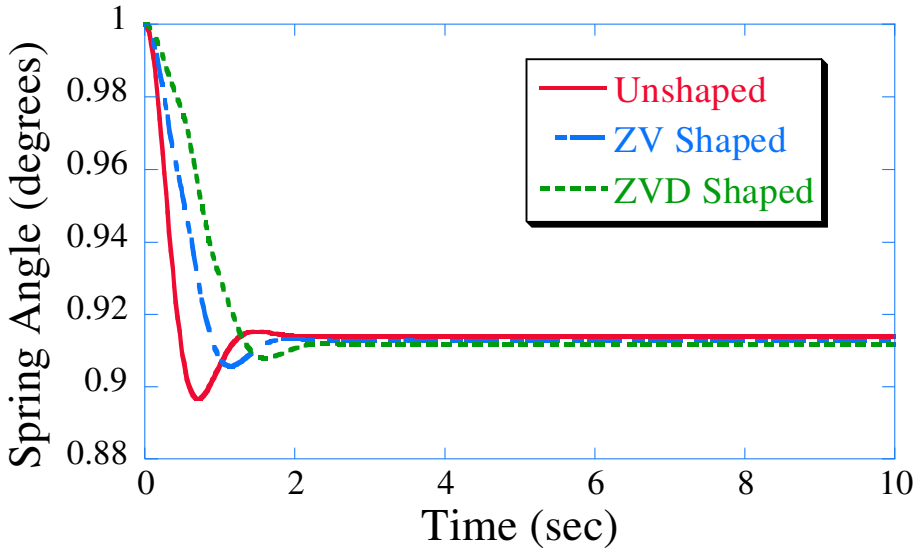

Figure 72: Separation Distance for Shaped Pushing-Same Orbit Maneuver.

therefore the vibration reduction seen by the follower satellite is independent of its placement. Whether the follower satellite is being "pulled" or "pushed", it still sees vibration benefits from the leader satellite's shaped trajectory. Figure 72 shows the separation distance for the "pushing" case. Comparing Figure 70 and Figure 72 the separation distances are symmetric around the desired separation distance of 1 m. The only difference between the figures is that for the "pulling" case, the separation distance is greater than the desired

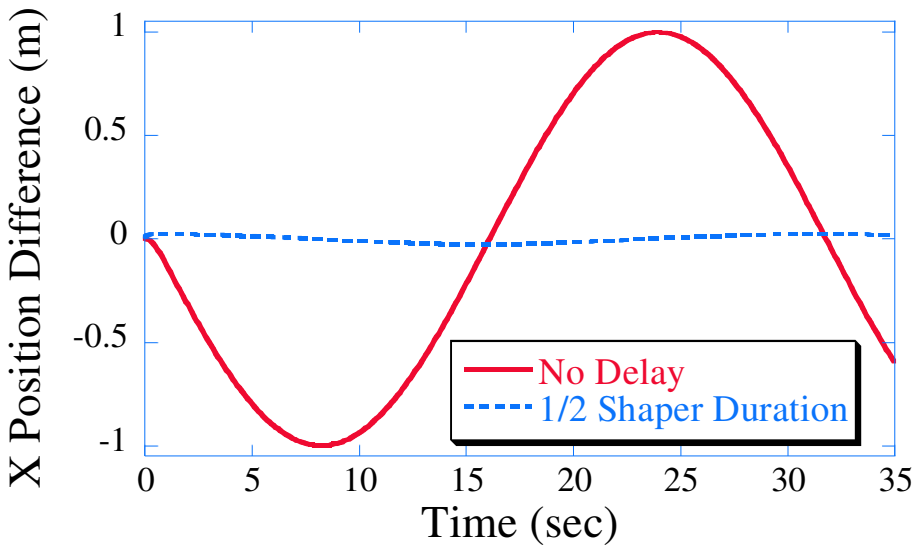

Figure 73: X Position Difference for Unshaped and ZVD Shaped Desired Trajectories.

value. For the "pushing" case, the separation distance is smaller than the desired value. However, the amount the separation distances deviate from the desired value is the same (approximately 0.8m for both).

As with the straight-line trajectories, the same-orbit trajectories are delayed in time. The delay time is related to the duration of the input shaper used to generate the trajectories. For circular trajectories, the amount of the delay needed is not exactly equal to $\frac{1}{2}$ the shapers duration, although that is a good approximation of the delay time. Figure 73 shows the position difference with respect to time for the unshaped and ZVD shaped trajectory. If there is no time delay between the starting of the unshaped and the ZVD shaped trajectories, then the position difference varies sinusoidally. However, if the difference in the starting times is equal to $\frac{1}{2}$ the shaper duration (0.5 seconds for ZVD shaper), then the position differences between the unshaped and ZVD shaped cases is significantly smaller. The same holds for the position differences in the y direction as shown in Figure 74. Therefore, for any circular trajectory, the temporal tracking differences between the unshaped and shaped trajectories can be lessened by starting the shaped trajectories earlier than the unshaped trajectories. The time that the shaped cases must be started earlier is $\frac{1}{2}$ the shaper's duration.

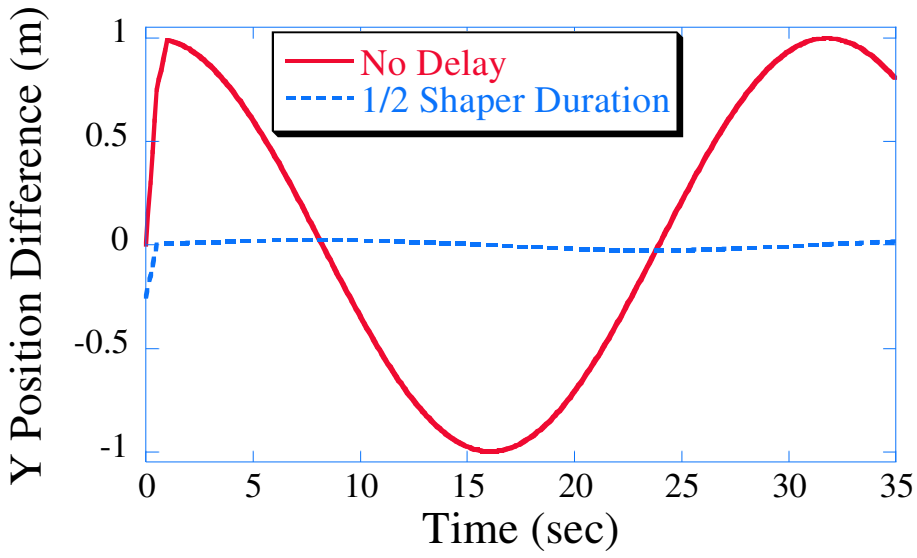

Figure 74: Y Position Difference for Unshaped and ZVD Shaped Desired Trajectories.

3.3.3 Case 3: Synchronized Orbit Maneuvers

The next simulations discussed are the synchronized orbit maneuvers shown in Figure 41. For these simulations the follower satellite is radially outward or radially inward from the leader satellite at the desired separation distance. Unlike the previous cases, the follower's velocity for this case cannot be equal to the leader's velocity. If the velocities matched, then the follower would not be in a synchronous orbit. Figure 75 shows the desired trajectories and the responses of both satellites. For this case, the leader satellite starts at a location of (1,0) and the follower satellite starts at (2,0). The leader satellite moves along the desired trajectory in a counterclockwise direction. For this particular simulation, it was desired that the separation distance be equal to 1 m pointing radially outward.

Figure 76 shows the spring angle response for the leader satellite. Shaping the desired trajectory significantly reduces the vibration in the spring angle. The ZV shaper reduces the vibration 54% compared to the unshaped case. The ZVD shaper reduces the vibration 77% compared to the unshaped response. Figure 77 shows the spring angle responses for the follower satellite. The ZV shaped case reduces the follower's maximum spring angle deflection approximately 50%, whereas the ZVD shaped case reduces the spring angle 72%. Also present in both Figures 76 and 77, is a low vibration mode. This vibration mode

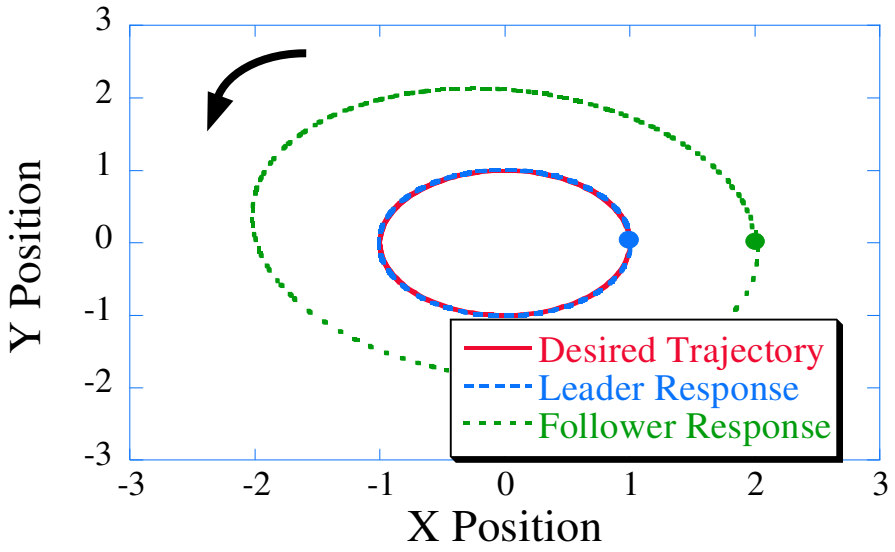

Figure 75: Formation Response to Synchronized Orbit Maneuvers.

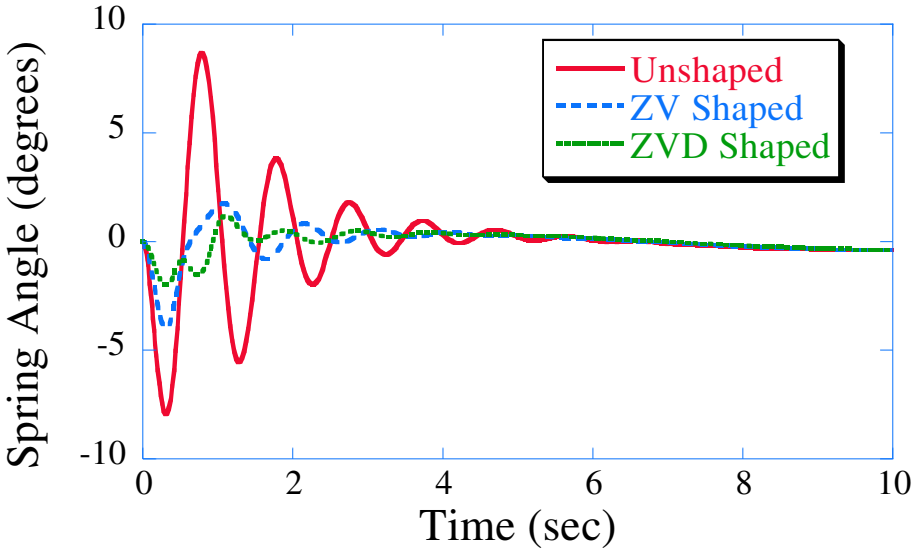

Figure 76: Spring Angle Response for Synchronized Orbit Maneuvers.

results from the circular trajectory. For this case, the frequency of the circular trajectory is equal to 0.5 $\frac{rad}{sec}$.

Figure 78 shows the separation distance between the two satellites as a function of time. The separation distance oscillates about the desired separation distance of 1 m for all cases. For the case where the natural frequency of the desired trajectory, ω, is equal to $4\frac{rads}{sec}$, input shaping does not significantly affect the separation distance. In fact, the only effect

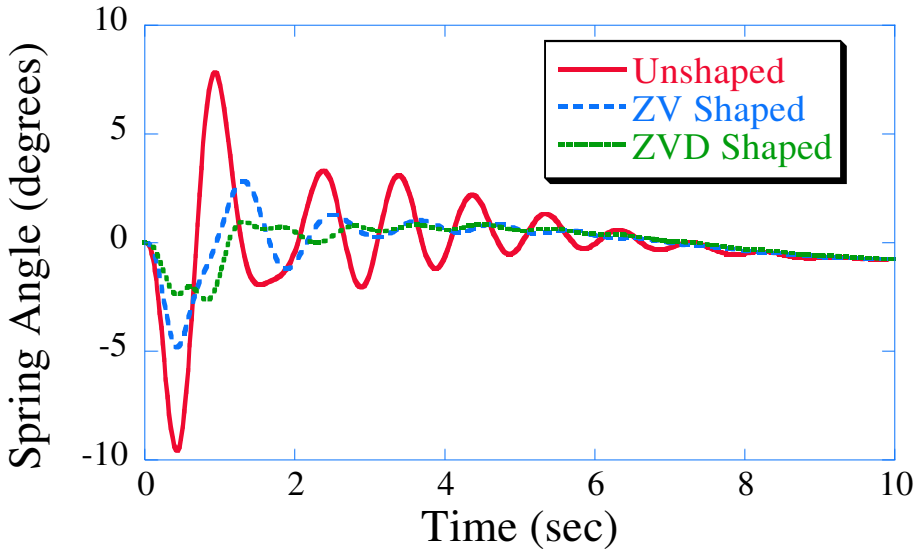

Figure 77: Follower Satellite's Spring Angle Response for Synchronized Orbit.

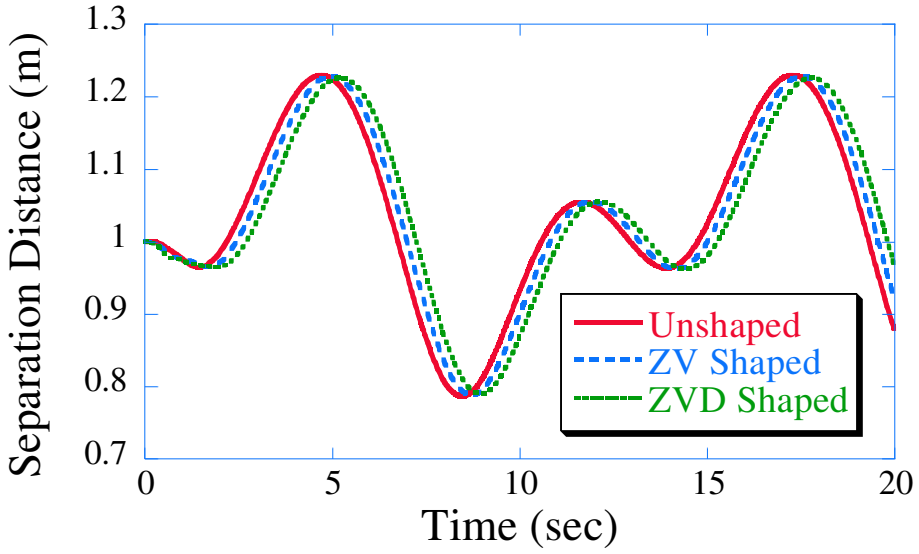

Figure 78: Separation Distance for Synchronized Maneuver for $\omega = 4\frac{rads}{sec}$.

input shaping has is to delay the oscillations slightly.

Figure 79 shows the separation distance when the desired trajectory has a natural frequency of 0.2 $\frac{rads}{sec}$. Comparing Figures 78 and 79 it is clear to see that the frequency of the circular trajectory directly affects the separation distance. The separation distance between the satellites is much smaller for the trajectory with the lower frequency. For the lower trajectory frequencies ($\omega < 0.8\frac{rads}{sec}$) the unshaped and shaped cases have almost

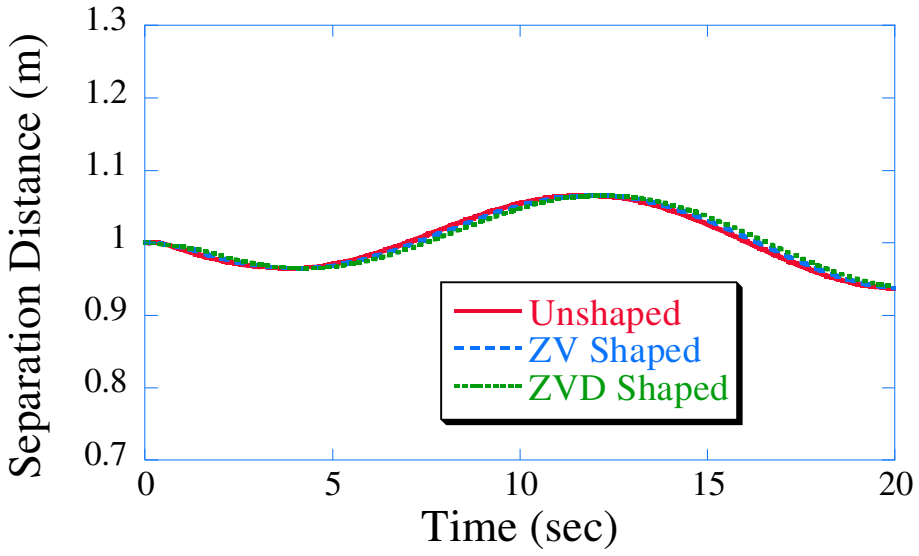

Figure 79: Separation Distance for Synchronized Maneuver for $\omega = 0.2\frac{rads}{sec}$.

identical maximum separation distances. This effect was shown in Figure 78 and Figure 79. However, as the trajectory frequency increases, the maximum separation error for the unshaped case increases rapidly. The ZV and ZVD shaped responses are almost 75% less than the unshaped cases even for very high frequencies. As expected, the ZVD shaped trajectory has the lowest maximum separation distance.

As the radius of the desired trajectory increases, for a constant trajectory frequency, ω, the K_p and K_d gains must increase. This is because of the assumed linear relationship between velocity, frequency, and radius, for circular travel. For large radii, the low controller gains are unable to keep up with the desired trajectory. However, if the gains are matched according to the radius and the trajectory's frequency, the shaped trajectories will yield smaller maximum separation distances and superior vibration reduction.

3.3.4 Case 4: Tangential Pursuit Maneuvers

The next class of maneuvers studied are the tangential pursuit maneuvers shown in Figure 43. For these maneuvers, the trailing satellite always tries to remain parallel to the leader satellite's velocity. The desired trajectory and responses for both satellites is shown in Figure 80. For this case, the leader satellite starts at (1, 0) and the follower satellite starts at (1,-1). The leader satellite travels counterclockwise around the desired trajectory. The

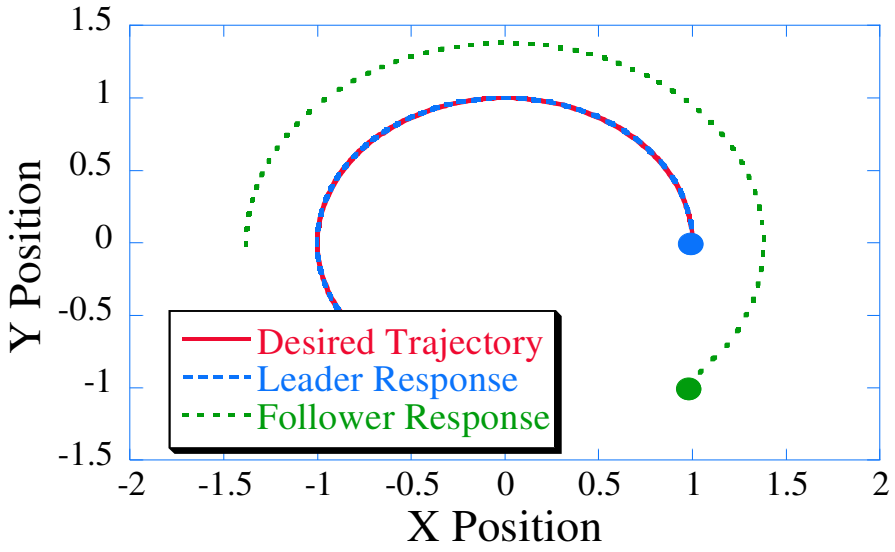

Figure 80: Formation Response to Tangential Pursuit Maneuver.

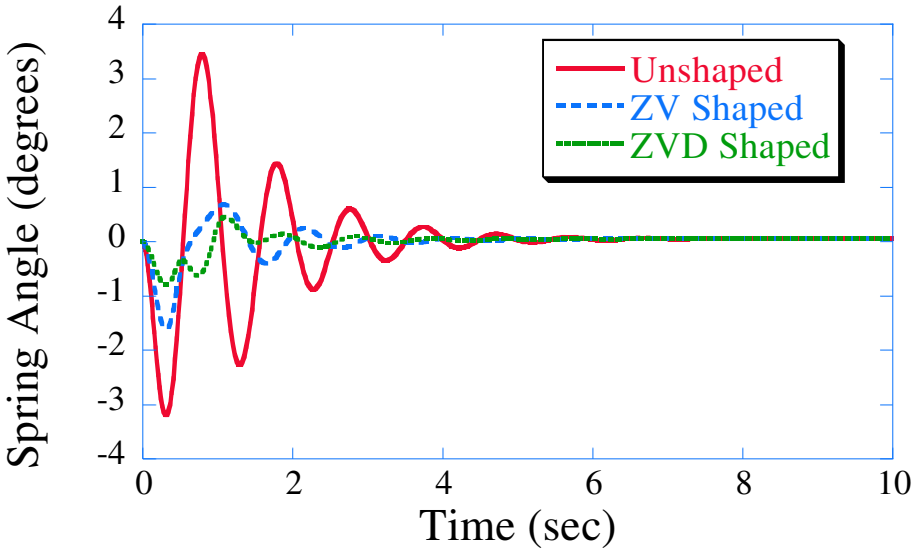

Figure 81: Leader Satellite's Spring Angle Response for Tangential Pursuit Maneuver.

desired separation distance between the leader and follower satellites is 1 m.

Figure 81 shows the leader satellite's spring angle response for the unshaped and shaped cases. As expected, the shaped trajectories provide excellent vibration reduction for the leader satellite's spring angle. Figure 82 shows the follower satellite's spring angle response. The ZV shaped trajectory reduces the follower satellite's maximum spring angle approximately 50% compared to the unshaped chase. The ZVD shaped trajectory reduces the

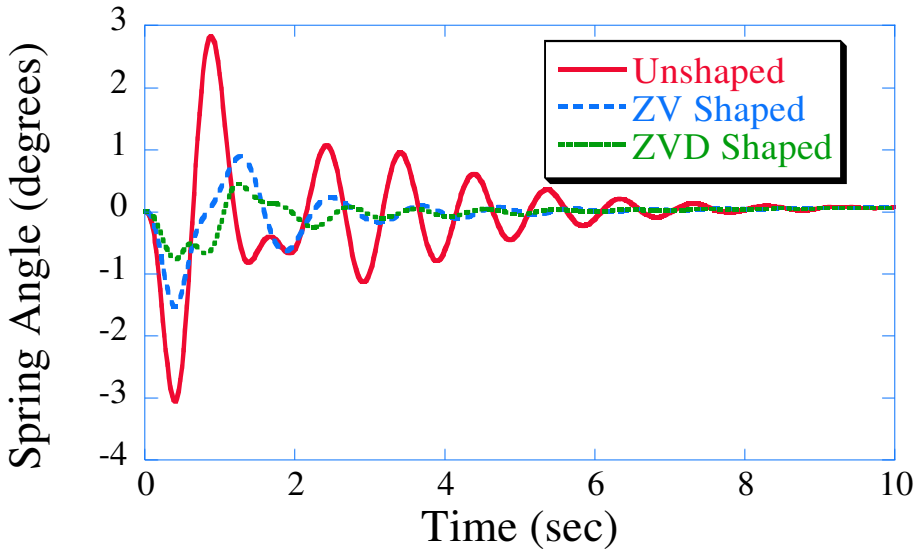

Figure 82: Follower Satellite's Spring Angle Response for Tangential Pursuit Maneuver.

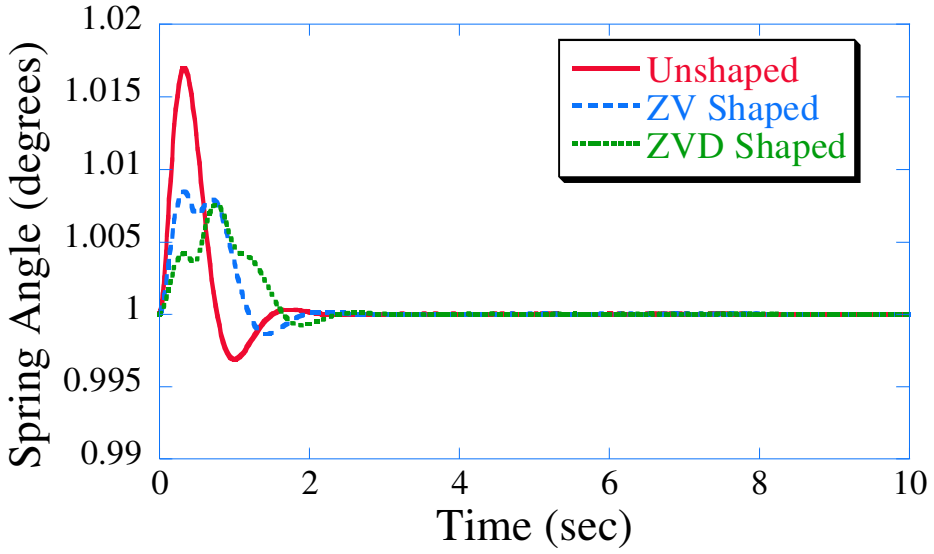

Figure 83: Separation Distance for Tangential Pursuit Maneuver.

maximum spring angle approximately 75%.

Figure 83 shows the separation distance for the unshaped and shaped trajectories. Both the ZV and ZVD shaped trajectories reduce the maximum spring angle of the follower approximately 84%. The ZVD shaped trajectory has a smaller undershoot, and it has approximately the same settling time as the unshaped case.

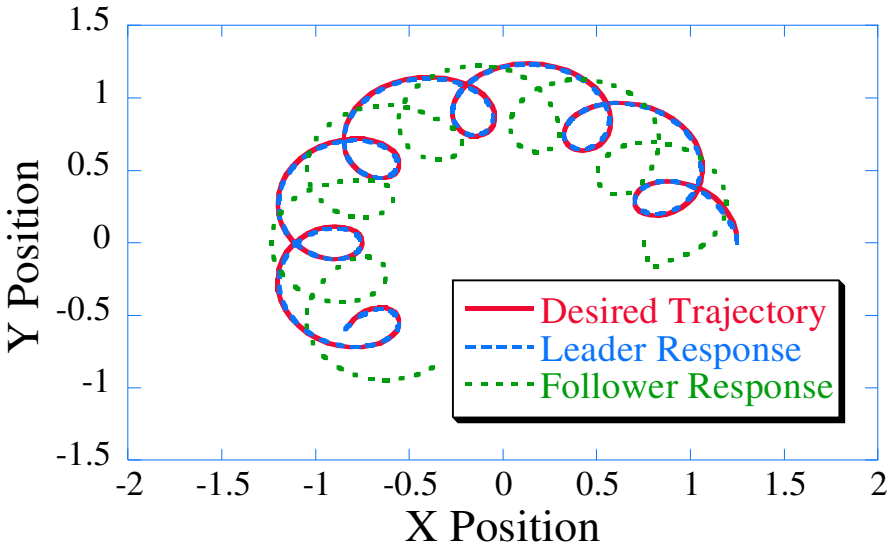

Figure 84: Leader Satellite's Response to Epi-Cyclic Maneuver.

3.3.5 Case 5: Epi-Cyclic Maneuvers

The final maneuver studied using the leader-follower architecture is the Epi-Cyclic Maneuver. This trajectory is a complex path composed of two circular orbits. This trajectory is similar to the path the moon makes around the sun. The moon orbits around the earth while the earth orbits around the sun. However for this maneuver, both the satellites in the formation are like the moon. They are orbiting around a center point which orbits another center point.

Figure 84 shows the desired trajectory and the response of the leader and follower satellites. For the maneuver shown in the figure, the leader satellite starts at (1.25,0) and the follower starts at (0.75,0). The frequency of the smaller circle is $2\frac{rads}{sec}$ with a radius of 0.25 m. The frequency of the larger circle is $.2\frac{rads}{sec}$ with a radius of 1 m. The desired separation distance between the satellites is .5 m which is two times the radius of the smaller circle.

As with any circular trajectory, using input shaping changes the radius of the trajectory. Figure 85 shows the leader's desired trajectory for the unshaped, ZV and ZVD shaped cases. In addition to the radial shortening, input shaping changes the beginning and ending portion of the trajectory. This results from the convolution of the input shaper's delayed

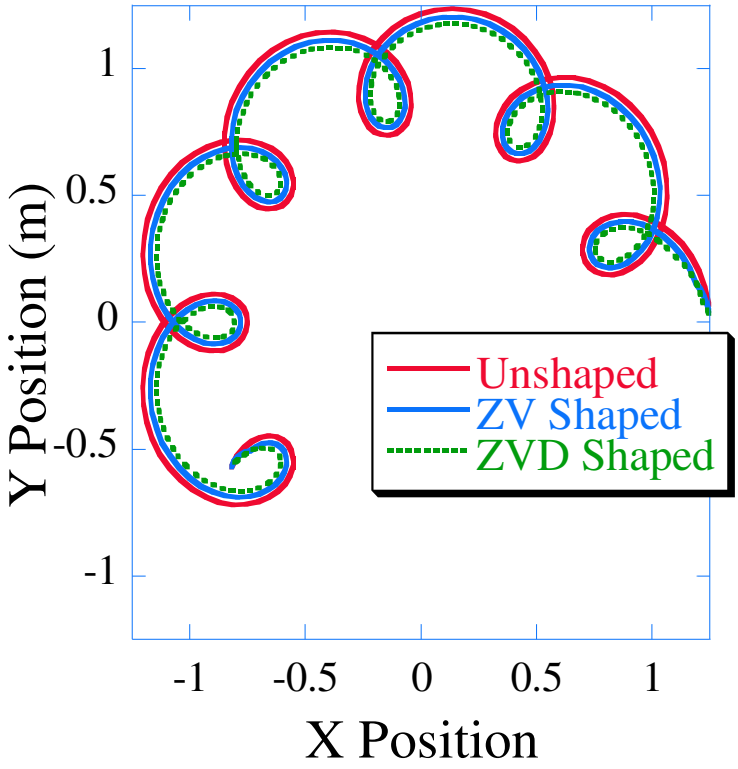

Figure 85: Leader Satellite's Desired Trajectory for Epi-Cyclic Maneuver.

amplitudes.

Figure 86 shows the spring angle response for the leader satellite. Now, instead of only feeling the effect of one circular trajectory, the satellites feel the effects of two circular trajectories. These effects manifest as oscillations in the spring angle. The frequency of one of these oscillations is 0.318 Hz which is equal to the frequency of the smaller circle ($2\frac{rads}{sec}$). However, the shaped trajectories are still able to decrease the maximum spring angle deflection. The ZV shaped trajectory decreases the maximum spring angle approximate 60% while the ZVD shaped trajectory decreases the maximum spring angle 80%.

Figure 87 shows the spring angle response for the follower satellite. For the Epi-Cyclic maneuver, it is desired that the follower satellite be 180° degrees behind the leader satellite. The large amount of vibration in the system comes from the complicated desired trajectory. Although the position of the follower satellite is supposed to be directly opposite the leader

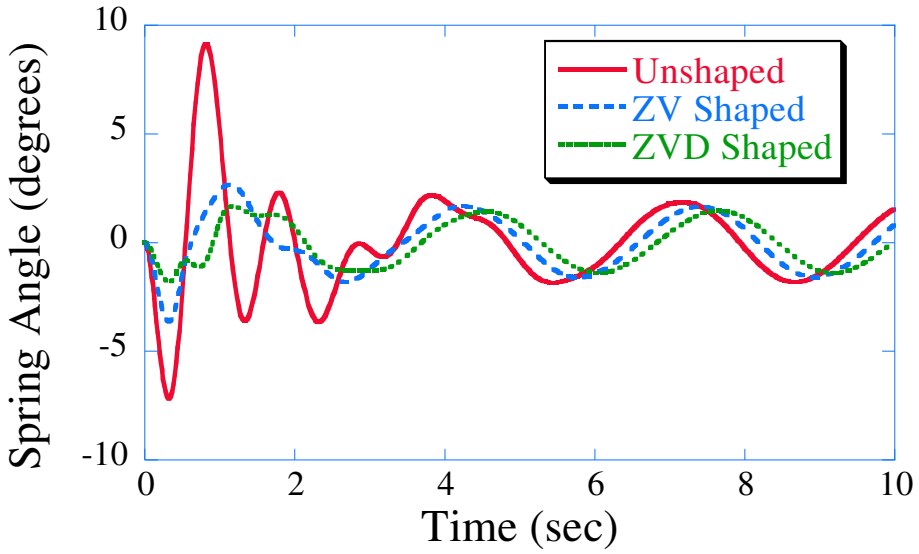

Figure 86: Leader Satellite's Spring Angle Response for Epi-Cyclic Maneuver.

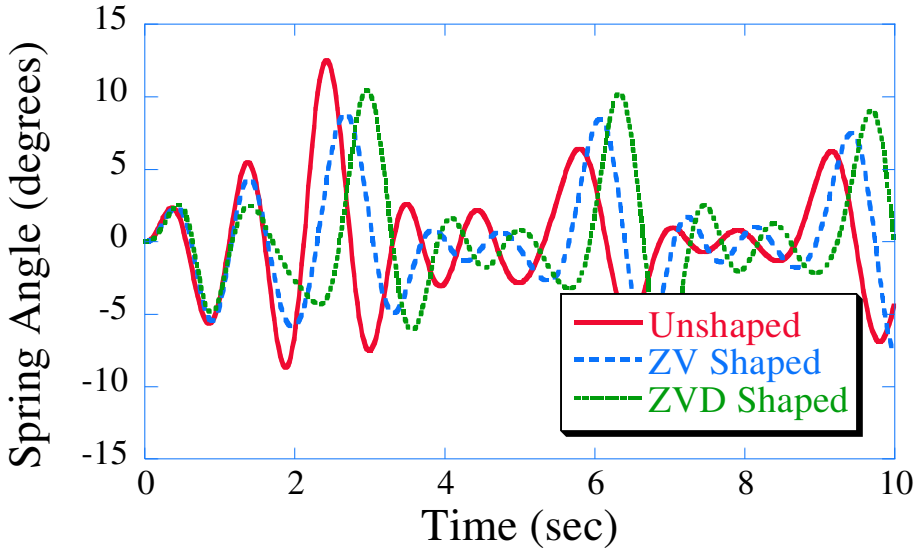

Figure 87: Follower Satellite's Spring Angle Response to Epi-Cyclic Maneuver.

on the smaller circle, this is not always the case as shown in Figure 88. This figure shows the x position of both satellites as a function of time. The position of both the satellites should vary sinusoidal at two frequencies. Notice that the position of the leader satellite is smooth and even, the follower satellite's position is not. As the satellites travel along the large circle, the follower satellite's should be opposite the leaders (shown in the figure by the high frequency oscillation). When the leader satellite is at a maximum, the follower

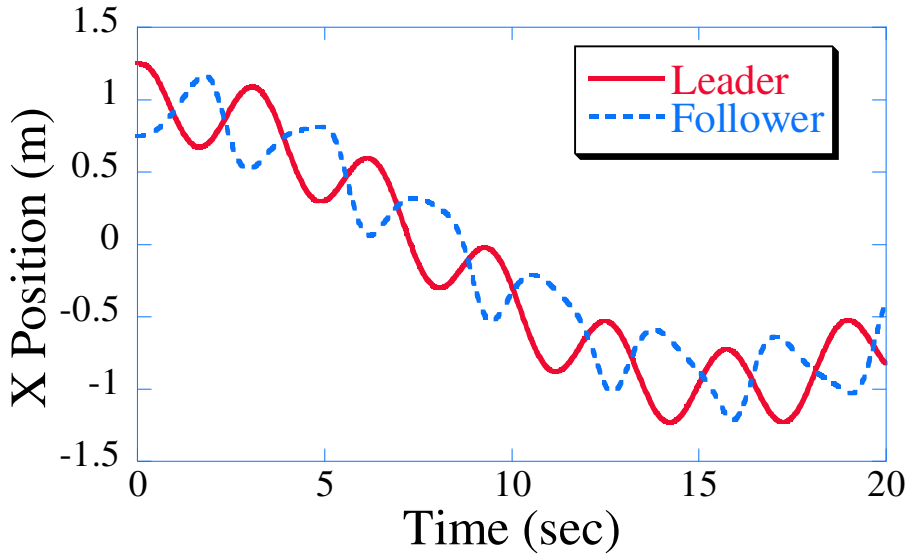

Figure 88: X-Position for the Epi-Cyclic Maneuver.

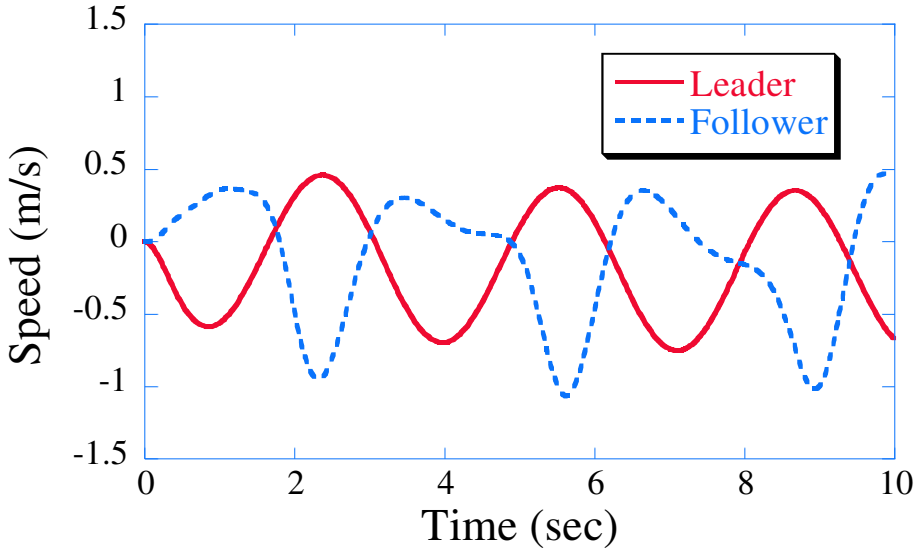

Figure 89: Speed Profile in the X-direction for the Epi-Cyclic Maneuver.

should be at a minimum. As seen in the figure, the shape of the follower satellite's path is distorted. The peak of the maximum amplitude is elongated, and the trough is shortened. There are times when the follower satellite is nearly stopped. Then it must move rapidly to try and maintain the desired separation distance. This effect can be clearly seen by examining the speed profile in the x direction for both satellites as shown in Figure 89. The desired velocity for the leader satellite can be calculated at any time by taking the derivative

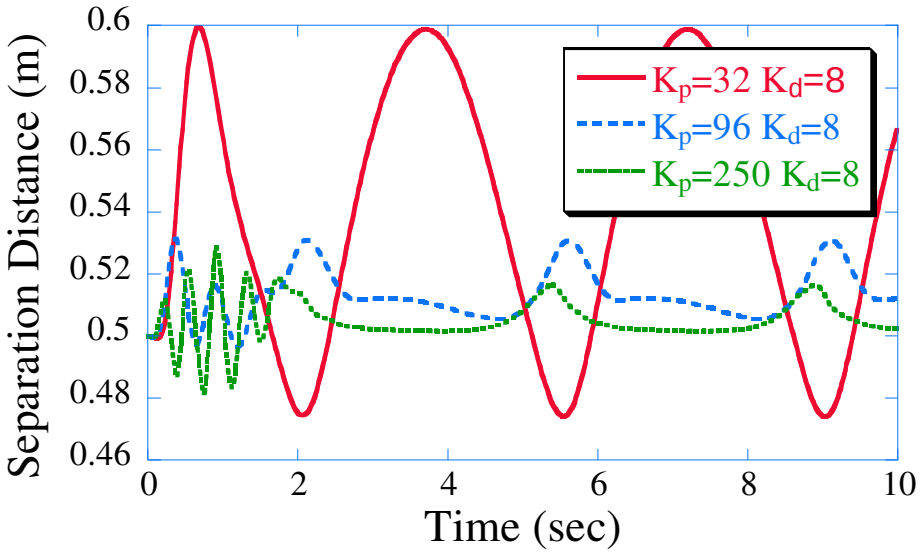

Figure 90: Separation Distance for Epi-Cyclic Maneuver

of (58) with respect to time. Calculating the desired velocity from the position leads to a smooth velocity profile; however, the follower satellite's desired velocity is unknown. For these simulations, the follower's desired velocity was calculated to be equal to the leader's velocity, but in the opposite direction. Ideally, the follower's velocity would be an identical copy of the leader's velocity profile, only it would be phase shifted 180° relative to the leader's velocity profile. As the desired trajectory becomes more complex, the selection of PD gains becomes more important.

Increasing the PD gains does decrease the separation error between the two satellites as shown in Figure 90. As the proportional gain is increased, the maximum separation distance significantly decreases. However, more oscillation is introduced, especially at the beginning of the maneuver when the satellite is converging onto the trajectory. Because the velocity of the follower satellite does not match the leader's velocity, input shaping the leader satellite does not significantly affect the follower satellite's behavior. Increasing the PD gains for better trajectory tracking does not improve the vibration reduction for the follower satellite as shown in Figure 91.

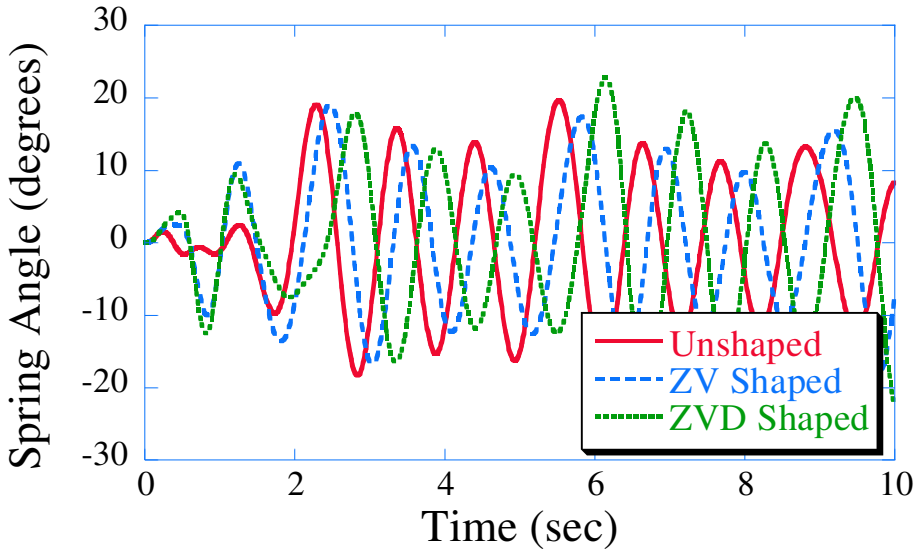

Figure 91: Follower Satellite's Spring Angle Response for Epi-Cyclic Maneuver for $K_p = 96$, $K_d = 8$.

3.3.6 Summary of Single Flexible Mode

For the straight-line trajectory, input shaping the leaders trajectory also benefited the follower's satellite. However, the extent of the benefits depends on the starting position of the follower satellite. If the follower satellite is very near to its desired initial conditions, then maximum vibration reduction is achieved. However, if the satellite starts far away from its desired initial position, then simply shaping the leader satellites desired trajectory will not significantly affect the vibration response. However, if a more robust input shaper is the vibration reduction seen in the follower satellite will be increased. Table 13 compares the maximum spring angle deflections for the different maneuvers. For any circular trajectory, the temporal tracking differences between the unshaped and shaped trajectories can be lessened by starting the shaped trajectories earlier than the unshaped trajectories. For Same-Orbit maneuvers, it does not matter whether the follower satellite is being "pushed" or "pulled". The follower satellite experiences the benefits of shaping the leader's trajectory regardless of its placement on the orbit.

Table 13: Follower Satellite's Maximum Spring Angle Deflection Reduction.

	Follower Satellite's Reduction in Maximum Spring Angle
Straight-Line ZV	34%
Straight-line ZVD	50%
Same-Orbit ZV	63%
Same-Orbit ZVD	75%
Synchronous Orbit ZV	50%
Synchronous Orbit ZVD	72%
Tangential Pursuit ZV	50%
Tangential Pursuit ZVD	75%

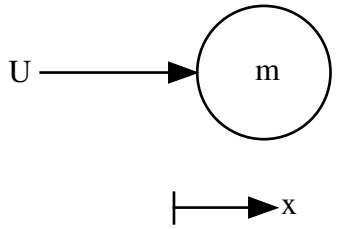

Figure 92: Open-Loop Control Scheme for Point Mass.

3.4 Two Sets of PD Gains

3.4.1 Simulation Results

The previous cases focused on the effect of input shaping on a leader-follower architecture when all of the satellites in the formation are identical. In reality, however, the satellites will not be identical. Different types of satellites are needed to fulfill different functions; therefore, this section examines the effect of input shaping when the flexible mode on each satellite is different. The simplest way to investigate this effect is by modeling the satellites as point masses. Although point mass satellites do not have flexible modes, when they are coupled with a PD controller, the closed-loop system will have a single flexible mode. Consider the open-loop control scheme and equations of motion for the point mass shown in Figure 92.

$$U = m\ddot{x} \tag{60}$$

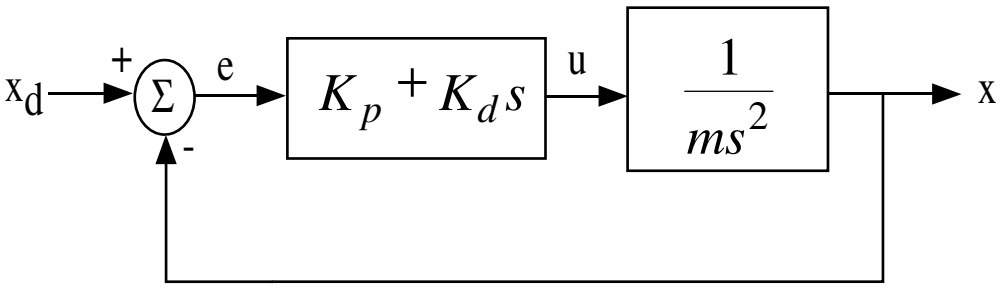

Figure 93: Block Diagram for Point Mass Satellite System.

The open-loop transfer function for this equation is

$$\frac{X(s)}{U(s)} = \frac{1}{ms^2} \tag{61}$$

However, when a proportional plus derivative feedback controller is added to this system the open-loop transfer function is now

$$\frac{X\,(s)}{X_d\,(s)} = \frac{K_p + K_d s}{ms^2} \tag{62}$$

The block diagram of the system is shown in Figure 93, and the closed-loop transfer function is

$$\frac{X(s)}{X_d(s)} = \frac{K_p + K_d s}{ms^2 + K_d s + K_p} \tag{63}$$

$$ms^2 + K_d s + K_p = 0 \tag{64}$$

Equation 64 is the characteristic equation for the system. Notice in (64) that the characteristic equation is identical to that of a second-order-damped harmonic oscillator. The solution for the roots of (64) is

$$s = \frac{-K_d \pm \sqrt{{K_d}^2 - 4mK_p}}{2m} \tag{65}$$

Therefore, by simply adding proportional plus derivative feedback control to a point mass, the system now has a single flexible mode. The frequency of the flexible mode is controlled by the K_p and m and the damping ratio is a function of K_d, K_p, and m. If the PD gains of the controller are tuned to different values, then each of the satellites will have a different flexible mode frequency. It is the effect of input shaping on these different flexible mode satellites that is of interest. The trivial cases for the solution of (64) such as two identical

real roots, or two overdamped roots will not be considered. Only the case of a distinct flexible pole for each satellite will be investigated.

It was desired that the leader satellite have a closed-loop natural frequency of 1.0 Hz. RLTOOL, a MATLAB function, was used in order to determine the appropriate values of K_p and K_d, as well as the damping ratio. A small damping ratio was desired so that the system would mimic a lightly damped second-order system. The gains were chosen to be: $K_p = 1658.4$ and $K_d = 55.3$. This led to a damping ratio of $\zeta = 0.105$, and a damped natural frequency of 1.0 Hz.

The equations of motion for the system are:

$$\ddot{x} = \frac{K_p\left(x_{desired} - x\right) + K_d\left(\dot{x}_{desired} - \dot{x}\right)}{m_1} \tag{66}$$

$$\ddot{y} = \frac{K_p\left(y_{desired} - y\right) + K_d\left(\dot{y}_{desired} - \dot{y}\right)}{m_1} \tag{67}$$

The ZV and ZVD input shapers used to shape the leader's desired trajectories are slightly different than those used in the previous section. This is because the input shapers are calculated using the damped natural frequency and damping ratio. For the point mass system, the ZV shaper has the following time locations and amplitudes:

$$\begin{bmatrix} A \\ t \end{bmatrix} = \begin{bmatrix} 0.5822 & 0.4178 \\ 0 & 0.5027 \end{bmatrix} \tag{68}$$

The ZVD shaper time locations and amplitudes are:

$$\begin{bmatrix} A \\ t \end{bmatrix} = \begin{bmatrix} 0.3389 & 0.4865 & .1746 \\ 0 & 0.5027 & 1.055 \end{bmatrix} \tag{69}$$

Figure 94 shows the desired trajectory and main satellite body response for the formation when the gains for both satellites are identical. Both of the satellites have gains that correspond to a 1.0 Hz closed-loop natural frequency. As expected, both the satellites are able to follow the desired trajectory. Figure 95 shows the x position for both satellites as a function of time. As seen in the figure, the shaped responses have zero residual vibration. Because this system is linear, there should not be any residual vibration in the system when the natural frequency of the closed-loop system is known exactly. The follower satellite

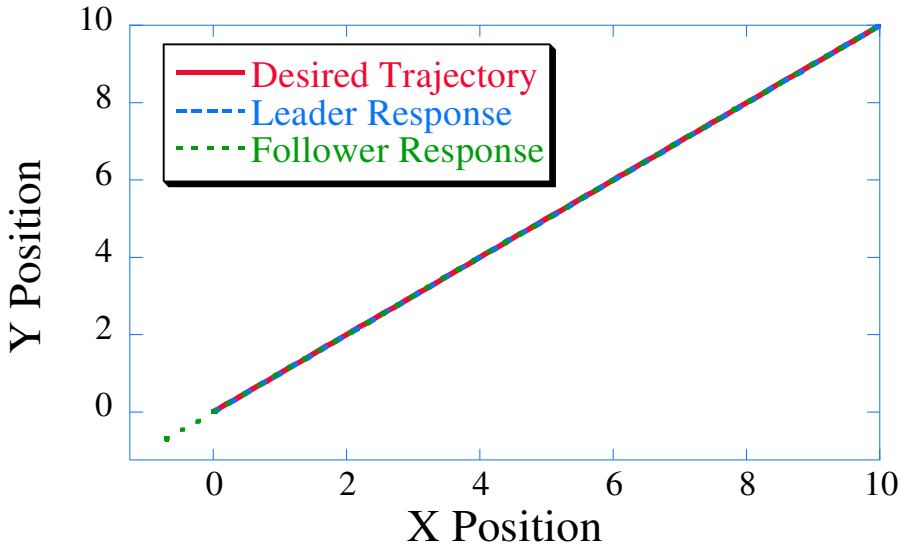

Figure 94: Point Mass Satellite Response to Straight-Line Maneuver Using Identical PD Gains.

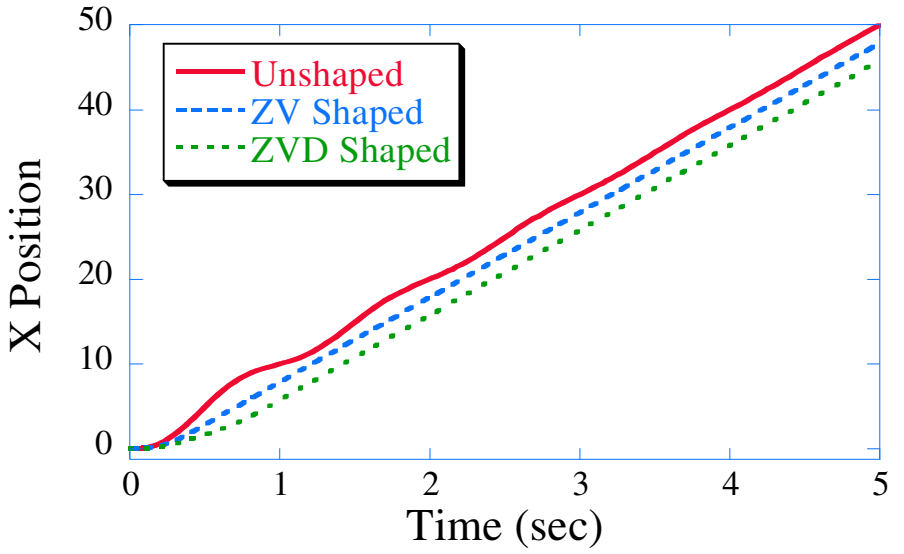

Figure 95: Point Mass Leader Satellite Response to Straight-Line Maneuver.

receives benefits from shaping the leader's trajectory. Figure 96 shows the x position for both satellites as a function of time. Note that the follower satellite vibrates at a 1.0 Hz frequency when shaping is not used. The follower satellite for the ZV shaped case has almost no vibration, and the follower satellite for the ZVD shaped case has no vibration.

Because these satellites do not have any flexible appendages, the separation distance

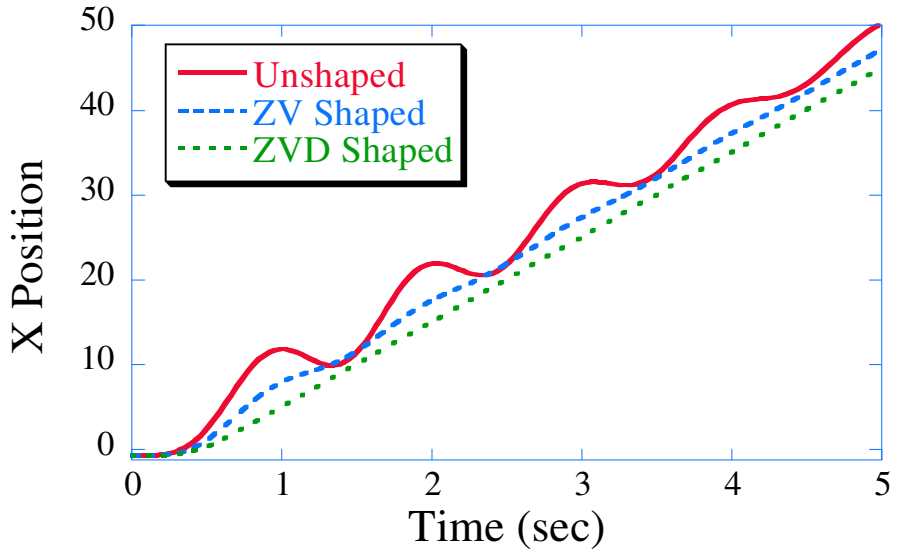

Figure 96: Point Mass Follower Satellite Response to Straight-Line Maneuver.

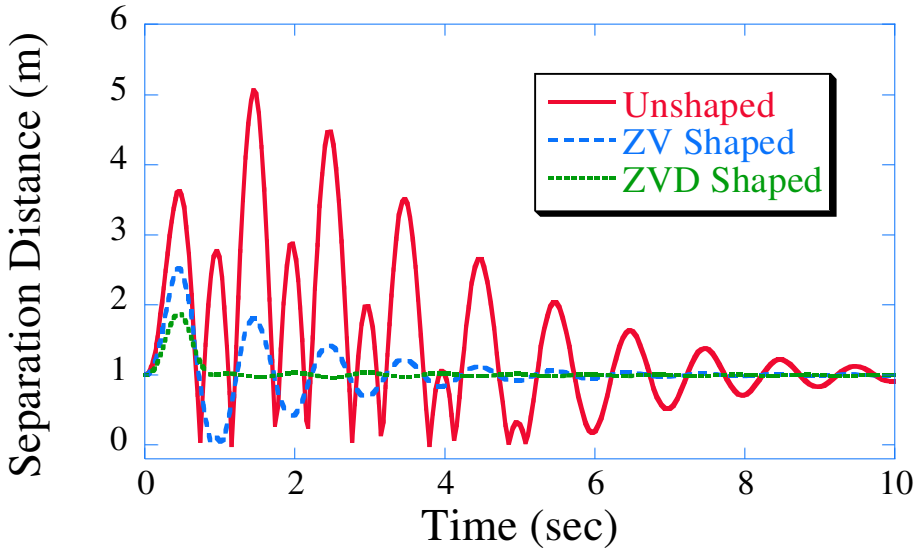

Figure 97: Separation Distance for Point Mass Satellites with Identical PD Gains.

between these satellites is the most important parameter. Figure 97 shows the separation distance between the satellites for the unshaped, ZV and ZVD shaped cases. As expected, the point mass satellites following the unshaped trajectory have the largest separation distance. There are also times for the unshaped case when the satellites would collide. The separation distance oscillates between the maximum amplitude and zero. The satellites would collide whenever the separation distance reaches zero. When this occurs, the follower

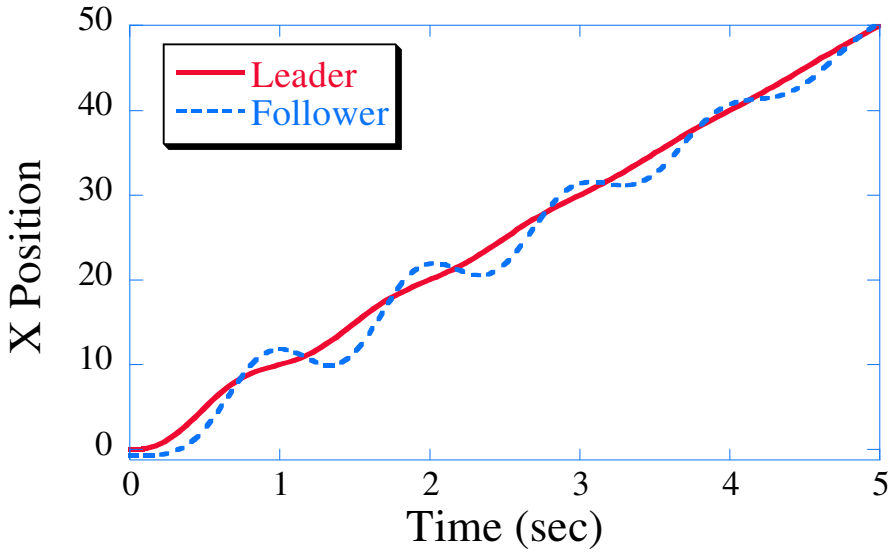

Figure 98: X Position Versus Time for Unshaped Straight-Maneuver.

satellite races past the leader satellite. The follower satellite then tries to resume the desired position of 1 unit behind the leader satellite. This behavior can be seen by examining the x position of the leader and follower satellites shown in Figure 98. In order to avoid collisions, the x position of the follower satellite must always lag the leader's position. However, as seen in the figure, this is not the case. For the ZV shaped case, the maximum separation distance is reduced 50%, however, there are two places where the satellites may collide. On the other hand, the ZVD shaped trajectory reduces the maximum separation distance 63%, and the separation distance remains at the desired value after the 1.0 sec. This corresponds to the duration of the ZVD shaper. The satellites using the ZVD shaped trajectory will never collide. So, in addition to providing excellent separation distance, the ZVD shaper also provides some degree of collision avoidance (for this particular case). It is important to note that for this case, the PD gains for both satellites were identical. Next, the effect of input shaping will be evaluated for cases where the PD gains of the point mass satellites are not identical.

The PD gains for the leader satellite were chosen so that its closed-loop frequency remained constant at 1.0 Hz. The PD gains for the follower satellite were varied so that its closed-loop frequency varied from 0.1 Hz - 10 Hz. Figure 99 shows the maximum separation

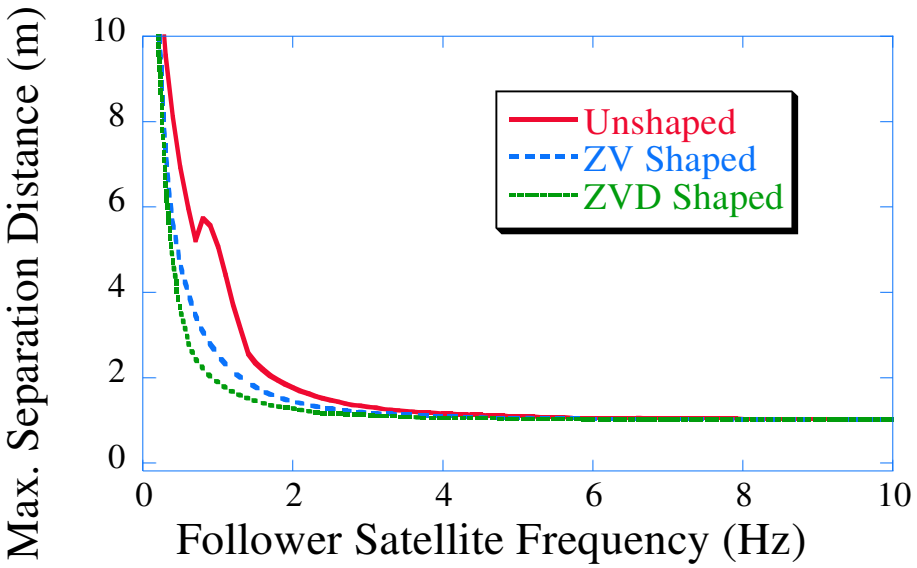

Figure 99: Maximum Separation Distance versus Follower Satellite Frequency for Straight-Line Maneuvers.

distance as a function of the follower satellite's closed-loop frequency. From the figure, it is apparent that input shaping has a significant effect on the maximum separation error for a large range of follower satellite frequencies. Input shaping begins to have an effect on the maximum separation distance for follower satellite frequencies greater than 0.2 Hz. At approximately 6.0 Hz, the maximum separation distance for the ZV and ZVD shaped trajectories converge to the same value of approximately 1.02 m. As the frequency of the follower satellite increases, the shaped trajectories approach the desired separation distance of 1.0 m. The unshaped trajectory also approaches the desired separation distance of 1.0 m.

The maximum separation distance is not symmetric about the leader satellite's frequency of 1.0 Hz. This is because the follower satellite's frequency is increasing due to increasing proportional and derivative gains. As the PD gains increase, the follower satellite is better able to maintain the desired separation distance, and the maximum separation distance decreases. As the frequency increases beyond 3 Hz the differences between the unshaped and shaped cases vanish. This is because the PD controller dominates the response of the system and the follower satellite is able to remain close to the desired separation distance.

Figure 100 shows the minimum separation distance as a function of follower satellite

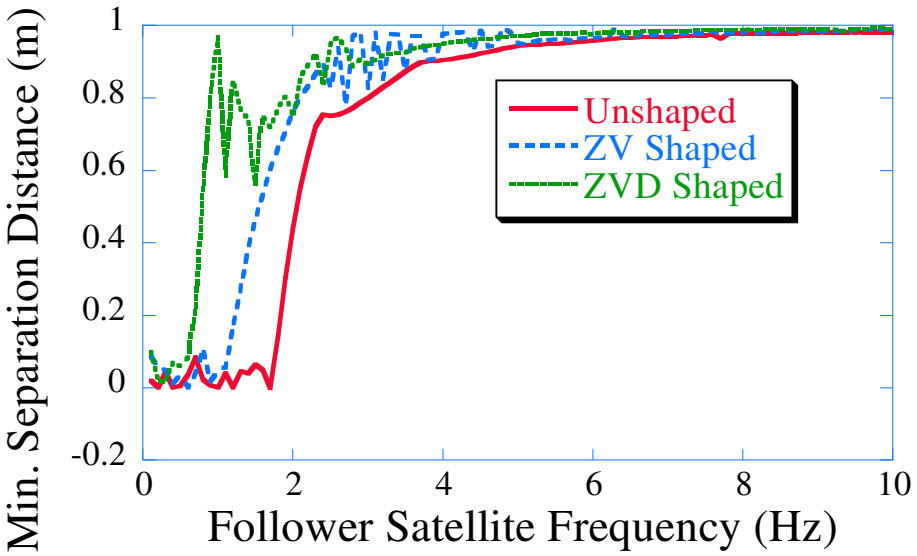

Figure 100: Minimum Separation Distance versus Follower Satellite Frequency for Straight-Line Maneuvers.

frequency. From the figure, it is clear that input shaping the leader satellite's trajectory provides improved performance for the follower satellite over a large range of frequencies. The ZVD shaped case also provides additional collision avoidance for low follower satellite frequencies. For all follower satellite frequencies greater than 0.3 Hz, if the ZVD shaped trajectory is used, then the satellites will not collide. If a ZV shaped trajectory used, then the satellite will not collide for frequencies greater than 0.9 Hz. If no shaped trajectories are used, then the satellites will not collide for follower frequencies greater than 1.7 Hz. However, it is important to note that the chance for a collision between the satellites depends on the desired separation distance. As the separation distance increases, the chance for a collision decreases. This is because even with the overshoot of the controller, the satellites are still farther apart. Using a ZVD shaper permits tighter formation structures.

The starting position of the follower satellite determines how much benefit it will receive from following the shaped leader satellite. An array of simulations was performed for the point mass satellites. Figure 101 shows the maximum separation distance for the satellites following the unshaped trajectories. For this case, the damped closed-loop frequency of the follower satellite was equal to 0.5 Hz and the leader satellite had a damped closed-loop frequency of 1.0 Hz.

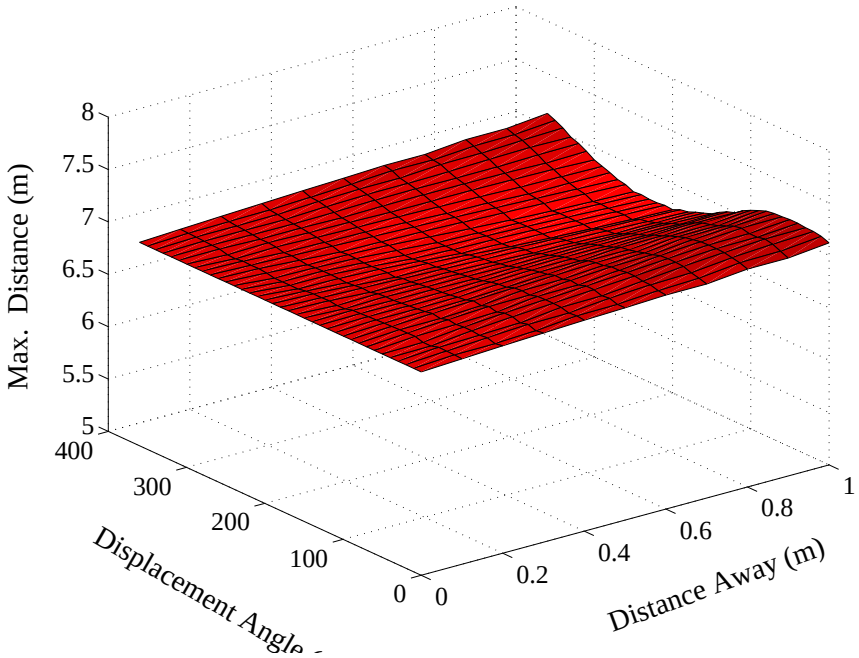

Figure 101: Maximum Separation Distance for Different Follower ($\omega_d = 0.5$ Hz) Starting Positions.

Figure 102 shows the maximum separation distance for the ZVD shaped leader satellite. Although the starting positions of the follower satellites change, using a ZVD shaper for the leader satellite's desired trajectory significantly reduces the maximum separation distance. This holds true for cases when the follower satellite's damped closed-loop frequency is larger than the leader satellites.

Figure 103 shows the unshaped maximum separation distance for the case when the follower satellite has a damped closed-loop frequency of 2.0 Hz. As expected, the maximum separation distance decreases as the frequency increases. This can be seen by comparing Figure 101 and Figure 103. An increase in the damped closed-loop frequency corresponds to increase in K_p and K_d values. Figure 104 shows the maximum separation distance for the ZVD shaped trajectory.

Figure 105 shows the minimum separation distance for the unshaped case when the follower satellite has a damped closed-loop frequency of 2.0 Hz. Figure 106 shows the minimum separation distance for the ZVD shaped case when the follower satellite has a damped closed-loop frequency of 2.0 Hz. Although both cases show that the satellites will

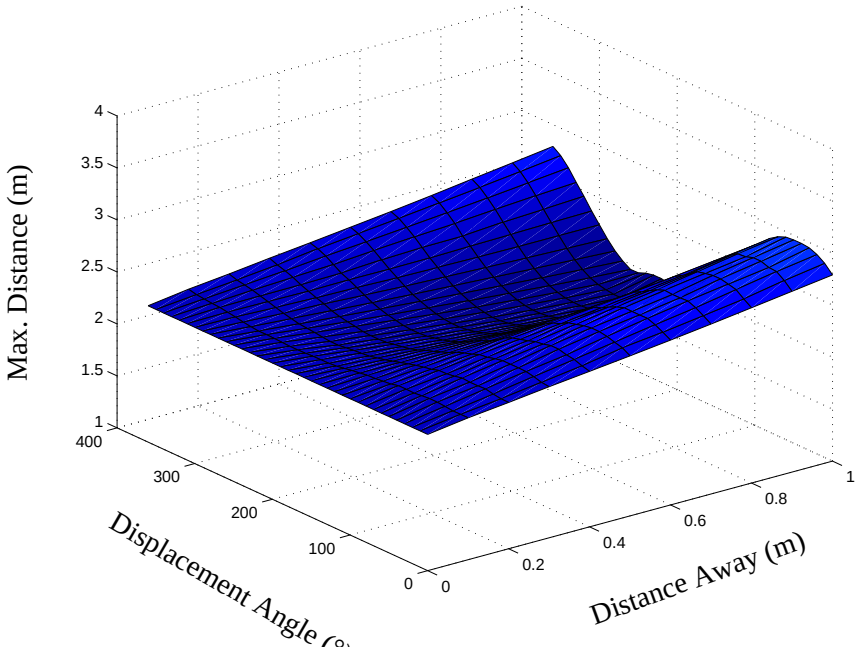

Figure 102: Maximum Separation Distance for Different Follower Starting Positions Using ZVD Shaping ($\omega_d = 0.5$ Hz).

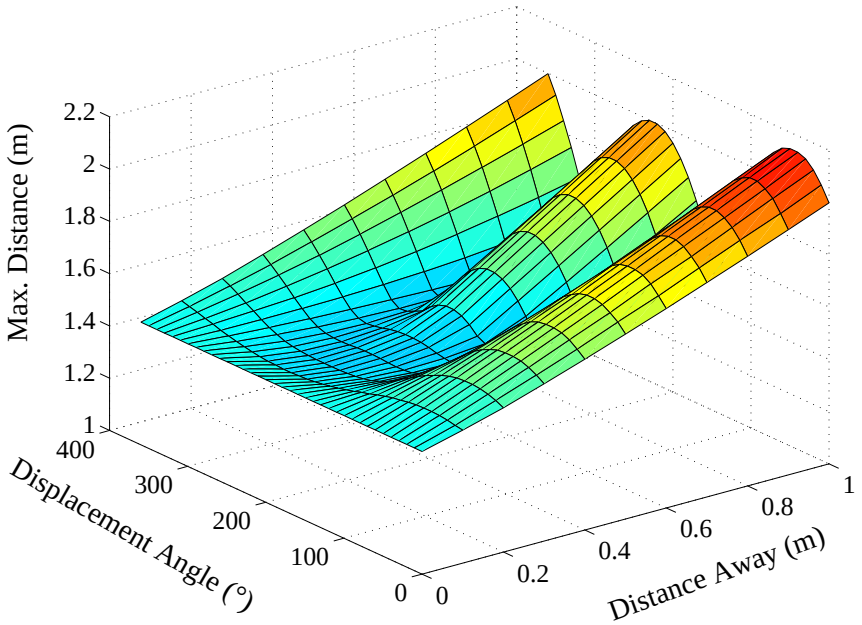

Figure 103: Maximum Separation Distance for Different Follower ($\omega_d = 2.0$ Hz) Starting Positions.

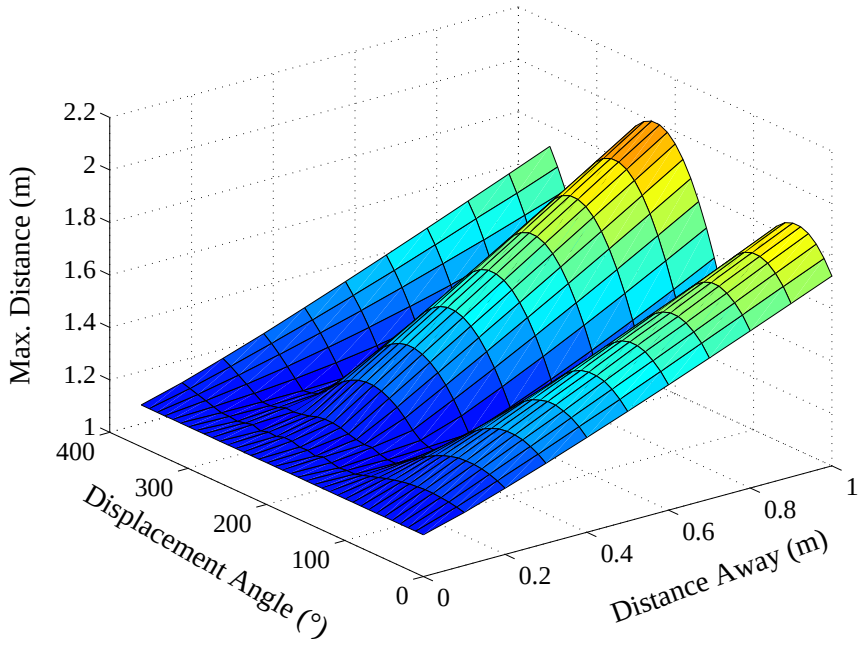

Figure 104: Maximum Separation Distance for Different Follower Starting Positions Using ZVD Shaping $\omega_d = 2.0$ Hz

not collide for any of the offset initial positions, the ZVD shaped case maintains a safer distance away from the leader satellite.

3.4.2 Summary of Two Sets of PD Gains

In this section, the satellites were modeled as point masses, and a PD feedback controller was used to control the motion. Input shaping generated the leader satellite's desired trajectory providing enhanced system performance. The damped closed-loop frequency was controlled by varying the proportional and derivative controller gains. As the frequency of the follower satellite is increased, the proportional and derivative gains also increased. Increasing the PD gains provides better trajectory tracking. As the PD gains increased, the maximum separation distance between the two satellites decreased. Increasing the closed-loop frequency increases the oscillation of the satellite and can also increase the chance for a collision.

Input shaping provided two benefits. First, input shaping the leader's trajectory led to decreased maximum separation distances for a wide range of follower frequencies. Second,

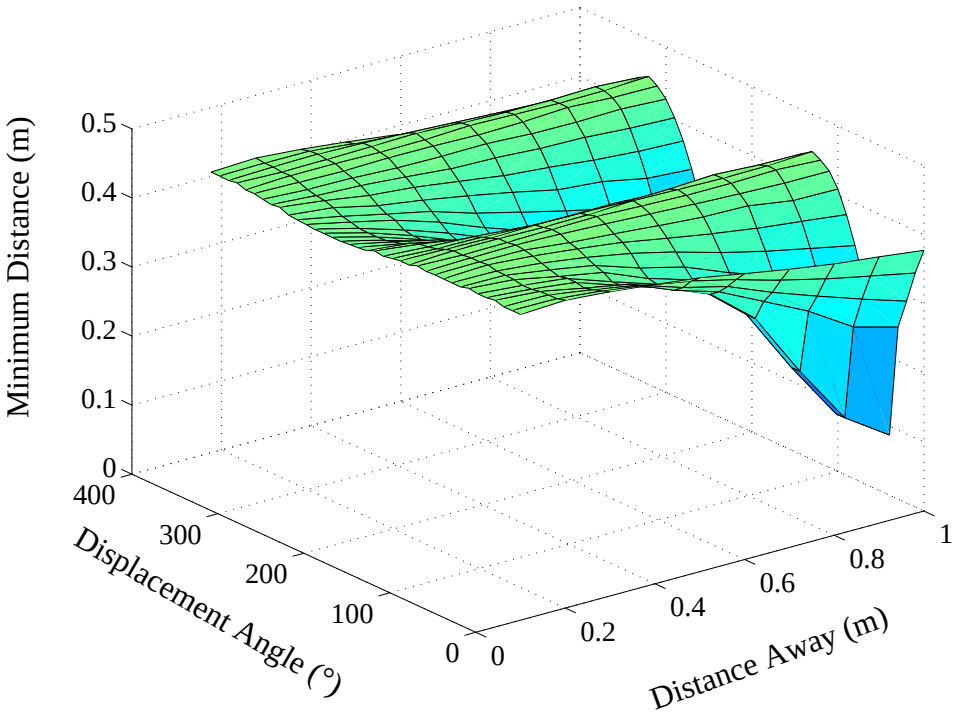

Figure 105: Minimum Separation Distance for Different Follower Starting Positions.

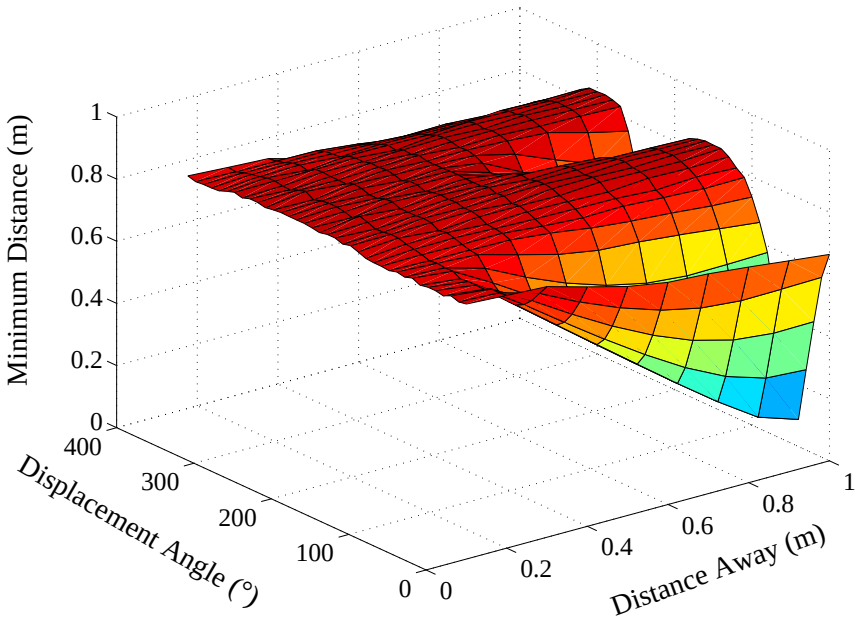

Figure 106: Minimum Separation Distance for Varying Follower Starting Positions Using ZVD Shaping.

using input shaping provided the formation with some collision avoidance. In order to ensure collision avoidance, a ZVD shaper should be used to generate the leader satellite's desired trajectory. As the gains for the follower satellite are increased, the two satellites will not collide. This is an extremely important benefit for leader-follower formation architectures where the cost of a single collision could mean the destruction of one or both the satellites in the formation. However, it is also important to note that as the separation distance for the satellites increases, the likelihood of collision for either the unshaped or shaped cases decreases, but the ZVD case will always decrease the risk of a collision.

3.5 Two Flexible Modes

3.5.1 Simulation Results

The final study for the leader-follower architecture investigates what happens when the satellites have flexible modes that are different. Unlike the previous case where the satellites were modeled as point masses, and the PD controller provided the flexible mode, the work discussed in this section uses the flexible satellite model developed in Chapter 2. The value of the spring constant, K, of the follower satellite's flexible appendage is directly related to the natural frequency of the flexible appendage.

The trajectories used for this study are the straight-line trajectories. Because this system is nonlinear, the natural frequency of the system is not easily calculated. Therefore, the approximation for the natural frequency of the flexible appendage used in Chapter 2 is used. The natural frequency of the flexible appendage is estimated to be

$$\omega_n = \sqrt{\frac{K}{m_2 L^2}} \tag{70}$$

From (70) the necessary spring constant for a desired natural frequency can be calculated.

$$K = {\omega_n}^2 \cdot m_2 \cdot L^2 \tag{71}$$

The frequency of the follower satellite is varied from 0.1 Hz to 5.0 Hz. This corresponds to changing the spring constant from $K = 0.3948$ to $K = 986.9604$, where $K = 39.5$ for a 1.0 Hz natural frequency.

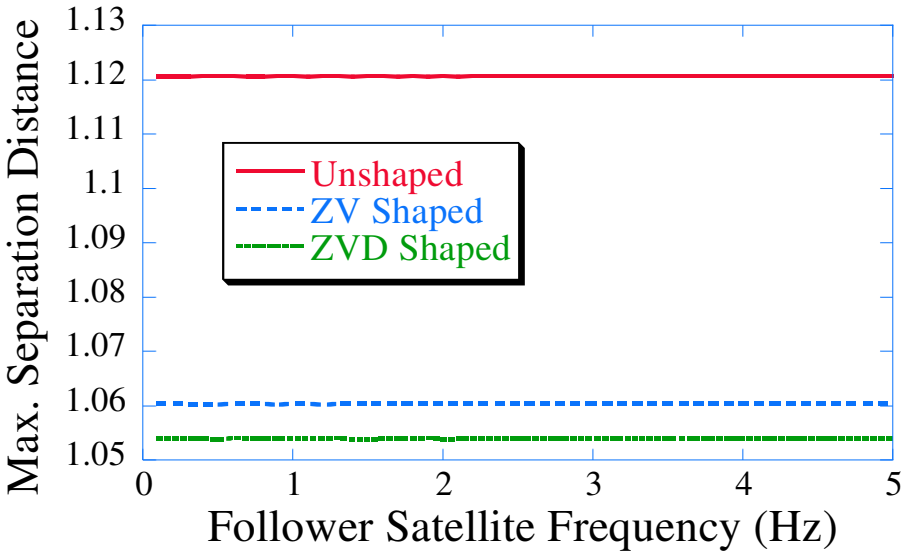

Figure 107: Maximum Separation Distance versus Follower Satellite Frequency.

The leader satellite follows either an unshaped or shaped trajectory while the follower satellite tries to remain at the desired separation distance. Figure 107 shows the maximum separation distance between the two satellites as a function of the follower satellite's frequency. As seen from the figure, the frequency of the follower satellite has no effect on the maximum separation distance. The maximum separation distance is controlled only by the controller gains and the satellite masses. Increasing the controller gains decreases the maximum separation distance. However, for a particular set of controller gains, using a ZV or ZVD shaped trajectory does lower the maximum separation distance.

Figure 108 shows the follower satellite's maximum spring angle deflection versus the follower satellite's natural frequency. The leader satellite's natural frequency is fixed at 1.0 Hz. For the frequencies below 1.0 Hz, the behavior of the follower satellite is as expected. As the frequency deviates from 1.0 Hz, the maximum spring angle of the follower satellite increases. This result is consistent with the sensitivity curves for the shapers. Recall that for the ZV shaper as system's frequency deviates from the modeled frequency, the percent of residual vibration increases linearly.

Even though the frequency of the follower satellite is significantly different from leader satellite, input shaping the leader satellite still affects the follower satellite. This is especially

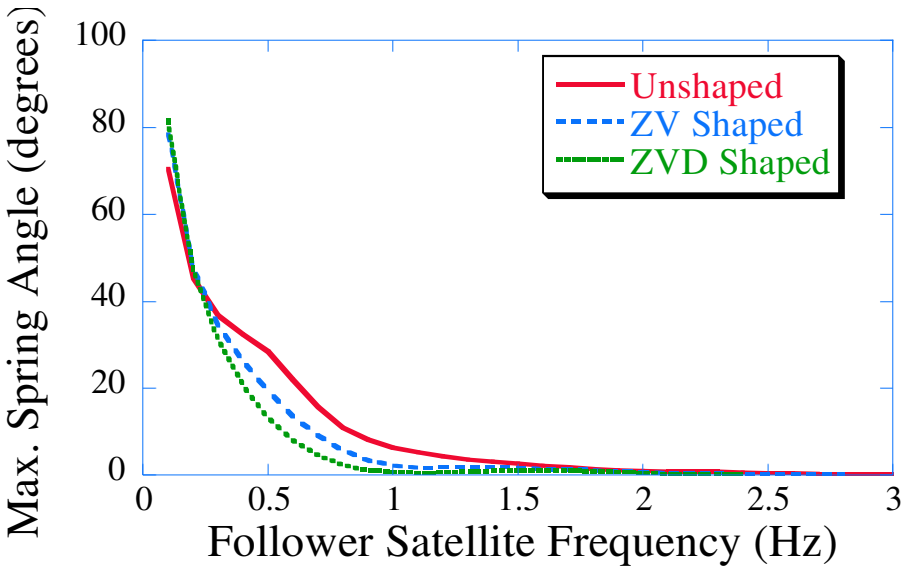

Figure 108: Follower Satellite's Maximum Spring Angle Deflection for Varying Natural Frequencies.

true for frequencies between 0.2 Hz and 1.0 Hz. For this range, the ZVD shaped trajectory provides the greatest suppression in the spring angle. One might expect that the vibration suppression would be symmetric about the leader satellite's natural frequency of 1.0 Hz; however, from the figure 108 this behavior is not present. As the frequency increases from 1.0 Hz to 5.0 Hz, the follower satellite's maximum spring angle deflection decreases for all of the trajectories. One explanation for this behavior is that the nonlinear nature of the system is magnified at higher frequencies. This phenomena can be seen in Figure 109. This figure shows a detailed portion of Figure 108. As seen from the figure, after the frequency of 1.0 Hz, the ZV and ZVD shaped responses do increase as expected from their sensitivity curves. However, the increase is only for a small range of frequencies. By 1.5 Hz, both the ZV and ZVD shaped trajectories begin to decrease. At this point, the controller frequency begins to manifest itself in the spring angle response as shown in Figure 110. This is because the follower satellite's frequency is much closer to the controller frequency, so now the response is a combination of the two frequencies. At lower follower satellite frequencies, the flexible appendage frequency dominates the response.

It is possible to reduce the follower satellite's vibration by changing the frequency of the input shaper used to modify the leader satellite's trajectory. If the follower satellite's

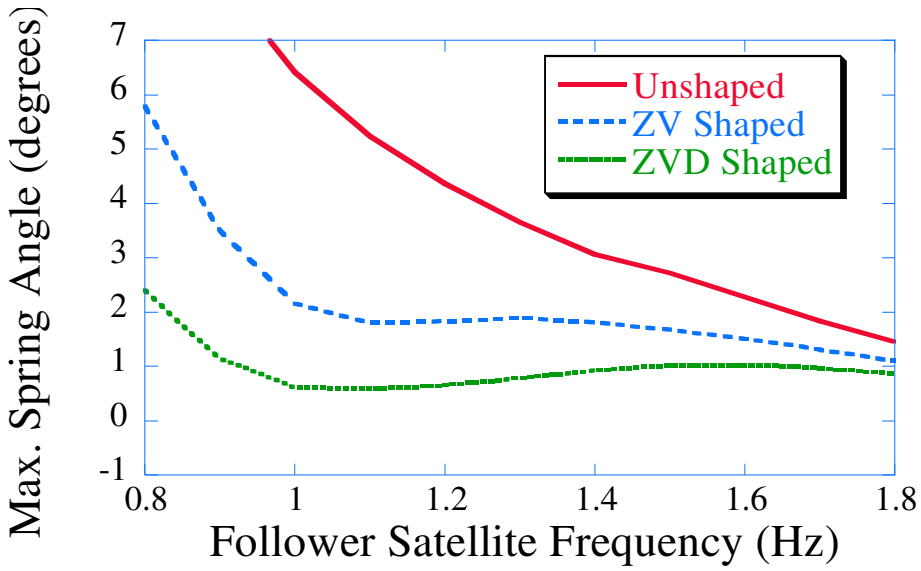

Figure 109: Follower Satellite's Max. Spring Angle Deflection for Varying Natural Frequencies.

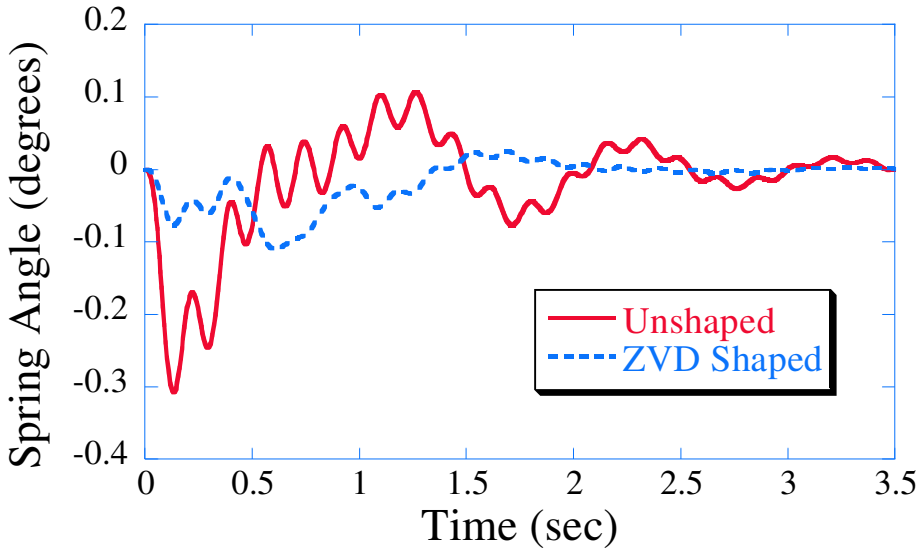

Figure 110: Spring Angle Response for Follower Frequency of 5.0 Hz.

frequency is known, then the frequency of the input shaper can be modified. One solution for two different frequencies is to take the average of the frequencies and use this average value to design the input shaper. Another, and perhaps easier solution is to use a multi-mode shaper. Figure 111 shows the maximum spring angle deflection of the follower satellite for the unshaped and ZVD shaped trajectories. The average value input shaper reduces

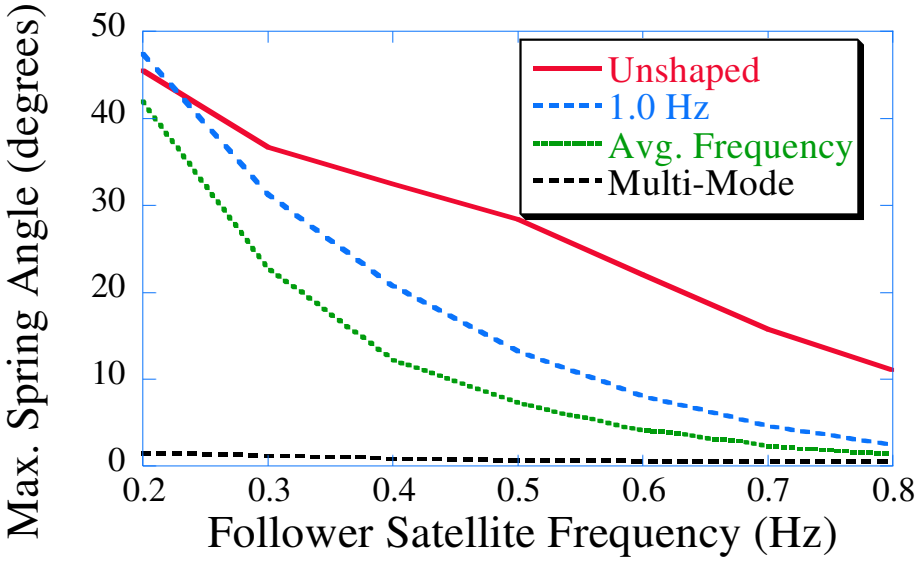

Figure 111: Maximum Spring Angle Response for Different Input Shaper Frequencies.

the maximum spring angle deflection for a larger range of follower satellite frequencies, but the multi-mode shaper provides superior vibration reduction for the range of frequencies shown. As the frequencies of the follower and leader satellites approach each other, the average frequency response,the 1.0 Hz frequency response, and the multi-mode responses all converge.

Changing the frequency of the input shaper away from 1.0 Hz affects the response of the leader satellite. If the multi-mode shaper is not used, then the leader satellite follows a shaped trajectory for a different frequency. This causes an increase in the maximum spring angle deflection as shown in Figure 112. The response of the leader satellite is similar to the response predicted by the sensitivity curves. As expected the response using the 1.0 Hz ZVD shaper has the best response. The ZVD shaped trajectory has an increased robustness to the difference between the leader and follower's frequencies.

However, by utilizing a multi-mode shaper, the vibration characteristics of the leader and follower satellites can both be improved. Figure 113 shows the spring angle response of the leader satellite. The response shown in the figure represents the extreme case when the frequency of the follower satellite is 0.2 Hz and the frequency of the leader satellite is 1.0 Hz. As seen from the figure, even with largely spaced modes, the shaping still provides

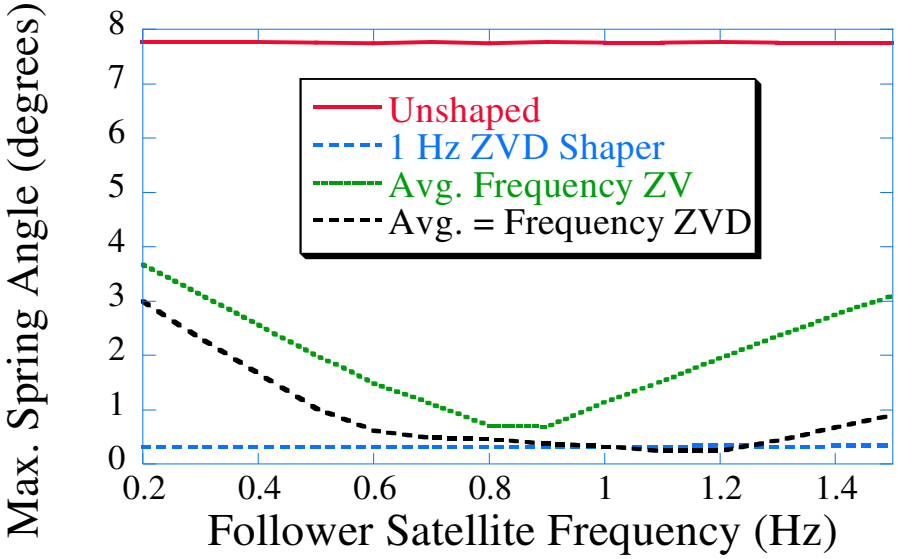

Figure 112: Leader Satellite's Maximum Spring Angle Response for Varying Follower Satellite Frequencies.

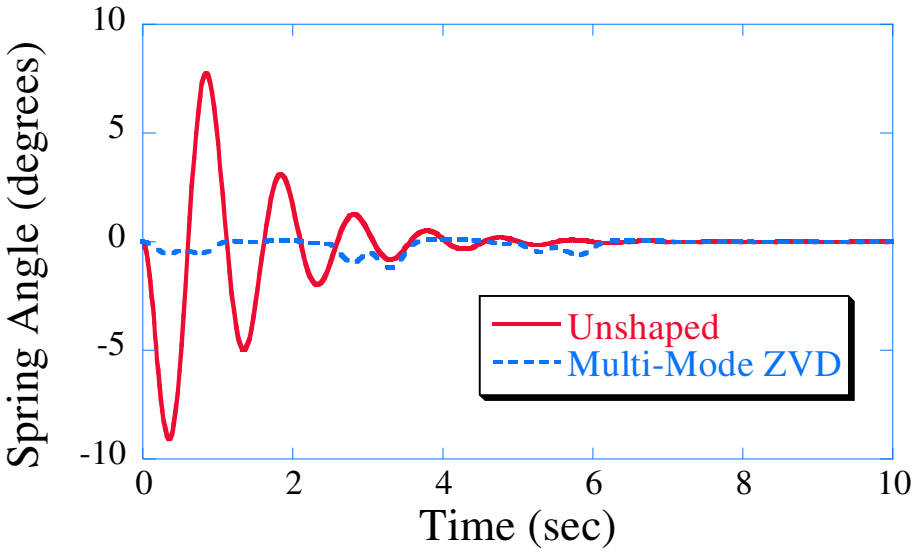

Figure 113: Leader Satellite's Spring Angle Response for Multi-Mode Shaped Trajectory.

superior vibration reduction for the leader satellite. So, both the leader and follower satellite have superior vibration reduction of the flexible appendages when the multi-mode shaper is utilized.

The price for using a multi-mode shaper is an increase in the shaper's duration. As the frequency range between the leader and follower satellites increases, the duration of the

multi-mode shaper increases. For example, the amplitudes and time locations for the 1.0 Hz shaper are:

$$\begin{bmatrix} A \\ t \end{bmatrix} = \begin{bmatrix} 0.25 & 0.5 & 0.25 \\ 0 & 0.5 & 1.0 \end{bmatrix} \tag{72}$$

The amplitudes and time locations for a multi-mode ZVD shaper designed for 1.0 Hz and O.2 Hz frequencies are:

$$\begin{bmatrix} A \\ t \end{bmatrix} = \begin{bmatrix} 0.0625 & 0.125 & 0.0625 & 0.125 & 0.25 & 0.125 & 0.0625 & 0.125 & 0.0625 \\ 0 & 0.5 & 1.0 & 2.5 & 3.0 & 3.5 & 5.0 & 5.5 & 6.0 \end{bmatrix} \tag{73}$$

The duration of the shaper is six times the 1.0 Hz ZVD shaper. This affects the temporal tracking delay. As the duration of the shaper increases, the time the shaped trajectories must be started before the unshaped trajectory also increases. In addition, the time period where the trajectories can never be equal (during the duration of the shaper) also increases; however, compared to the overall length of the maneuver, this may be an insignificant time penalty.

3.5.2 Summary of Two Flexible Modes

As the frequency of the follower satellite deviates from the natural frequency of the leader satellite, the vibration reduction seen by shaping the leader satellite's desired trajectory decreases unless a multi-mode shaper is used. If a multi-mode shaper is used, then superior vibration reduction is experienced by both the leader and follower satellites for a wide range of frequencies.

The initial starting position of the follower satellite plays an important role in determining how much benefit it receives from the leader's shaped trajectory. For low follower satellite frequencies, the farther the satellite starts away from its desired initial position, the less input shaping benefits it receives. Input shaping also provides a measure of collision avoidance for the low follower satellite frequencies. For situations where collision between the satellites is possible due to small separation distances, a ZVD input shaper should be used to shape the leader satellites trajectory.

As the frequency of the follower satellite is increased, the benefits felt from input shaping the leader's trajectory decrease. This is due to the increasing dominance of the PD feedback

controller. As the frequency of the satellite increases, the controller mode becomes more important. The maximum spring angle of the follower satellite decreases for all cases. The range of follower satellite frequencies where input shaping significantly effects the vibration characteristics, is not symmetric about the leader satellite's frequency. Instead, it is more effective for a larger range of lower satellite frequencies (when the follower satellite has a lower frequency than the leader satellite). For a follower satellite frequency of two times the leader's frequency, the unshaped, and shaped cases have almost identical maximum spring angle deflections.

It is possible to further increase the benefits received by input shaping the leader satellite's trajectory using the average of the leader and follower satellite's frequencies, or a multi-mode shaper for superior vibration reduction. Using the average frequency increases the spring angle deflection of the leader satellite, but decreases the spring angle deflection for the follower satellite. Using a multi-mode shaper decreases the maximum vibration amplitude for both the leader and follower satellites. For maximum benefit, this technique should be applied to systems where the follower satellite has a lower frequency than the leader satellite. The response of the follower satellite does not follow the linear behavior predicted by the input shaping sensitivity curves. The leader satellite's behavior however, more closely follows the predicted response. The price for using the multi-mode frequency input shaper is an increase in the shaper duration.

As the frequency of the follower satellite varies from the leader satellite, the separation distance between the two satellites does not change. This is because the proportional and derivative feedback controller gains dominate the separation distance. However, the type of shaping determines what value the maximum separation distance is equal to. Using a ZVD shaper on the leader satellite's trajectory yields the smallest maximum separation distance.

CHAPTER IV

VIRTUAL STRUCTURE FORMATION FLYING ARCHITECTURE

The previous chapter investigated the effect of input shaping on a leader-follower formation flying architecture. This chapter extends the study by focusing on a more complex algorithm, a virtual-structure algorithm. As discussed in Section 1.4.3, the virtual-structure algorithm is based off the formation architecture presented in [12]. This architecture has elements of centralized and decentralized control and virtual structures.

The motion of the formation is governed by the formation supervisor. The formation supervisor knows the state of each satellite and is responsible for coordinating the motion of every satellite in the formation. Each satellite however, does not know the position or attitude of any of the other satellites in the formation. Its only responsibility is to ensure it follows its desired trajectory. The desired trajectories for each of the satellites is generated by the corresponding formation state.

There are many different ways to implement command shaping with this architecture; however, this chapter studies the effect of implement the shaping at the supervisor level and the local satellite level. For this work, the formation supervisor is assumed to have instant knowledge of the formation states and the states of each of the satellites in the formation. The formation investigated is composed of three satellites in a triangular configuration.

4.1 Design Procedure for Utilizing Command Generation with Virtual-Structure Formation Flying Architecture

The goal of investigating the virtual-structure architecture is to produce design procedures. These procedures can be used to help the controls engineer implement trajectory shaping with a virtual-structure or similar formation flying architecture. The design procedure for the virtual-structure architecture is as follows:

- *Select PD gains to provide excellent tracking performance.*(The detailed explanation for choosing the gains is discussed in Sections 2.3.2 and 4.7.)

- *Convolve the satellites' desired trajectories with a robust shaper.* (The benefit of utilizing a robust shaper will be discussed in Sections 4.5.1-4.9.)

- *For circular maneuvers, increase the desired radius before shaping.*(The justification and clarification for this step was given in Section 2.3.4.)

- *When temporal tracking is of paramount importance, generate the satellite's desired trajectories using small step changes.* (The justification and clarification for this step is given in 4.6.2 and 4.6.3.)

- *When temporal tracking is of paramount importance, start the shaped maneuvers early.* (This explanation for this step is discussed in Sections 2.3.3 and 4.7.3.2.)

- *For largely spaced multi-mode formations use a supervisor level multi-mode shaper.* (The clarification for this step is discussed in Sections 4.9.1 and 4.9.2.)

- *For closely spaced multi-mode formations use a supervisor level robust shaper.*(The explanation for this step is given in Sections 4.8 and 4.9.2.2.)

The following sections discuss the structure of the architecture in more detail, and examine the effect shaping the satellites' desired trajectories has on the overall structure of the formation.

4.2 Formation Frame

A schematic representation of the architecture is shown in Figure 114. The formation states are used to describe the configuration and motion of the virtual structure. The virtual structure is assumed to be a completely rigid body, and contains a specified center point. The location of the center point is arbitrary and does not have to be coincident with the centroid of the virtual structure. This control architecture requires three references frames: internal, formation, and satellite. The relationship between these frames is shown in Figure 115. The inertial reference frame shown in the figure is the same inertial frame

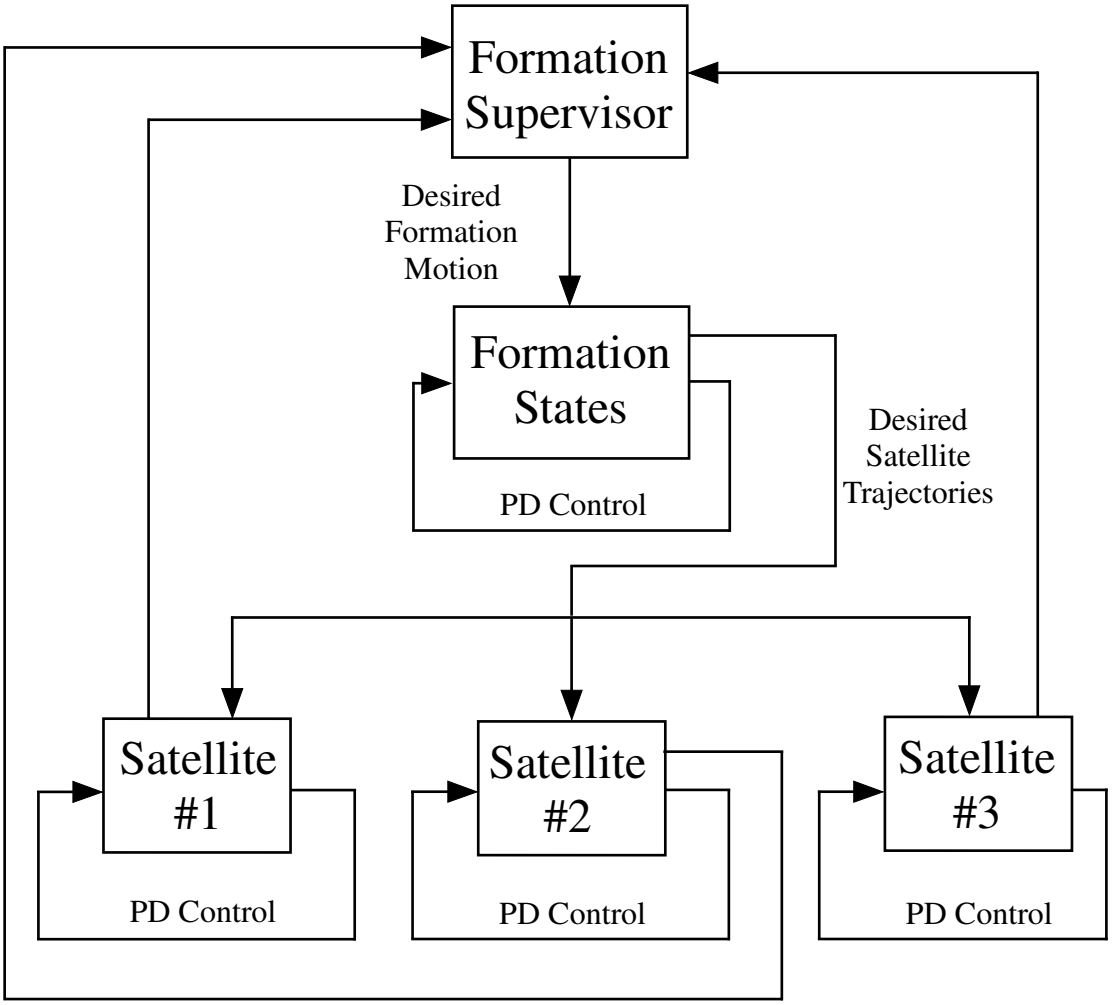

Figure 114: Virtual Structure Formation Flying Architecture.

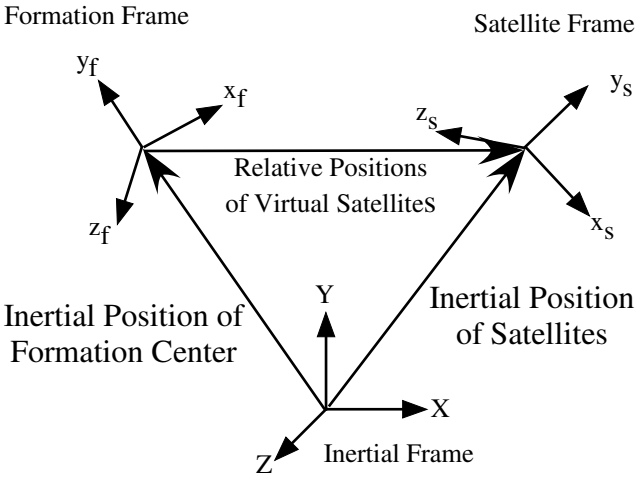

Figure 115: Coordinate Frame Geometry.

used for the leader-follower calculations discussed in Chapter 3. The position, velocity, and orientation of the virtual structure's center is measured with respect to the inertial frame. The formation frame is body fixed,and is attached to the virtual structure at its center point. The position, velocity, orientation and angular velocity are described by $\vec{r}_f$, $\vec{v}_f$, $\vec{\theta}_f$, and $\vec{\omega}_f$. The sate of the formation's center is

$$\vec{\bar{x}}_f = \left(\vec{r_f}', \vec{v_f}', \vec{\theta_f}', \vec{\omega_f}'\right) \tag{74}$$

The formation frame is used to describe the positions, and velocities of the *virtual satellites*. The attitude of the virtual satellites is measured with respect to the inertial frame. These virtual satellites are modeled as point masses and act as placeholders for the actual satellites. The position, velocity, orientation, and angular velocity of the virtual satellites with respect to the formation frame is $\vec{r}_{if}$, $\vec{v}_{if}$, $\vec{\theta}_{if}$, and $\vec{\omega}_{if}$ respectively. Accordingly let

$$\vec{\bar{x}}_{if} = \left(\vec{r_{if}}', \vec{v_{if}}', \vec{\theta_{if}}', \vec{\omega_{if}}'\right) \tag{75}$$

represent the states of the virtual spacecraft where i is the spacecraft number. For this work only three satellites were used so $i = 1:3$. The state of the formation is given by

$$\vec{x}_f = \left(\vec{\bar{x}}'_f, \vec{\bar{x}}'_{1f}, \vec{\bar{x}}'_{2f}, \vec{\bar{x}}'_{3f}\right) \tag{76}$$

4.3 Satellite Frame

The position, velocity, orientation, and angular velocity of the satellites is measured with respect to the inertial reference frame and described by: $\vec{r}_i$, $\vec{v}_i$, $\vec{\theta}_i$, and $\vec{\omega}_i$. The state of the satellites is

$$\vec{x} = \left(\vec{x_1}', \vec{x_2}', \vec{x_3}'\right) \tag{77}$$

The formation states are used to generate the desired position trajectories for the satellites, and they must be transformed from the formation frame to the inertial frame. This is accomplished by utilizing the following position transformation:

$$\vec{r}_{id} = \vec{r}_{fd} + R \cdot \vec{r}_{ifd} \tag{78}$$

where $\vec{r}_{id}$ is the desired position of the i^{th} satellite, $\vec{r}_{fd}$ is the desired position of the formation frame (i.e. the virtual structure's center), $\vec{r}_{ifd}$ is the desired position of the i^{th} virtual

satellite, and R is a rotation matrix given by

$$R = \begin{bmatrix} \cos\theta_{fd} & \sin\theta_{fd} & 0 \\ \sin\theta_{fd} & \cos\theta_{fd} & 0 \\ 0 & 0 & 1 \end{bmatrix} \tag{79}$$

θ_{fd} is the desired rotation of the virtual structure with respect to the inertial frame.

4.4 Flexible Satellite States

In [12] both the formation states and satellites were modeled as point masses and the equations of motion and control laws were developed accordingly. Here, the satellites in the formation are modeled as flexible bodies, and the equations of motion developed in Chapter 2 are incorporated into the formation flying architecture. This is accomplished by substituting the point mass model with the flexible satellite model. The formation states are still modeled as point masses.

There is one factor which facilitated the ease of integrating the flexible model, the architecture was developed for deep space applications. Because the architecture was developed for deep space applications, the gravitational effects of the earth, and sun are neglected. In addition, any disturbance forces that may result from an earth orbit, such as solar pressure and atmospheric drag are also neglected. Using an architecture that does not include these simplifications would require either:

1. a derivation of the flexible model that can account for these disturbance forces
2. a simplification that would uncouple the flexible dynamics from the motion of the main satellite body

It is important to note that neglecting these disturbance forces does not affect the focus of this work. The focus of the work presented here is to investigate how shaping the trajectory affects the trajectory tracking and temporal tracking of the satellites in the formation. Therefore, the effect of the disturbance forces on this focus can be disregarded.

Utilizing a flexible model for the satellites changed the equations that define the state of the satellites given in (77). Now, instead of utilizing only four states to define the motion of

the satellite, six states are utilized. These states are the position of the main satellite body, $\vec{r}_i$, the velocity of the main satellite body, $\vec{v}_i$, the orientation of the main satellite body, $\vec{\theta}_i$, the angular velocity of the main satellite body, $\vec{\omega}_i$, the spring angle, $\vec{\phi}_i$, and the flexible appendage angular velocity, $\dot{\vec{\phi}}_i$. It is important to note that both the additional states $\vec{\phi}_i$ and $\dot{\vec{\phi}}_i$ are measured using a body fixed frame attached to the main satellite body at the flexible appendage's connection point as discussed in Chapter 2.

4.5 Motion of the Virtual Structure

The motion of the formation (i.e. the virtual structure) and satellites is composed of two regimes: Initialization, and General Motion.

4.5.1 Initialization

The goal of the initialization stage is to move the virtual structure and the satellites from their starting positions to a desired initial position and orientation. This is accomplished by commanding a step change in the desired position and orientation. It is assumed that both the formation states, or virtual satellites, and the satellites will be starting and ending with zero velocities and accelerations. Therefore, only step changes in the desired position or orientation are commanded. Once given the desired positions and orientations, the formation states and satellites are allowed to maneuver to their destinations using a PD control algorithm. It is important to note that the formation states and satellite states converge to their desired locations independent of one another. That is, the motion of the satellites is not dependent on the convergence of the virtual structure for the initialization portion of the maneuver.

4.5.2 General Motion

Once the virtual structure and satellites are in their initialized positions and orientations, the architecture switches to the general motion stage. The switch to the generalized motion is regulated by an error function. The purpose of the general motion stage is to maneuver or reorient both the formation and the satellites according to the desired motion. For example, suppose a group of satellites is released from their transportation vehicle. The

initialization stage would be used to maneuver the satellites from their launch position to the desired formation structure. Now suppose that the purpose of the formation is to observe a particular cluster of stars. The general motion stage would be used to point the satellites to the desired star cluster.

In order to maneuver the satellites during the general motion stage, first the formation states must converge to their desired locations. The formation states are given the appropriate step changes in position, velocity and orientation from the formation supervisor. Next, the formation states are driven toward their desired locations using a PD feedback control algorithm. The response of the formation states is used to drive the satellites.

There are several benefits to utilizing the formation states in this way. One of the benefits is that the satellites have smooth desired trajectories. Instead of step changes, the satellites have continuous trajectories. This is because the response of the formation states is smooth and continuous. The second benefit is collision avoidance is guaranteed. As long as the satellites are able to reasonably follow the desired trajectories, they will not collide with one another. This comes from the virtual structure. Once initialized, the formation states form a virtual rigid structure, and it is impossible for two points on this structure to collide, provided there is no deformation of this structure. Consequently, the satellites achieve collision avoidance by simply following the desired trajectories. The satellites are commanded to follow the desired trajectory by utilizing a PD feedback control algorithm.

There are many different ways to utilize input shaping for such a complicated architecture. This work focuses on two areas: supervisor level, and the local satellite level. The input shapers are convolved with the trajectories generated by the formation states, and the resulting shaped trajectories are used to drive the satellites. A computer program was developed using MATLAB to simulate the architecture in [12]. The virtual structure simulation was developed so that translation and rotation maneuvers are available. The following section discusses the two types of investigated motions.

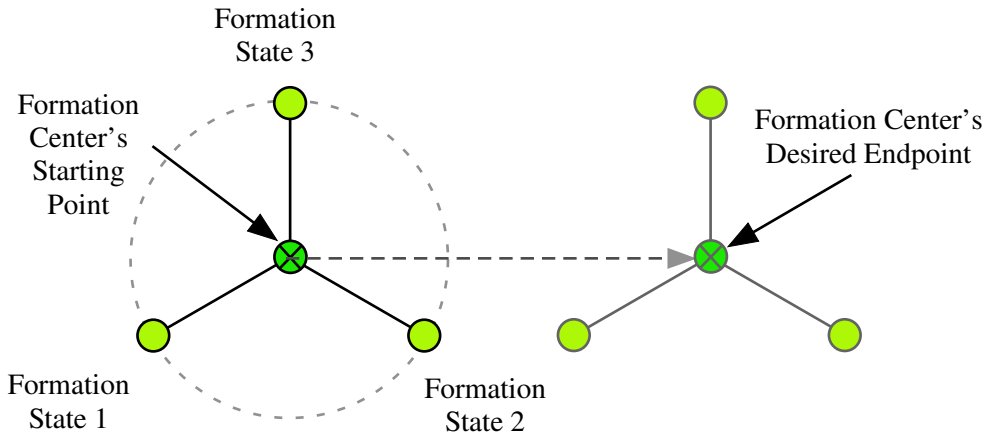

Figure 116: Formation States for Straight-Line Maneuver.

4.6 Investigated Motions

Two types of motions were used to evaluate the effect of input shaping on a virtual-structure architecture: straight-line motion and circular motion. For both of these motions, the satellite formation is composed of three satellites. Each of the satellites has a flexible appendage and is modeled using the equations of motion developed in Chapter 2.

4.6.1 Initialization

During the initialization phase, the formation frame and the satellites converge from their starting locations to the desired initialization position and orientation. The desired location for each satellite on the virtual structure is determined by their satellite number (1,2 or 3) and the corresponding formation number on the rigid body. Both the satellites and the formation's center are given their desired position and orientation directly from the formation supervisor. They converge to their desired ending states independent of one another.

4.6.2 General Motion: Straight-Line Maneuver

For this motion, the formation states maintain a fixed relative position to the formation center. Next, the formation frame's center is given the step change in desired position as shown in Figure 116. As the center of the formation converges to its desired location, the desired trajectories for each of the satellites is generated by its corresponding formation

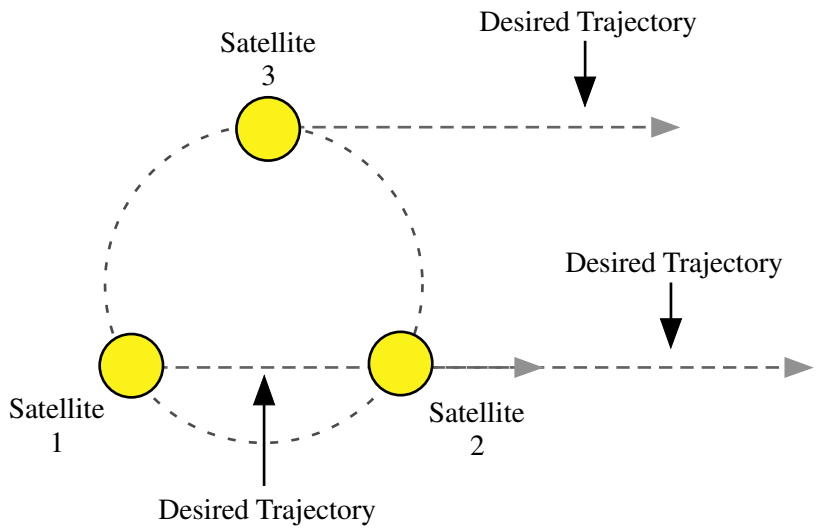

Figure 117: Straight-Line Maneuver.

state. For example, the desired trajectory for the first satellite is generated by the response of the second formation state. The first formation state represents the formation's center point. Once the desired trajectory for each of the satellites is generated, the satellites move along their desired trajectory as shown in Figure 117.

4.6.3 General Motion: Circle Maneuver

The second type of maneuver performed by the virtual-structure satellites was a circular maneuver. For this type of general motion, the formation states maintain fixed positions relative to the formation's center point. The formation's center does not translate, it simply rotates about its axis. The desired rotation angle for the center's formation is given as a step change as shown in Figure 118. As with the straight-line maneuvers, the responses of the formation states are set as the desired trajectories for the satellites as shown in Figure 119. In addition to moving in a circle, the satellites are able to rotate about a body fixed axis. The desired trajectory for this motion is also generated by the convergence of the formation states. The next sections discuss the simulation results for the straight-line and circular motions.

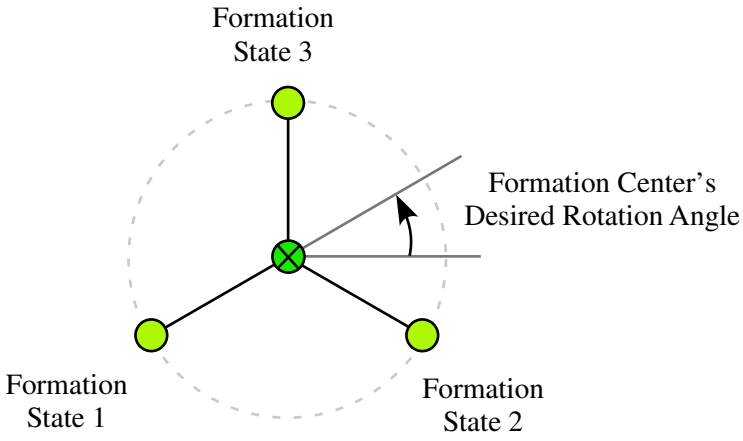

Figure 118: Formation Frame Circular Motion.

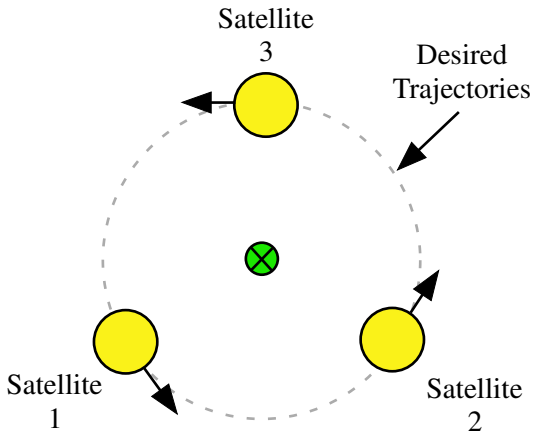

Figure 119: Desired Satellite Trajectories for a Circular Maneuver.

4.7 Simulation Results: Supervisor Level Input Shaping

The formation architecture employs centralized control, and the desired motion for each of the satellites comes from the formation supervisor directly. The virtual-structure formation flying architecture, uses two sets of feedback controller gains. The first set of controller gains governs the response of the formation states. The second set of controller gains governs the response of the satellites.

The choice of gains for the formation frame is very important since its response ultimately determines the satellites' desired trajectories. Figure 120 shows the response of the formation center for different feedback controller gains. If the derivative gains are too low, as is the case when $K_p = 10$ and K_d=0, then the formation frame's response will have

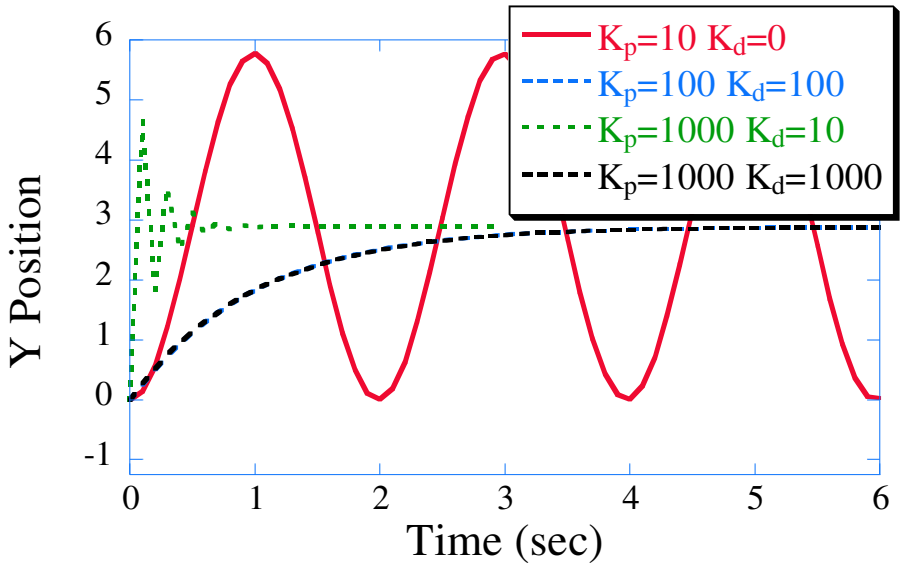

Figure 120: Controller Gains for Formation States.

large oscillations. Derivative gains of zero are not acceptable since the vibration of the formation states would continue indefinitely. If the proportional gains are too high, as is the case when $K_p = 1000$ and $K_d = 10$, the response has a large peak overshoot which may be unacceptable. Although this set of gains provides the fastest settling time, it is not desirable to have any oscillation. The desired changes in the formation frame are given as step changes; consequently, it is important to pick gains that provide a good response to step changes. The desired step response is smooth with little or no oscillations, yet has a reasonable settling time. There are two responses shown in Figure 120 that match these criteria: $K_p = 100$, $K_d = 100$ and $K_p = 1000$, $K_d = 1000$. Both of these responses have no oscillation. However, they both have much longer selling times compared to $K_p = 1000$, $K_d = 10$. The formation frame controller gains used are

$$K_p = 100 \tag{80}$$

$$K_d = 100 \tag{81}$$

$$K_\theta = 100 \tag{82}$$

$$K_{\dot{\theta}} = 100 \tag{83}$$

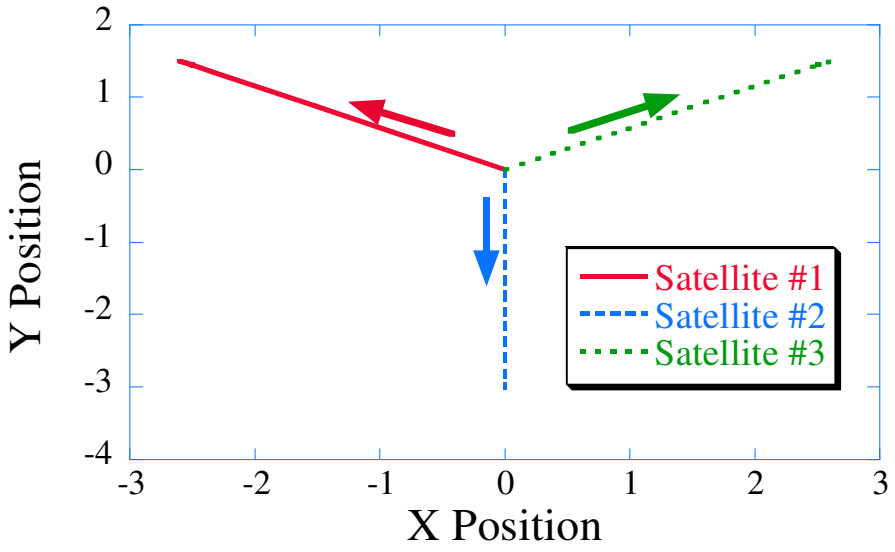

Figure 121: Initialization of Formation.

The formation frame feedback controller gains given in (80)-(83) provide a smooth continuous trajectory for the satellites. Once the formation states have settled to their desired final states, input shaping can be utilized. For input shaping applied at the supervisor level, the same input shaper is used for all of the trajectories. After the new shaped trajectories are generated, they are passed from the supervisor to the corresponding satellite. A 1.0 Hz ZV and ZVD input shaper was used to generate the desired satellites' trajectories.

4.7.1 Initialization

This section discusses the effect input shaping has on the initialization portion of the desired maneuver. Figure 121 shows the main satellite body position responses for the three satellites. For this case, all three satellites start at the origin and move to their desired positions. The satellites form an equilateral triangle whose center is located at the origin. Figure 121 shows the spring angle responses for each satellite. The spring angle responses for the first and third satellites are similar. This is because their desired maneuvers are mirror images of one another (about the y axis). The second satellite has the largest spring angle deflection. The starting configuration for the satellites is such that they are oriented at 0° with respect to the x axis. That is, the flexible appendage is parallel to the x axis and the desired motion of the second satellite is in the negative y direction. A motion

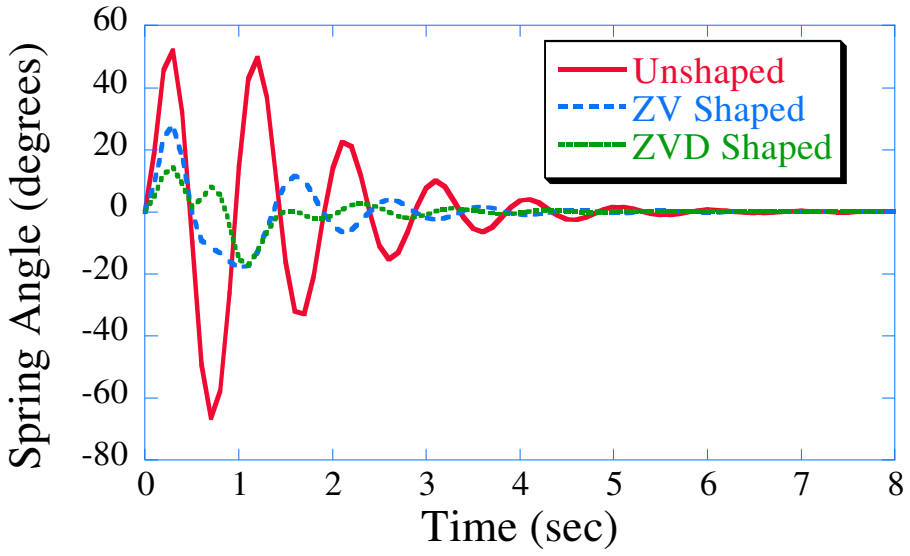

Figure 122: Spring Angle Response for Satellite #2.

that is perpendicular to the orientation of the flexible arm produces the largest amount of deflection (as seen in the figure).

Figure 122 compares the unshaped and shaped spring angle responses for the second satellite. Using a shaped trajectory reduces the amount of vibration in the flexible appendage. The ZV shaped trajectory for the first satellite reduces the maximum spring angle approximately 56% and the ZVD shaped trajectory reduces the maximum spring angle approximately 74%. Figure 123 shows the spring angle response for the first satellite. The ZV shaped trajectory for the second satellite reduces the vibration 63% and ZVD shaped trajectory reduces the vibration 77%. The spring angle response for the third satellite is similar to the response of the first satellite.

The maximum spring angle of the flexible appendage is related to the required change in desired position. Figure 124 shows the relationship between starting position and spring angle response. For each of the responses shown in the figure, the endpoint was the same (-2.5, 1.44), but the starting position of the satellite was varied. As the difference between the starting and ending position increases, the amplitudes of the spring angle response also increase. Figure 125 shows the spring angle responses for different ending positions. Comparing Figure 124 and Figure 125, it is easy to see that even as the starting position

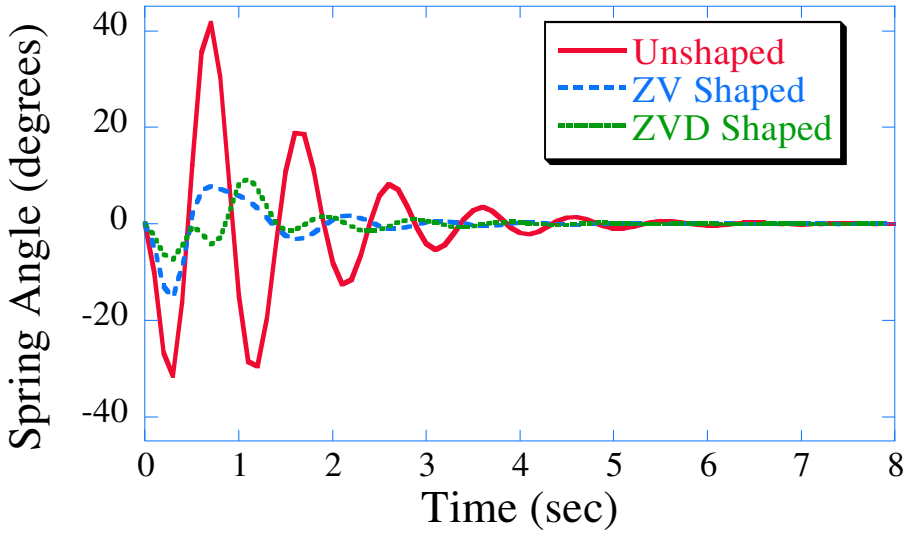

Figure 123: Spring Angle Response for Satellite #1.

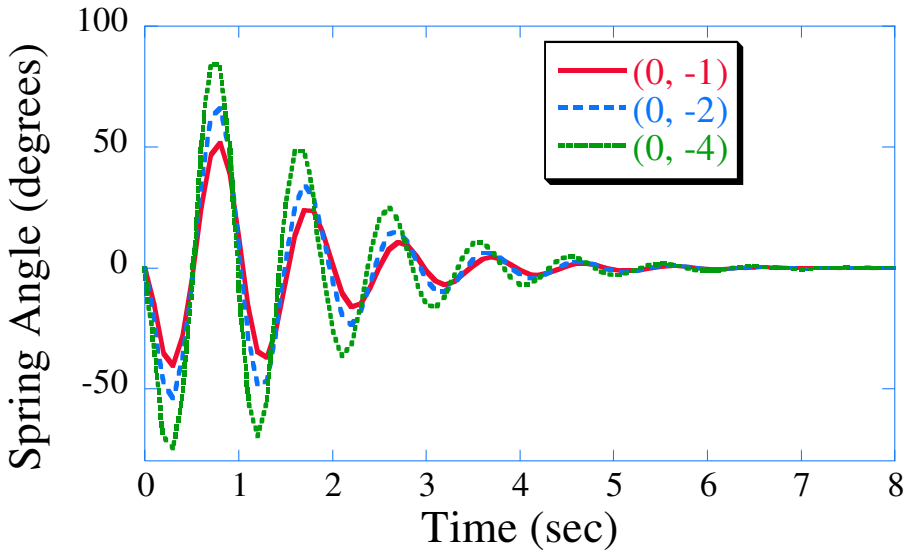

Figure 124: Spring Angle Response for Different Satellite #1 Starting Positions.

of the satellite changes, input shaping is still able to reduce the maximum amplitude of vibration. Using a ZVD input shaper further reduces the maximum vibration amplitude.

4.7.2 General Motion: Straight-Line Maneuver

The first general motion maneuver investigated was the straight-line maneuver. It was desired that the satellites maintain the triangular shape and move together in a straight

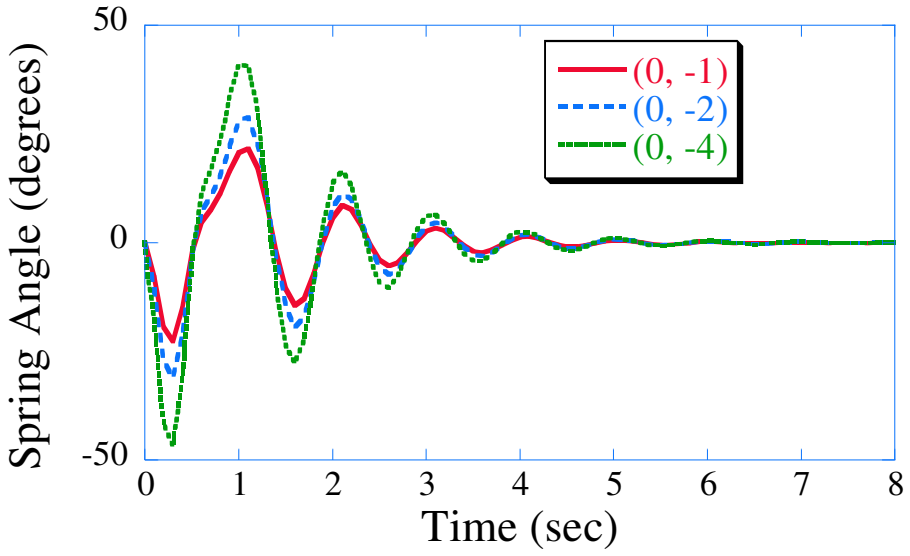

Figure 125: Spring Angle Response for Different Satellite Starting Positions Using ZV Shaped Steps.

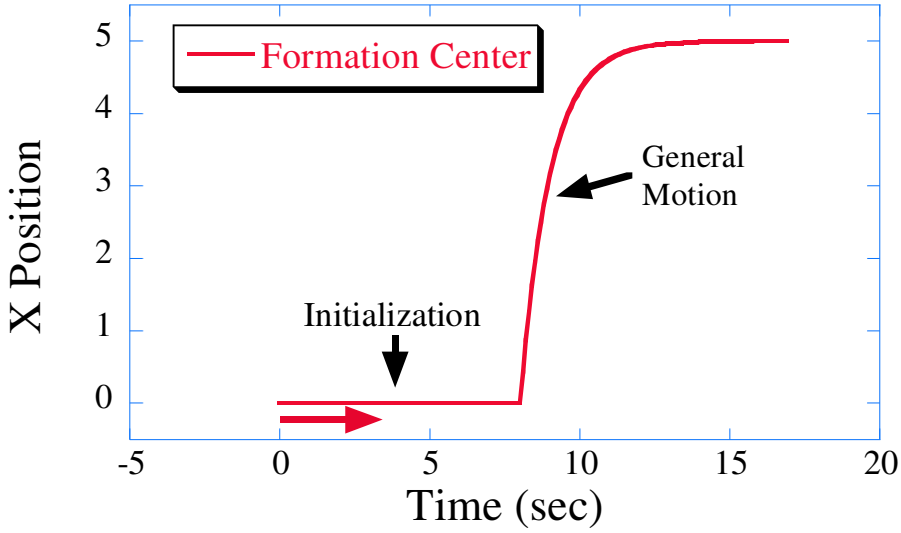

Figure 126: X Position of Formation States Versus Time.

line. All of the formation states, including the center point, start at a position of (0,0). The response of the formation center is Figure 126. During the initialization portion of the maneuver, the formation center does not move. During this time, the formation states shown in Figure 127 converge to the desired setpoints ($t = 0 - 8$ seconds). The position of the formation states is relative to the body fixed coordinate system attached to the formation's

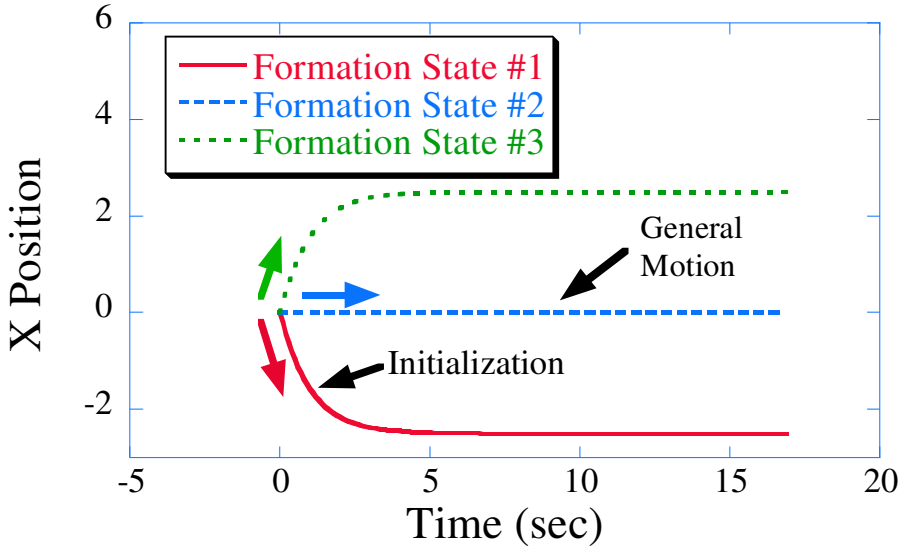

Figure 127: X Position of Formation States Relative to Body Fixed Frame.

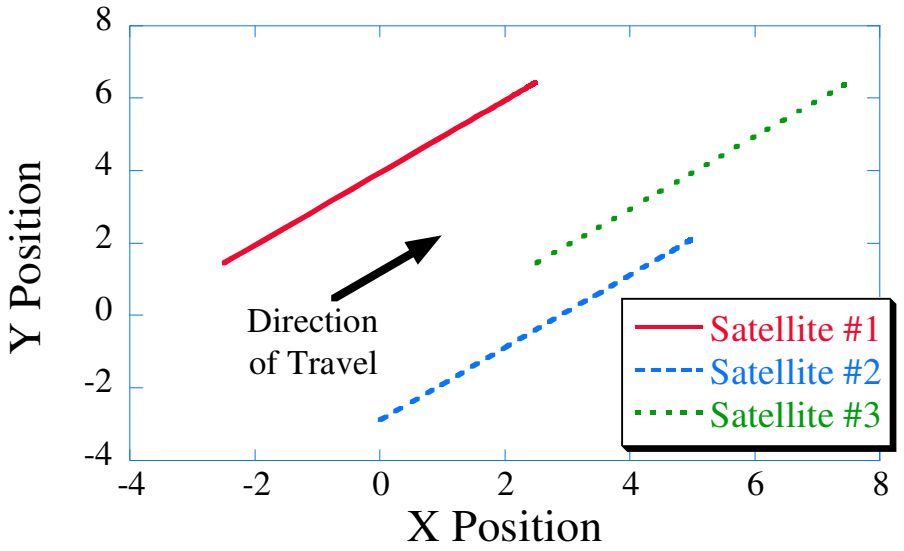

Figure 128: Straight-Line Maneuver.

center. At this time, the center of the formation begins the straight-line motion and moves from the origin to the desired position of (5,5). As the center moves, the formation states remain at their body fixed locations.

The response of the formation states is with respect to the formation frame, and when transformed to the inertial frame, generate the trajectories for the satellites. Figure 128 shows the response of the main satellite bodies.

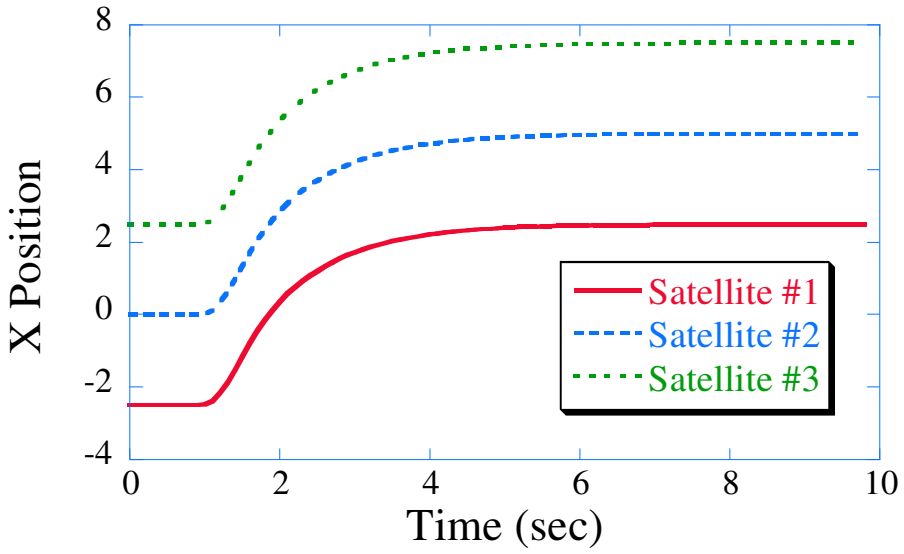

Figure 129: X Position of the Formation Versus Time.

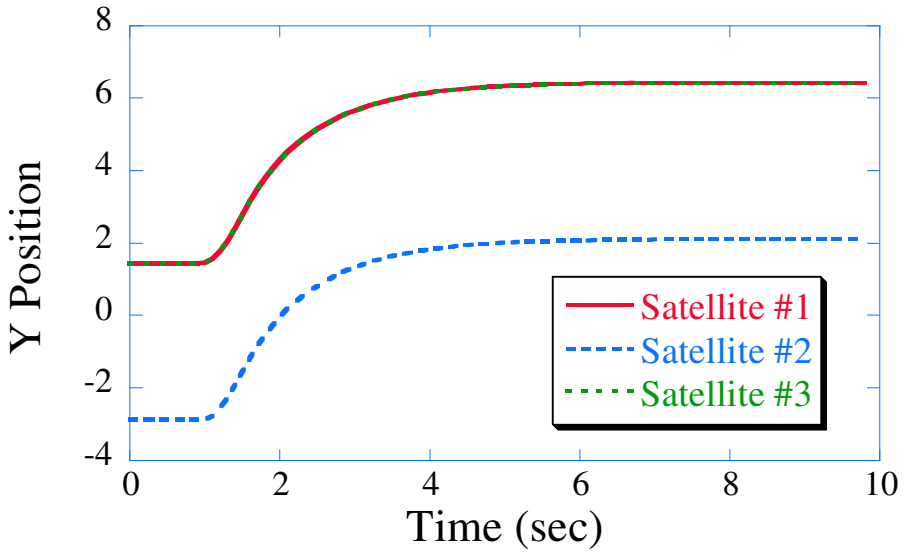

Figure 130: Y Position of the Formation Versus Time.

Figure 129 and Figure 130 show the responses of main satellite bodies versus time. Because the satellites start in the desired triangular configuration, they do not move during the initialization portion of the maneuver. As seen from the figures, the satellites are able to follow the desired trajectory and have a smooth response.

The trajectories generated from the formation states are convolved with an input shaper and form the desired shaped trajectories. Figure 131 shows the unshaped and shaped x

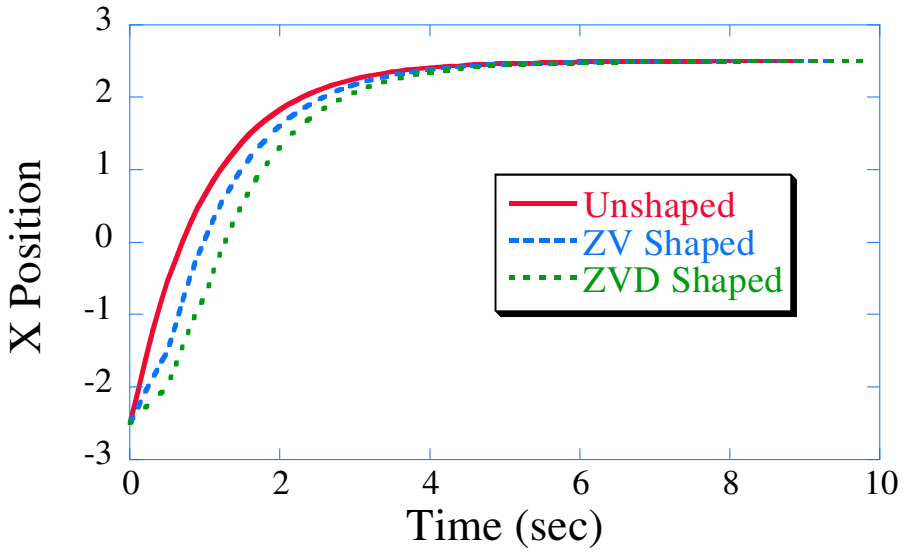

Figure 131: Unshaped and Shaped X Trajectory for Satellite #1.

trajectory of the first satellite. From the graph, it is apparent that the shaped trajectories lag the unshaped trajectory. The delay between the unshaped and shaped curves is not constant.

In order to determine the relationship between the unshaped and shaped trajectories, a series of simulations was completed. The desired end position of the formation center changed; however, it was only varied in the y direction. The position difference between the unshaped and ZV shaped desired trajectories for the first satellite was calculated as a function of time and is shown in Figure 132. As seen from the figure, the difference between the unshaped and shaped trajectories depends on the magnitude of the formation center's desired step change. As the distance the formation center travels increases, the difference between the unshaped and shaped trajectories also increases. The response of the formation states depends on this distance. The maximum difference between the unshaped and ZV shaped trajectories occurs at $t = 0.5$ seconds which corresponds to the duration of the 1.0 Hz ZV shaper. The 1.0 Hz ZVD shaper has a duration of 1.0 seconds. Figure 133 shows the difference between the unshaped and ZVD shaped trajectories versus time for the same maneuvers completed in Figure 132. The maximum difference for the ZVD shaped trajectories occurs at $t = 0.5$ seconds, which corresponds to the shaper's second impulse

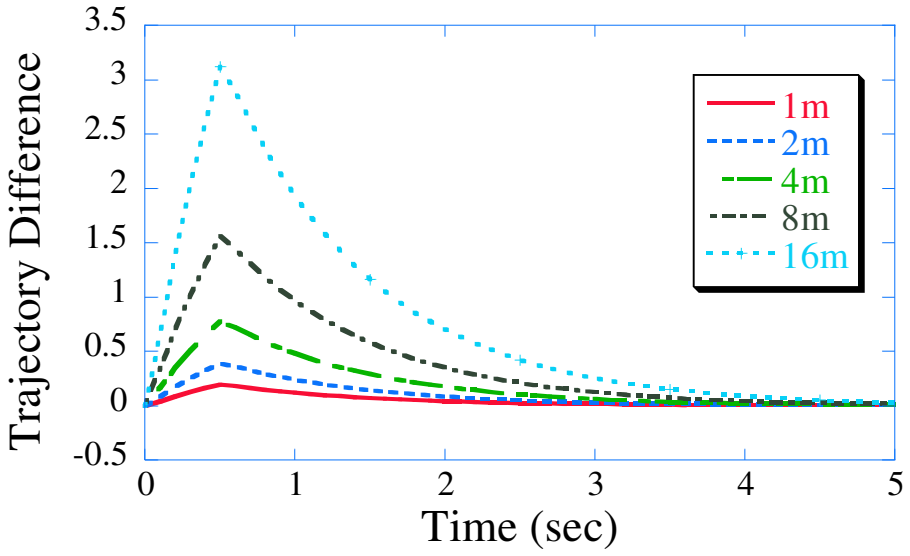

Figure 132: Position Difference Between Unshaped and ZV Shaped Trajectories.

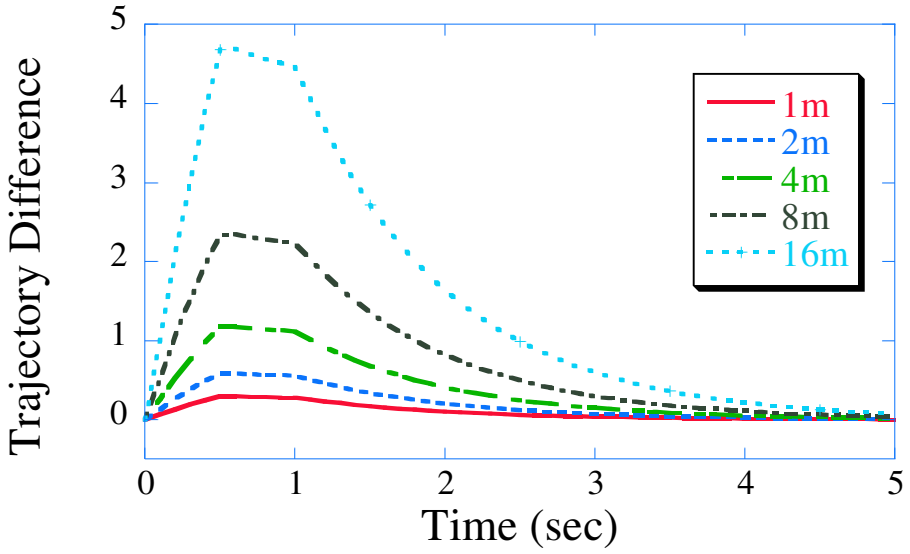

Figure 133: Position Difference Between Unshaped and ZVD Shaped Trajectories.

time location. In addition to increasing the maximum difference, the width of the peak increases. The difference between the unshaped and shaped trajectories decreases rapidly after the time of the third and final impulse (corresponding to $t = 1.0$ seconds). The delay between the unshaped and shaped trajectories is not constant, and it is impossible to align the unshaped and shaped trajectories.

Although the temporal tracking of the formation is important, the spatial tracking is

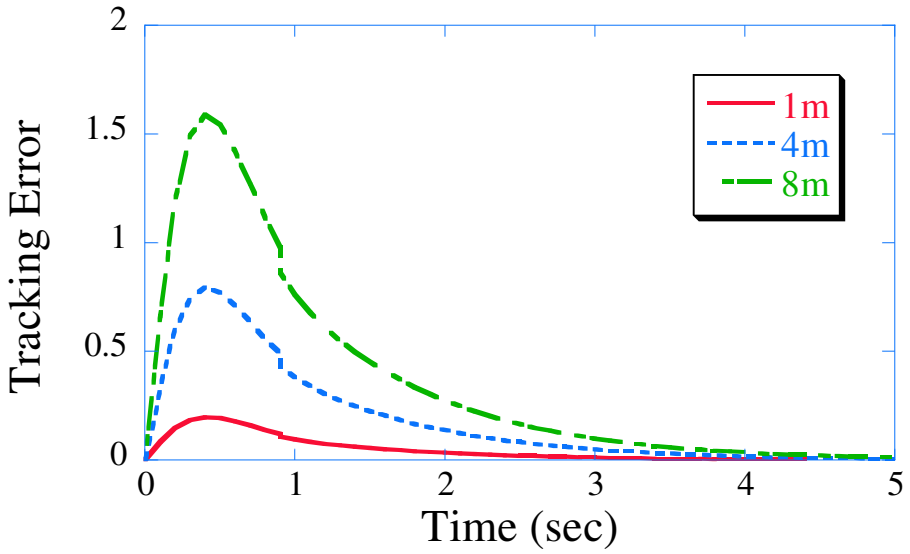

Figure 134: Tracking Error for Unshaped Straight-Line Maneuvers.

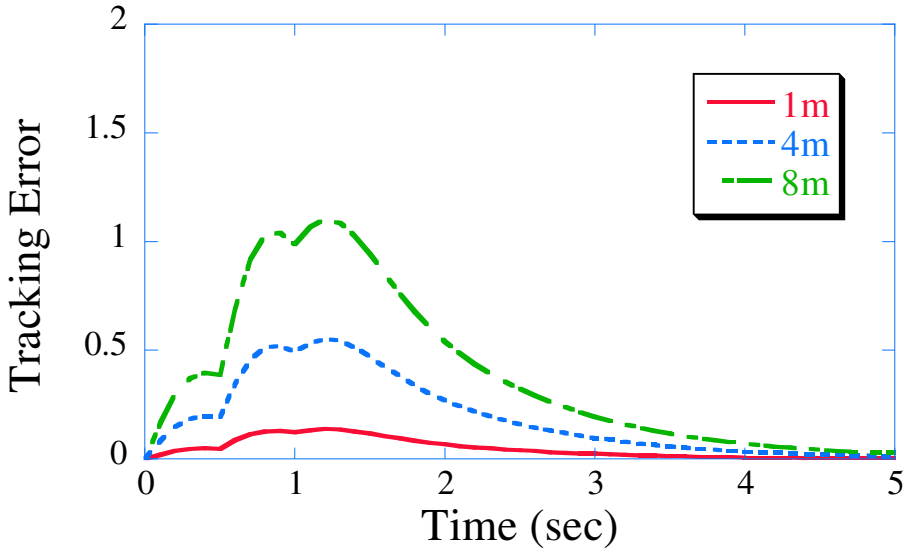

Figure 135: Tracking Error for ZVD Shaped Straight-Line Maneuvers.

also important. Figure 134 shows the trajectory tracking error of the first satellite for a series of vertical maneuvers. The vertical straight-line maneuver was chosen since it causes the maximum amount of deflection in the flexible appendage when it is oriented horizontally. As the maneuver distance increases, the tracking error also increases. Figure 135 shows the ZVD shaped trajectory tracking error. Comparing Figure 134 and Figure 135 it is clear that input shaping reduces the maximum tracking error. The tendency for input shaping is

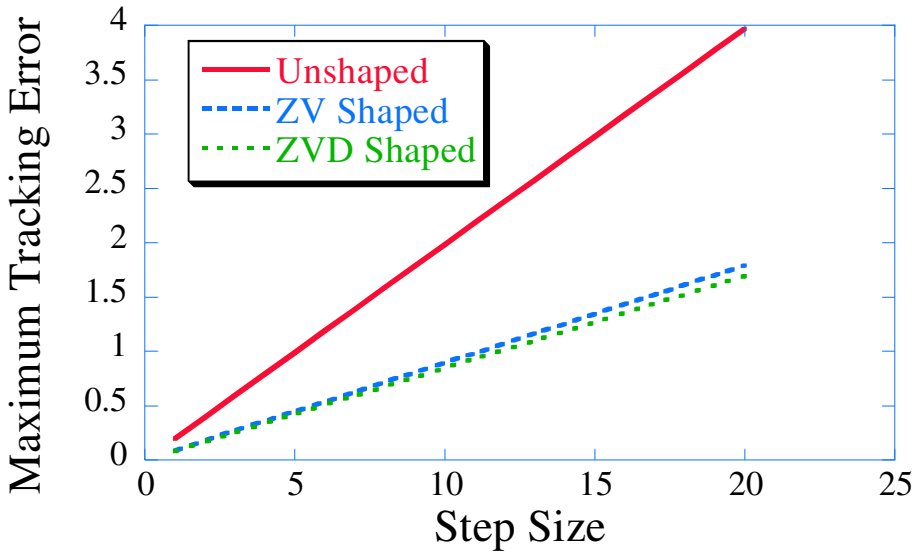

Figure 136: Maximum Trajectory Tracking Error Versus Formation Center Ending Locations.

to shift the tracking error peak to the right, but to lower the amplitude. Figure 136 shows the maximum tracking error versus the step change in the formation center's y position. As the desired ending location for the formation center increases, the maximum trajectory tracking error also increases. However, input shaping the desired trajectories decreases the maximum trajectory tracking errors. For a desired formation center step change of 20 units, the ZV shaped trajectory decreases the maximum tracking error 55% and the ZVD shaped trajectory reduces the maximum tracking error 57%. Both input shaped trajectories decrease the maximum tracking error by more than 50%. This reduction is constant over the range of move distances examined.

Figure 137 shows the spring angle response for the 1.0 m shaped and unshaped straight-line motions. The ZV shaped trajectory reduces the maximum spring angle deflection 51% and the ZVD shaped trajectory reduces the maximum spring angle approximately 75%. Figure 138 shows the maximum spring angle deflection for various formation center step changes. The satellites were oriented with the flexible appendage initially parallel to the x axis and the step change was given in the y direction only. This is the worst possible case for exciting vibration in the flexible appendage. As the desired endpoint increases, the maximum spring angle for both the unshaped and shaped cases also increases. The ZV and

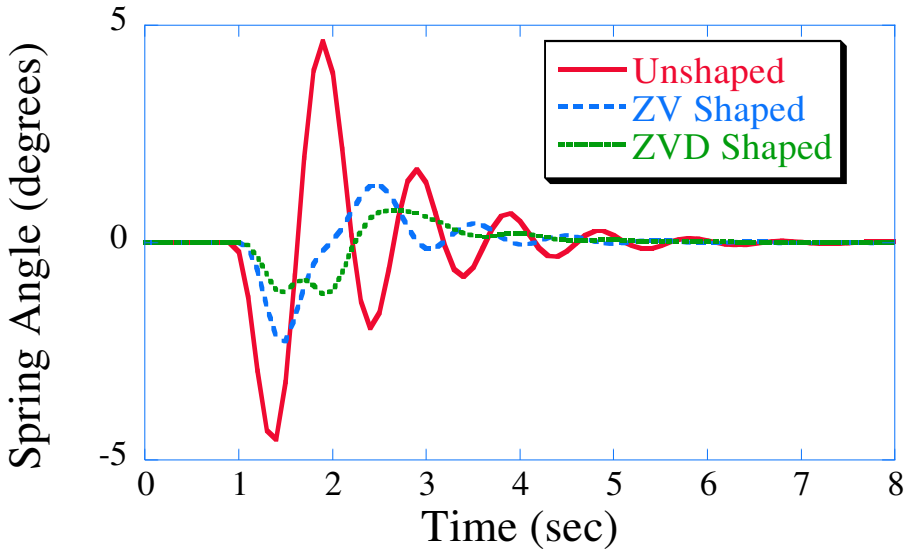

Figure 137: Satellite #1 Spring Angle Response to Straight-Line Maneuver.

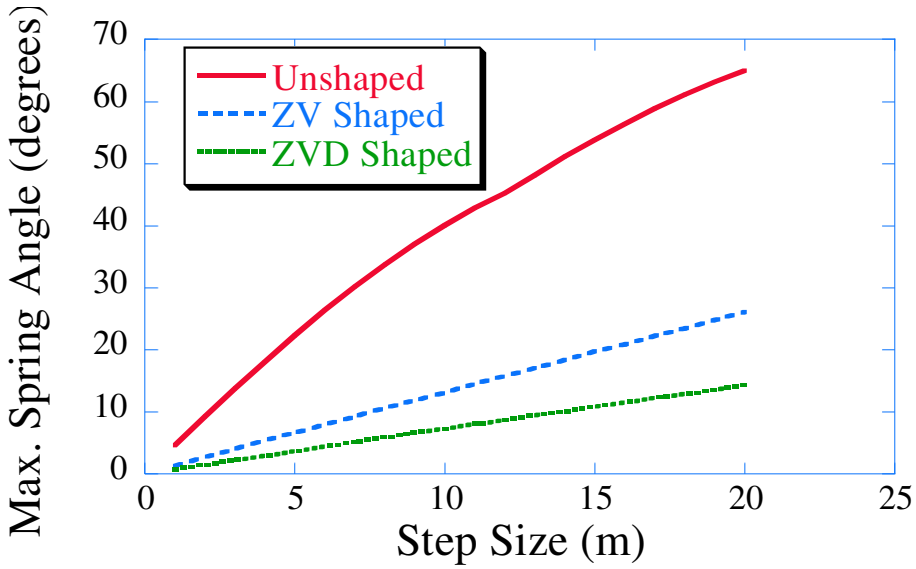

Figure 138: Maximum Spring Angle Deflection Versus Formation Center Move Distance.

ZVD shaped trajectories significantly reduce the maximum spring angle for the entire range of move distances. For a desired step change of 20 units in the y direction, the ZVD shaped trajectory reduces the maximum spring angle from 45° to 14° (a 69% reduction). The ZV shaped trajectory reduces the maximum spring angle 42%.

The benefits of using input shaping are apparent for straight-line maneuvers. Although it is not possible for the unshaped and shaped maneuvers to align temporally, the vibration

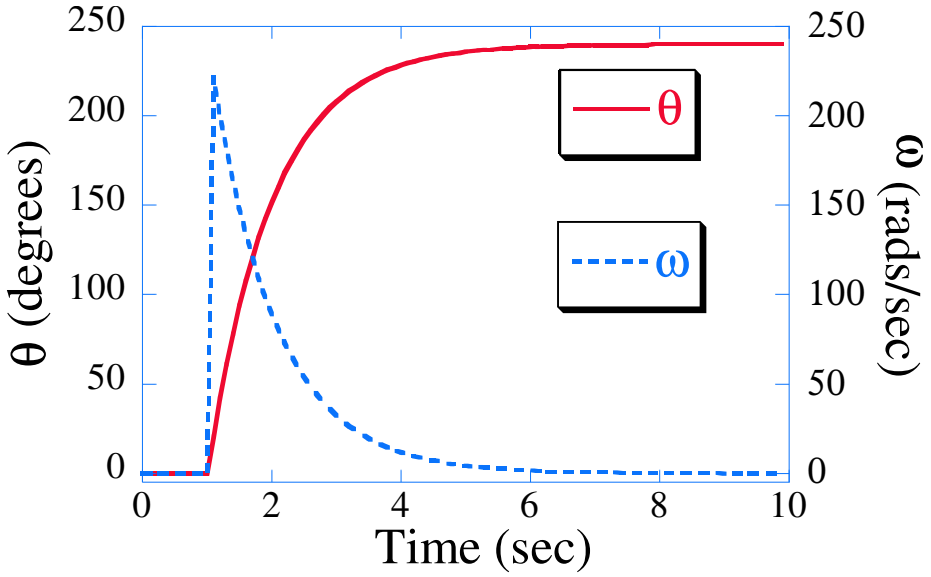

Figure 139: Rotation Angle and Angular Velocity for 240° Maneuver.

reduction benefits are overwhelming. Both the maximum tracking error and the maximum spring angle deflection are significantly reduced. The next type of maneuver investigated was a circle maneuver and the simulation results are discussed in the next section.

4.7.3 General Motion: Circle Maneuver

For the circular motion investigated, the position of the formation center remains fixed, and the entire formation rotates about the center point. The position of the virtual satellites, or formation states, remains fixed relative to the formation's center, so as the center rotates, the virtual satellites sweep out circular trajectories. If the position of the formation states varies during the maneuver, then spiral trajectories are created.

4.7.3.1 Varying ω

This section discusses the effect of input shaping on the circular trajectory whose rotation rate, ω, varies. For this motion, the formation's center is given a desired step change in rotation angle. Because a step change in rotation angle is commanded, the frequency of formation rotation is not constant. Figure 139 shows the response of the rotation angle, θ, and the angular velocity, ω, of the formation's center for a 240° rotation. The response shown in Figure 139 is similar to the straight-line maneuver responses discussed in the previous

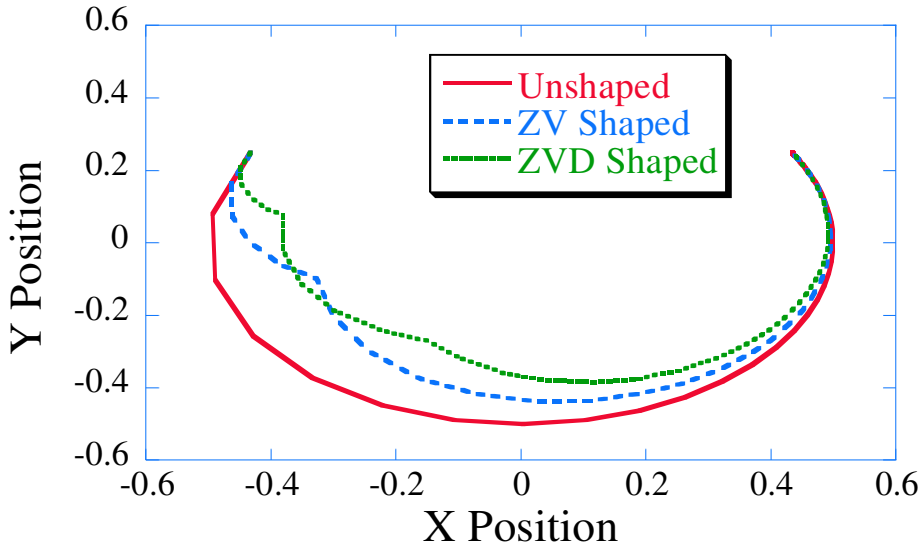

Figure 140: Desired Trajectories for Satellite #1.

section. Step changes in position or rotation produce similar response characteristics.

Figure 140 shows the unshaped and shaped trajectories for the first satellite. The satellite starts at the initial position of (-.433, 0.25) and moves counterclockwise until it reaches the final position of (.433, 0.25). Unlike the circular motion trajectories discussed in Chapter 3, shaping these formation state generated trajectories does not produce a circular trajectories. Instead, a spiral trajectory is produced as shown in Figure 141. This figure shows the trajectory's radius of curvature for the maneuver as a function of time. The unshaped trajectory remains at the desired radius of 0.5 m for the entire maneuver, whereas the radius of the shaped trajectory deviates significantly. The ZV shaped trajectory has a minimum radius of 0.34m, and the ZVD shaped trajectory has a minimum radius of 0.30m. The satellite starts out at the desired formation radius of 0.5 m, and as time progresses, the satellite moves inward and then back out to the desired setpoint. Instead of completing a circular maneuver, the satellite completes two spirals. At the end of the maneuver, all of the satellites converge back to the desired formation radius of 0.5 m. Because all of the satellites' desired trajectories are shaped using the same shaper, the effect is the same on all the satellites. That is, the satellites maintain a triangular shape. The distance between the satellites changes as the satellites follow the shaped trajectories. The percent the shaped

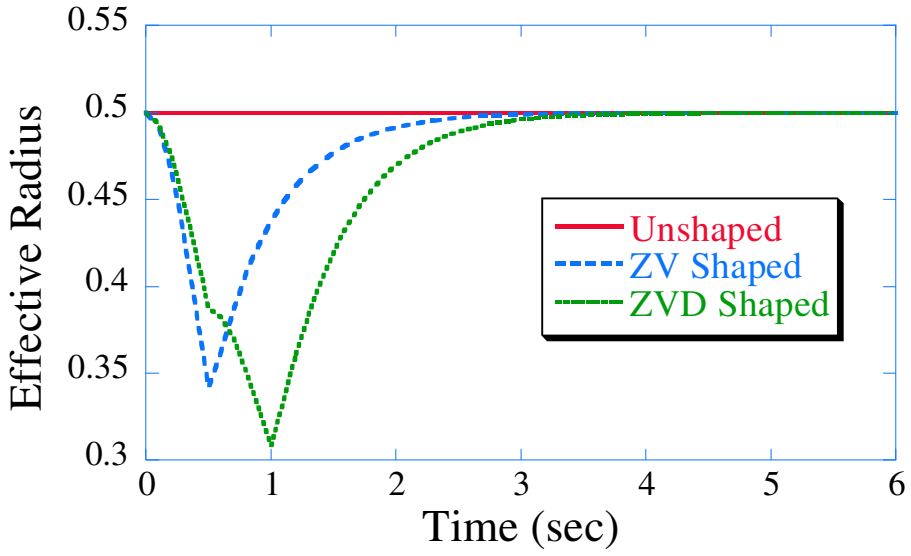

Figure 141: Effective Maneuver Radius for Satellite #1.

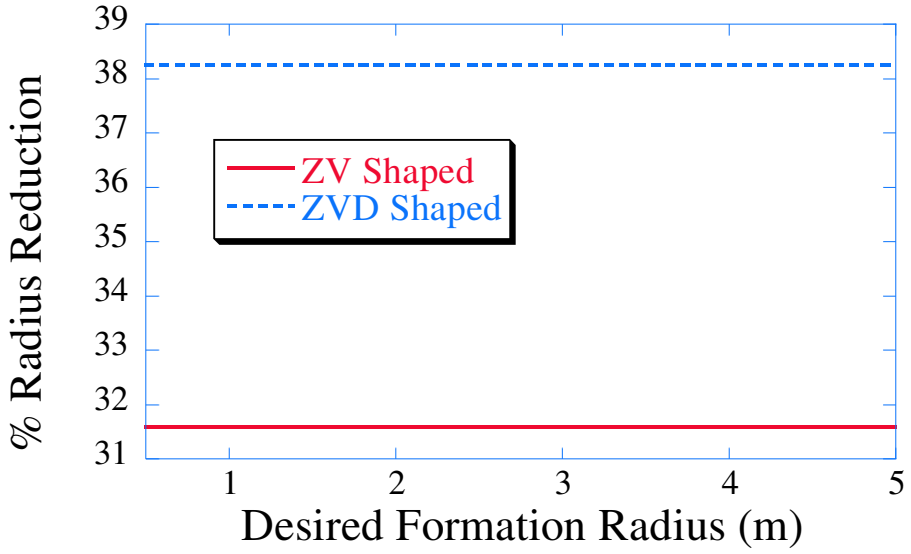

Figure 142: Percent Reduction in Desired Formation Radius.

trajectory's radius of curvature decreases is constant. Figure 142 plots the percent reduction versus desired formation radius. Using a ZV shaper to generate the desired trajectories will cause a 32% reduction in the radius of curvature, and the ZVD shaper will cause a 38% reduction.

For the straight-line maneuvers, it is impossible to temporally align the shaped trajectories to the unshaped trajectory. The same holds true for the circular maneuvers that

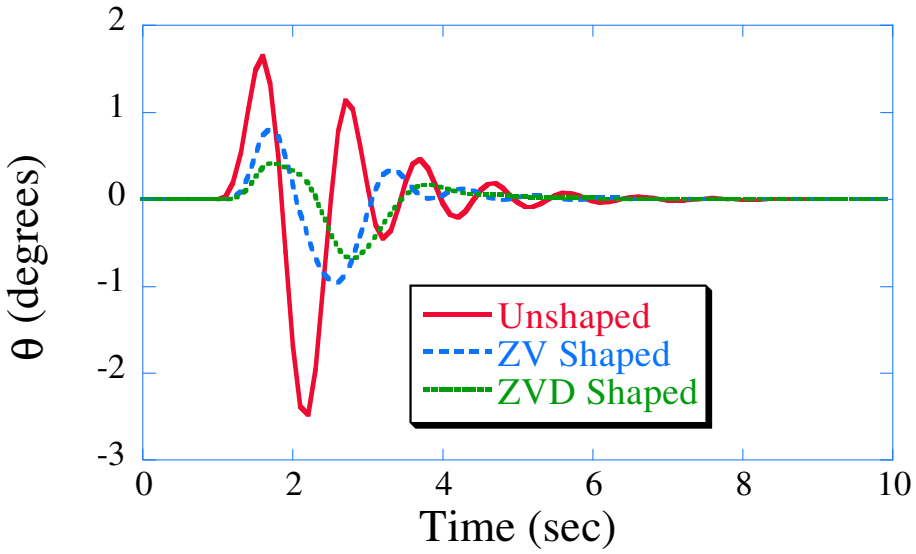

Figure 143: Main Satellite Body Response to 240° Rotation.

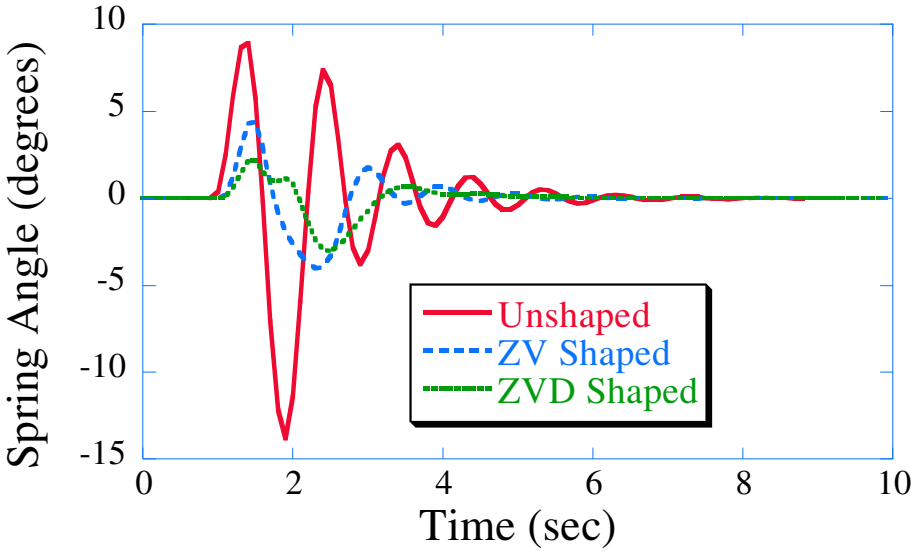

Figure 144: Spring Angle Response of Satellite #1.

are generated from a single step change. Both the desired trajectories are generated the same way. The benefit of shaping the trajectories is evident in the reduction of vibration in the main satellite body and flexible appendage. Figure 143 shows the main satellite body response for the first satellite. Figure 144 shows the response of spring angle of the first satellite for the 240° maneuver. Shaping the trajectory reduces the maximum spring angle deflection of the satellite and decreases the settling time. As the desired formation

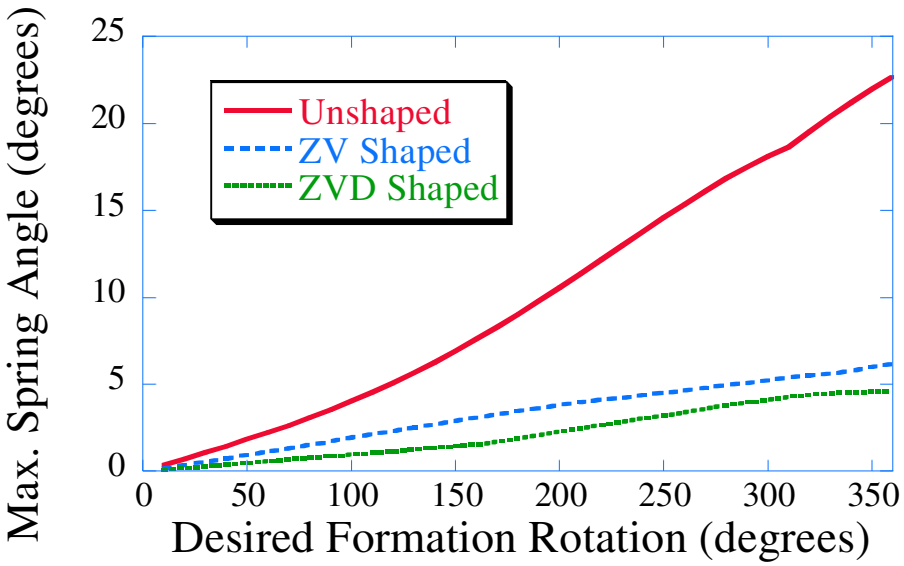

Figure 145: Maximum Spring Angle Deflection versus Desired Formation Rotation.

angle of rotation increases, the maximum spring angle deflection also increases. However, shaping the satellites' trajectories decreases the maximum spring angle when compared to the unshaped maximum as shown in Figure 145.

4.7.3.2 Constant ω

In the previous section, the trajectories of the satellites were formulated by commanding a single step change in the desired formation rotation angle. This led to a varying formation frequency, ω. To generate trajectories that have a constant formation rotation frequency, the desired rotation of the formation's center is specified as a continuous function. This is the case for the maneuvers discussed in this section. Attitude control for the satellites is also employed, and the satellites' flexible arms point radially outwards for the entire maneuver. Figure 146 shows the desired configuration for the formation satellites.

The period of the circular rotation is 30 seconds. This corresponds to $\omega = 0.2094\frac{rads}{sec}$. During the initialization phase, the satellites orient themselves to the desired starting angle. Their position does not change, only the orientation of the flexible appendage changes. Once the satellites complete the initialization phase, the general motion of maintaining $\omega = 0.2094\frac{rads}{sec}$ begins. Figure 147 shows the formation center's rotation angle as a function

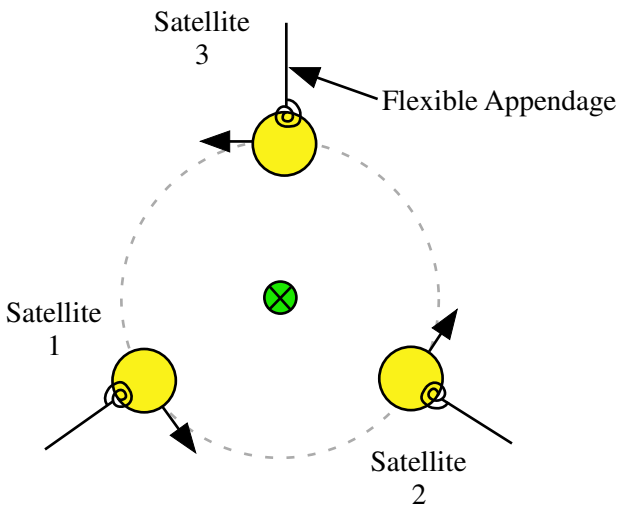

Figure 146: Desired Configuration of Formation Satellites.

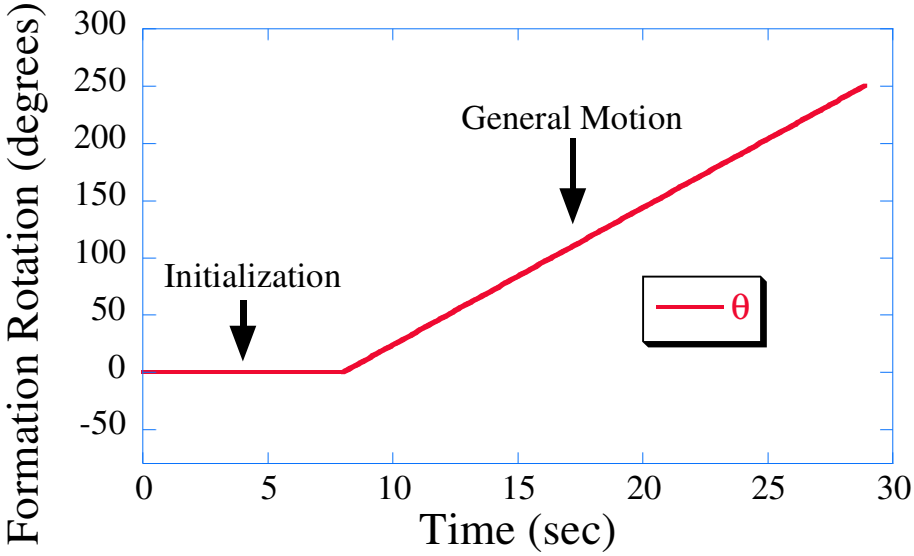

Figure 147: Formation Center's Rotation Response.

of time. During the initialization portion of the maneuver, the formation states representing the virtual satellites converge to the desired triangular shape and desired orientation. During the general motion portion of the maneuver, the formation center rotates about its center at the desired angular velocity until it reaches 240°.

Figure 148 shows the responses of the main satellite bodies. The satellites start at the indicated starting positions and move counter-clockwise around the center of the formation. Figure 149 shows the attitude response for each of the satellites. The desired satellite

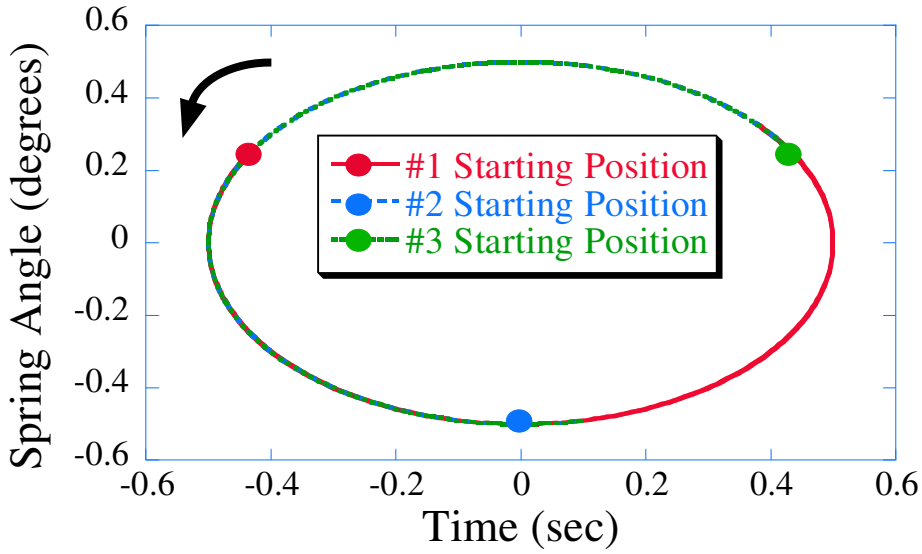

Figure 148: Main Satellite Body Response to Constant ω Maneuver.

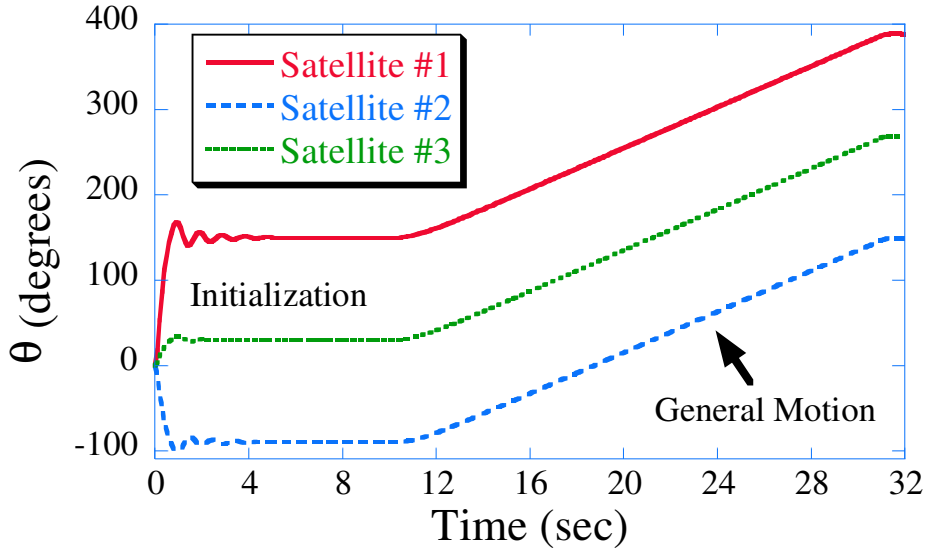

Figure 149: Main Satellite Rotation Angle (θ).

attitude of the satellites is for each flexible appendage to point radially outward throughout the entire maneuver. During the initialization portion of the maneuver, the first and third satellites have some oscillation in the satellites' attitude angle, θ, due to the high step change in desired attitude. During the general motion portion of the maneuver, the satellites' desired trajectories are smooth, and the response is oscillation free.

Input shaping a circular trajectory decreases the effective radius. The radial shortening

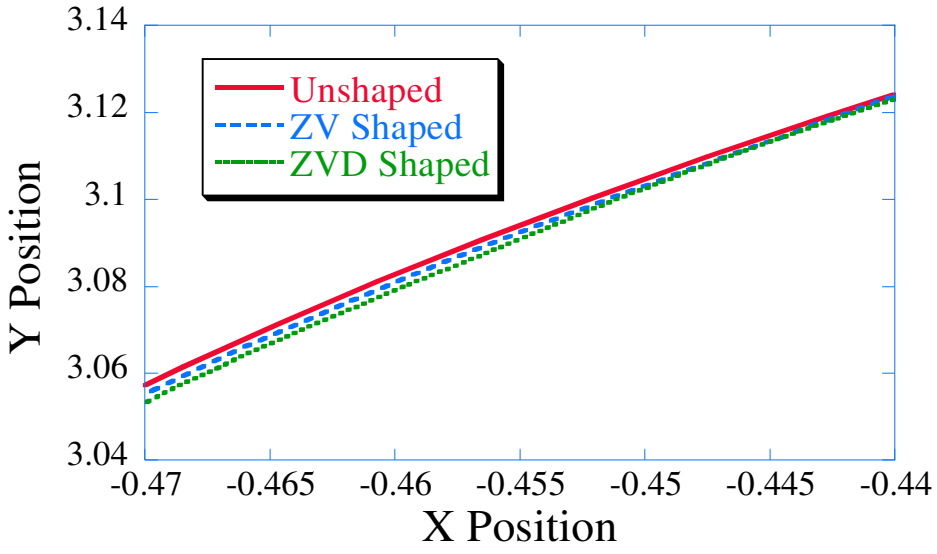

Figure 150: Desired Trajectory for Satellite #1.

effect from input shaping can be seen in Figure 150. The starting position of the first satellite is in the upper right portion of the graph. The satellite moves down and left. As seen in the figure, the ZV and ZVD shaped trajectories diverge from the unshaped trajectory. They still follow a circular path, but it has a smaller radius. The differences between the unshaped and shaped trajectories is very small.

Figure 151 shows the spring angle response for the first satellite during the initialization portion of the maneuver. The input shaped trajectories decrease the maximum spring angle. The ZV shaped trajectory provides a 57% reduction and the ZVD shaped trajectory provides a 74% reduction in the maximum spring angle. Figure 152 shows the spring angle response during the first portion of the general motion. The time was normalized so that the general motion for each trajectory started at $t = 0$.

One of the benefits of input shaping is that the time it takes for the system to settle to the desired setpoint decreases. Many times, the formation following the shaped trajectories can begin the generalized motion portion of the maneuver before the unshaped system is able to. When general motion begins, the deflection of the spring is smaller in magnitude for both the unshaped and shaped trajectories. This is because the desired attitude change of the satellites is smaller than the step change commanded during the initialization. Figure

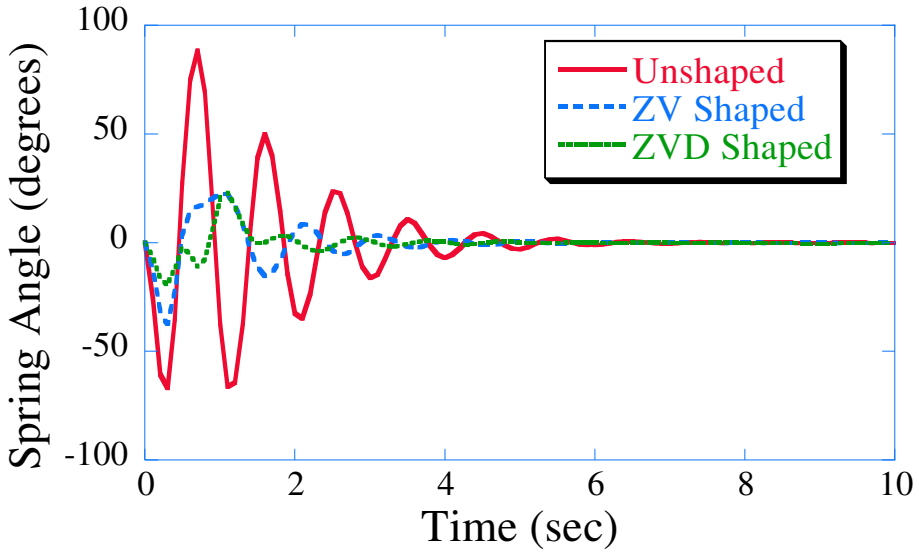

Figure 151: Spring Angle Response for Initialization Phase of Satellite #1.

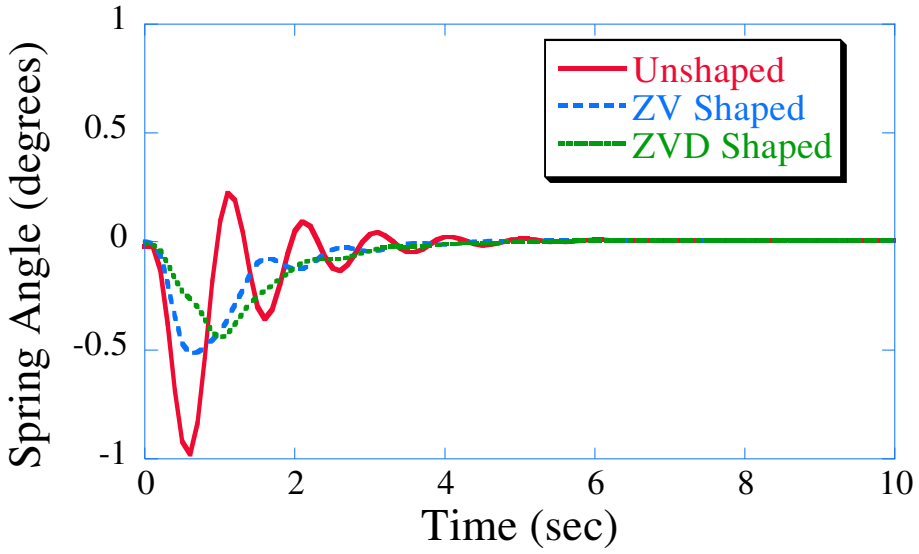

Figure 152: Spring Angle Response for General Motion Phase of Satellite #1.

152 shows the spring angle responses for the generalized motion. It is clear that shaping the trajectories reduces the maximum spring angle for a constant ω maneuver. The ZV shaped trajectory reduces the maximum spring angle 50% and the ZVD provides a reduction of 66%.

If the frequency of rotation is held constant at $\omega = 0.2094 \frac{rads}{sec}$ and the formation radius is increased, the maximum spring deflection increases. Figure 153 shows the linear relationship

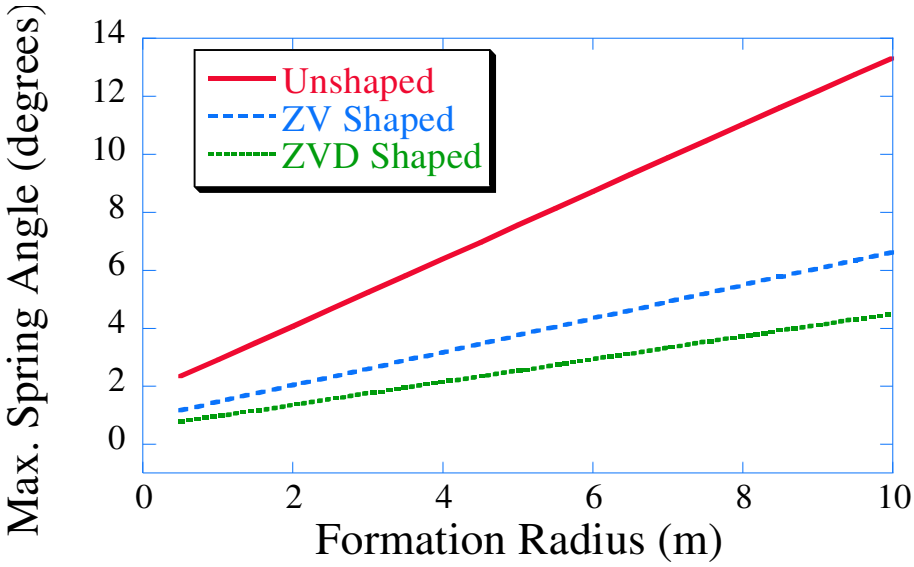

Figure 153: Maximum Spring Angle for Satellite #1 versus Formation Radius.

between the radial increase and the maximum spring deflection for the general motion circular maneuver. The maximum spring angle for the initialization is independent of the formation radius assuming the satellites start at their desired initial positions. The reduction the shaped trajectories provides is relatively constant for the entire range of formation radii studied. The ZV shaped trajectory provides a 50% reduction compared to the unshaped maximum spring angle. The ZVD shaped trajectory provides a 66% reduction. The maximum spring angle increases as the formation's radius increases because of the relationship between rotation frequency and speed shown below.

$$v = r \cdot \omega \tag{84}$$

From (84) it is clear that as the radius, r, increases, the speed, v must also increase when ω is constant. If the velocity of the satellites is held constant then ω must decrease as the radius increases. Figure 154 shows the effect of keeping the speed of the satellites constant while changing the formation's radius. As the radius of the formation increases, the maximum spring angle decreases for a constant satellite speed of $0.1047 \frac{m}{sec}$

The trajectories the satellites follow for the constant ω cases are generated from the formation states; however, the desired endpoint for the formation center is no longer one step change, but a series of small step changes. The size of the step change is a function

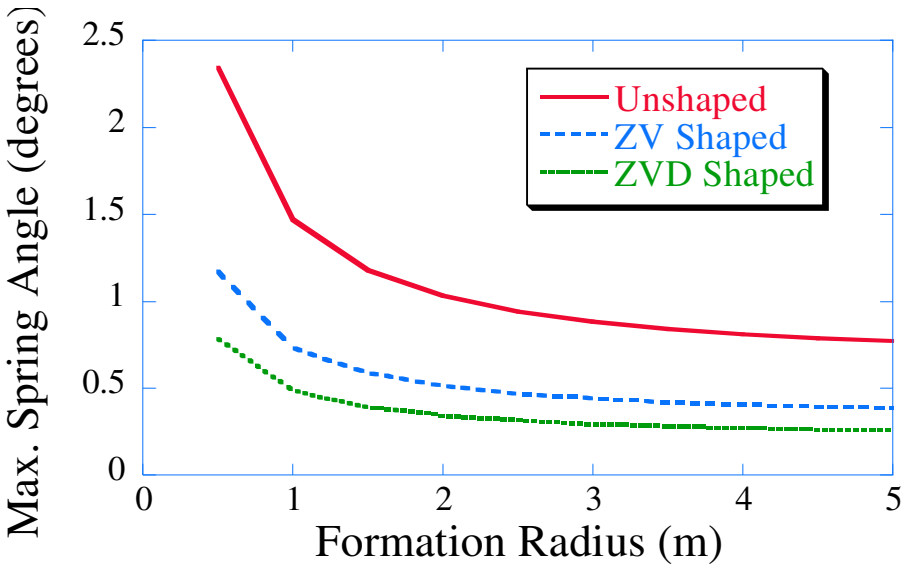

Figure 154: Maximum Spring Angle for Satellite #1 for $V = .1047\frac{m}{sec}$.

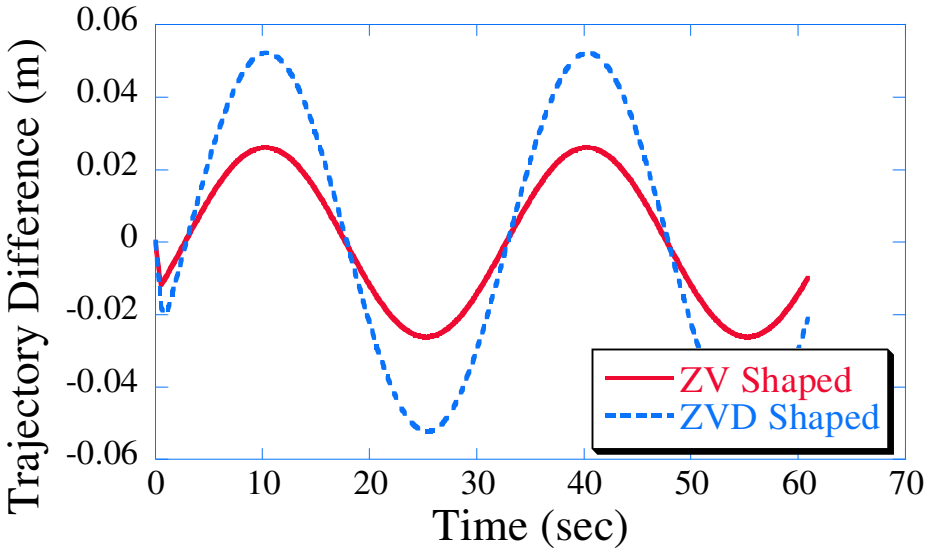

Figure 155: Temporal Position Difference For Constant ω Maneuver.

of the integration time-step: the smaller the time-step, the smaller the step change. By giving the formation center a series of small step changes, the frequency of the formation's rotation is constant. This affects the shape of the trajectories generated for the satellites. The position difference between the unshaped and shaped trajectories as a function of time is shown in Figure 155. The difference between the trajectories is sinusoidal and more closely resembles the trajectory differences for the leader-follower circular trajectories. If

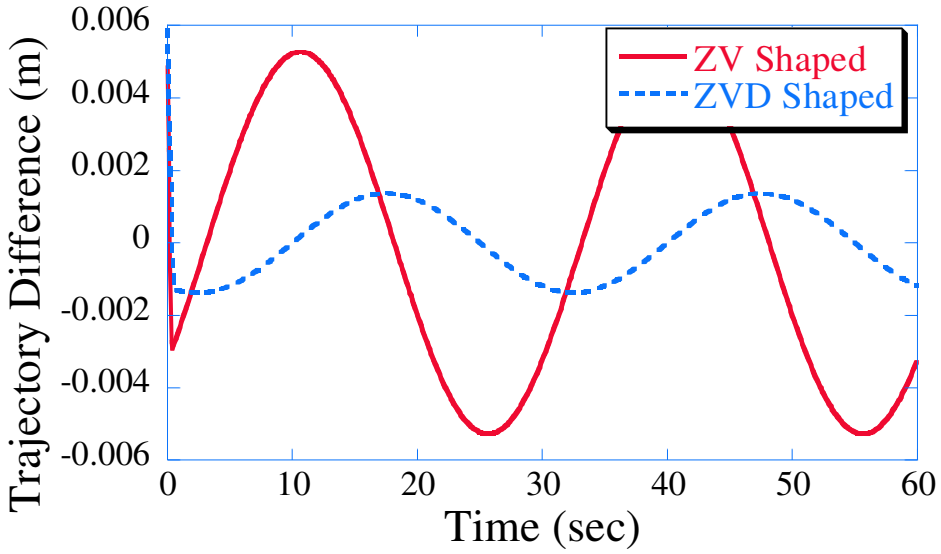

Figure 156: Temporal Position Difference for Time Shifted Trajectories.

the position delay for the shaped trajectories is assumed to be equal to $\frac{1}{2}$ the shaper's duration, then the difference between the unshaped and shaped trajectories becomes much smaller as shown in Figure 156. This plot compares the unshaped positions at a particular time to the shaped positions at a corresponding time in the future. For example, the desired unshaped position at time $t = 1.0$ seconds is compared to the desired ZV shaped position at time $t = 1.25$ seconds and the desired ZVD shaped position at time $t = 1.5$ seconds. Using a delay equal to one-half the shapers duration decreases the temporal position difference one order of magnitude. Now, the maximum position difference is approximately 5 mm for the ZV shaped trajectory and 1.3 mm for the ZVD shaped cases. The initial spike seen in the figure corresponds to position differences times before the duration of the shaper.

4.7.4 Summary: Shaping at the Supervisor Level

For straight-line maneuvers, and circular maneuvers generated from single large step changes, the delay between the unshaped and shaped trajectories is not constant. As the duration of the shaper increases, the temporal difference between the trajectories also increases. Therefore, it is not possible to temporally align the shaped and unshaped trajectories by starting the shaped trajectories earlier as was the case for the leader-follower formation architecture. However, for small changes in position or rotation, the difference between the unshaped and

shaped trajectories is small.

For straight-line maneuvers, shaping should be used to control the maximum spring deflection of the flexible appendages, and the maximum tracking error. Both the ZV and ZVD shaped trajectories reduce the maximum tracking error over 50% when compared to the unshaped case. As the desired final position of the formation center increases, the deflection of the spring also increases. However, using input shaping to change the satellite's trajectories significantly decreases the deflection. For large maneuvers, shaping can reduce the maximum deflection 69%. Over the entire range of the step distances investigated, shaping the trajectories decreases the maximum spring deflection by over 50%.

For circular maneuvers that are generated from a single step change in the formation center's rotation, using input shaping affects the radius of curvature of the satellites' trajectories. The more robust the input shaper used, the greater the decrease in the satellite's radius of curvature during the beginning portion of the maneuver. The ZV shaper decreases the formation's radius by 32% and the ZVD shaper decreases the radius 38%. Although the vibration in the flexible appendage is reduced, the formation no longer moves in a circle. Instead, the formation moves in a series of spiral maneuvers. Temporally, the positions of the unshaped and shaped trajectories cannot be aligned for trajectories generated by a single step change in rotation. However, both the spatial and temporal tracking can be resolved by specifying the rotation of the formation as a continuous function of time, as is the case for the constant ω maneuvers.

For the constant ω maneuvers, shaping the trajectories reduces the maximum spring angle during the initialization phase and the general motion phase by over 50%. The ZVD shaped trajectories have the largest reduction in the maximum spring angle for both phases of the maneuver. The temporal differences between the unshaped and shaped trajectories can be lessened. This is accomplished by starting the shaped trajectories before the unshaped trajectory. The time the trajectories must be started ahead is equal to one-half the shaper's duration. After the time equal to the shaper's duration passes, the position of the unshaped and shaped trajectories will be more closely aligned. The effect of input shaping on the spatial tracking is a shortening of the radius. Unlike the shortening for the varying

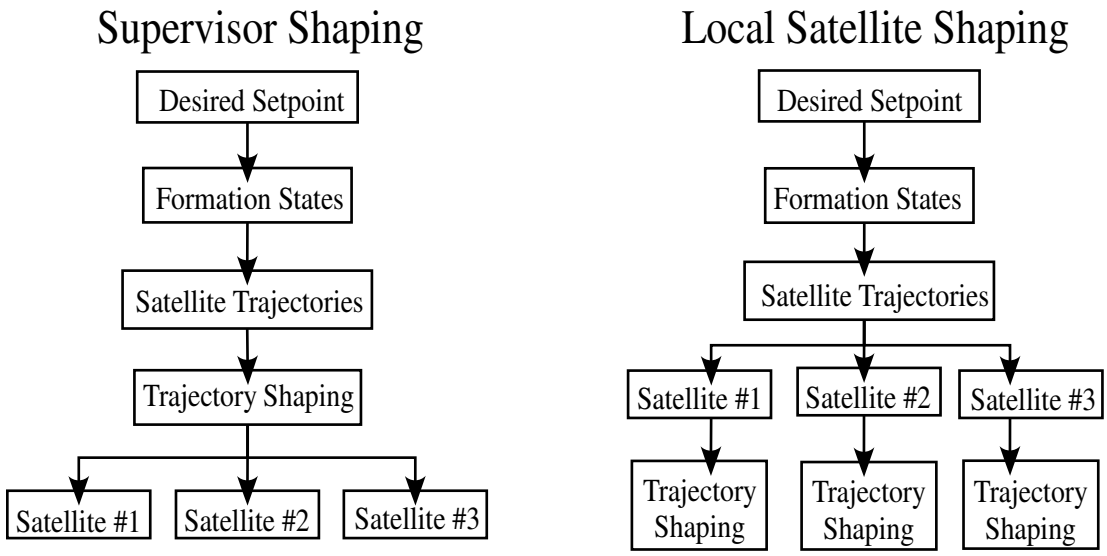

Figure 157: Trajectory Shaping.

ω, this radial shortening is small and remains constant for the duration of the maneuver.

4.8 Local Level Input Shaping

The previous section discussed the effect of shaping trajectories at the supervisor level. It is also possible to utilize input shaping by applying it at the local satellite level. When all of the satellites in the formation are identical, there is no difference between shaping at the supervisor or local satellite level. This idea is illustrated in Figure 157.

A desired setpoint or trajectory is given to the formation states from the formation supervisor. Their responses form the satellites' desired trajectories. If the input shaping is implemented at the supervisor level, then the shaper is convolved with all of the trajectories at the same time. The shaped trajectories are then sent to the corresponding satellites. For shaping at the local level, once the trajectories are generated from the formation states, they are sent to the corresponding satellite. Each satellite then shapes the trajectory to generate its desired trajectory. Once the desired shaped trajectory is generated, the satellite then implements the trajectory. So, if the satellites are identical and the shaper used on all the satellites is the same, then there is no difference between shaping at the supervisor level or local level. The end result is identical. The satellites would have the same shaped trajectory.

Table 14: Frequency Range of Satellite #3.

a	f (Hz)
0.2	0.4473
1.0	1.0
2.0	1.4146
4.0	2.00

For systems where the satellites are not identical, then a difference between shaping at the supervisor level or local level may arise. The differences between shaping at the supervisor level or local level for multi-mode formations is addressed in the next section.

4.9 Simulation Results: Multi-mode Analysis

This section studies the effects of shaping on multi-mode formations. Two of the formation satellites (#1 and #2) are identical and have a flexible mode of 1.0 Hz. The third satellite's flexible mode can vary. The frequency of the satellite's flexible appendage is adjusted by changing the spring constant, K. First the effect of applying the trajectory shaping at the supervisor level will be studied. The effect of shaping at the local satellite level will follow.

4.9.1 Supervisor Level Trajectory Shaping

4.9.1.1 Circle Maneuver: Varying ω

When the shaping is applied at the supervisor level all of the trajectories are shaped using the same shaper. The spring constant for the third satellite varies according to

$$K_3 = a \cdot K_1 \tag{85}$$

where K_3 is the spring constant for the third satellite, K_1 is the spring constant for the first and second satellites, and a is a percent multiplier. The value of a ranges from 0 to 4. Suppose it is desired that K_3 be equal to 80% of K_1, then a would be equal to 0.8. Table 14 shows the estimated natural frequency of the third satellite, ω_3, for a range of a. When the value of a is close to 1.0, then the frequency of the third satellite is approximately 1.0 Hz.

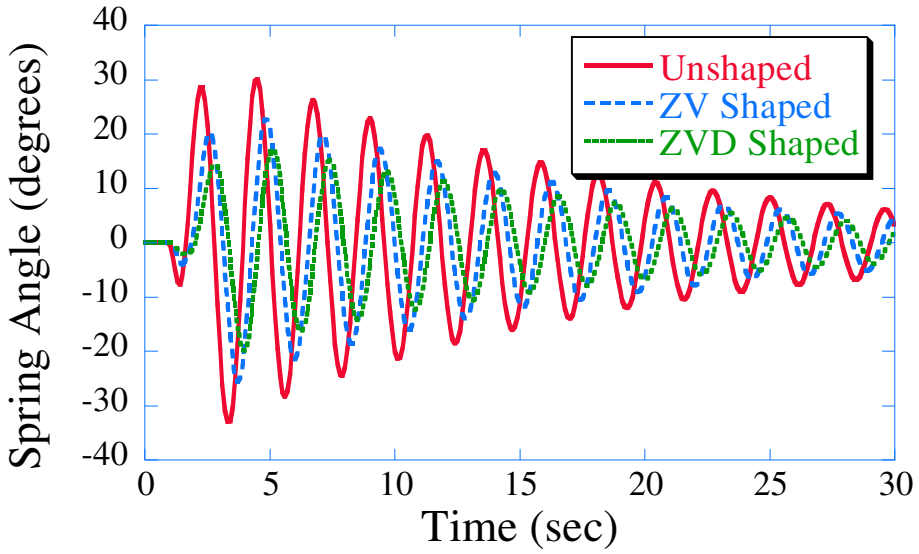

Figure 158: Spring Angle Response for Satellite #3.

Figure 158 shows the response of the third satellite's spring angle when its frequency is 0.4 Hz, and a 1.0 Hz shaper is used. From the ZV and ZVD sensitivity curves, it is expected that as the frequency of the third satellite deviates from 1.0 Hz, the shaped response should approach the unshaped response. It is important to note that the time it takes the formation to accomplish the desired maneuver is significantly lengthened. This is because the third satellite takes a much longer time to settle due to the residual vibration present in the system. When all the satellites are identical, the maneuver is completed in 9.9 seconds. When the third satellite has a frequency of 0.4 Hz, the ZV shaped maneuver takes 51.9 seconds, and the ZVD shaped maneuver takes 48.9 seconds. This is a significant increase in the maneuver time but the unshaped response time is longer than either of the shaped responses.

As the frequency of the third satellite deviates from 1.0 Hz, the maximum spring angle deflection changes as shown in Figure 159. When the frequency of the third satellite is below 1.0 Hz, the behavior of the maximum spring angle is close to the behavior predicted from the sensitivity curves. The farther the actual frequency of the satellite is from the shaper's frequency, the larger the maximum spring angle deflection. The shaped responses have smaller spring deflections. The ZVD shaped trajectory generates the smallest deflection.

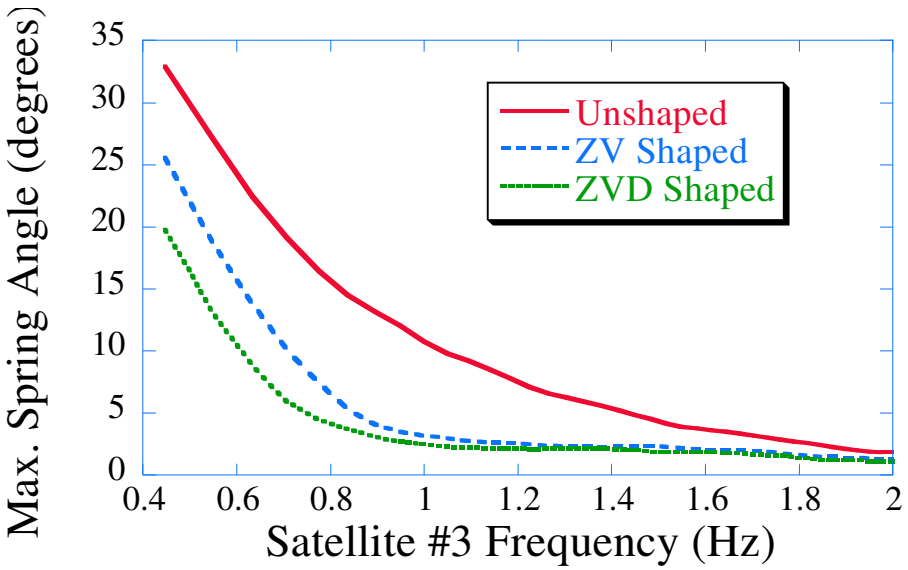

Figure 159: Maximum Spring Angle Deflection versus Satellite Frequency.

This is because the ZVD shaper is the more robust to frequency variations. When the frequency of the third satellite is above 1.0 Hz, the behavior is much different. As the frequency increases, the spring constant increases. An increasing spring constant correlates to a stiffer flexible appendage. The mass at the end of the appendage does not change, and its inertia is unable to deform the spring. so, the bar acts more like a stiff, rigid bar.

The easiest way to reduce the maximum spring deflection for the third satellite is to utilize a multi-mode input shaper. A multi-mode input shaper is designed to eliminate frequencies at two or more frequencies. Figure 160 shows the maximum spring angle deflection of the third satellite for the unshaped, 1.0 Hz ZV , and the multi-mode ZV shaped cases. The 1.0 Hz ZV shaped trajectory suppresses the vibration for the first and second satellite. The multi-mode shaper is designed to eliminate the 1.0 Hz mode of satellites one and two and the frequency of satellite three. Only the range of frequencies below 1.0 Hz were studied. The multi-mode ZV shaper generates a smaller maximum spring deflection for the entire observed range of satellite frequencies.

For even better vibration suppression, a multi-mode ZVD shaper can be used. Figure 161 shows the maximum spring angle deflection for the ZVD multi-mode shaper. Comparing Figure 160 and 161 it is clear to see that the ZVD multi-mode shaper provides the best

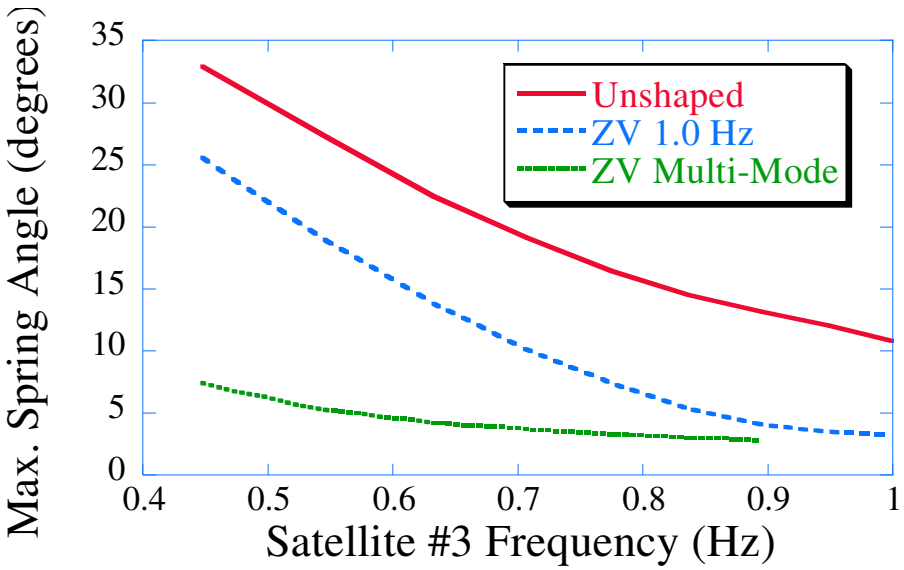

Figure 160: Maximum Spring Angle Deflection Using Multi-Mode ZV Shaper.

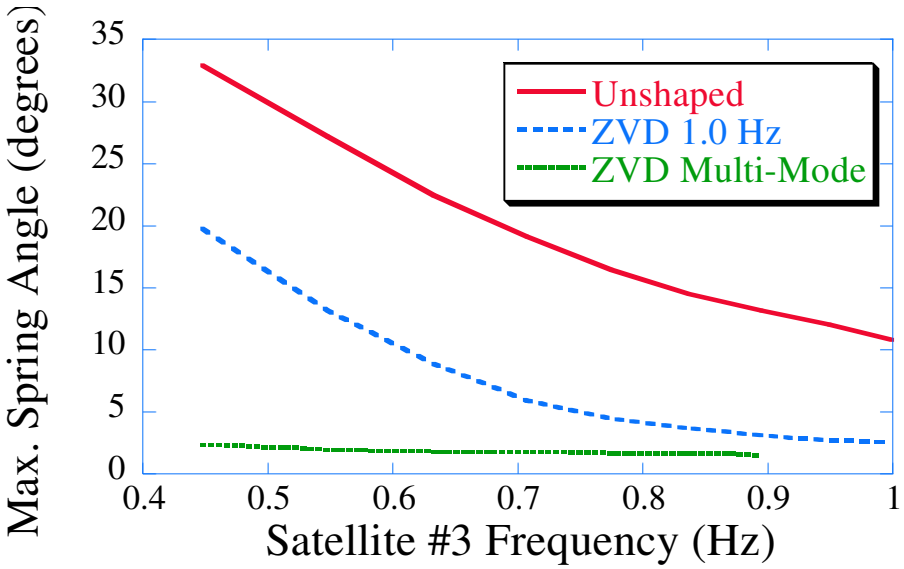

Figure 161: Maximum Spring Angle Deflection Using Multi-Mode ZVD Shaper.

vibration suppression over the range of frequencies studied. The maximum spring deflection is less than 5% for the entire range of frequencies.

Utilizing a multi-mode shaper also reduces the maneuver time. Figure 162 shows the maneuver time as a function of the third satellite's frequency. When the frequencies of the third satellite and the other satellites in the formation are far apart, using the ZVD multi-mode shaper to generate the trajectory significantly reduces the maneuver time. The

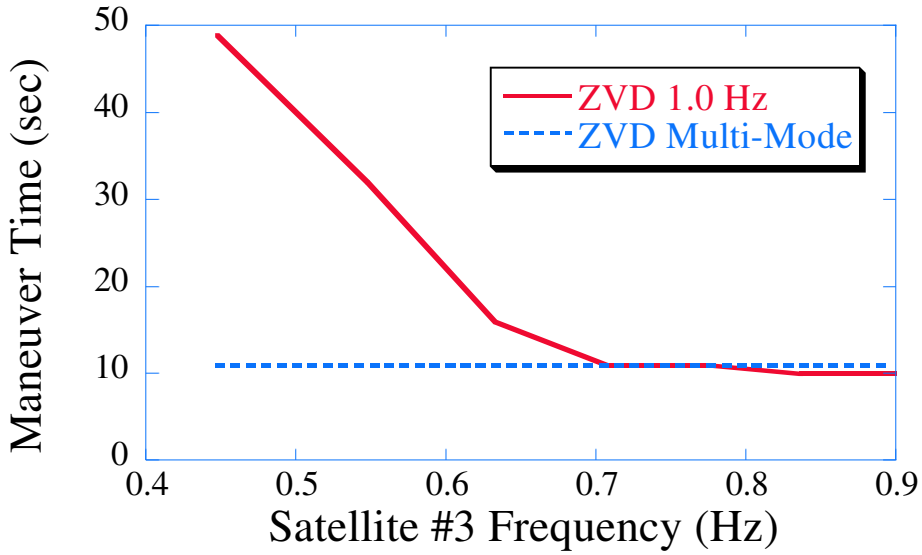

Figure 162: Maneuver Time Versus Satellite Frequency.

maneuver time is calculated as the time when the position, velocity, orientation and angular velocity of all the satellites is below a specified error limit. The maneuver time is reduced almost 75% when the frequency of the third satellite is 50% of the other two. When the ZVD multi-mode shaper is used, the maneuver time stays constant at 10.9 seconds.

The multi-mode input shaper has two effects on the formation. The first effect is the vibration reduction for all the satellites, even when the frequencies are far apart. The second effect is the reduction in the radius of curvature of the formation. Figure 163 shows the percent reduction as a function of satellite frequency. For the circle maneuver with a varying rotation frequency, using a multi-mode shaper increases the deviation from the desired formation radius. As the frequency difference between the third and other formation satellites increases, the amount the radius is reduced increases. This is because the multi-mode shaper is generated using both satellite frequencies. When the frequencies are close together, the shaper's duration is shorter than when the frequencies are far apart. Consider the multi-mode ZV shaper's amplitudes and time locations when the frequencies used to generate it are 1.0 Hz and 0.8 Hz.

$$\begin{bmatrix} t \\ A \end{bmatrix} = \begin{bmatrix} 0 & 0.5 & 0.625 & 1.0 & 1.125 & 1.25 & 1.625 & 1.75 & 2.25 \\ 0.625 & 0.125 & 0.125 & 0.0625 & 0.25 & 0.0625 & 0.125 & 0.125 & 0.625 \end{bmatrix} \quad (86)$$

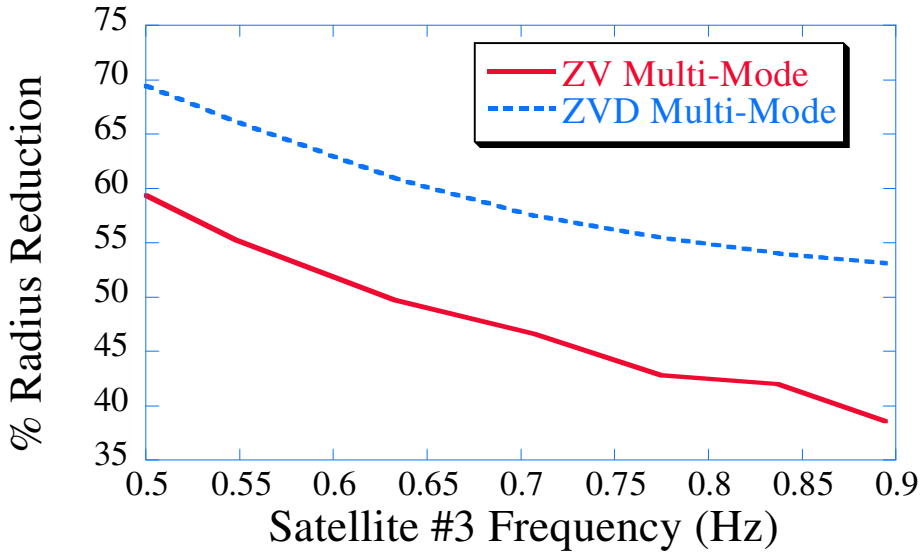

Figure 163: Percent Reduction in Formation Radius for Multi-Mode Shapers.

The duration of this shaper is 2.25 seconds. When the frequencies used to generate the multi-mode shaper are 1.0 Hz and 0.4 Hz, the amplitudes and time locations are as follows:

$$\begin{bmatrix} t \\ A \end{bmatrix} = \begin{bmatrix} 0 & 0.5 & 1.0 & 1.25 & 1.75 & 2.25 & 2.5 & 3.0 & 3.5 \\ 0.0625 & 0.125 & 0.0625 & 0.125 & 0.25 & 0.125 & 0.0625 & 0.125 & 0.0625 \end{bmatrix} \quad (87)$$

The duration of this shaper is 3.5 seconds which is 1.25 seconds longer than the previous shaper. As the frequencies get farther apart, the duration of the shaper increases.

4.9.1.2 Circular Motion: Constant ω

The previous section studied the effect of two formation modes for varying ω circle maneuvers. This section studies the effects of two formation modes when the frequency of the rotation, ω is constant. Figure 164 shows the spring angle responses for $\omega = 0.2094 \frac{rads}{sec}$ during the initialization portion of the maneuver. The frequency of the third satellite's flexible appendage is approximately $0.4 \frac{rads}{sec}$, and the desired formation radius for this maneuver is 0.5m. The shaped trajectories were generated using with a 1.0 Hz shaper. Recall that the first and second satellites both have natural frequencies of 1.0 Hz. Because the frequency of the third satellite is less than half that of the other two satellites, the unshaped and shaped spring angle responses are almost identical (as predicted by the sensitivity curves).

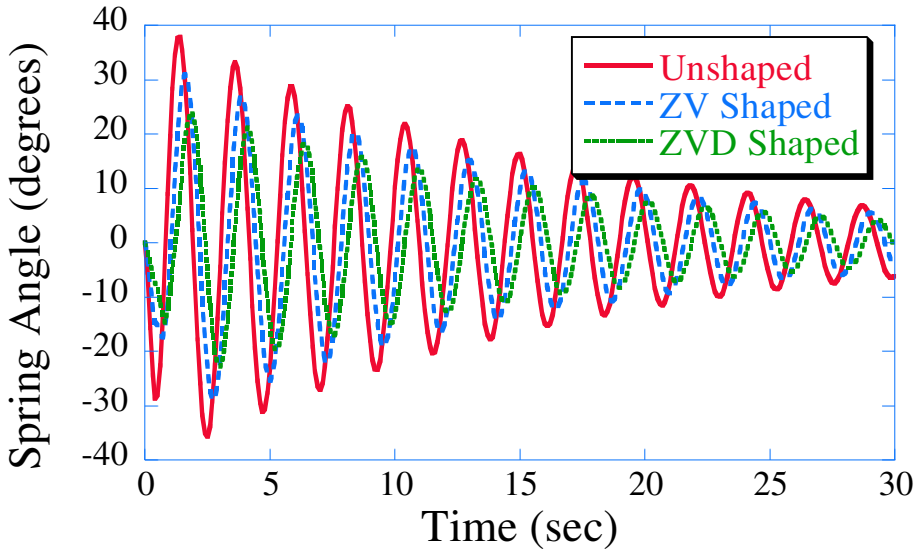

Figure 164: Spring Angle Response for Satellite #3 for Constant ω Maneuver.

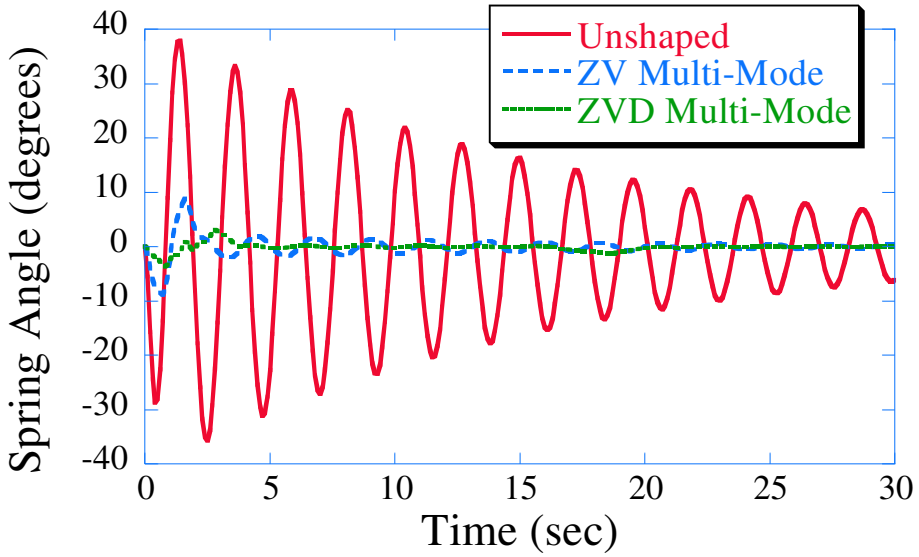

Figure 165: Spring Angle Response For Multi-Mode Shapers for Satellite #3.

A multi-mode shaper can be used to generate a trajectory that will eliminate the vibration for the two identical satellites (#1 and #2) and for the third satellite. Figure 165 compares the unshaped and multi-mode shaped spring angle responses for the third satellite frequency of 0.4 Hz. Clearly, the multi-mode shaper provides a reduction in the satellite's spring angle. It is also important to note the significant reduction in the settling time. Figure 166 compares the shaped spring angle response for the first satellite during

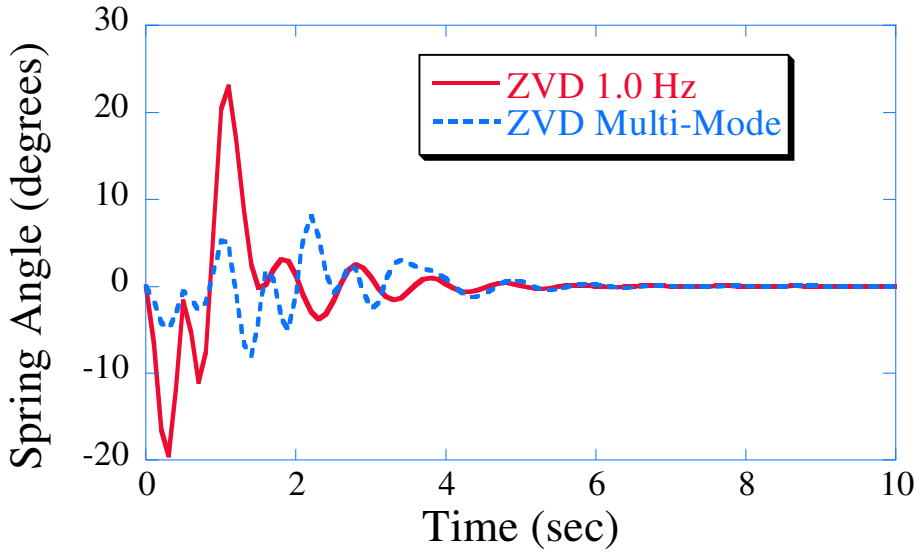

Figure 166: Spring Angle Response for Satellite #1 During Initialization.

the initialization portion of the maneuver The multi-mode shaper causes less vibration in the flexible appendage than the single mode shaper. The initialization maneuver is a step change in satellite attitude, but the multi-mode ZVD shaper has more impulses than the 1.0 Hz ZVD shaper, so the commanded step changes are not as large. This leads to reduced vibration in the flexible appendage for the first and second satellites.

Figure 167 compares the 1.0 Hz and multi-mode shapers for a range of satellite frequencies. The multi-mode shapers drastically reduce the maximum spring deflection in the flexible appendage for the range of frequencies shown. When the frequency of the third satellite is half that of the other two satellite, the multi-mode shapers provide over a 50% reduction in the maximum spring angle. The ZV multi-mode shaper has a 66% reduction and the ZVD multi-mode shaper has an 80% reduction when compared to the 1.0 Hz shaped trajectories. However, as the frequency of the third satellite approaches the frequency of the other satellites, the responses generated from using the 1.0 Hz shaper and multi-mode shaper converge.

Although it is clear that the multi-mode shapers provide superior vibration reduction, the multi-mode shapers have much longer durations. In the previous section (varying formation frequency), the effect of the multi-mode shapers on trajectories generated by large

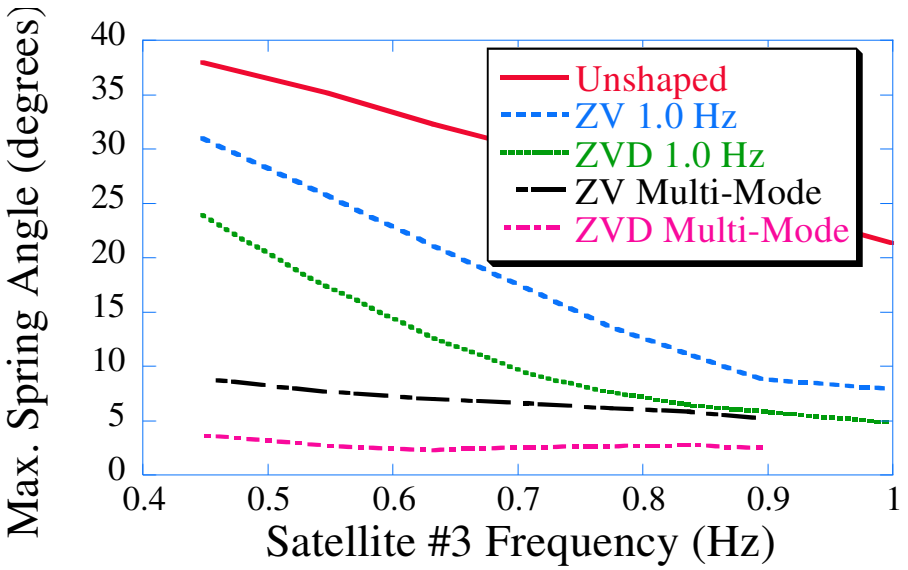

Figure 167: Maximum Spring Angle Response versus Satellite Frequency.

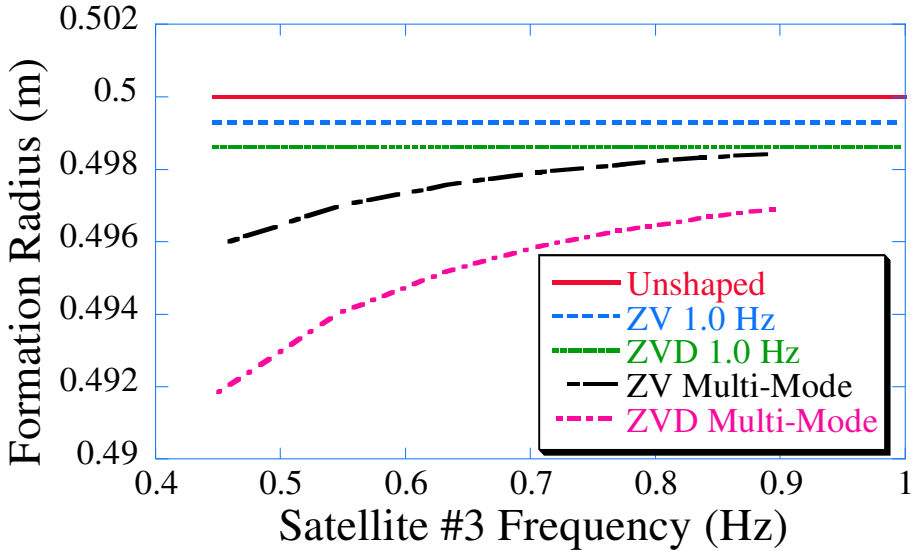

Figure 168: Formation Radius Versus Satellite Frequency for Constant ω Maneuver.

step changes in rotation was a large reduction in the trajectories' radii of curvature. When a constant ω maneuver is performed, this is not the case. Figure 168 shows the change in the third satellite's formation radius as a function of its frequency. The unshaped and single mode shapers have a constant formation radius over the entire range of the third satellite's frequencies. This because they are independent of the third satellite's frequency. On the other hand, the multi-mode shapers depend on the third satellite's frequency. As the

frequency of the third satellite gets farther away from the frequency of the other satellites (1.0 Hz), the multi-mode shaper increases in duration. This increase in duration causes a decrease in the effective radius, albeit a small one. This is less than a two percent reduction in the radius. Although there is a decrease in the formation's radius, it is constant throughout the entire maneuver. This means that the formation satellites still travel in a circle, although it is a slightly smaller circle.

When the shaping is implemented at the supervisor level, all the satellites in the formation are affected the same way. The structure of the formation is not altered. The satellites maintain their triangular shape although the relative position between the satellites changes depending on the way the desired trajectories are generated. For situations where the satellites are not identical, multi-mode shapers can be used to eliminate the flexible modes in all of the satellites. The price is an increase in the shaper's duration and a small decrease in the formation's radius. The next section discusses the effects of implementing the trajectory shaping on the local satellite level.

4.9.2 Local Level Trajectory Shaping

When the shaping is implemented on the local satellite level, each satellite is responsible for shaping its desired trajectory. The unshaped trajectory is given to each satellite by the supervisor. For situations where the satellites in the formation are not identical, each satellite would use an input shaper designed to eliminate its own mode of vibration. However, doing this causes a change in the formation's structure. This effect is discussed next.

4.9.2.1 Circular Motion: Varying ω

For the varying ω circular motion, the desired step change in rotation is given to the formation states. The response of the formation is generated from this single step change. When the shaping is completed on the local satellite level, each of the satellites is responsible for generating a shaped trajectory that will reduce the vibration of its flexible appendage.

For circular motions, shaping the desired trajectory reduces the radius of curvature as shown in Figure 169. The amount the radius of curvature deviates from the desired radius depends on the frequency of the satellite's flexible appendage. The shaper used to generate

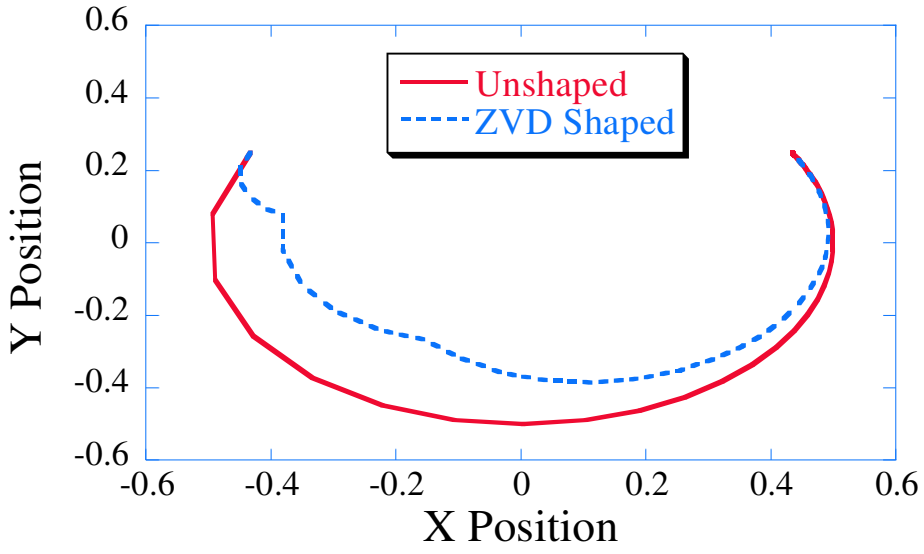

Figure 169: Desired Trajectory for Satellite #1 for 240° Maneuver.

the shaped trajectory is designed from the frequency of the flexible appendage.

When all the satellites in the formation have identical flexible modes, the trajectories all have the same shape. However, when one of the satellites has a different mode, then the shape of the trajectories no longer matches and the amount the radius of curvature changes also no longer matches. Because the effective radius of the formation depends on the frequency of the flexible mode, an interesting problem arises when the satellites in the formation are not identical. If the frequency of the flexible appendage for the third satellite is far from the frequency of the other two satellites in the formation, then the duration of the shapers used will be significantly different. Consider the case when the frequency of the third satellite is 0.4 Hz and the frequency of the other two satellites is 1.0 Hz. The time locations and amplitudes for the 1.0 Hz and 0.4 Hz ZVD shapers are:

$$1.0Hz \rightarrow \begin{bmatrix} A \\ t \end{bmatrix} = \begin{bmatrix} 0.25 & 0.5 & 0.25 \\ 0 & 0.5 & 1.0 \end{bmatrix} \tag{88}$$

$$0.4Hz \rightarrow \begin{bmatrix} A \\ t \end{bmatrix} = \begin{bmatrix} 0.25 & 0.5 & 0.25 \\ 0 & 1.25 & 2.50 \end{bmatrix} \tag{89}$$

Notice the increase in the ZVD shaper's duration from 1.0 seconds to 2.5 seconds. The duration of the shaper affects the radius of curvature of the trajectory. Figure 170 shows

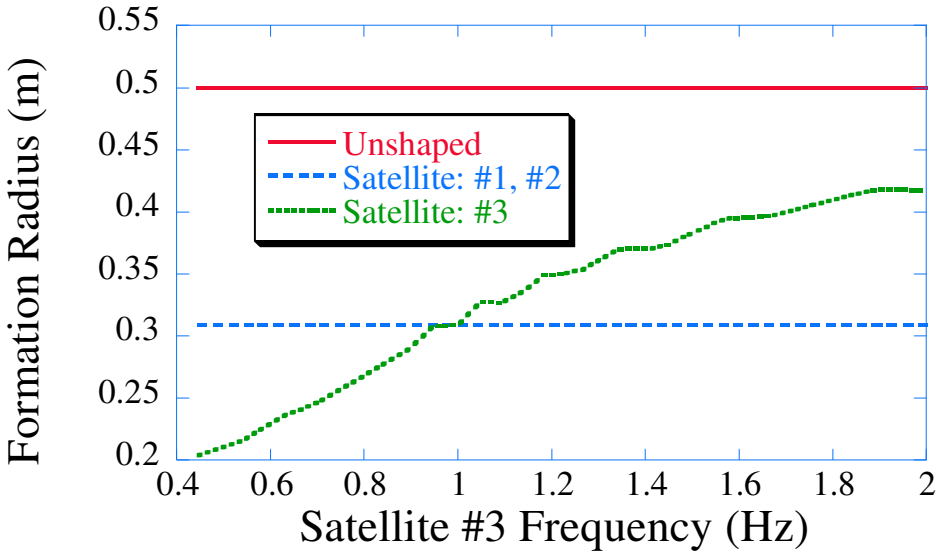

Figure 170: Minimum Formation Radius Versus Satellite Frequency for ZVD Shaped Trajectories.

the minimum formation radius as a function of the frequency of the third satellite's flexible arm. The minimum radius of curvature for the first and second satellite's trajectories is independent of the third satellite's frequency; therefore, it remains constant over the range of frequencies. The lower the frequency of the third satellite's arm, the smaller the minimum radius of curvature. When the frequency of the third satellite is 0.4 Hz, the minimum radius of curvature is 0.2 m. This is a 60% reduction. The first and second satellite have a 38% reduction in the radius of curvature. Now the changes in the trajectories are different

When the trajectory shaping is completed at the local level, the satellites have different radii of curvature throughout the entire maneuver. Spatially, this means that the formation no longer maintains its desired equilateral triangular shape. The satellites begin the maneuver in the desired triangular shape. When the motion begins and the satellites follow their desired shaped trajectories, the triangular structure of the formation degrades slightly. The amount of the degradation depends on how close the different satellites' frequencies are to each other. When the frequencies are close, the differences between the desired trajectories are small. When the frequency of one of the satellites is far away (as is the case for $\omega_3 = 0.4$ Hz), the differences in the trajectories are large.

Consider the case where the frequencies of the first and second satellite are identical at

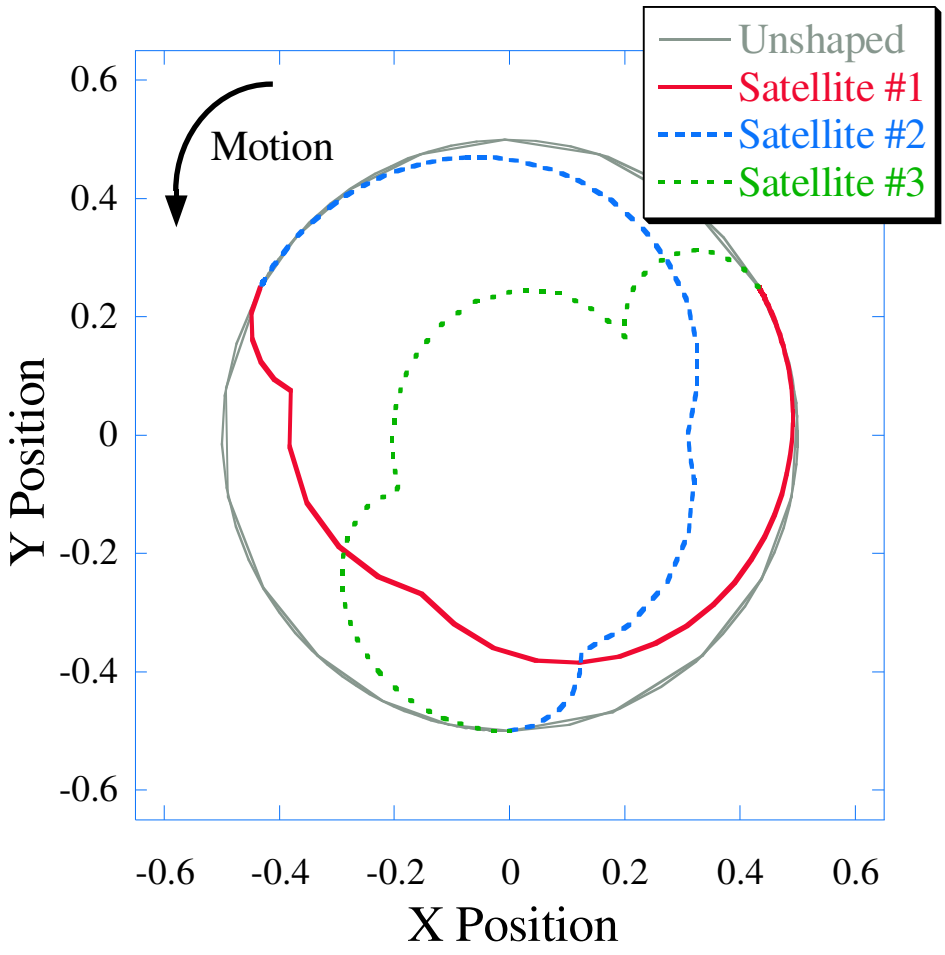

Figure 171: ZVD Shaped Trajectories for Multi-Mode Formation.

1.0 Hz. The frequency of the third satellite is less than half at 0.4 Hz. Figure 171 shows the desired trajectories for all of the satellites. From the figure, it is clear that the satellites do not travel in a circle, but rather a series of spirals. Therefore, when spatial tracking and maintaining the desired formation structure are the primary objectives, input shaping at the local satellite level should not be used. This is especially true when the trajectory is generated from a single step change. However, if the trajectory is generated from a series of step changes or a continuous function, then input shaping at the local level should be used. This is discussed in the following section.

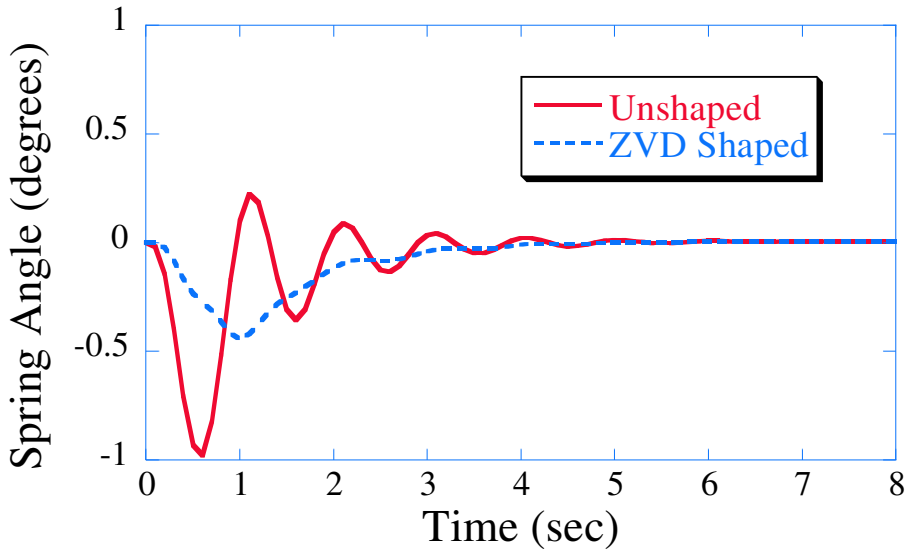

Figure 172: Spring Angle Response for Satellite #1 During General Motion.

4.9.2.2 Circular Motion: Constant ω

Shaping the desired trajectories at the local level ensures that the maximum vibration reduction in the flexible appendage occurs. Each satellite's trajectory is shaped according to its frequency. Figure 172 shows the spring angle response for the first satellite undergoing a constant ω maneuver. The frequency of the first satellite is 1.0 Hz and the frequency of the third satellite is 0.4 Hz. Figure 173 shows the spring angle response for the third satellite for the same maneuver. The data shown in Figures 172 and 173 is during the general motion part of the maneuver. The time has been normalized to zero. For both of the satellites, shaping the desired trajectory reduces the spring angle vibration.

Shaping the satellites' desired trajectories at the local level, changes the effective formation radius for circular maneuvers, which affects the spatial tracking. The amount the radius is shortened is directly related to the shaper's duration. The longer the shaper, the more the formation's radius is decreased. Figure 174 shows the effective radius versus frequency of the third satellite for ZVD shaped trajectories. The desired formation radius is 0.5m. The shaper for the third satellite is generated using the frequency of the third satellite. The radii of the first and second satellites is constant and are not influenced by the frequency of the third satellite. The shaper used for the first and second satellite is a

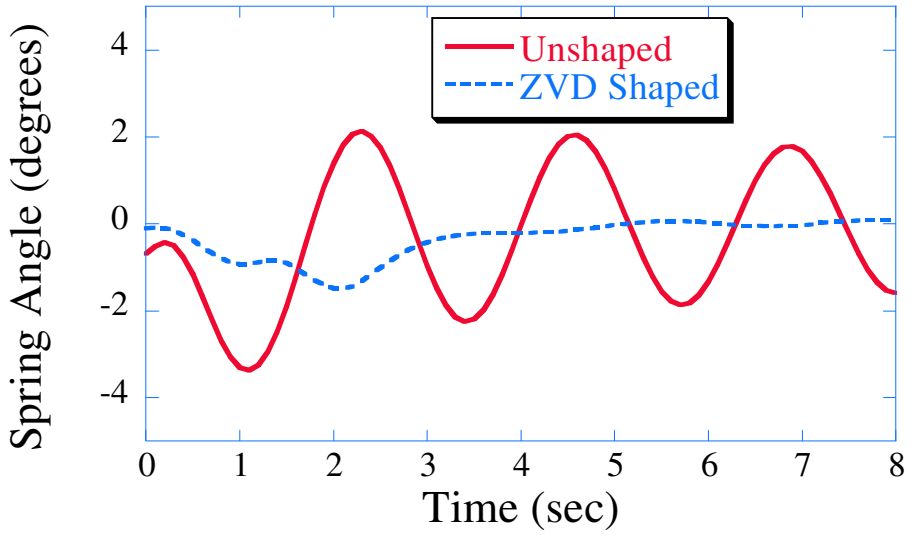

Figure 173: Spring Angle Response for Satellite #3. During General Motion.

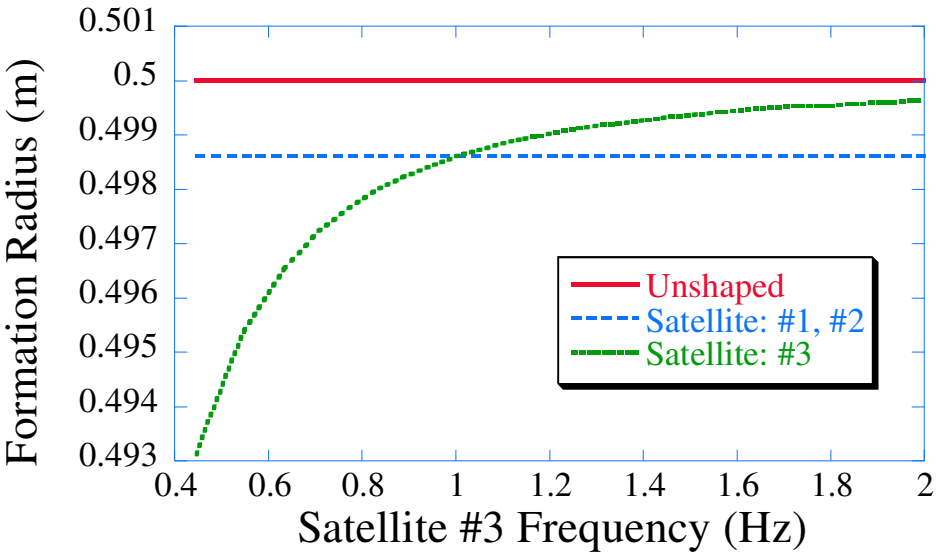

Figure 174: Effective Shaped Radius Versus Satellite Frequency.

1.0 Hz ZVD shaper. However, when the frequency of the third satellite is below 1.0 Hz, its effective radius is smaller. When its frequency is greater than the other satellites, its radius of curvature is larger and more closely approaches the desired radius of 0.5m. Figure 175 shows the desired trajectories for the formation satellites. Although the frequency of the third satellite is less than one-half the other two (0.4 Hz compared to 1.0 Hz). The satellites in the formation still travel in a circular path. The duration of the 0.4 Hz shaper

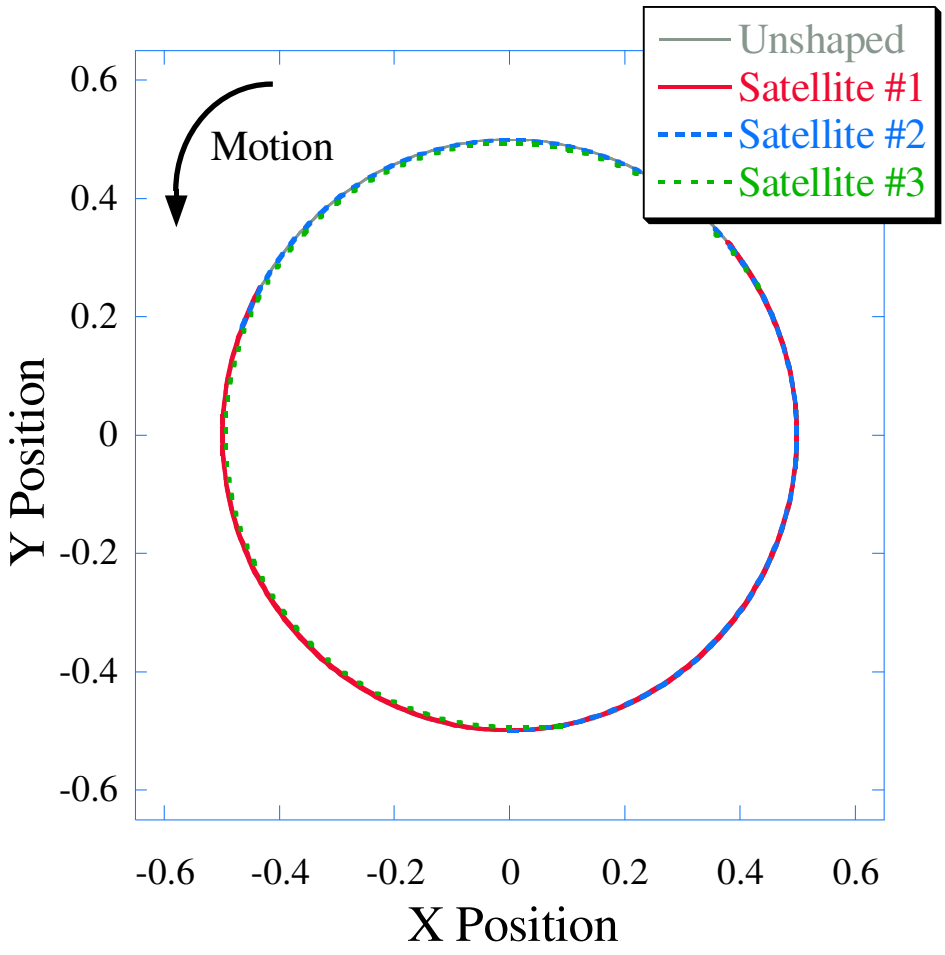

Figure 175: ZVD Shaped Trajectories for Multi-Mode Formation.

is 2.5 times as long as the 1.0 Hz shaper. The first and second satellite's effective radius is 0.4993 m and the third satellite's effective radius is 0.496 m. The desired radius is 0.5m

Because the satellites are no longer travelling circles with the same radius, the equilateral triangular shape of the formation is no longer maintained. However, the change in configuration is extremely small. Figure 176 plots the distances between the satellites as a function of time. The frequency of the third satellite is 0.4 Hz. The distance between the first and third satellite increases, while the distance between the second and third satellite decreases. The distance increase between the first and third satellites can be explained by looking at the speed profile for each of the satellites shown in Figure 177. The speeds for the first and second satellites are almost identical. This leads to the very small change in separation distance between these satellites as seen in Figure 176. The third satellite's

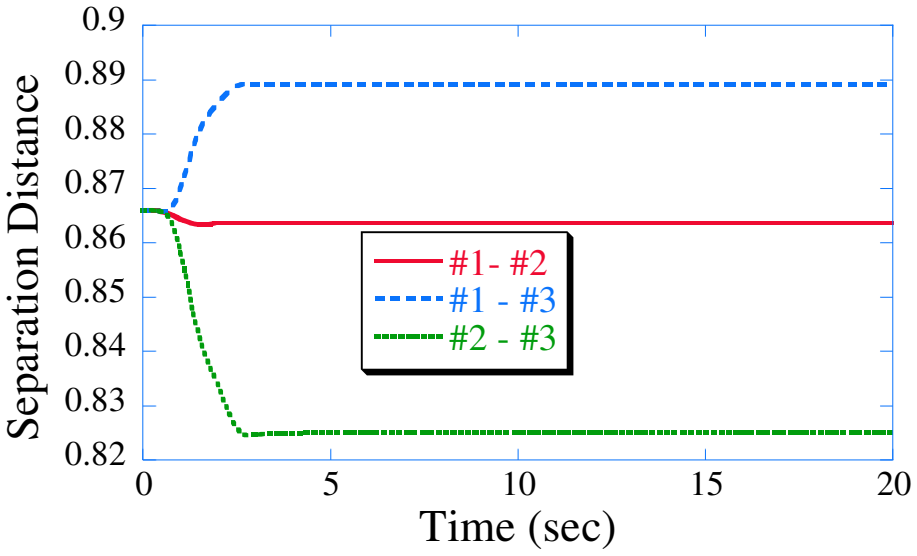

Figure 176: Separation Distance Between the Formation Satellites Using ZVD Shaped Trajectories.

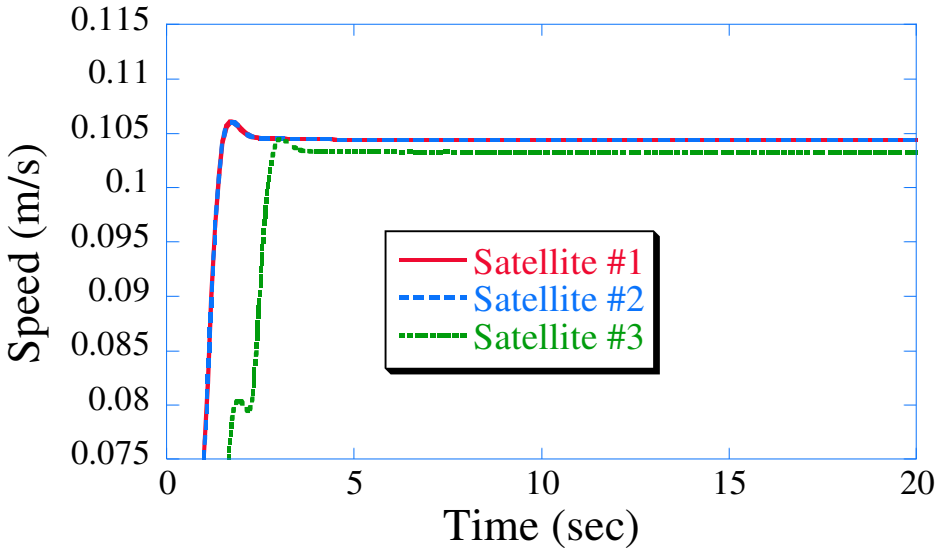

Figure 177: Satellite Speed Profile.

speed is smaller than either of the other satellites. Because the rotation of the formation is counter-clockwise, the first satellite travels farther than the third satellite does in the same amount of time; therefore, the distance between them increase. Similarly, the second satellite also travels farther than the third satellite, but because of the orientation, the distance between these satellites decreases.

Shaping the desired trajectories of the satellites affects the temporal tracking. For constant frequency circular maneuvers, the temporal tracking differences between the unshaped and shaped cases can be reduced. Shaping at the supervisor level affects the entire formation the same, but shaping on the local level affects each satellite differently. The time delay between the unshaped and shaped trajectories depends on the duration of the shaper. When all of the satellites are identical, this is not a problem for the formation because all of the satellites have the same delay. When one of the satellite has a different flexible appendage frequency, and input shaping is performed on the local level, then the time delay for each of the satellites is different. However, this can be resolved by starting the shaped trajectories at different times. The satellite with the lowest frequency would be started first, followed by the satellite with the next lowest frequency, and so on. After all the satellites have begun to move, and the time is greater than the duration of the longest input shaper, the trajectories of the satellites would be aligned.

4.10 Summary: Multi-Mode Formations

When the input shaping is completed at the supervisor level, a multi-mode input shaper should be used when the formation has different satellite modes, and these modes are largely spaced. A multi-mode ZVD shaper provides the best reduction in the maximum spring angle when the frequency of one of the satellites is below the frequency of the other two satellites. In addition to reducing the maximum spring angle, the settling time of the maneuver also decreases. If a multi-mode shaper is not used, then the overall time of the maneuver increases as the frequency difference between the satellites increases. Using a multi-mode input shaper significantly decreases the maneuver time when the frequencies are far apart.

For motions that are generated from a large single step change (such as the varying ω case), using a multi-mode shaper significantly increases the deviation in the formation's radius of curvature. If spatial tracking is of utmost importance, then the trajectories should not be generated from a single large step change. However, if response of the flexible appendage is of primary concern then the multi-mode shapers should be utilized as they

provide excellent vibration suppression over the range of frequencies studied.

For motions that are generated using continuous functions, such as the constant ω case, the temporal tracking difference between the unshaped and shaped trajectories can be decreased. This is accomplished by starting the shaped trajectories before the unshaped trajectories. The time they must be started is equal to the one half the shaper's duration. As the frequency between the satellites increases, the duration of the multi-mode shaper also increases. Spatially, the formation remains unchanged except for a small decrease in the effective radius. However, this may be eliminated by using a slightly larger formation radius.

CHAPTER V

INPUT SHAPING USING PULSE WIDTH MODULATION

5.1 Pulse Width Modulation

In many models, the control force or torque is modeled as a continuous variable amplitude signal. In reality, however, this is not the case. On-off thrusters are commonly used to maneuver a spacecraft. In addition to thrusters, momentum wheels or gyros can be used to control the spacecraft's attitude. Therefore, sometimes a mismatch occurs between the desired modeled control effort and the on-off control effort required by the satellite. The easiest way to convert a continuous control effort signal to an on-off thruster profile is by using a technique known as Pulse Width Modulation.

Pulse Width Modulation (PWM) is a method for converting continuous time varying amplitude signals into pulses and is used to drive many different types of systems. PWM is commonly used to drive DC motors and other actuators, such as thrusters, that require a full-on, full-off actuation. The width of the fixed amplitude pulse is proportional to the continuous signal amplitude [27]. The parameter that denotes the proportionality of the pulse train to the continuous signal amplitude is the duty cycle. The duty cycle is the ratio of the pulse duration to the pulse period. For example a 50% duty cycle means that the pulse duration is half of the total pulse period.

Figure 178 shows a PWM conversion of a sine wave. The sampling rate of the PWM is 5 Hz which corresponds to 0.2 seconds. So every 0.2 seconds, the PWM converts the continuous signal into the corresponding duty cycle. As seen from the figure, when the amplitude of the sine curve is very small, the corresponding duty cycle is also small. As the amplitude increases, the duty cycle also increases until it reaches 100%. The amplitude of the modulated signal is either ± 1. For thrusters, their duty cycle would correspond exactly

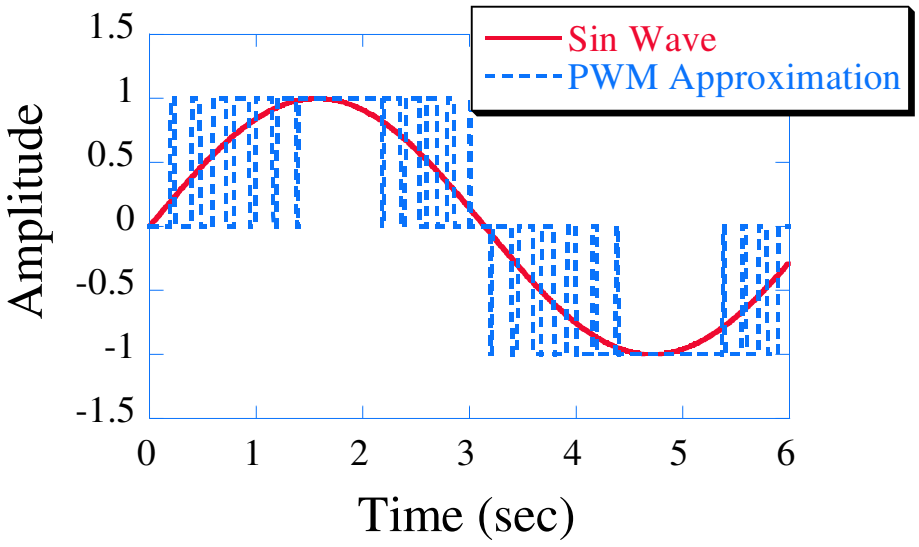

Figure 178: 5.0 Hz PWM Approximation of 0.15 Hz Sine Wave.

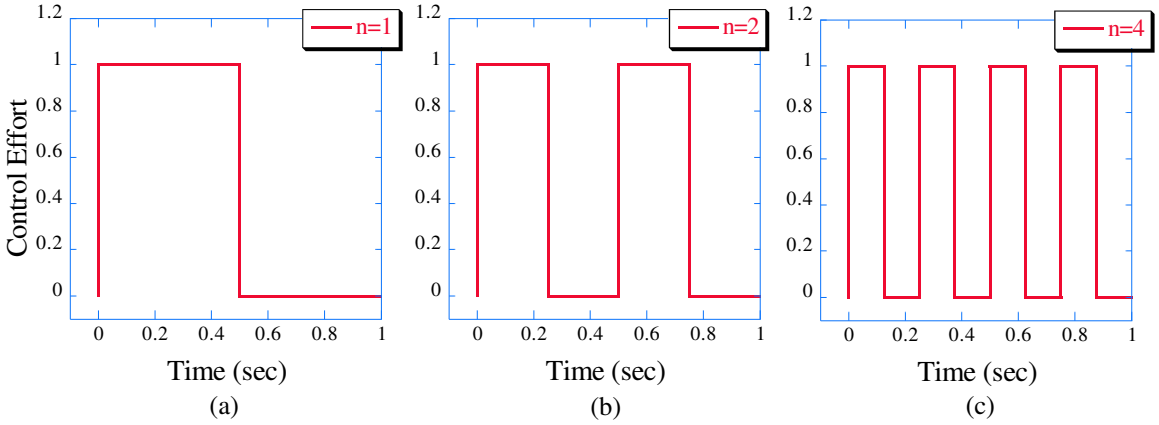

Figure 179: PWM Cycles for 50% Duty Cycle.

to the duty cycle of the PWM. Every time the modulated signal has an amplitude of either ± 1, the thrusters would be turned on. A positive amplitude of one would turn one set of thrusters on, and an amplitude of negative one would turn on the opposite set of thrusters.

The number of complete PWM cycles for a given time interval is defined as n. Figure 179 shows the pwm command assuming a 50% duty cycle for different values of n. The time interval for this case is 1 second. When $n = 1$ as shown in Figure 179a, the command only has one pulse. Figure 179b shows the modulated command when $n = 2$, and Figure 179c shows the command when $n = 4$. As the number of PWM cycles for the given time

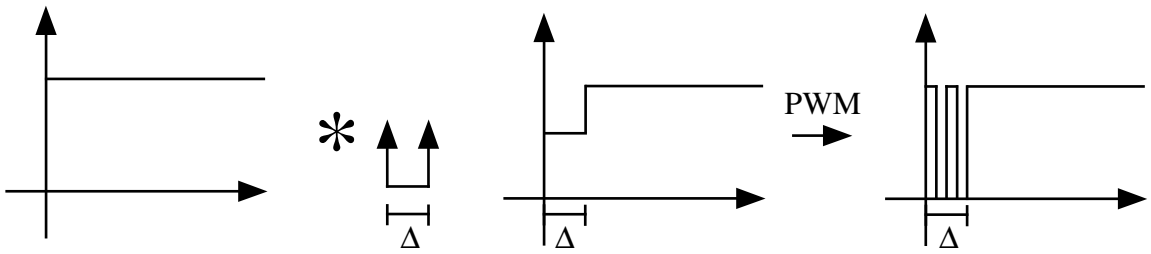

Figure 180: Combined ZV Input Shaping and PWM.

interval increases, the number of pulses in the pulse train also increases. The total area for each case remains constant.

5.2 Combined Input Shaping and Pulse Width Modulation

It is well established that convolving a step command with a shaper generates a staircase command. If generated correctly, this command can provide complete eliminate of the system's residual vibration. The command no longer has a constant amplitude, but PWM can be used to generate an on-off thruster profile. Combining input shaping and PWM can be completed as shown in Figure 180. First, the command is shaped by convolving it with the desired input shaper. The command signal can be continuous and time varying. Next, the shaped command is converted to an on-off profile using PWM as shown in Figure 180. In this process the input signal (in this case a step command) is convolved with a ZV input shaper. The convolved signal is then sent to the PWM and is converted into the appropriate on-off pulse train. The resulting command is knows as an input-shaped pulse-width-modulated (ISPWM) command.

In order to convert the convolved signal into a matching PWM signal, an appropriate period for the PWM cycle must be established, or some of the important signal characteristics will be lost. For shaped commands, the locations of the impulse amplitudes are important. A ZV shaper two amplitudes, one located at time $t = 0$ and the other at $t = \frac{1}{2}T$, where T is the system's period. The PWM command must maintain this crucial change at $t = \frac{1}{2}T$. Therefore, for the staircase command shown in Figure 180, the maximum allowable duration of the PWM cycle is equal to the shaper duration, Δ. If the duration of the PWM cycle is larger than Δ, then the modulated command would not be able to capture the

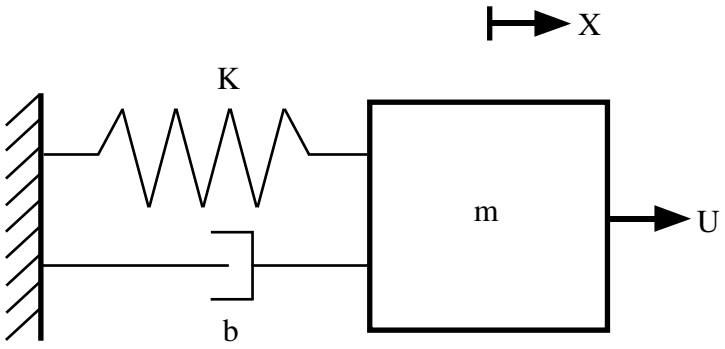

Figure 181: Second-Order Benchmark System.

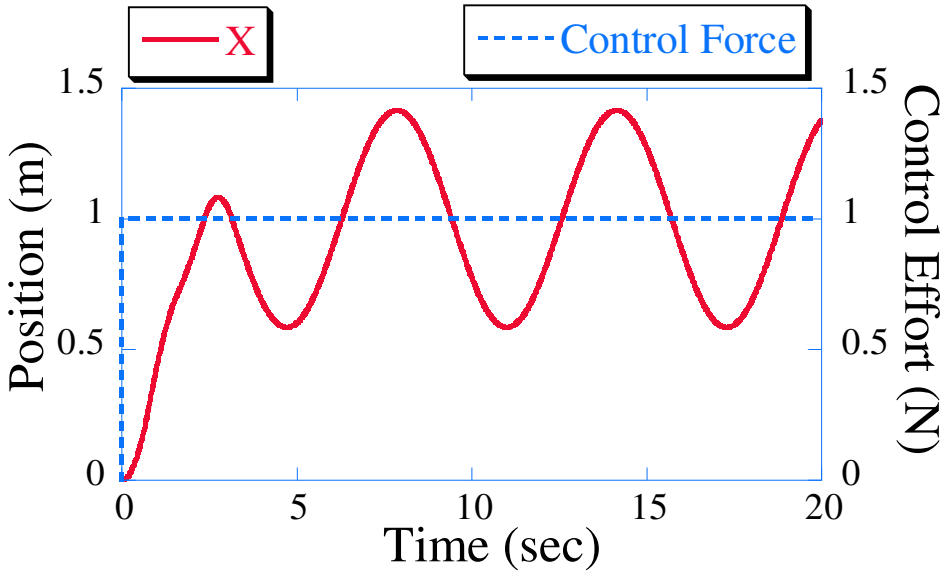

Figure 182: Undamped Benchmark System's Response to Step Change in Actuator Effort.

necessary change in the staircase command. This would in effect cancel out the shaping and the system's vibration would not be reduced. The duration of the PWM cycle can be smaller than the shaper's duration and its size is only limited by thruster capability.

5.2.0.3 Benchmark System

Consider the mass-spring-damper benchmark system shown in Figure 181. The mass and spring constants for this simple system are both equal to one, thus the system has a natural frequency, ω_n, equal to $1\frac{rads}{sec}$. For undamped systems, the damping coefficient, b, is zero. If a step change in actuator effort is given to the undamped system, the open-loop response of the system is shown in Figure 182. As seen in the figure, the position response of the

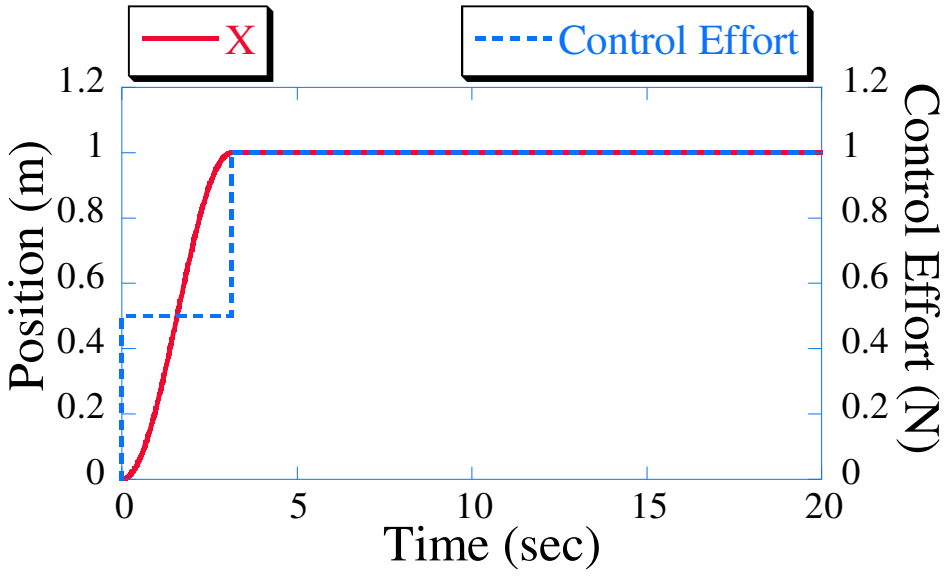

Figure 183: Undamped Benchmark System's Response to ZV Shaped Actuator Effort.

system is sinusoidal, and the oscillation of the mass will never damp out. If the step change in control effort is convolved with a ZV shaper and the resulting shaped command is used on the system, then the system will have the response shown in Figure 183. As seen from the figure, the oscillation of the mass is completely eliminated, but the rise time of the system is slightly increased.

Unfortunately, the control signal used in Figure 183 does not have a constant amplitude, but it can be modulated so that it has a constant amplitude. This modulated signal is used to command the system, and the response of the mass is shown in Figure 184. For this case, only 1 PWM cycle was used ($n = 1$). The duration of the PWM cycle is equal to the duration of the shaper, Δ. As seen in the figure, the PWM has a 50% duty cycle. The 50% duty cycle results from modulating the first part of the staircase command shown in Figure 183. Unlike the response seen in Figure 183, the response shown in Figure 184 has considerable residual vibration. The amplitude of the residual vibration is greater than the residual vibration amplitude for the unshaped case shown in Figure 182.

If the number of PWM cycles, n, used to modulate the input shaped staircase command is increased, the response of the system to the input shaped PWM commands improves. Figure 185 shows the response of the benchmark system for different values of n. As seen

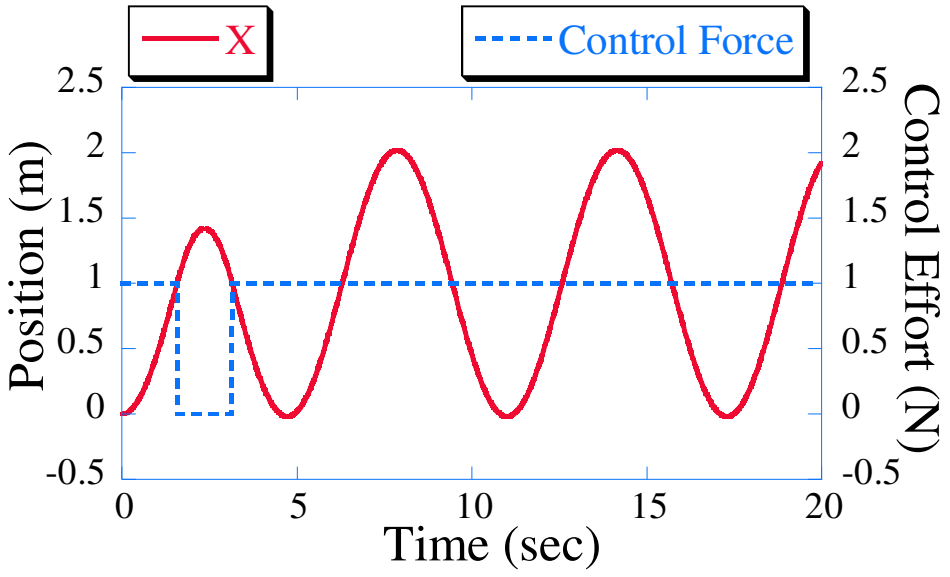

Figure 184: Open Loop ZV Input Shaped Pulse Width Modulated System Response.

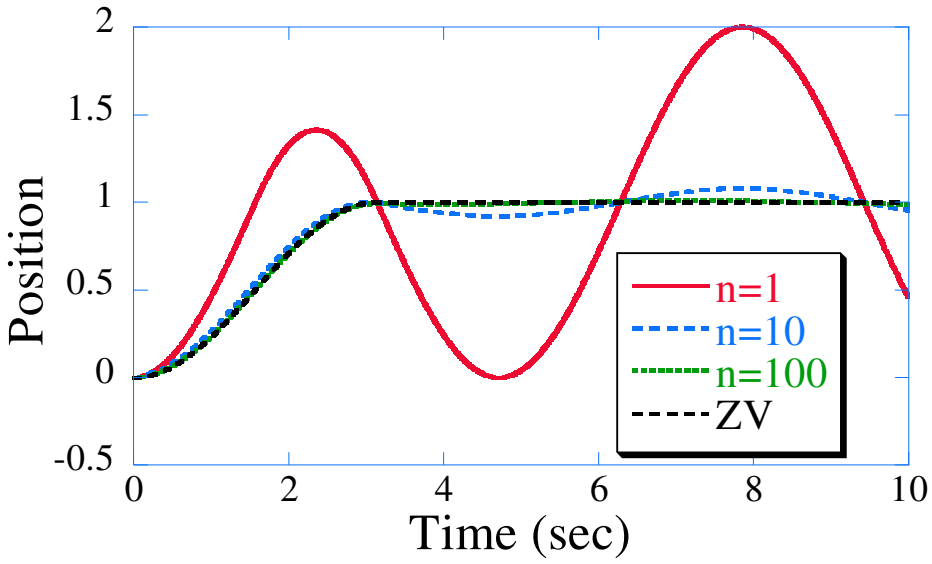

Figure 185: Input Shaped Pulse Width Modulated System Response.

from the figure, as the number of cycles, n, increases, the residual oscillation of the mass decreases. When the number of PWM cycles is significantly increased, then the response of the system to the combined input shaped PWM command more closely resembles the ZV input shaped response shown in Figure 183. In order to get the best vibration suppression, n should set equal to ∞. This, however, is not realizable.

For spacecraft applications, the number of pulses in the command profiles corresponds

to the number of times the thrusters must fire. So as n increases, the number of thruster fires also increases. In addition, there is also a minimum amount of time the thruster must be turned on in order for the thruster firing to be considered effective. For this research, the minimum on-time for any spacecraft thruster is 10 ms, and the thruster is assumed to have an finite amount of firings available (approximately 10 million cycles). It is also assumed that the first 5 ms of thruster firing is considered wasted fuel, while the rest of the time the thruster is on, is considered useful fuel.

5.3 Combined Input Shaped Pulse Width Modulated Sensitivity

The previous section showed how the number of PWM cycles affected the open-loop response of the benchmark system. This section evaluates the sensitivity of the input-shaped-pulse-width-modulated (ISPWM) shaper to changes in natural frequency and number of PWM cycles.

Some of the input shaping research has focused on developing shapers that generate on-off command profiles. The unity magnitude shapers can generate commands that are on-off in nature [43]. The amplitudes of the unity magnitude shapers are ± 1. Although these shapers eliminate the residual vibration of a system, they can also induce excitation of higher system modes. ZV and ZVD shapers cannot excite higher system modes.

When PWM is combined with either a ZV or ZVD shaper it generates an effective shaper that is similar to the unity magnitude shapers. Therefore, it is possible that higher modes present in the system will be excited. Investigating the sensitivity of this generated shaper will show if the high modes will be excited and the extent of the excitation.

The first step in generating the sensitivity curves for this system is to identify the shaper working on the system. Although the ZV shaper is used to shape the command, when the signal is modulated, the effective shaper of the system changes. The effective shaper can be determined by de-convolving the input shaped PWM signal into a step command and an ISPWM shaper. The ISPWM shaper is the shaper that determines the vibration response of the system. This de-convolution process is shown in Figure 186. Notice that the amplitudes

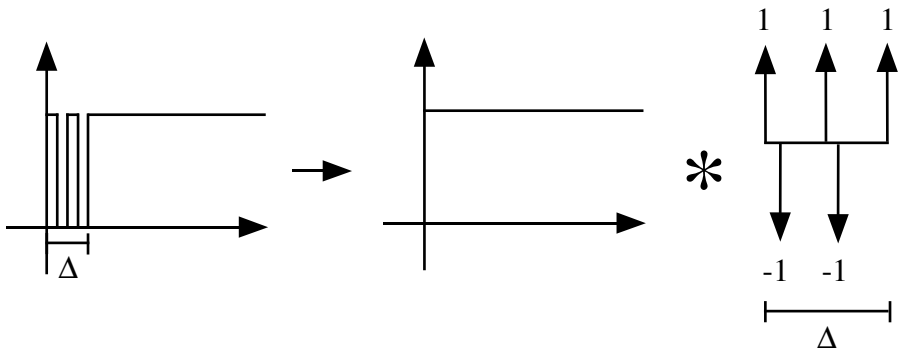

Figure 186: ISPWM De-convolved Input Shaper.

of the ISPWM shaper are equal to (1, -1, 1, -1, 1).

The amplitudes for the ISPWM shaper are similar to the amplitudes of the Unity Magnitude shapers discussed in [43]. The duration of the ISPWM shaper is equal to that of the ZV shaper, Δ. The duration of an undamped unity magnitude ZV shaper is $\frac{T}{3}$ and the duration of an undamped ZV shaper is $\frac{T}{2}$. Therefore, the ISPWM shaper is slightly longer than a unity magnitude shaper generated using the same frequency as the ZV shaper. The frequency of the ISPWM shaper is determined by the number of PWM cycles and the shaper used to initially shape the command.

5.3.1 Zero Vibration Pulse Width Modulation Sensitivity

5.3.1.1 Undamped Benchmark System

The first sensitivity study was performed assuming an undamped system and a ZV shaper. The ZV shaper is the base shaper for the system. The base shaper is the shaper that initially changes the original command signal to the shaped signal that gets modulated.

The ISPWM shaper is dependent on the number of PWM cycles, n, used generate the command. The number of impulses and the time locations of these impulses changes depending on the number of PWM cycles used. It is important to note that the duration of the PWM cycle cannot exceed the duration of the ZV shaper.

Generalized expressions describing the amplitudes and time locations of the ISPWM shaper were developed so that for any value of n, the corresponding ISPWM shaper could be generated. The following equations represent the generalized expressions for the ISPWM

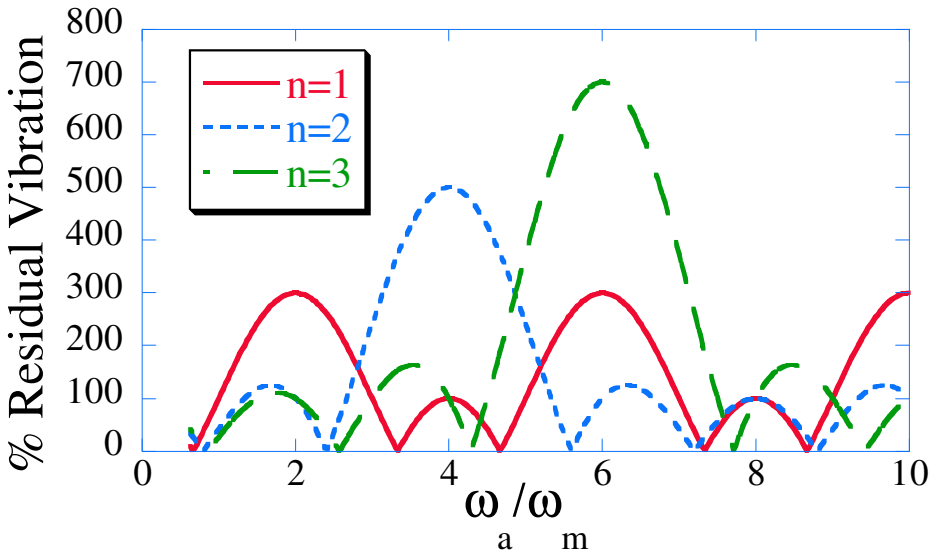

Figure 187: ZV Input Shaped PWM Sensitivity Curves.

amplitudes and time locations when the base shaper is the ZV shaper. First the number of impulses in the ISPWM shaper is calculated from:

$$2 \cdot n + 1 \tag{90}$$

where n is the desired number of PWM cycles. The amplitudes of the ISPWM impulses always alternate between ± 1, starting with $+1$ and ending with $+1$. The impulse amplitudes and time locations for the ISPWM shaper are calculated from:

$$A = \begin{bmatrix} 1 & -1 & 1 & \dots & 1 \end{bmatrix} \tag{91}$$

$$t = \begin{bmatrix} 0 & \frac{1 \cdot \Delta}{2n} & \frac{2 \cdot \Delta}{2n} & \dots & \frac{n \cdot \Delta}{2n} \end{bmatrix} \tag{92}$$

where Δ is the duration of the ZV shaper ($\Delta = \frac{T}{2}$). It is important to note that the preceding equations are only valid for undamped systems.

Once the impulse amplitudes and time locations for the ISPWM shaper are determined, the sensitivity curve for the shaper can be determined using the SENSPLOT command in MATLAB. Figure 187 shows the sensitivity of the ISPWM shaper using a ZV base shaper for different PWM values. The percent residual vibration is the ratio of the unshaped to shaped vibration for a step command, ω_a is the actual frequency of the system, and ω_m is the modeled frequency.

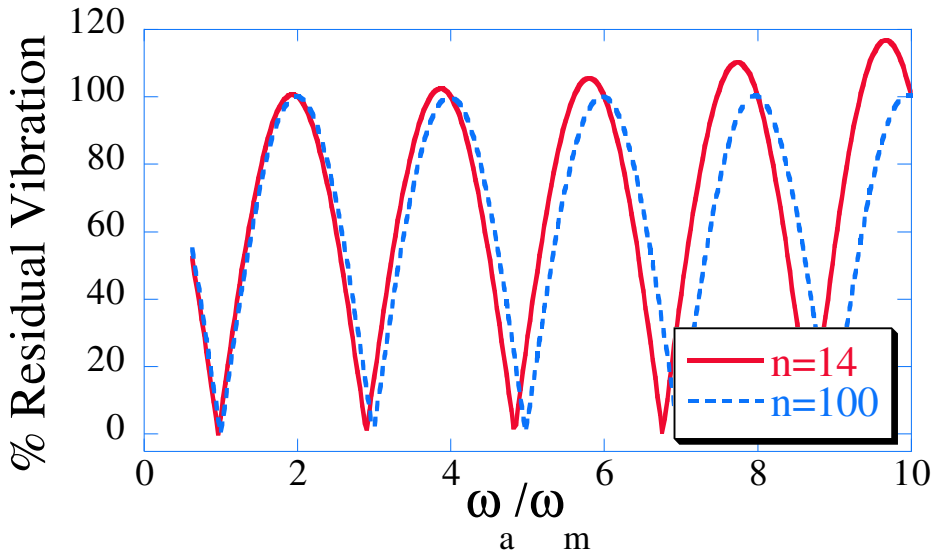

Figure 188: ZV Input Shaped PWM Sensitivity Curves.

As seen in the figure, the number of PWM cycles, n, affects the robustness of the ISPWM shaper. For n=1, the sensitivity curve shows that modes at approximately two times the natural frequency will be excited to three times their unshaped levels. As n increases, the frequencies of the excited modes shift to the right, but their amplitudes increase. When $n = 3$, the peak for the largest, excited higher mode has shifted to approximate six times the lowest natural frequency, but the amplitude has increased from three times to approximately seven times the unshaped level.

One advantage that the ISPWM shaper has and the unity magnitude shapers does not possess, is the ability to shift the excited high mode so far to the right that it will not significantly impact the response of the system. This effect is shown in Figure 188. The sensitivity curves for n=14 and n=100 are shown. For n=100, the sensitivity curve approximates the ZV curve and has no high mode excitation for the range studied ($0.1 \leq \omega_a \leq 31$). The sensitivity curve also shows that for n=14, the ZV ISPWM begins to approximate the ideal ZV shaper sensitivity.

It is possible to combine a ZV shaper and pulse width modulation in order to eliminate the residual vibration. As the number of PWM cycles increases, the effect of the PWM high mode excitation decreases. However, increasing the number of cycles, n, increases the

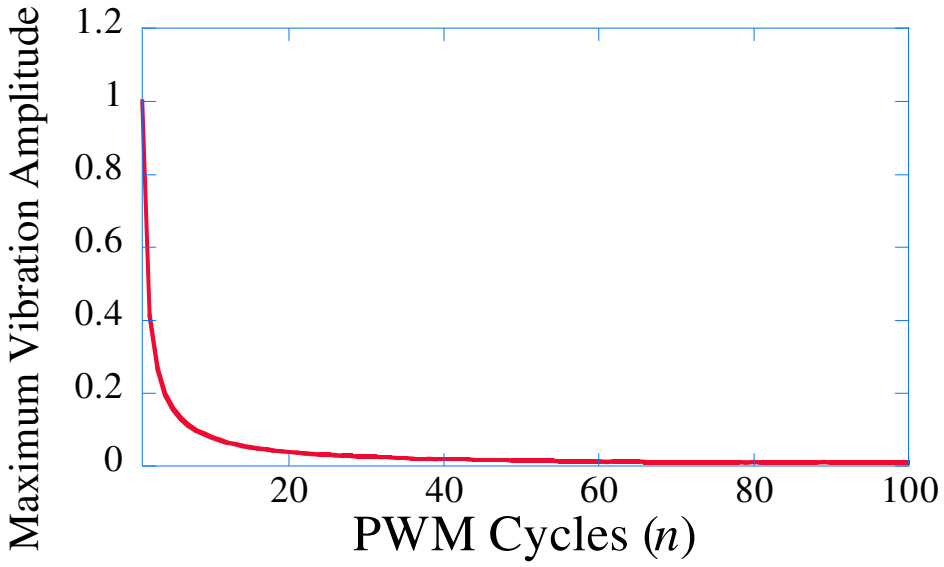

Figure 189: Normalized Maximum Residual Vibration Amplitude.

amount of wasted fuel. In order to determine how many PWM cycles are needed for a particular situation, one must first decide on the acceptable level of vibration. Once the acceptable level of residual vibration is determined, it is possible to utilize Figure 189 in order to pick the smallest value of n that will guarantee that the level of vibration will not exceed the required specification. Figure 189 shows the normalized maximum residual vibration amplitude for a unit step change on the benchmark system. The maximum residual vibration is calculated as follows:

$$\text{MaximumResidualVibration} = \max(Y) - 1 \tag{93}$$

where $\max(Y)$ is the maximum vibration amplitude of the system's response. Given that the signal generates an oscillation about 1, the magnitude of the response can be normalized by subtracting one.

As the number of PMW cycles increases, the amplitude of the residual vibration decreases. However, it is clear from the figure, that using n=100 does not further reduce the maximum vibration amplitude when compared to maximum vibration amplitude for n=60. In order to effectively use the information in the graph, one must first decide on the acceptable level of residual vibration. For many cases, a 5% residual vibration level is acceptable and Figure 190 can be used to determine the value of n. As seen in the figure,

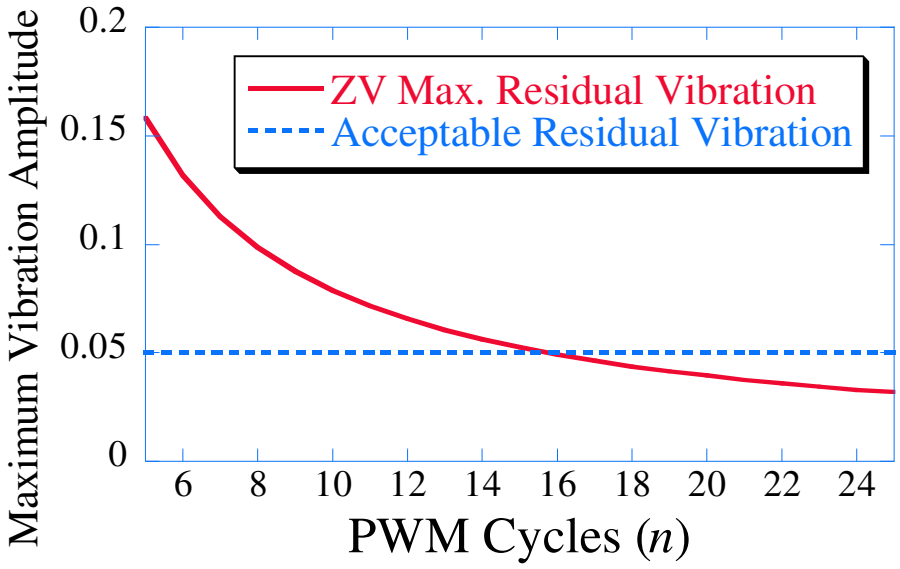

Figure 190: Maximum Residual Vibration Amplitude.

the value of n is determined using the intersection of the acceptable vibration amplitude limit (shown as the dashed line) and the maximum vibration amplitude (shown as the solid line). For the ZV shaped case where the shaper duration, Δ, is equal to π, the optimum value of n is 16.

5.3.1.2 Damped Benchmark System

Although the damping ratio for spacecraft's flexible appendages is very low, it is important to study the effect of damping on combined input shaped PWM system. Input shaping depends on both the natural frequency and damping ratio of the system. Damping changes both the time locations and amplitudes of the impulses. When a damping ratio of 0.2 is added to the system, the input shaper for the damped benchmark system is:

$$A = \begin{bmatrix} 0.655 & 0.345 \end{bmatrix}$$

$$t = \begin{bmatrix} 0 & 3.20 \end{bmatrix} \tag{94}$$

The duration of the shaper, Δ is slightly smaller for the damped system than for the undamped system. Also, the magnitude of the amplitudes has changed from 0.5 to 0.655 for the first amplitude and 0.345 for the second amplitude.

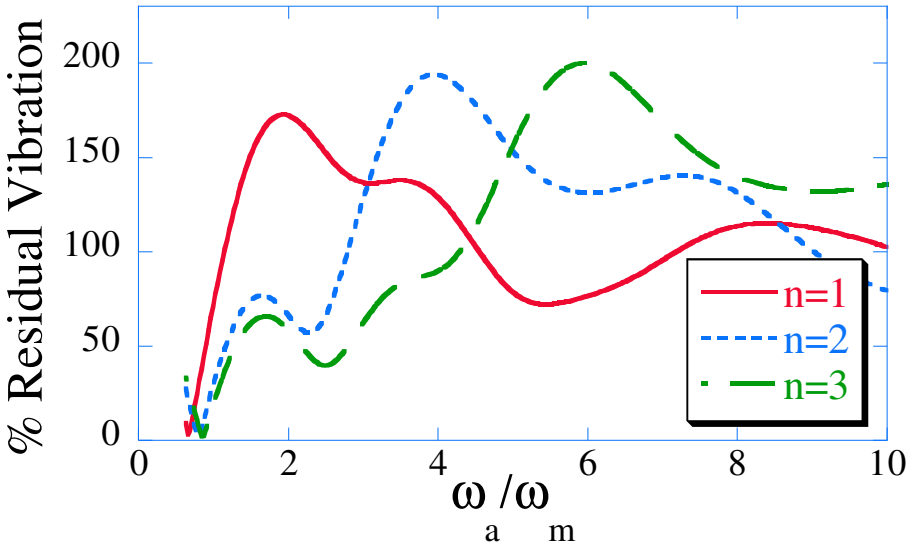

Figure 191: ZV Input Shaped PWM Sensitivity for $\xi = 0.2$.

In order to calculate the sensitivity of a damped ISPWM shaper, first the generalized expressions must be developed. The time locations for the impulse amplitudes for the damped ISPWM shaper are:

$$t = \left[0 \quad \frac{\Delta}{n} \cdot (0 + A_1) \quad \frac{1 \cdot \Delta}{n} \quad \frac{\Delta}{n} \cdot (1 + A_1) \quad \ldots \quad \frac{(\Delta)}{n} \cdot (n + A_1) \quad \frac{n \cdot \Delta}{n}\right] \tag{95}$$

where A_1 is the magnitude of the first impulse for the base ZV shaper. The amplitudes of the ISPWM shaper are still calculated from (91). Unlike the time locations for the undamped system shown in expression (92), the time locations for the damped system shown in (95) depend on the magnitude of the first amplitude, A_1.

Using this expression for the impulse time locations, the sensitivity plot of the damped ISPWM shaper can be generated. Figure 191 shows the sensitivity of the ISPWM shaper for $\xi = 0.2$ As seen in the figure, as n increases, the high mode excitation shifts to the right. However, the amplitude of the high mode excitation is increased. Similar to the undamped sensitivities, as the number of pulse width modulation cycles increases, the sensitivity curve approaches the ideal damped ZV curve. Figure 192 shows the sensitivity curves for n=14 and n=100.

Figure 193 shows the relationship between the lowest n value that satisfies a given maximum residual vibration level. As seen in the figure, as the damping ratio increases,

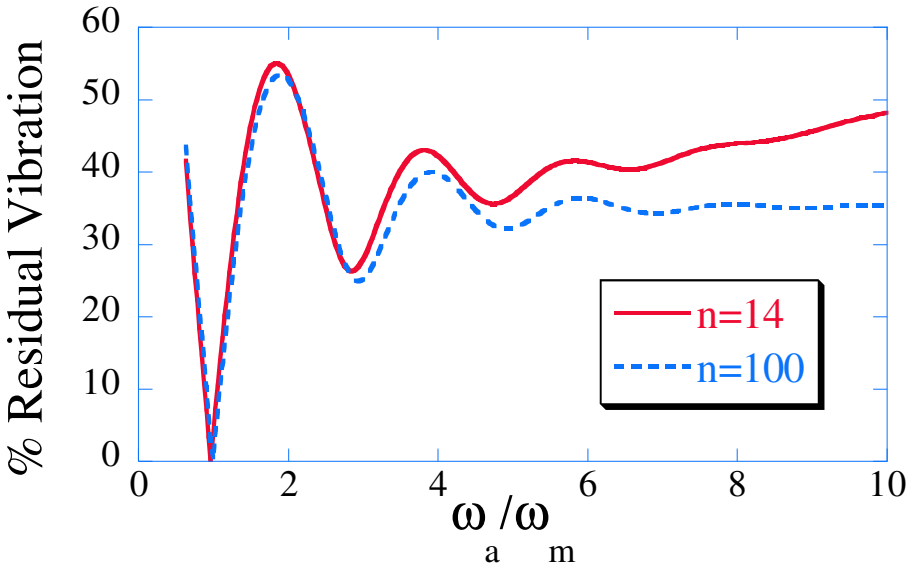

Figure 192: ZV Input Shaped PWM Sensitivity Curves for $\xi = 0.2$.

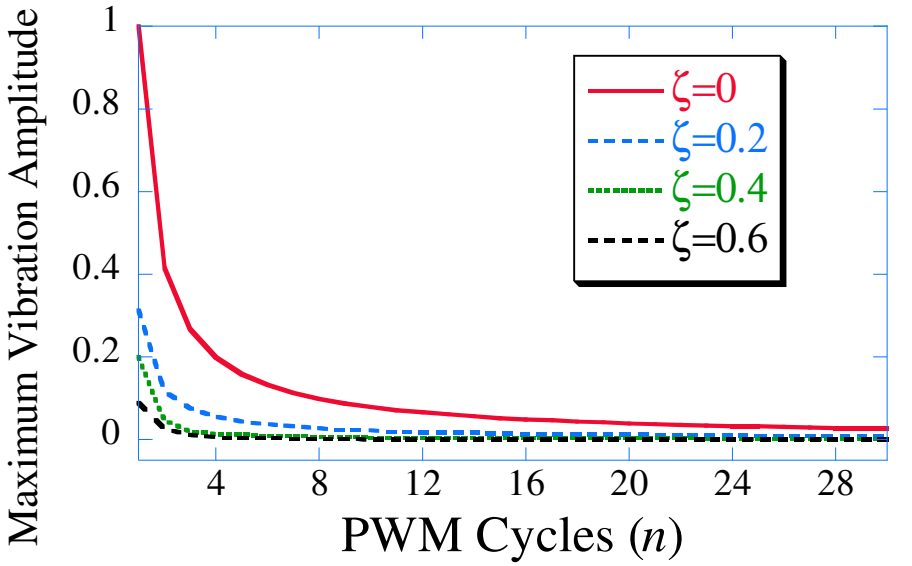

Figure 193: Maximum Residual Vibration Amplitude for Damped Benchmark System.

the number of pulse width modulation cycles needed to satisfy a vibration limit decreases. In general, increasing the damping for a second-order system, decreases the maximum peak overshoot and increases the system's rise time. Because damping decreases the maximum peak overshoot naturally, the lowest value of n required to meet a specified maximum vibration limit should also decrease. Figure 194 shows the number of pulse width modulation cycles needed to meet the specified residual vibration limit.

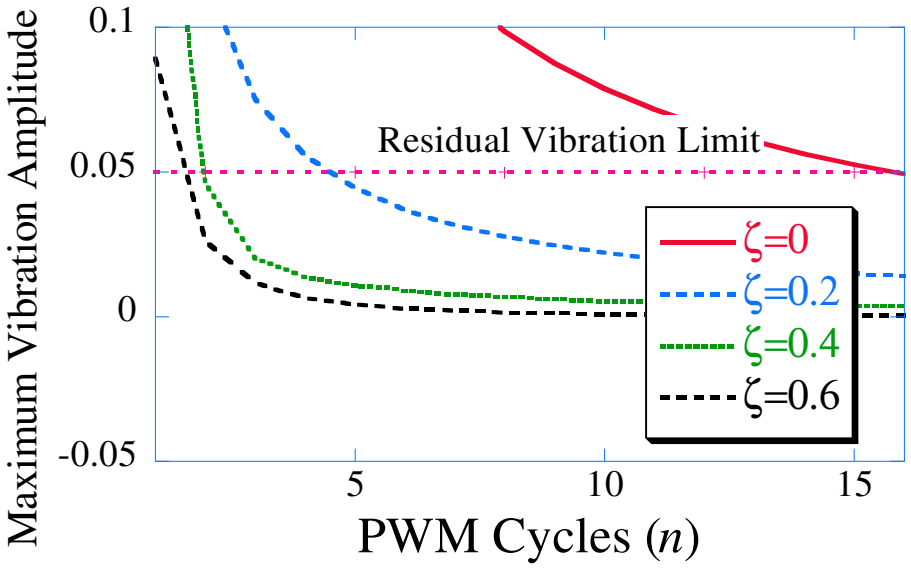

Figure 194: Lowest value of n for Damped Benchmark System.

From Figure 194, for $\zeta = 0$, the lowest value of n satisfying the 5% vibration requirement (for a unity magnitude step change) is 16. For $\zeta = 0.2$, the lowest value of n satisfying the vibration requirement is 5. For $\zeta = 0.4$, the lowest value of n satisfying the vibration requirement is 5. For $\zeta = 0.4, or 0.6$, the lowest value of n is equal to 2.

Although the sensitivity curves for the both the undamped and damped ISPWM approach the ideal ZV sensitivity curves, the ZV shaper is the least robust type of input shaper. From the sensitivity curves, it is obvious that a small deviation in estimated natural frequency can cause the amount of residual vibration to increase linearly. The ZVD shaper, however, is much more robust to modeling errors. As shown in section 1.6.1, the ZVD input shaper is more insensitive to variations in the system's natural frequency. The next section will discuss the ZVD ISPWM sensitivity.

5.3.2 Zero Vibration and Derivative Pulse Width Modulation Sensitivity

5.3.2.1 Undamped Benchmark System

A ZVD input shaper and PWM can be used in the system as shown in Figure 195. The input signal is convolved with a ZVD input shaper, and the PWM uses the staircase command in order to generate the thruster profile. The amplitudes and time locations for the ZVD

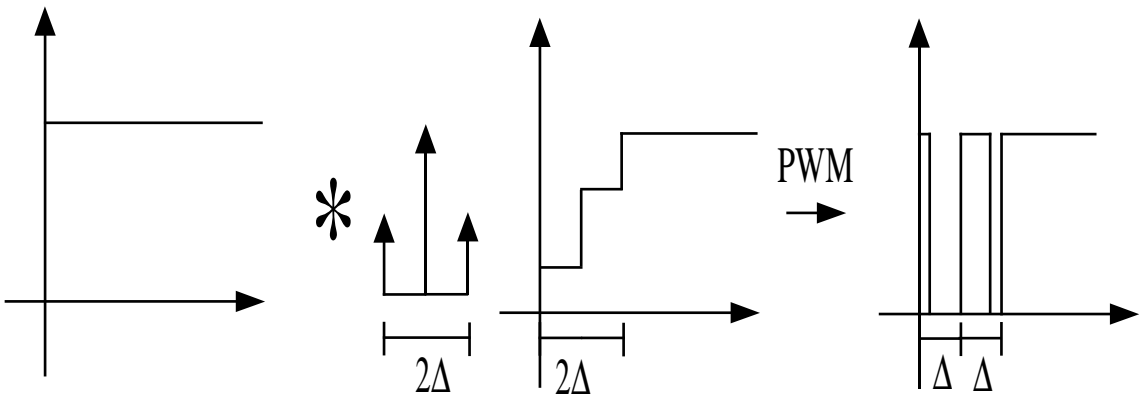

Figure 195: Combined ZVD Input Shaping and PWM.

shaper developed for the benchmark system are:

$$A = \begin{bmatrix} 0.25 & 0.5 & 0.25 \end{bmatrix}$$

$$t = \begin{bmatrix} 0 & 3.14 & 6.28 \end{bmatrix} \tag{96}$$

Notice that the ZVD shaper duration is twice that of the ZV shaper.

Because of the shape of the staircase command, the command is divided into two equal segments of duration Δ. One of the important parameters for the PWM is the number of PWM cycles, n, used in each of the time segments. For the case shown in Figure 195, n is equal to 1 for both cycles For the first time segment, the PWM has a 25% duty cycle, and for the second time segment, the PWM has a 75% duty cycle.

The sensitivity of this combined ZVD input shaped PWM (ISPWM) system must be evaluated. Like the ZV shaper, the ZVD shaper will not excite higher flexible modes in the system. However, because the staircase command is combined with a PWM, the effect of high mode excitation must be studied.

Similar to the ZV shaped ISPWM, the ZVD ISPWM shaper impulses and amplitudes were initially developed assuming zero damping. Because the ZVD shaped staircase command is divided into two distinct regimes, two sets of impulse amplitudes are needed to describe the entire ISPWM amplitude sequence. In order to completely describe the ISPWM shaper,

$$4n + 1 \tag{97}$$

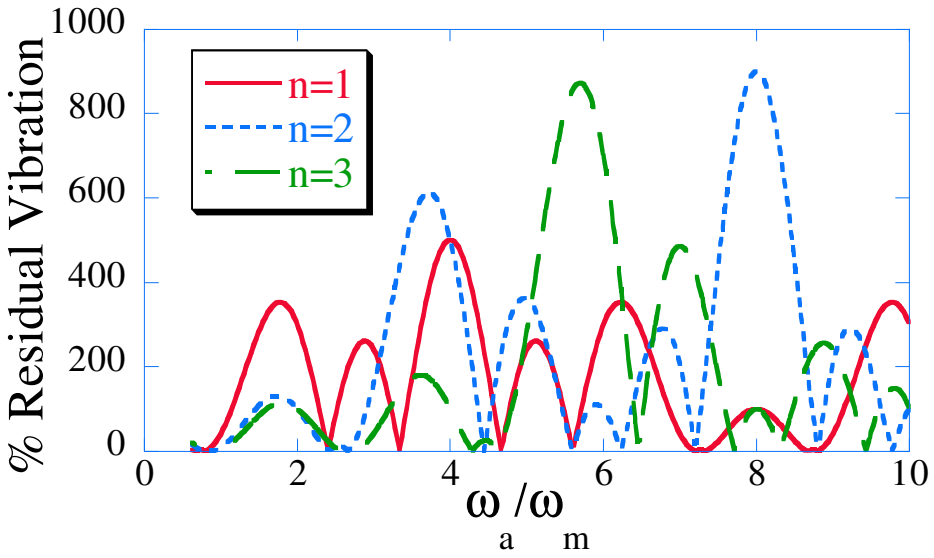

Figure 196: ZVD Input Shaping and PWM Sensitivity Curves.

impulses are needed, where n is the number of PWM cycles during each of the time segments. The amplitude and time locations of the impulses are calculated as follows:

$$A = \begin{bmatrix} 1 & -1 & 1 & -1 & 1 & \dots & 1 \end{bmatrix} \tag{98}$$

$$t = \begin{bmatrix} 0 & \frac{\Delta}{4} & \Delta & \frac{5\cdot\Delta}{4} & \dots & \frac{4(n-1)\Delta}{4} & \frac{(4\cdot n-3)\Delta}{4} \end{bmatrix} \tag{99}$$

Figure 196 shows the sensitivity curve of this combined ZVD ISPWM system. As seen in the figure, the number of PWM cycles affects the robustness of the ISPWM. For this case, the same number of PWM cycles was used for both time segments. For n=1, the sensitivity curve shows that modes 1.78 times the natural frequency will be excited higher than 3.5 times their unshaped levels. Similar high mode excitations are also seen at around three and four times the modeled frequency. As n increases, the frequency of the excited high modes shifts to the right, and the amplitude increases. When n=3, the highest peak has shifted to approximately 5.8 times the lowest natural frequency, but the amplitude has increased from three times the unshaped vibration to over eight times the unshaped vibration.

It is possible to shift the high mode excitation so far to the right that it will not significantly impact the response of the system. This effect is shown in Figure 197. For n=100, the sensitivity curve approximates the ideal ZVD sensitivity curve and has no high

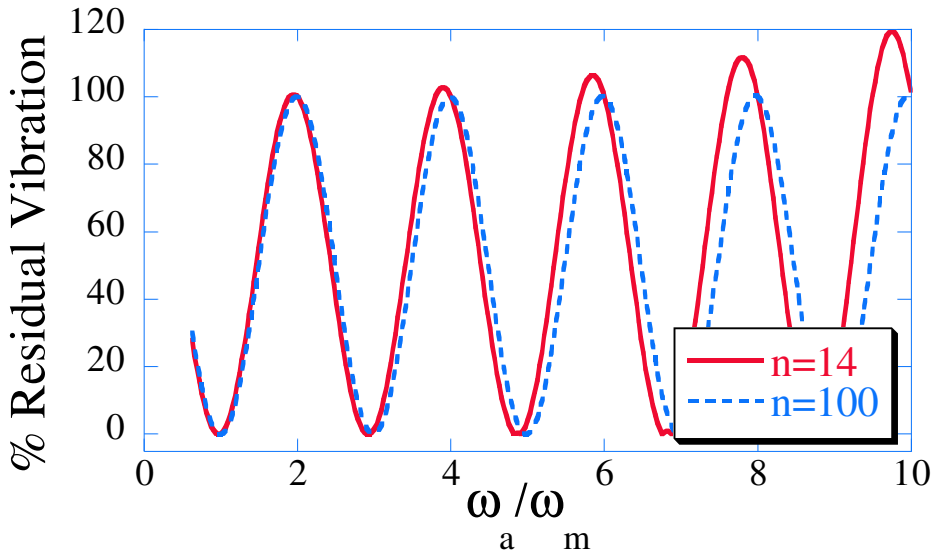

Figure 197: ZVD Input Shaping PWM Sensitivity Curves.

mode excitation for the range studied ($0.1 \leq \omega_a \leq 31$). The sensitivity curve also shows that for n=14, the ZVD ISPWM begins to approximate the ideal ZVD shaper sensitivity.

It is possible to combine a ZVD shaper and pulse width modulation in order to eliminate the residual vibration. As the number of PWM cycles increases, the effect of the PWM high mode excitation decreases. However, increasing the number of cycles, n, increases the amount of wasted fuel. In order to determine how many PWM cycles are needed for the ZVD shaper, first the acceptable maximum residual vibration amplitude must be determined. Once this level has been determined, it is possible to utilize Figure 198 in order to pick the smallest value of n that will guarantee the level of vibration will not exceed the required specification. Figure 198 shows the maximum residual vibration amplitude for a ZVD shaped step input on the benchmark system. As the number of PMW cycles increases, the amplitude of the residual vibration decreases. However, it is clear from the figure, that for $n \geq 20$ the level of residual vibration is approximately zero. So, there is no advantage to more PWM cycles.

If the acceptable amount of residual vibration is 5%, then Figure 199 can be used to determine the value of n. As seen in the figure, the value of n is determined using the intersection of the acceptable vibration amplitude limit (shown as the dashed line) and

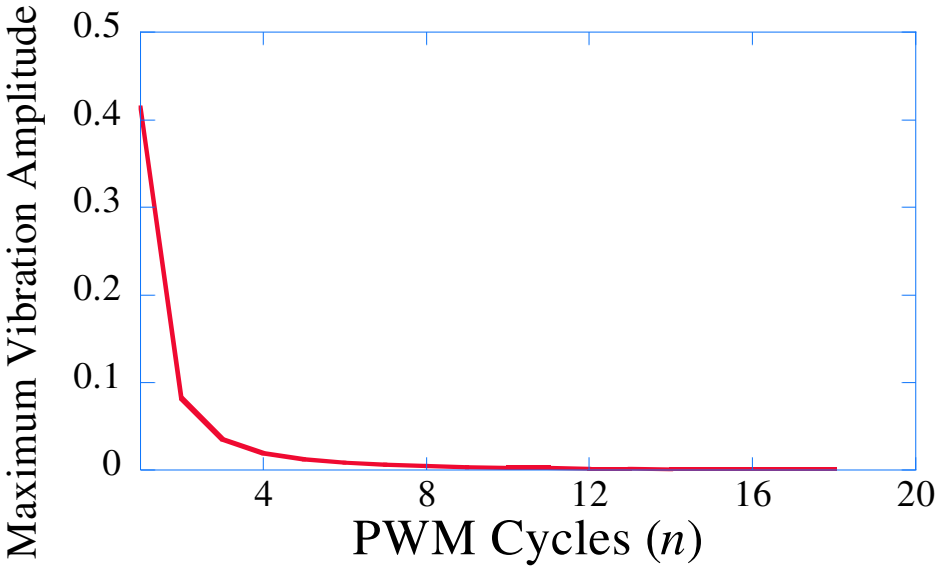

Figure 198: Maximum Residual Vibration Amplitude for ZVD Shaper.

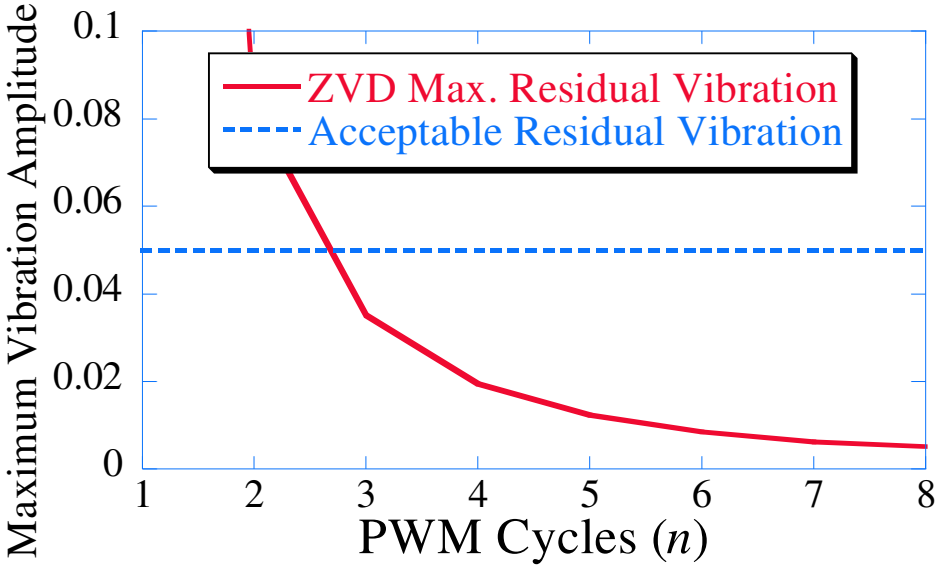

Figure 199: Maximum Residual Vibration Amplitude for ZVD Shaped Step.

the maximum vibration amplitude (shown as the solid line). For the ZVD shaped case where the shaper duration, 2Δ, is equal to 2π, the optimum value of n is 3. However, it is important to note that this method assumes the unshaped maximum vibration to be equal to one.

5.3.2.2 Damped Benchmark System

Damping affects ZVD input shapers in the same manner as the ZV shapers. Damping changes the impulse time locations and magnitudes. For $\zeta = 0.2$, the amplitudes and time locations of a ZVD shaper generated for the damped benchmark system are:

$$A = \begin{bmatrix} 0.4291 & 0.4519 & 0.1190 \end{bmatrix} \tag{100}$$

$$t = \begin{bmatrix} 0 & 3.20 & 6.41 \end{bmatrix} \tag{101}$$

Comparing (102) and (101), the duration of the damped ZVD shaper is slightly longer than the corresponding undamped ZVD shaper. The amplitudes of the damped ZVD shaper are different when compared to the undamped case. The first amplitude increases from 0.25 to 0.4291 and the second amplitude decreases from 0.5 to 0.4519. The third amplitude decreases from 0.25 to 0.1190. From (101), it is clear that the time locations and amplitude magnitudes depend on the damping ratio of the system.

In order to calculate the ISPWM sensitivity for the damped cases, generalized expressions were developed.

$$t_1 = \begin{bmatrix} 0 & PWM \cdot A_1 & \ldots & (n-1) \cdot PWM & (n-1) \cdot PWM + PWM \cdot A_1 \end{bmatrix} \tag{102}$$

$$t_2 = \begin{bmatrix} 0 & PWM \cdot (A_1 + A_2) & \ldots & (n-1) \cdot PWM & (n-1) \cdot PWM + PWM \cdot (A_1 + A_2) \end{bmatrix} \tag{103}$$

where n is the number of PWM cycles. Equation 102 shows the time locations for the amplitudes occurring in the first time segment. Equation 103 shows the generalized expressions for time locations of the amplitudes occurring in the second time segment.

The two expressions are combined in the following manner. The first expression is used to calculate the amplitudes during the first time segment. The second expression is used to calculate the amplitudes for the second time segment. The time locations for the two expressions are combined together to generate the damped ISPWM shaper.

The damped ZVD ISPWM shaped sensitivities are similar to the damped ZV ISPWM shaped cases. As the number of PWM cycles increases, the ISPWM shaper approaches the ideal damped ZVD sensitivity plot. The next section discusses a MATLAB program developed that calculates the lowest value of n that satisfies the Percent Residual Vibration constraints.

5.4 ISPWM MATLAB Code

The figures shown in the sections above were generated for the benchmark system using specific conditions; therefore, a general use program was written in MATLAB. The user enters the values of the required parameters as shown below:

$$\text{ISPWM}(\text{num}, \text{den}, \text{zeta}, \text{shaper}, \text{res\_vib}) \tag{104}$$

where *num* is the plant transfer function numerator, *den* is the plant transfer function denominator, *zeta* is the system's damping ratio, *shaper* is the desired shaper (ZV or ZVD), and *res_ vib* is the ratio of unshaped and shaped residual vibration limit (as a percentage).

From these inputs, the code determines the lowest value of n that meets the residual vibration requirements and utilizes the desired input shaper. Figure 200 shows the output of the ISPWM MATLAB Code. As seen in the figure, the program, produces three separate plots. The upper graph shows the shaped PWM command as a function of time. The middle graph shows the system response to a step command, a shaped command, and the shaped PWM command. The bottom graph displays the sensitivity curve for the shaped PWM for the value of n the program calculated. For the simulation shown in the figure, it is obvious that the shaped PWM has approximately the same system response as the shaped response. From the sensitivity curve, it is possible to identify where the high mode excitation will occur. Another advantage to using the ISPWM MATLAB program is that it can accommodate systems with non zero damping coefficients.

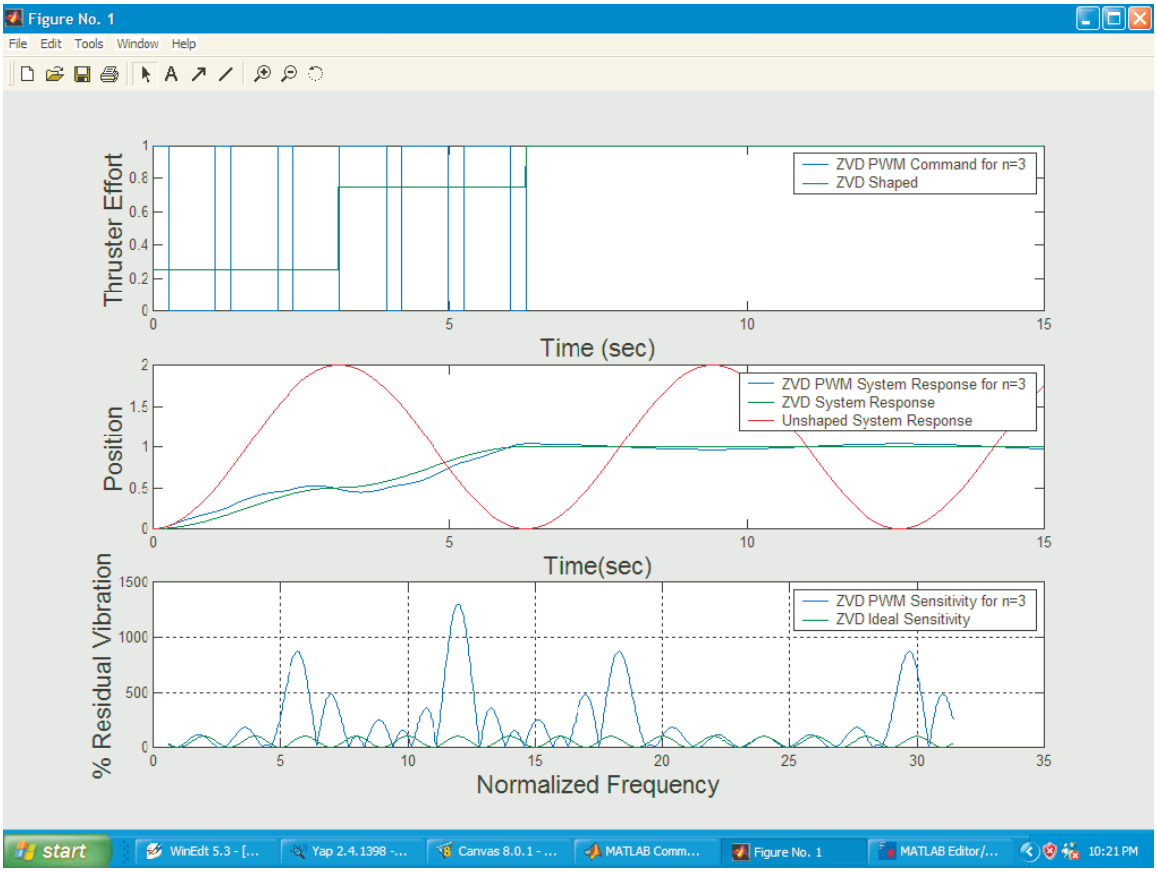

Figure 200: ISPWM MATLAB Simulation Figure Window.

5.5 Summary of Combined Input Shaped Pulse Width Modulated Commands

It is possible to combine the beneficial vibration reduction characteristics of shaping with the on-off nature of pulse width modulated commands. By using a ZV or ZVD shaper instead of a unity magnitude shaper, the excitation of the high modes can be controlled by the number of pulse width modulation cycles, n, used. As the number of PWM cycles increases, the higher the frequency of the excited modes. However, the amount the modes are excited also increases. The sensitivity plot of the ISPWM shaper is useful in determining where the excited higher mode occur. Increasing the number of PWM cycles also increases the fuel expenditure; therefore, it is desirable to pick the lowest value of n.

In order to facilitate this, a generalized MATLAB program was created which allows a user to enter in basic system information, to pick a shaper, and enter the desired level of

residual vibration. From this information, the program calculates the minimum number of PWM cycles that will satisfy all of the criteria and displays the system's response to a step input.

CHAPTER VI

FORMATION FLYING EXPERIMENTS AT TOKYO INSTITUTE OF TECHNOLOGY

Formation flying experiments were conducted at the Two-Dimensional Spacecraft Dynamics Simulator at the Tokyo Institute of Technology [38]. The formation flying experiments were conducted during summer 2002 and January-February 2003. The experiments completed during the winter months of 2003 were funded through a National Science Foundation Ph.D. Dissertation Enhancement Award.

6.1 Testbed Description

The satellite testbed consists of a 3 m x 5 m flat glass floor, three Dynamics and Intelligent control Simulators for satellite Clusters (DISC) units, an image processing system, and wireless communication devices.

The flat glass floor has a dark background with a equally spaced grid markers located underneath the glass. The glass floor allows the DISC units to move easily across its surface. Adjacent to the floor is a workstation that houses the main controls for the DISC units and the image processing system. From the workstation, the user is able to send commands remotely to each of the DISC units and operate the video recording equipment.

Figure 201 shows a picture and description of the DISC units. The DISC units consist of the following: aluminum frame, two air tanks and regulators, gyro, four air pads, eight thruster nozzles, battery, laptop personal computer, and wireless Local Area Network (LAN). The air tanks are filled using a portable air compressor. In order to simulate zero gravity conditions during operation, the DISC units float on air bearings. The four air pads provide enough lift so that the DISC units do not directly contact the glass floor. In addition to cancelling the weight of the unit, the air columns provide almost friction free movement across the glass floor.

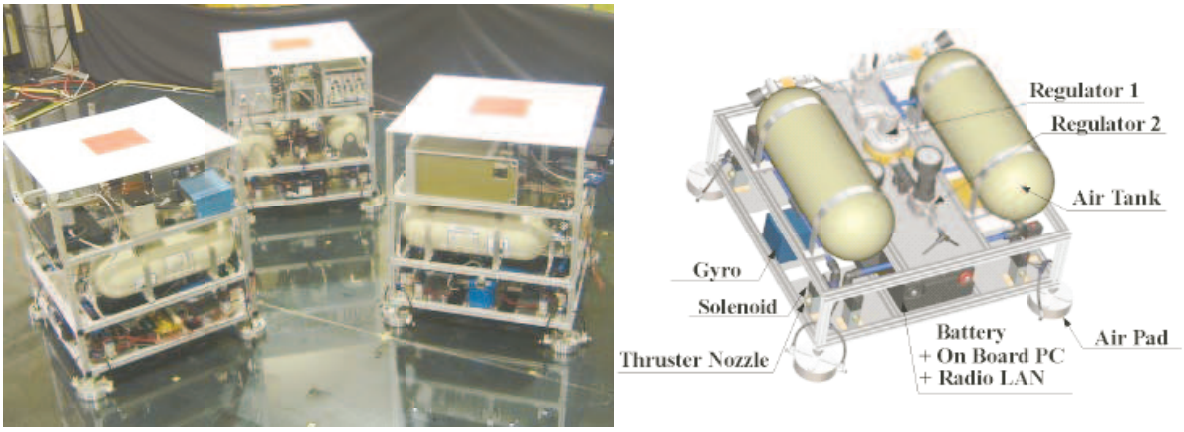

Figure 201: Dynamics and Intelligent Control Simulators for Satellite Clusters Units.

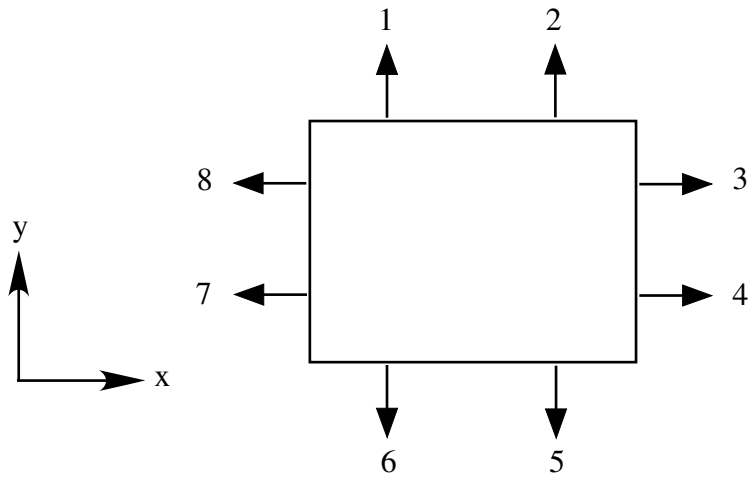

Figure 202: DISC Unit Thruster Location and Direction.

In order to maneuver the DISC units, eight thrusters are mounted on the corners of the frame. The direction of each thruster is shown in figure 202. The direction of the arrow indicates the direction the DISC unit will move when that thruster is turned on. A thruster map was developed in order efficiently determine which pair of thrusters is required for translational and rotational maneuvers.

The onboard gyro is used to determine the attitude of the DISC unit. At the beginning of each testing session, the gyro is calibrated in order to ensure attitude accuracy. Each DISC unit is equipped with an onboard laptop personal computer (pc). The pc is equipped with a wireless LAN card so that it can communicate easily with the workstation. The pc runs the operating system for the DISC unit. It receives the desired trajectories and its

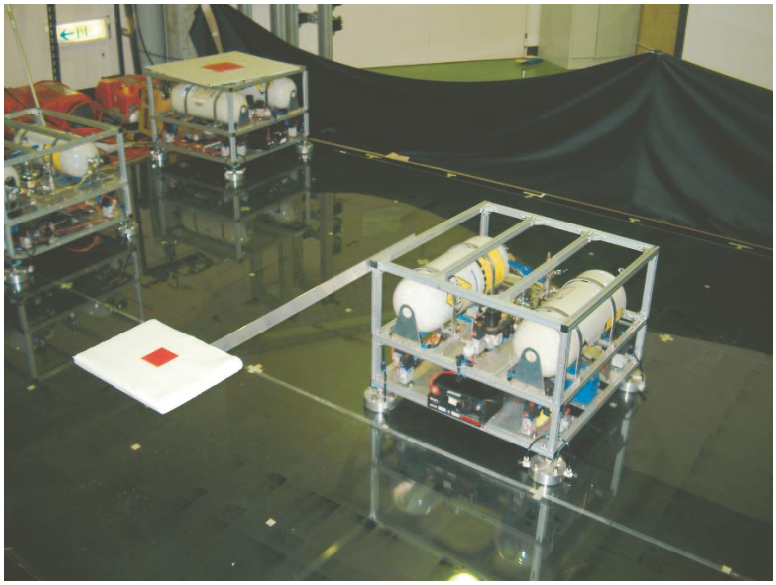

Figure 203: DISC Unit with Flexible Arm Attached.

current position from the workstation.

As stated earlier, an overhead camera is positioned so that it has a view of the entire glass floor. In addition, a video cassette recorder (vcr) is used to record the images from the overhead camera. The position of each DISC unit is calculated from digital images captured by an overhead camera. Colored markers placed on the top of the DISC unit are used by the tracking software. Tracking recognition software enables real time position determination of up to three DISC units and accounts for the fish-eye lens effect.

The DISC units shown in Figure 201 are extremely rigid. In order to test if input shaping can be used effectively on the DISC units, a flexible appendage was attached to simulate a solar panel or flexible antennae as shown in Figure 203. The flexible arm was constructed out of a thin aluminum beam. The arm was mounted so that the primary mode of vibration is parallel to the glass floor. The arm attaches to top of the DISC unit and has two sets of holes. The natural frequency of the arm can be controlled by changing the connection. The natural frequency of the flexible arm can vary between 0.9 - 1.3 Hz. At the end of the arm, a colored marker with a white background was placed on top. The colored marker is used to calculate the position of the arm's tip.

Figure 204 shows the flow diagram for the DISC control algorithm. The workstation

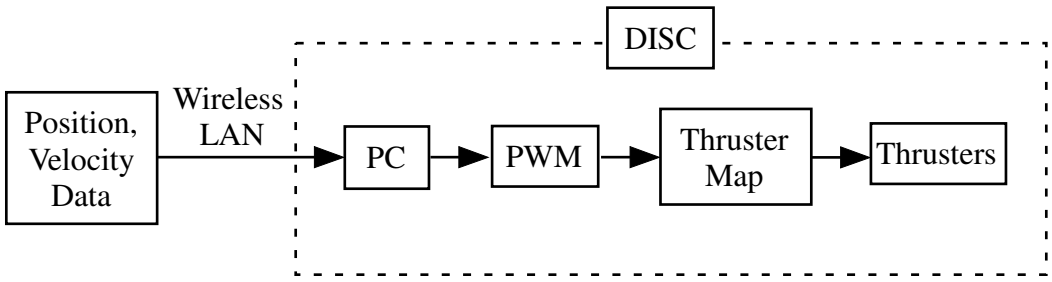

Figure 204: DISC Unit Control Diagram.

sends each DISC unit its desired position and velocity profiles, and the real time position and velocity via the wireless LAN card. Each DISC unit has no information about the position of the other units; therefore, it is a centralized control structure. Once the data is received by the DISC unit, it is passed to the onboard pc and used in the feedback controllers. Two feedback PD controllers are used on each DISC unit. The first feedback algorithm is used to control the position and velocity of the DISC unit and has the following form.

$$u = K_p \left(p_{desired} - p_{actual}\right) + K_v \left(v_{desired} - v_{actual}\right) \tag{105}$$

where p and v are the position and velocity respectively, u is the thruster force, K_p is the proportional gain, and K_v is the derivative gain. The thruster control force u is calculated every 60ms.

The second feedback algorithm is used to control the attitude of the DISC unit and has the following form:

$$u_{attitude} = Kp_{yaw} \left(\theta_{desired} - \theta_{actual}\right) + Kv_{yaw} \left(\dot{\theta}_{desired} - \dot{\theta}_{actual}\right) \tag{106}$$

where $u_{attitude}$ is the attitude thruster control force, Kp_{yaw} is the proportional gain, and Kv_{yaw} is the derivative gain. The thruster control force $u_{attitude}$ is calculated every 300ms.

The calculated thruster forces, u and $u_{attitude}$, are amplitude varying signals, but the thrusters can only utilize on-off commands. Therefore, the thruster signal is sent to a pulse width modulation program to convert the control signal, u or $u_{attitude}$, into a signal with a constant amplitude of 1.6 N. It is possible that the calculated amplitude of the thruster force will be larger than the thruster output of $1.6N$. If that is the case, the PWM program calculates the amount of time (in multiples of 60ms) that the thruster needs to be turned

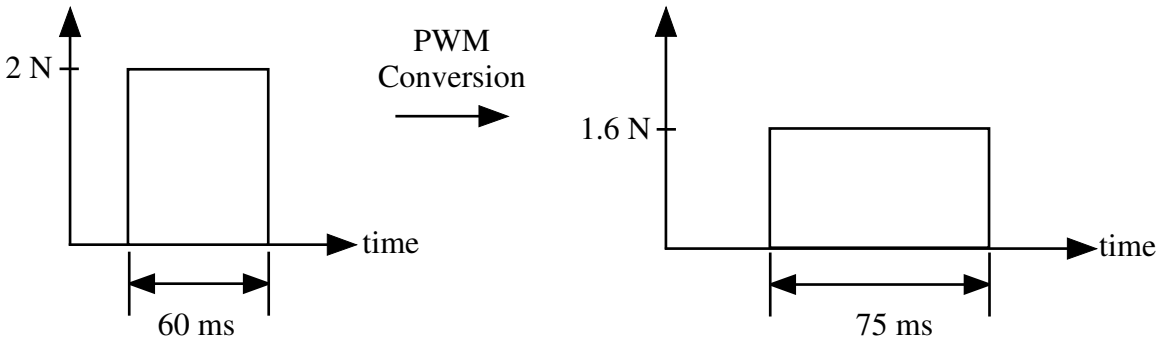

Figure 205: PWM Conversion of Thruster Force.

on in order to match the calculated thruster force. This process is shown in Figure 205, and the thrusters are sent the command resulting from the PWM conversion. The thruster command for the translation motion is recalculated every 60ms and sent to the DISC unit.

Once the modulated thruster pulse has been calculated, a thruster map is used to determine which pair of thrusters will be turned on. It is possible to have two pairs of thrusters turned on. This occurs when both u and $u_{attitude}$ are required. However, it is possible to maneuver the DISC unit without employing attitude control. This is accomplished by turning off the attitude feedback control program.

6.2 Verification of Input Shaping

It is important to verify that input shaping can be successfully used on flexible satellite systems. Figure 206 shows the experimental results of a flexible DISC unit performing a straight line translation maneuver with and without input shaping. The frequency of the flexible arm was calculated to be approximately 1.0 Hz. The DISC unit is controlled by a PD feedback controller and has a single flexible appendage. A strain gauge is attached at the midpoint of the flexible arm. As seen in Figure 206, the translation maneuver that utilizes input shaping has a much better system response than the translation maneuver that does not utilize input shaping.

In addition to translation maneuvers, input shaping has been experimentally verified for rotation maneuvers. Figure 207 compares an unshaped and a shaped rotation maneuver. The shaped commands were calculated from the closed-form solution presented in [53]. ZV

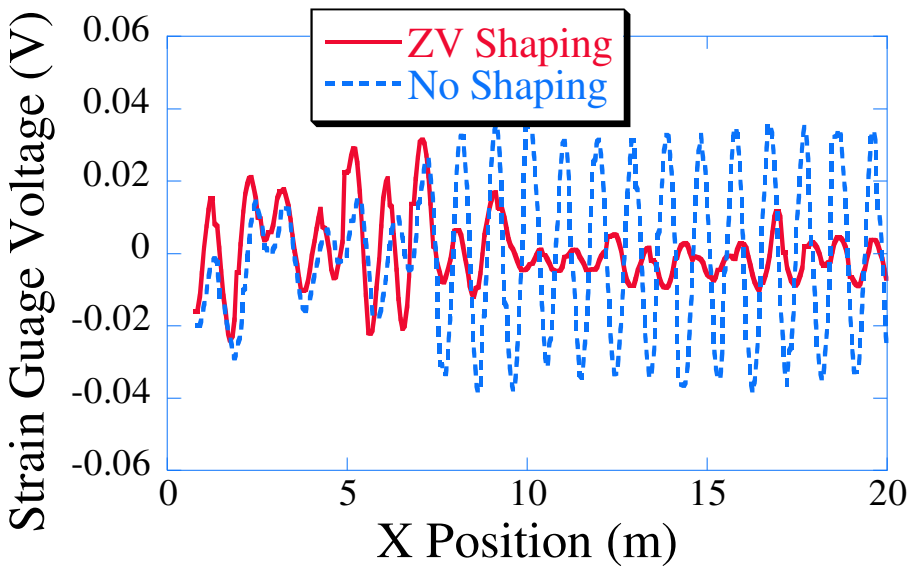

Figure 206: Flexible DISC Response to a Translation Maneuver.

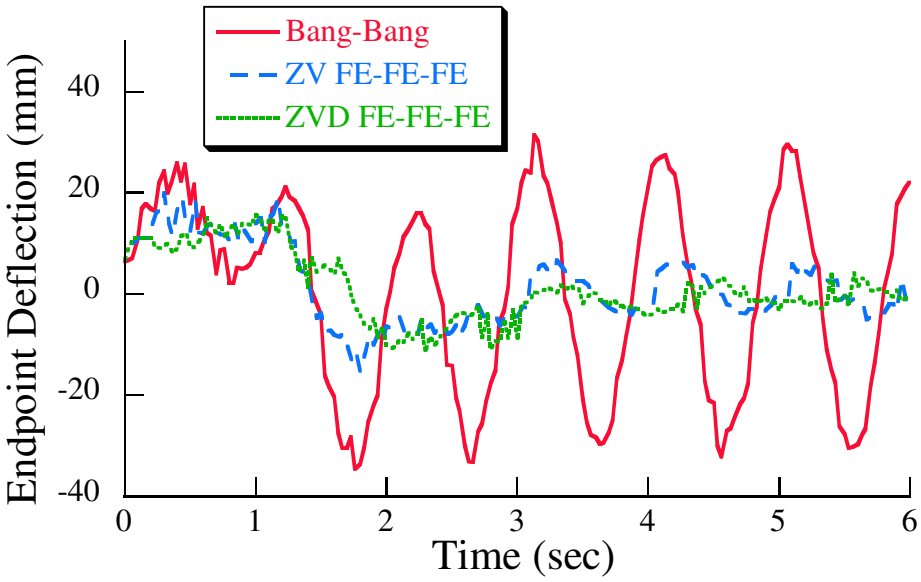

Figure 207: Flexible Appendage Endpoint Deflection for a Rotation Maneuver.

FE-FE-FE refers to a closed form Zero Vibration fuel efficient command. ZVD FE-FE-FE refers to a closed form Zero Vibration and Derivative fuel efficient command. More details on both of these analytic commands can be found in [53]. From the figure, it is clear that input shaping provides superior vibration reduction for the flexible appendage. The small amount of residual vibration present in the system after both the ZV FE-FE-FE and ZVD FE-FE-FE commands is due to the nonlinearities in the system and the estimation of the

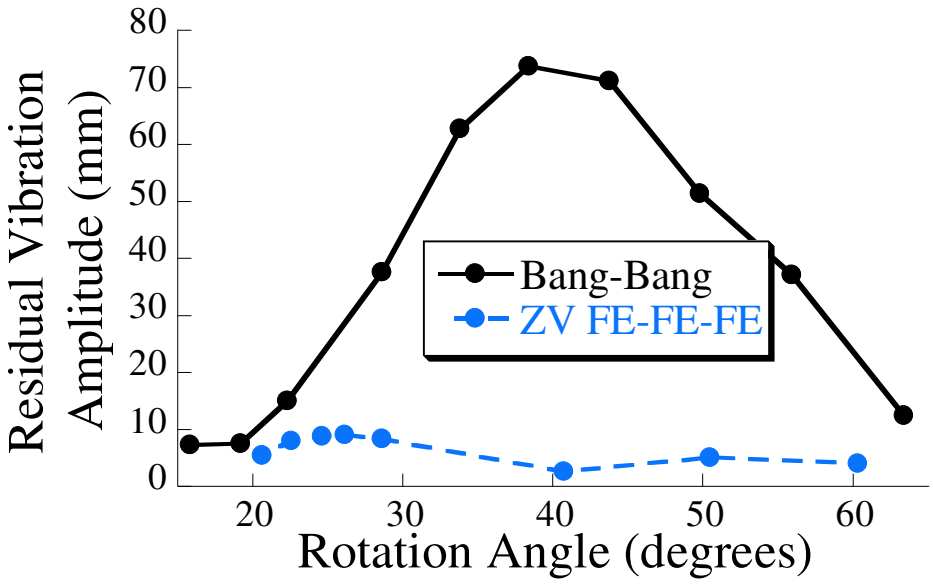

Figure 208: Residual Vibration Amplitude versus Rotation Angle.

flexible appendage's natural frequency.

Figure 208 demonstrates input shaping's ability to decrease the residual vibration present in the flexible appendage for different rotation maneuvers. For a large range of rotation maneuvers, input shaping is able to significantly decrease the system's residual vibration amplitude compared to a bang-bang command. As stated earlier, the frequency of the flexible appendage was adjustable. Figure 209 shows the residual vibration amplitude of the flexible appendage's endpoint for different appendage frequencies. Both the ZV and ZVD input shaped commands provide superior residual vibration reduction. As expected, the ZVD shaped command provides the greatest amount of vibration reduction. However, both shaped commands are far superior to the bang-bang command.

The transient deflection of the flexible spacecraft is also important. It is possible to damage the flexible appendage if the transient deflection is too large. Figure 210 shows the transient deflection of the DISC units flexible appendage. The deflection was measured at the endpoint of the arm. Using shaped commands to drive the DISC unit results in decreased transient deflections for a wide range of rotation maneuvers.

The above results experimentally verify the utility of applying input shaping to flexible systems. Not only does input shaping eliminate the residual vibration in the system, it

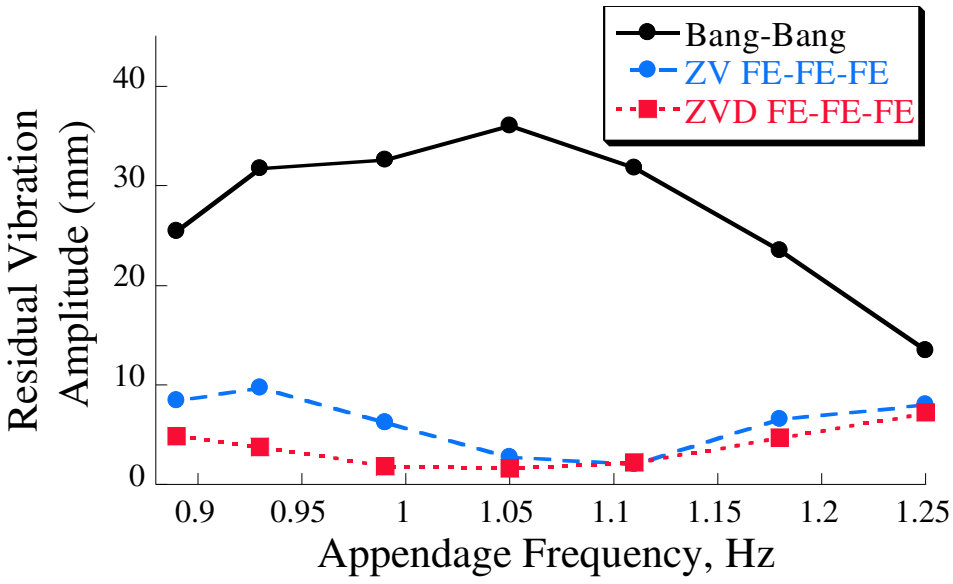

Figure 209: Residual Vibration Amplitude versus Flexible Appendage Frequency.

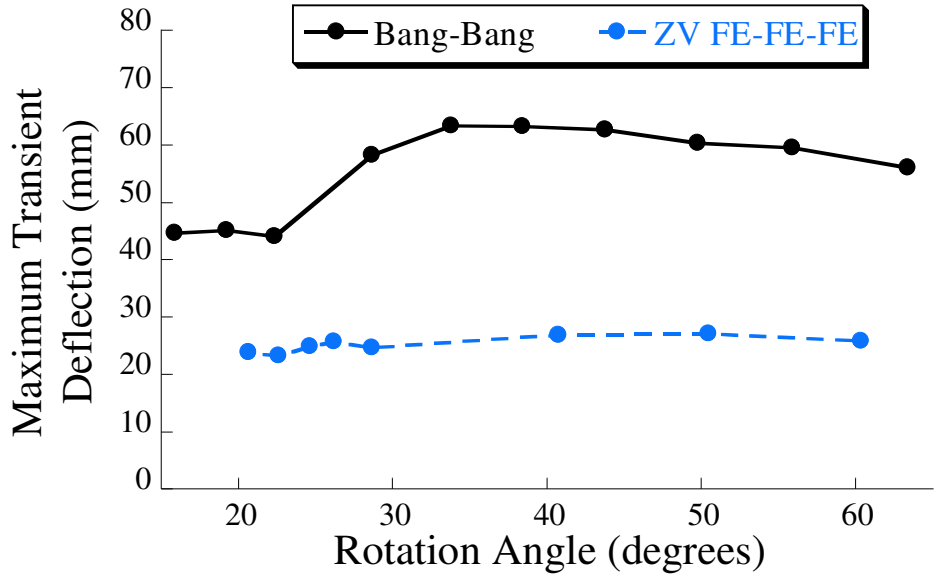

Figure 210: Transient Deflection of Flexible Arm versus Rotation Angle.

also decreases the amount of transient deflection during the maneuver. The next section discusses the formation flying experiments completed.

6.3 Formation Flying Experiments

The formation flying architecture used to command the DISC units is neither a leader-follower nor a virtual-structure architecture. Instead it is a completely centralized control

scheme. The desired trajectories for the DISC units are calculated before hand and are sent to the DISC units. Each DISC onboard computer receives its instructions from the main computer and has no information regarding the desired trajectory or response of the other DISC units. For many of the experiments, only one DISC unit was operated; however, the integrity of the formation is not compromised since each DISC unit is sent information regarding its desired path directly. The desired path sent to the DISC unit does not depend on the position or response of any other DISC unit. Therefore, the desired trajectory for each disc unit is the same whether one unit is in operation or three.

6.3.1 Straight-Line Maneuver

The first maneuver performed by the DISC units was a straight-line maneuver. For this maneuver, it was desired that the DISC unit translate across the workspace. The flexible arm was oriented so that it was perpendicular to the direction of travel. ZV and ZVD input shapers were designed for a 1.0 Hz undamped frequency. For the straight-line maneuver, the desired position, and velocity was convolved with either the ZV or ZVD input shaper. The resulting trajectory was used as the desired trajectory for the system. A strain gauge was attached to the midpoint of the flexible arm, and the voltage from the amplifier was transmitted from the DISC unit to the central computer. Figure 211 shows strain gauge voltage for a straight-line maneuver. Convolving the straight-line trajectory with the input shaper provides excellent vibration reduction. Both the ZV and ZVD shaper reduce the amount of vibration in the system. The ZVD shaper has addition robustness to parametric uncertainties.

6.3.2 Same-Orbit Maneuver

The second type of maneuver performed by the DISC units was a same-orbit maneuver. Basically, the DISC units are commanded to travel in a circle until their fuel is depleted. As mentioned earlier, the DISC units have two types of control: attitude control and position control. It is possible to operate the DISC unit without the attitude control enabled. When the attitude control is enabled for this maneuver, it is desired that the flexible appendage always be pointing radially outward from the center of the circle. The attachment point of

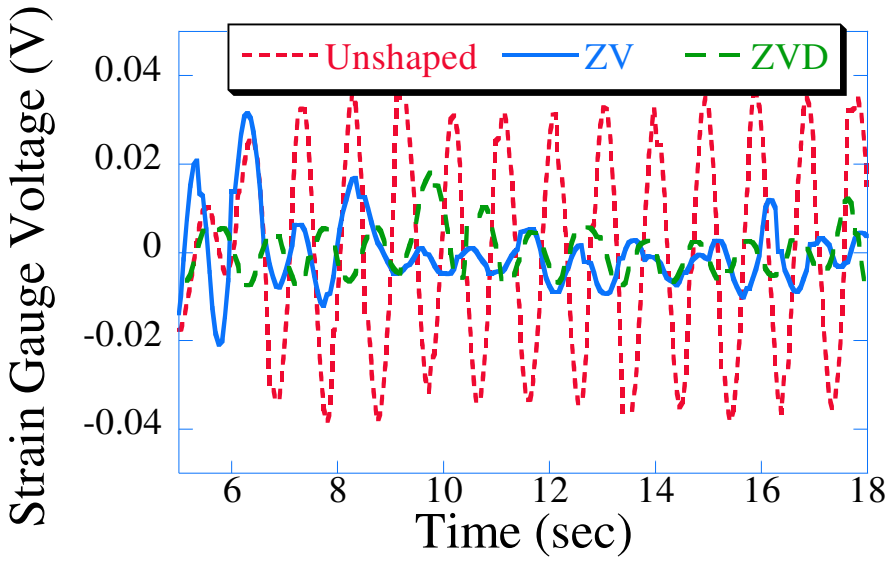

Figure 211: Strain Gauge Voltage for Straight-Line Maneuver.

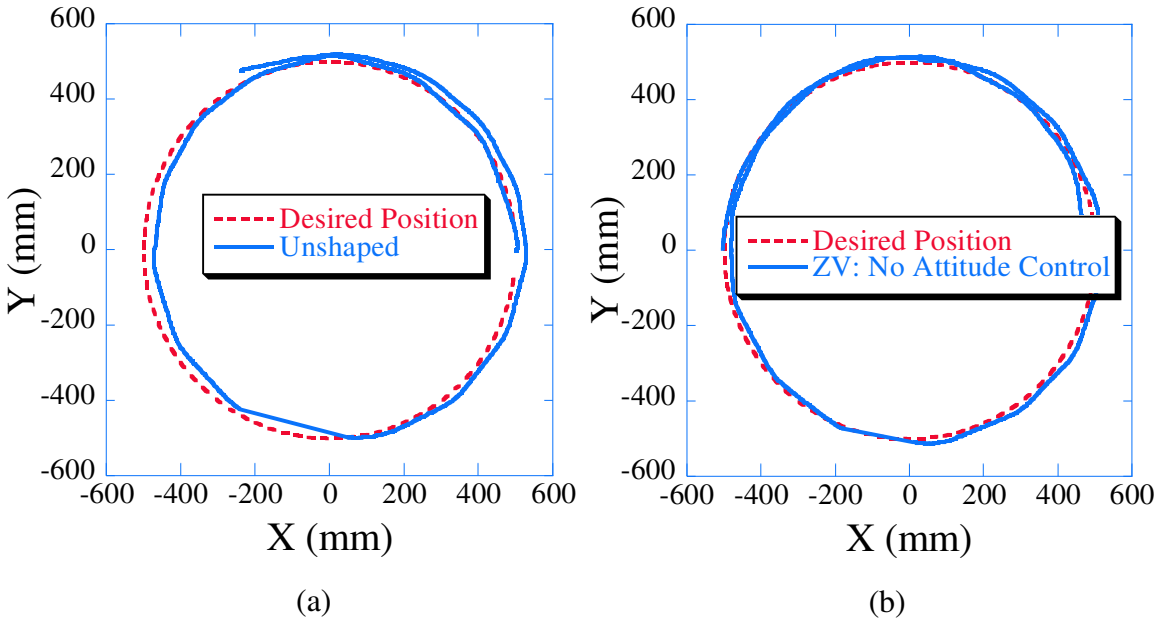

Figure 212: DISC Unit Response to Same-Orbit Maneuver.

the flexible appendage was adjusted so that its lowest vibration mode was approximately 1.0 Hz. Figure 212 shows the desired trajectory, unshaped and shaped responses of the DISC for the same-orbit maneuver. Figure 212a shows the unshaped response and Figure 212b shows the shaped response. The PD feedback gains do an excellent job of keeping the DISC unit on the desired circular trajectory. For this particular case, the attitude control

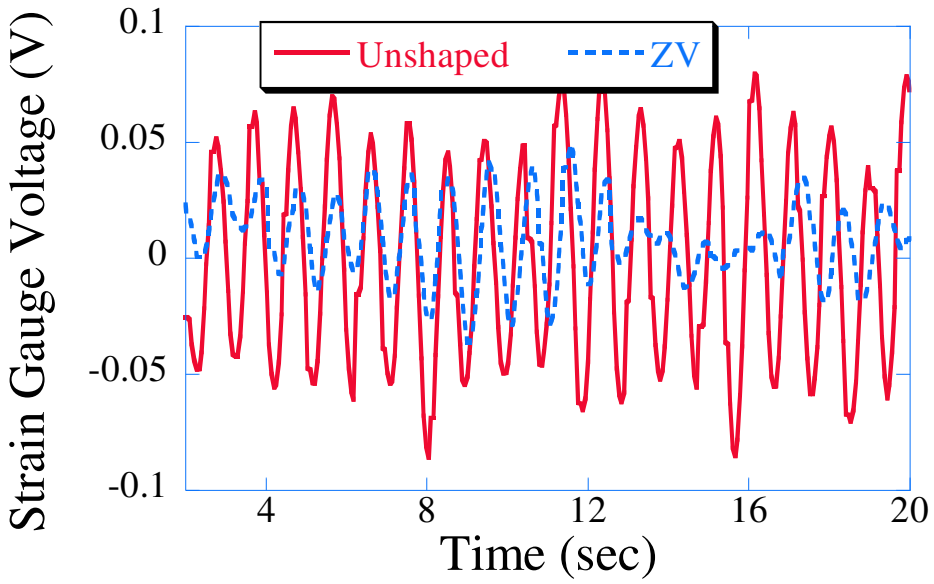

Figure 213: Flexible Arm Response for Same-Orbit Maneuver with No Attitude Control.

was disabled. So, although the flexible appendage starts the maneuver pointing radially outward, it does not maintain this desired position.

As with the unshaped case, the feedback controller is able to keep the DISC unit on the desired circular trajectory. Comparing Figure 212a and Figure 212b, the responses are very similar. For both trajectories, the DISC units remain near the desired trajectory, and they each travel around the circle at least once. Figure 213 shows the strain gauge voltage for the same-orbit maneuver when no attitude control is used. The figure shows the strain gauge voltage during the middle portion of the maneuver after the transient response is finished.

The ZV and ZVD input shapers were designed to eliminate a 1.0 Hz vibration. Although in theory both of these shaped trajectories should eliminate all of the vibration, nonlinearities and errors in the system prevent this from occurring. One of the largest errors in the system comes from the estimation of the natural frequency. The flexible arm was fabricated out of aluminum and is a thin beam. In reality, it has more than one mode. Also, the natural frequency of the arm was estimated by displacing the endpoint and recording the time it took for ten cycles. When the ZV and ZVD input shapers were generated for this system the damping was assumed to be zero, and this is a good approximation for

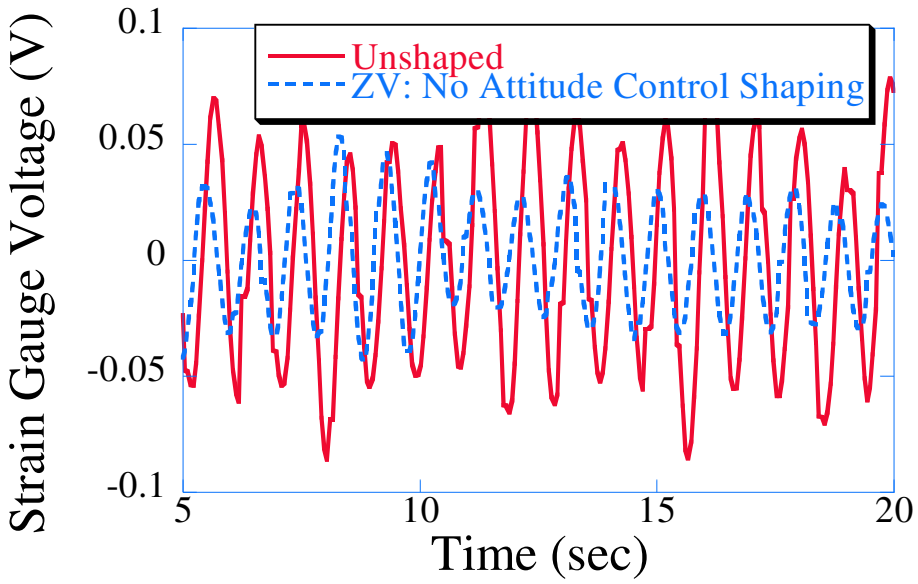

Figure 214: Flexible Arm Response for Same-Orbit Maneuver with Unshaped Attitude Control.

the lightly damped beam. The predominant nonlinearity in the system comes from the thrusters. When activated, the thrusters do not instantly reach their maximum force output, and once on, they do not maintain a constant output. However, as seen from the figure, the shaped trajectories significantly reduce the vibration in the system when compared to the unshaped trajectory response.

Figure 214 shows the response of the flexible appendage to a same-orbit maneuver when the attitude control is enabled. Although the attitude control is enabled, the desired attitude is not shaped. Only the desired position and velocity are shaped. As expected, the shaped trajectories have a lower level of deflection than the unshaped trajectory. Comparing Figure 213 and Figure 214 shows that the level of residual vibration is higher when attitude control is utilized. This is true for the unshaped case as well. Adding attitude control to the system increases the level of vibration. The attitude control is trying to keep the flexible appendage pointing radially outward, therefore every 300 ms the thrusters fire in order to accomplish this. Every time the thrusters fire, vibration is induced in the system. Input shaping the position and velocity eliminates the vibration that results from the thrusters turning on to follow these trajectories. However, it does not reduce the vibration that results from the attitude control. The shaped response does have a smaller level of deflection.

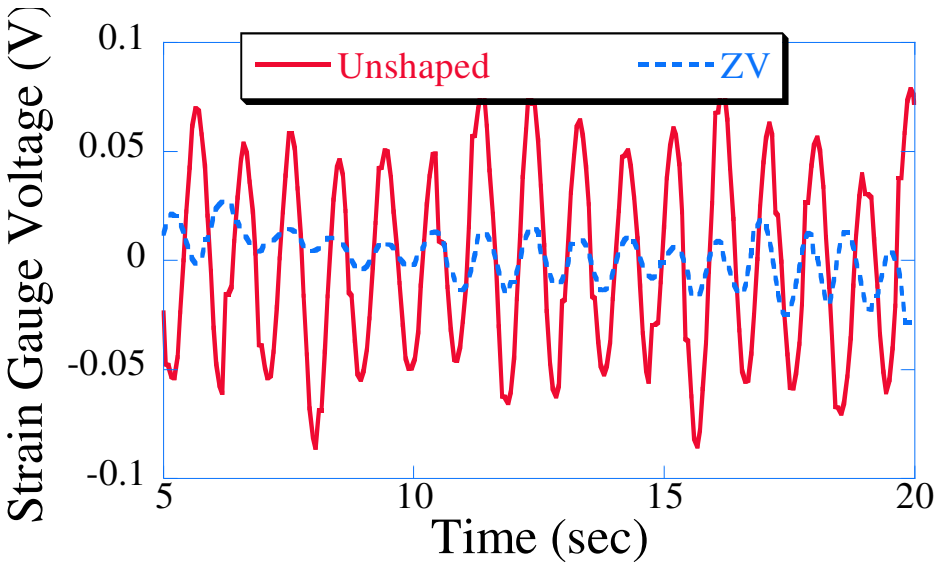

Figure 215: Flexible Arm Response for Same-Orbit Maneuver.

It is possible to shape the desired position, velocity and attitude. Figure 215 shows the response of the flexible arm when all the desired trajectories are shaped. From this figure, it is clear that input shaping the attitude control is important in eliminating the vibration in the system. The difference between the responses shown in Figure 214 and Figure 215 is that the attitude is shaped in the later figure. Therefore, input shaping should be used on both the position and attitude controllers.

Input shaping the desired position and attitude also reduces the amount of fuel needed to perform a same-orbit maneuver. Figure 216 shows the total fuel consumption for the same-orbit maneuver as a function of maneuver time. The total fuel consumption is calculated as the summation of time any of the thrusters are turned on. For example, suppose thrusters 1 and 2 are both turned on for 1 second. The total fuel consumption would be equal to two seconds. It was assumed that the thrusters could deliver a constant, instant 1.6 N of force. This figure captures the amount of fuel consumed for the same-orbit case when attitude control is enabled. The ZVD shaped trajectory consumes the least amount of fuel.

Although input shaping significantly reduces the amount of vibration in the system, it also introduces a delay in the system. Figure 217 shows the x position versus time for the unshaped and shaped trajectories. The ZVD shaped trajectory produces the largest

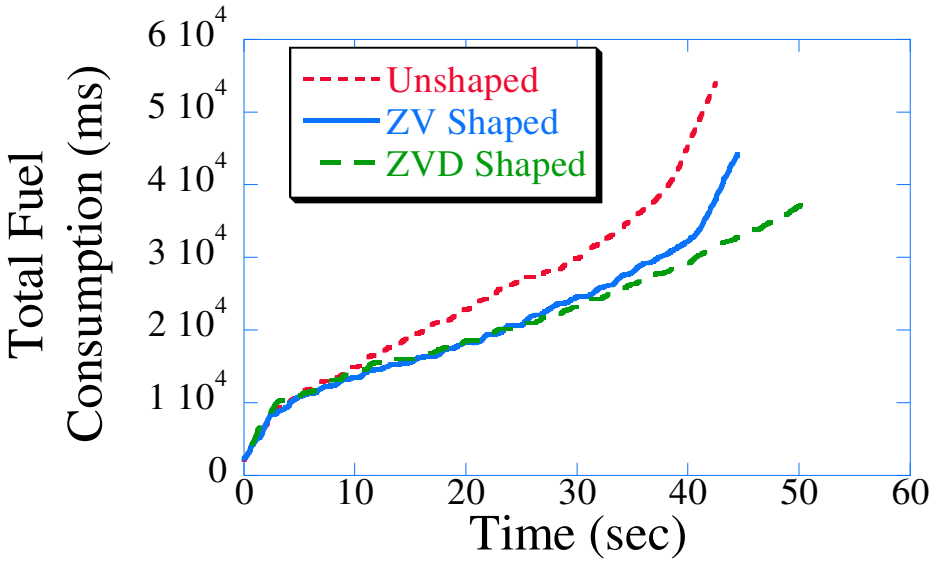

Figure 216: Total Fuel Consumption for Same-Orbit Maneuver.

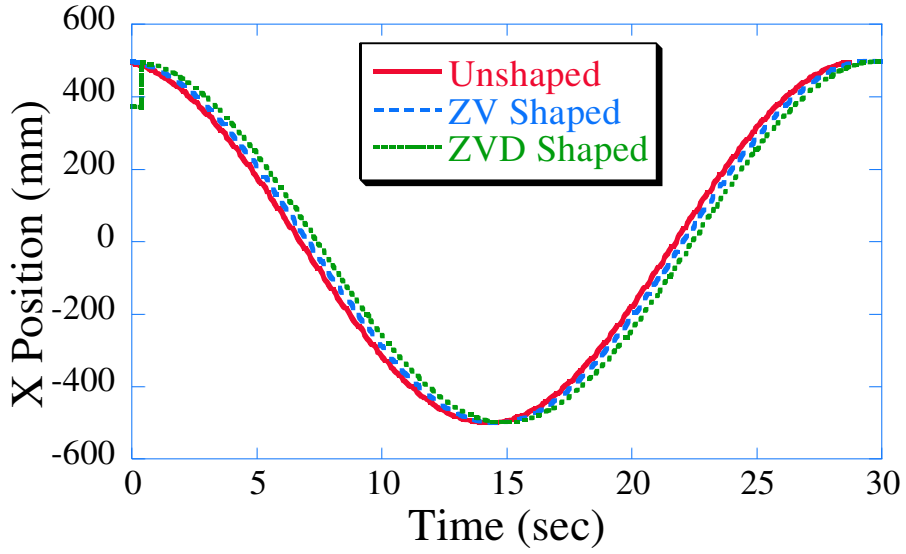

Figure 217: Desired X Position for Same-Orbit Maneuver.

amount of time lag into the system. However, by shifting the shaped maneuvers ahead in time by an amount equal to $\frac{1}{2}$ the shaper's duration, the positions can be more closely aligned. Figure 218 shows the shifted desired x positions for the same-orbit trajectory.

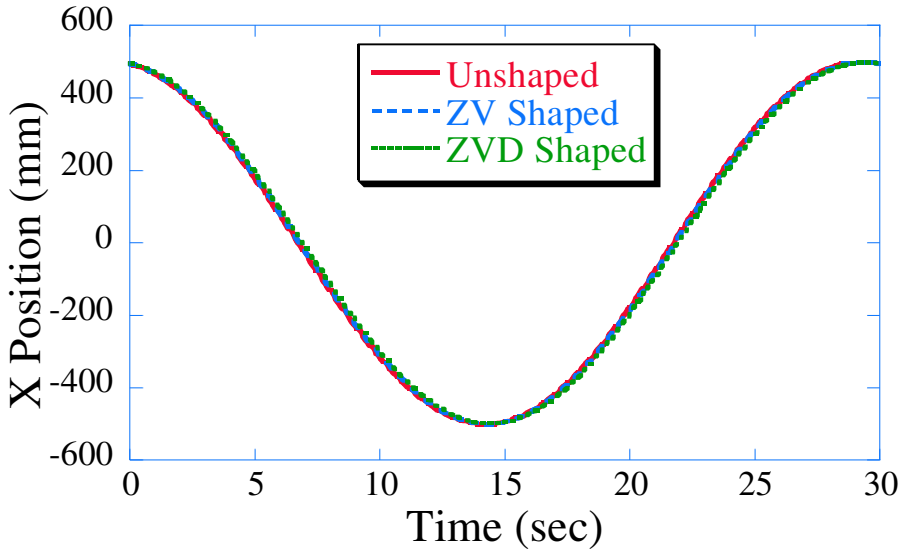

Figure 218: Shifted Desired X Position for Same Orbit Maneuver.

6.4 Summary of Input Shaping Experiments

Two types of motion were studied in the previous section: straight-line and same-orbit motion. For both of these maneuvers, utilizing input shaping greatly reduces the amount of vibration present in the system. This is true for both transient deflection and residual vibration.

For same-orbit maneuvers, input shaping the position control only should be used when the attitude control is disabled. When the attitude control is enabled, input shaping should be used for both. Doing so will yield a system response that has significant vibration reduction. For identical maneuvers, the input shaped cases will consume less fuel. For the spacecraft community, this means that the formation will have a longer life, and that they will be able to complete more missions. Increasing the life of the formation decreases the cost associated with a particular maneuver.

6.5 Trajectory Tracking Experiments

The imaging system used to calculate the position of the DISC units relies on colored markers that are placed on top of the units. When the flexible arm is attached to the DISC unit, a marker is also placed on the tip. The motion of the DISC unit is easier to track then

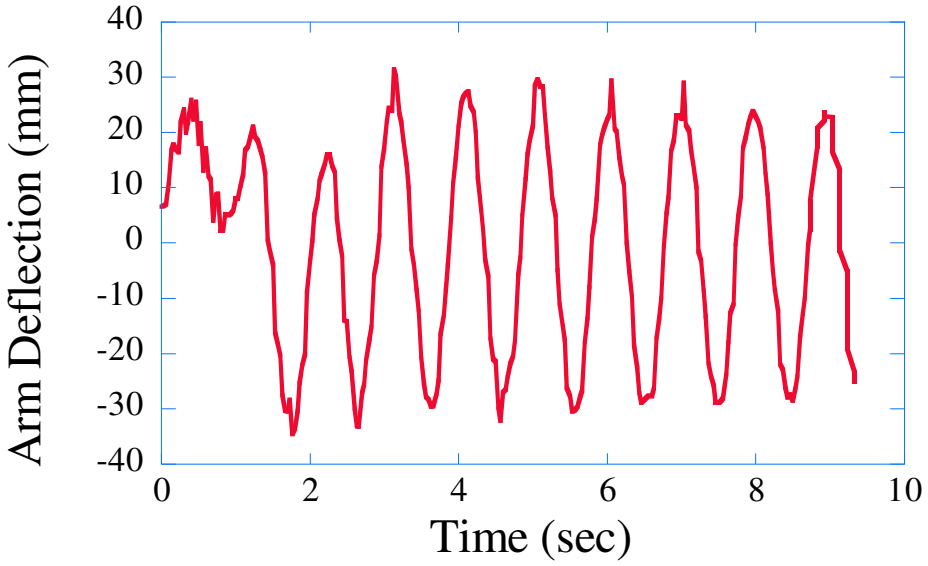

Figure 219: Flexible Arm Deflection for Bang-Bang Slewing Maneuver.

the endpoint motion of the flexible arm. This is because the flexible appendage oscillates at a much higher frequency than the DISC unit. The deflection of the flexible appendage is not small for a bang-bang command. Figure 219 shows the deflection of the appendage endpoint for a bang-bang rotational slewing maneuver. As seen in the figure, the endpoint of the arm has a maximum peak-to-peak amplitude of approximately 60 mm. This is a significant amount of deflection considering the entire length of the arm is only 1000 mm. The fast motion of the flexible appendage increases the difficulty of tracking it using any tracking algorithm.

A video tracking algorithm was used to calculate the position of the flexible arm as well as the position of the DISC units. The tracking code used to calculate the position of the DISC unit and the flexible appendage is an adaptation of an algorithm originally designed for tracking biomechanical motion, specifically that of pole-vaulters in action [24]. This original algorithm was based on techniques used to accomplish motion estimation for frame prediction in camera video sequences. More recently, the methods that inspired this implementation have been adapted to perform in biomedical applications aimed at reconstructing magnetic resonance imaging data sets [23].

First search regions are defined by the code operator in the initial frames of a video

sequence to identify the areas in respective images where the moving target is found. Next, thresholding is applied to each frame in order to isolate a differentiable region of the moving object. All pixels within the selected image that occupy this region are used to determine the centroid of the target. Based on the first and second order derivatives of motion, the algorithm predicts the location of the target in the next frame and the search region for that frame is centered at the prediction. The thresholding operation is repeated for this next frame and the true location of the target is determined via the centroid calculation. Using this methodology an entire video sequence can be tracked automatically following the user input required for the first few frames.

Because the centroid calculation is based on intensity information, varying lighting conditions can be problematic. A primary goal of the initial experiments is to identify optimal tracking conditions, such circumstances should be implemented when possible. In the event that lumination cannot be controlled, a dynamic threshold value can be effective in maintaining accurate results. Since manipulation of this threshold is allowed, the tracking algorithm presented here is able to perform with greater accuracy than some more complicated implementations based on block-matching and optical flow. A simple experimental setup was constructed to move a system in a straight line and then determine which marker most accurately indicated straight line motion.

6.6 Straight-Line Experiments

6.6.1 Testbed Description

Figure 220 shows the basic straight-line experimental setup. It consists of a track, marker background, and a marker. The colored marker is placed in approximately the center of the marker board. The marker board is then placed onto a cart that is constrained to move in a straight line by a track. The cart is then pulled along the track while an overhead camera records the movement. An overhead camera records the movement of the marker onto a VHS cassette. The track can be placed at any orientation relative to the camera field of view. Each of the experiments was digitized into a sequence of bitmaps. The tracking algorithm was then applied to the sequence of bitmaps to identify the position of the marker.

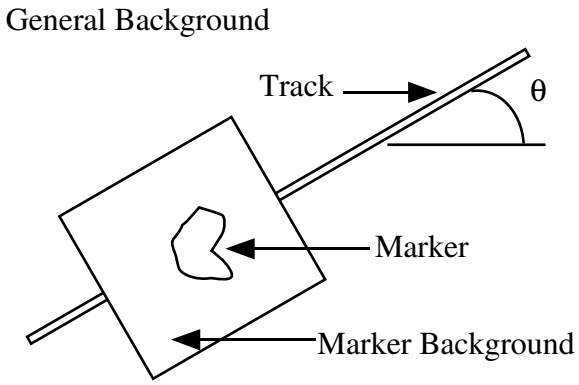

Figure 220: Straight Line Experimental Set Up.

Table 15: Straight-Line Experimental Variations.

Marker Background Colors	Marker Colors	Marker Shapes	Marker Sizes	Orientation
White	Red	Circle	Small	0°
Black	Blue	Square	Medium	30°
	White	Triangle	Large	60°

Table 15 shows the various combinations of marker shape and color tested. Table 16 shows the dimensions of the different marker sizes, track and marker background. Three different sizes were used for the markers: small, medium and large. For the large size, only the circle and triangle marker shapers were tested. The large size circle and triangle markers were adjusted so that they had an area equal to the area of the medium square marker. The large marker size experiments were completed in order to determine if tracking quality was a function of basic shape rather than area. Three orientations for the track were used: 0°, 30°, and 60°.

Table 16: Straight-Line Experimental Parameters.

Description	Size
Marker Background	450mm x 380mm
Track length	1m
Small Marker Size	Sides =6.25cm Radius = 6.25
Medium Marker Size	Sides = 12.5 cm Radius = 12.5 cm
Large Marker Size	Area of marker = 156.25 cm^2

There are many different factors that limit the effectiveness of the tracking algorithm. It is possible for the tracking algorithm to lose the location of the marker. If the color of the general background and marker do not have a large enough color contrast, it may be impossible for the algorithm to find the marker. For example, a black general background may be unsuitable for use with a black marker background, as it maybe difficult for the algorithm to distinguish between the general background and the marker background. Scaling the black and white threshold value may increase the grayscale difference between the two backgrounds. However, the best combination of marker background and general background is one that gives the greatest color difference. Another area of difficulty arises due to the overhead lights. If the overhead lights are too bright, the color intensity of the marker changes as it passes beneath the lights. If the change in intensity is severe enough, the algorithm will be unable to distinguish where the marker is. Another potential problem can occur due to the reflection of the bright overhead lights off of the glass floor. If the reflection is too bright, the contrast between the general background and a light colored background the algorithm will be unable to locate the marker. The experimental results are discussed in the following sections.

6.6.2 Experimental Results

Because the algorithm had difficulty tracking any of the markers when a dark marker background was used, all of the presented results are for the white marker background. Figure 221 shows the results of the tracking algorithm for a 0°, 30°, and 60° experiment. As seen in the figure, the algorithm shows that the centroid of the marker travels along a fairly smooth straight line. In order to avoid any distortion from the overhead camera's lens effect, the track was placed as close to the center of the workspace as possible. Figure 222 demonstrates the excellent consistency of results from the tracking algorithm. The figure shows three runs of the same experimental data - the medium sized red marker circle data. The Residual Y Position shown on the y-axis represents the difference between the experimental data and a best fit line through the data. As seen in the figure, there is less than a 1 mm difference between the three runs. This shows that the algorithm can provide

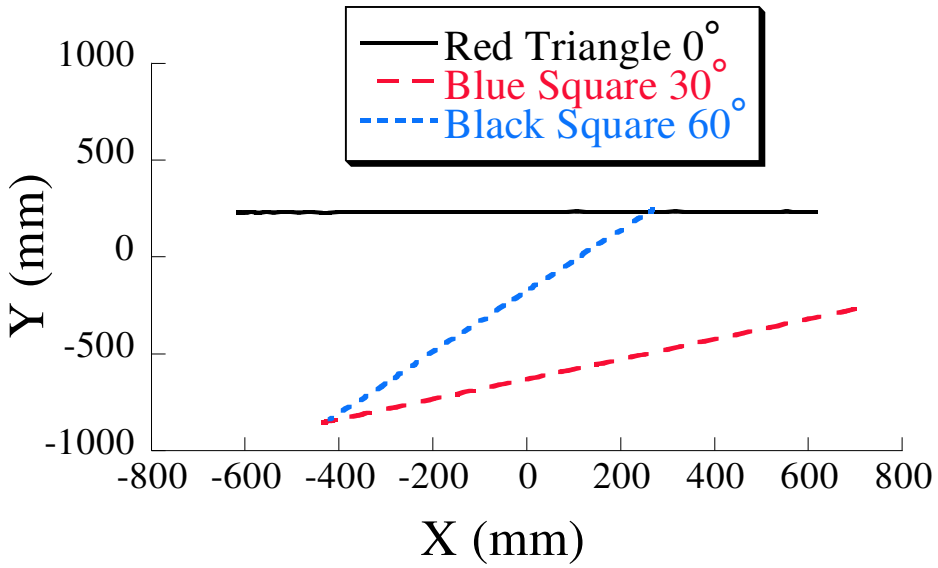

Figure 221: Straight-Line Experimental Results.

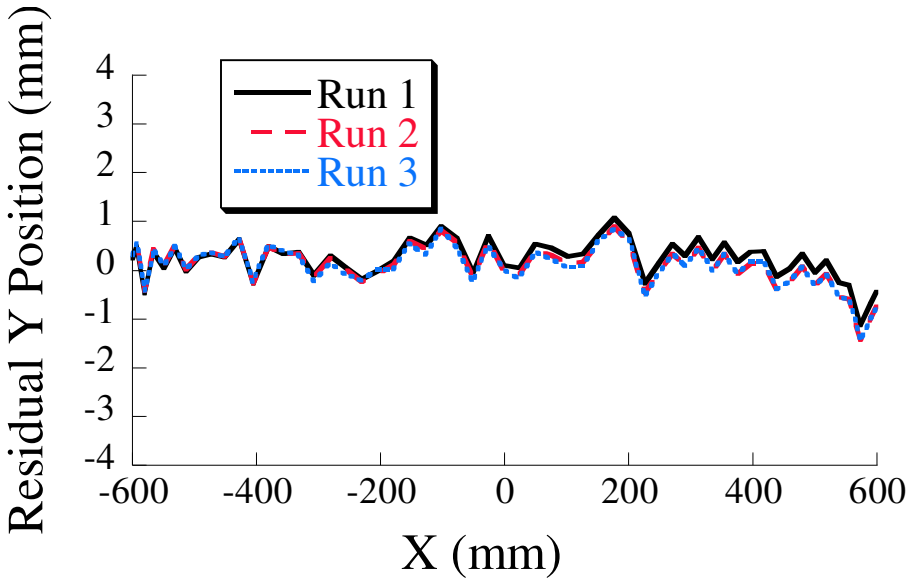

Figure 222: Repeatability of Tracking Algorithm.

consistent results for repeated experiments.

Although the experimental data shown in Figure 221 appears to be relatively smooth, upon closer inspection it is revealed that the tracking algorithm's calculated position is not as smooth. Figure 223 shows the results for the medium sized triangle experiments for the black and red markers. As seen in the figure, the general path of the marker is still a relatively straight line; however, the tracking algorithm's calculated position of the centroid

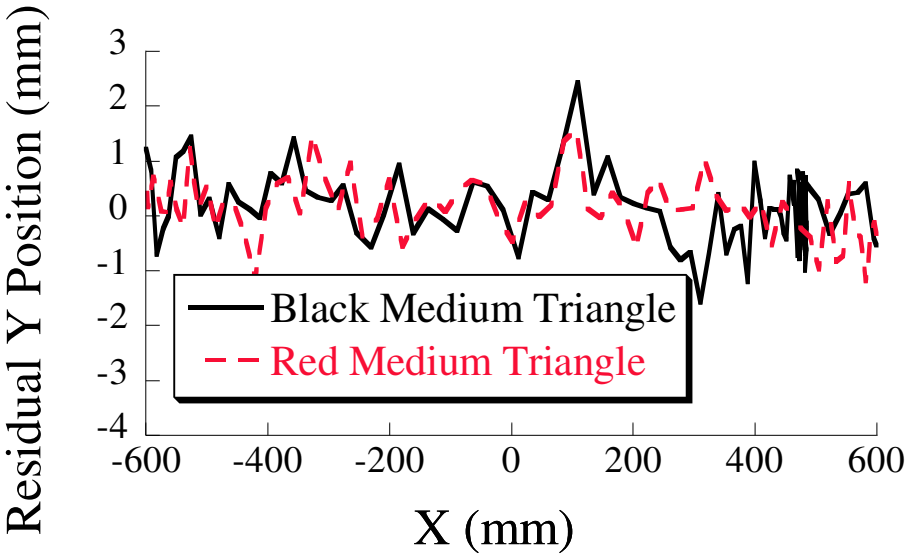

Figure 223: Medium Size Triangle 0° Experiments.

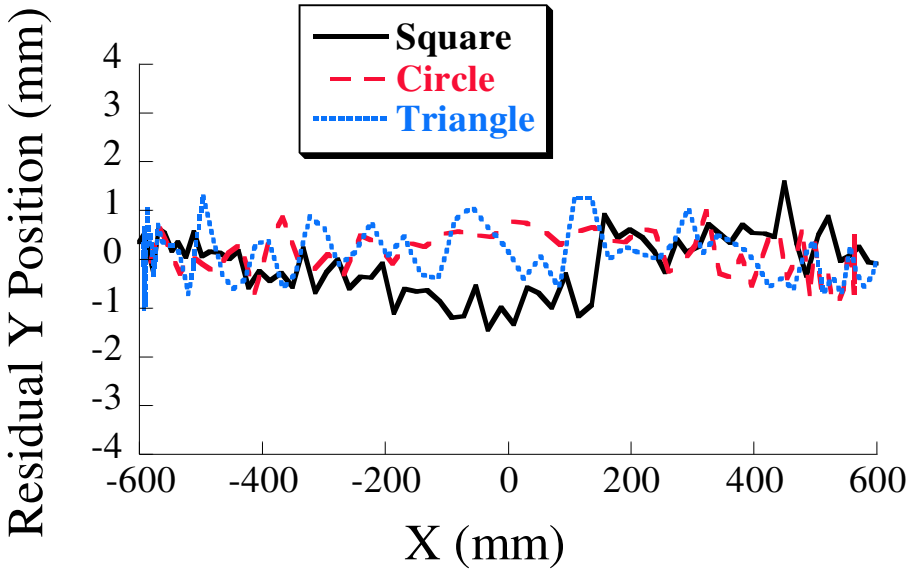

Figure 224: Black Marker Equal Area 0° Experiments.

varies up to 3 mm.

In order to test whether the precision of the tracking algorithm was independent of marker size, equal area experiments were conducted. Figure 224 shows the results for the equal area black marker 0° experiments. As seen in the figure, the calculated position of the centroid travels in a relatively straight line, and there is little difference between the three different shapes. Figure 225 shows the blue marker equal area 30° experiments.

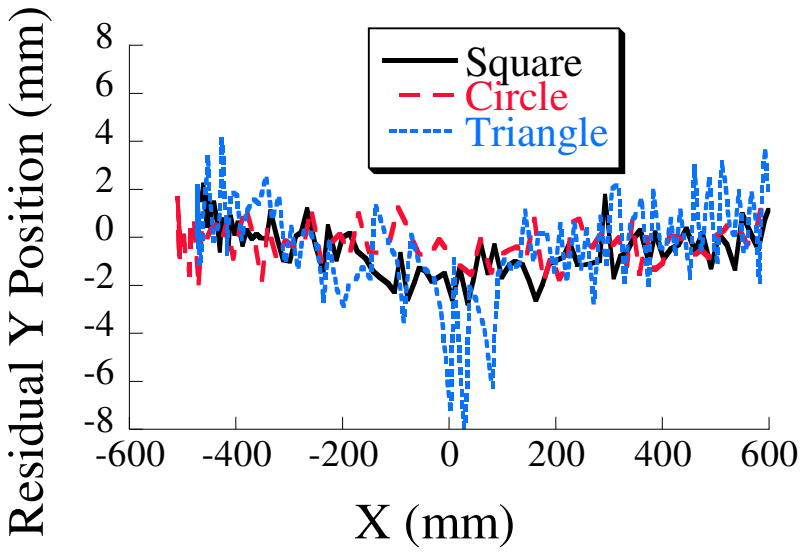

Figure 225: Blue Marker Equal Area 30° Experiments.

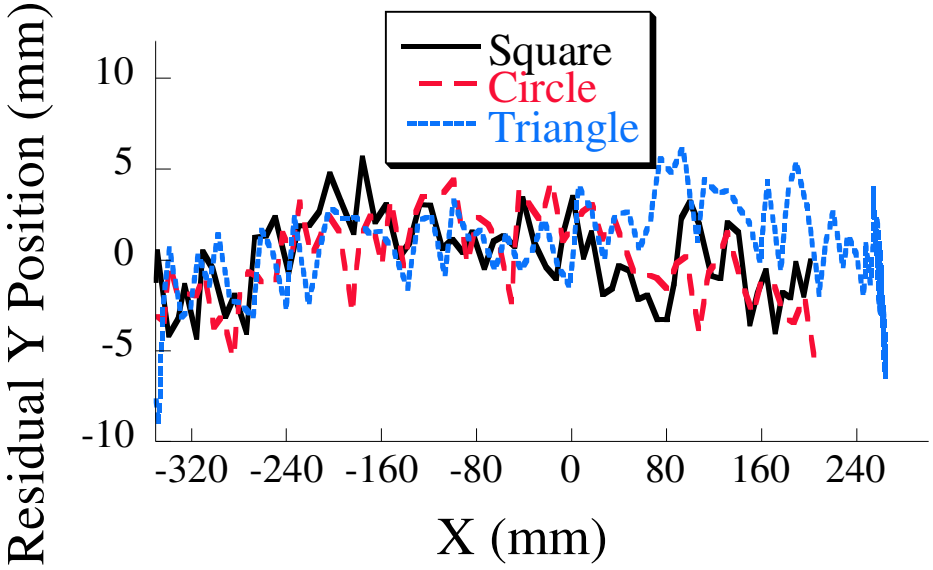

Figure 226: Blue Marker Equal Area 60° Experiments.

The tracking algorithm deviates from the best fit line through the data significantly more for $\theta = 30°$ experiment when compared to the $\theta = 0°$ experiment. Figure 226 shows the blue marker equal area 60° experiments. As θ increases, the tracking algorithm has an increased difficulty in tracking some of the shapes. The tracking algorithm does not track the triangular shape as well as the circular or square shape. Because the triangle is now at an angle with respect to the search region, it is possible for parts of the triangular marker

Table 17: Straight-Line $\theta = 0^\circ$ Statistical Results.

Marker Size	Marker Color	RMS	Standard Deviation
Medium Square	Black	0.53599	0.53773
Medium Square	Blue	0.26188	0.26317
Medium Square	Red	0.85659	0.86003
Medium Triangle	Black	0.65649	0.65882
Medium Triangle	Blue	1.2207	0.70446
Medium Triangle	Red	0.5717	0.57433
Large Circle	Black	0.36258	0.36355
Large Circle	Blue	0.37951	0.38199
Large Circle	Red	0.59118	0.59401
Large Triangle	Black	0.45075	0.45231
Large Triangle	Blue	0.60684	0.60989
Large Triangle	Red	0.55836	0.56055

to leave the search region and distort the calculated centroidal position.

6.6.3 Statistical Analysis

Although the graphical representations of the experiments is helpful, it is difficult to determine which marker size, shape and color is the best combination to utilize with the tracking algorithm. In order to differentiate between the experimental results, statistical analysis was performed on the data.

Table 17 shows the standard deviation and the RMS (root mean square) error for some of the $\theta = 0^\circ$ experiments. In general, the blue marker provided the best overall performance for the different shapes. The experiment with the lowest standard deviation was the blue square marker. The large black circle also had good performance. Overall, the tracking algorithm showed good success in tracking the circular shaped markers.

The statistical results for the $\theta = 30^\circ$ experiments are shown in Table 18. The circular shaped marker has the lowest error for all three different colors. The statistical results for the $\theta = 60^\circ$ experiments are shown in Table 19. For this particular set of experiments, the medium square marker (in all colors) and the large circular marker (in blue and black) significantly outperformed the triangular shaped marker. As the angle increases, the chance increases for more of the triangle marker to leave the predefined search region. Figure 227 shows the $\theta = 60^\circ$ residual y position for the medium sized square marker.

Table 18: Straight-Line $\theta = 30°$ Statistical Results.

Marker Size	Marker Color	RMS	Standard Deviation
Medium Square	Black	2.8511	2.8701
Medium Square	Blue	2.3146	2.3298
Medium Square	Red	2.0935	2.1072
Large Circle	Black	1.1071	1.1102
Large Circle	Blue	0.84140	0.84605
Large Circle	Red	1.2318	1.2377
Large Triangle	Black	1.5222	1.5268
Large Triangle	Blue	1.6915	1.696
Large Triangle	Red	1.5042	1.5073

Table 19: Straight-Line $\theta = 60°$ Statistical Results.

Marker Size	Marker Color	RMS	Standard Deviation
Medium Square	Black	2.8511	2.8701
Medium Square	Blue	2.3147	2.3299
Medium Square	Red	2.0887	2.1022
Large Circle	Black	3.5691	3.5948
Large Circle	Blue	2.4094	2.4256
Large Circle	Red	2.8011	2.8208
Large Triangle	Black	3.3485	3.3741
Large Triangle	Blue	2.0932	2.1086
Large Triangle	Red	2.0646	2.0788

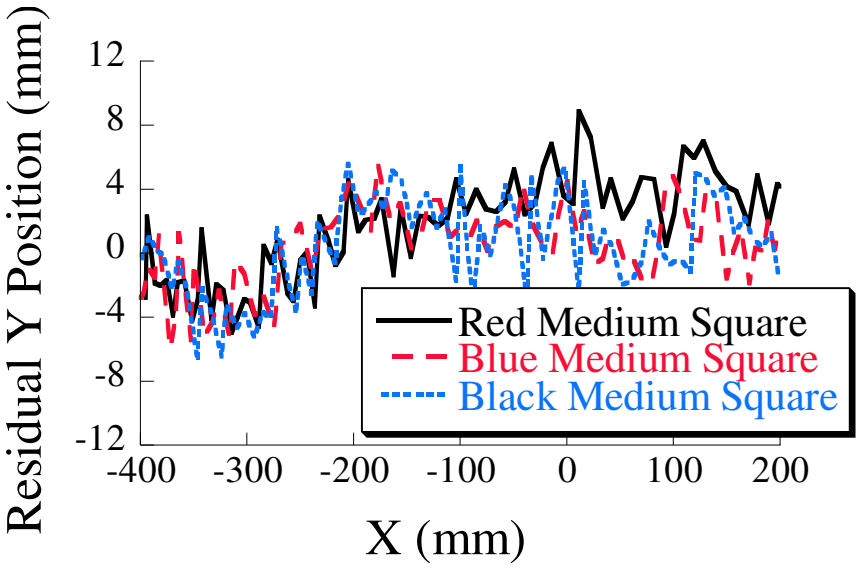

Figure 227: Medium Size Square $\theta = 60°$ Experiments.

6.6.4 Summary of Straight-Line Experiments

In general, the tracking algorithm is able to calculate the position of the DISC unit and its flexible appendage with high accuracy. Straight-line experiments were conducted to determine what kind of effect the marker color, shape and size has on the tracking algorithm. The algorithm had excellent success tracking all of the markers when using a white marker background.

The tracking algorithm produced excellent results. For the $\theta = 0^\circ$ experiments, the tracking algorithm had good success tracking all of the markers. However, when the angle was increased to 30°, and 60°, the algorithm showed better results when using the square and circular markers. In general, the algorithm had better success in tracking the blue markers when compared to the red and black markers.

CHAPTER VII

SUMMARY AND FUTURE WORK

7.1 Thesis Contributions

Formation flying is a difficult task with many performance requirements. This dissertation is the first significant investigation into the effect of integrating satellite flexibility into current state-of-the-art formation flying architectures, and utilizing trajectory shaping to eliminate the vibration. The important performance measures examined were the temporal tracking and the spatial tracking of the satellites. Temporal tracking refers to the satellite's ability to be at a specific position at a specified time. The base case for the temporal tracking is the desired unshaped trajectory. Trajectory tracking refers to the satellite's ability to follow the desired trajectory or to maintain the desired separation distance between satellites.

Utilizing input shaping with either a leader-follower architecture or virtual-structure architecture can improve the responses of the satellites in the formation. Using input shaping to generate the satellites' desired trajectories provides:

- decreased main satellite body oscillation
- improved separation distance between the satellites
- decreased trajectory tracking errors
- decreased deflection in the flexible appendage
- improved settling times

For spacecraft maneuvers, decreasing the settling time can correspond to an decrease in fuel consumption.

7.1.1 Leader-Follower Architecture

The choice of controller gains for the satellites in a leader-follower architecture is important and is discussed in Section 2.3.2. The feedback gains dictate the satellite's ability to

complete the desired maneuver and determine the time it takes to complete the motion. If the leader satellite's gains are chosen poorly, then it will not be able to track the desired trajectory. If the follower satellite's gains are chosen poorly, it will not be able to maintain the desired separation distance and the formation will degrade. High feedback controller gains can lead to better trajectory tracking, but it can cause an increase in the vibration of the system as discussed in Section 3.3.2. However, input shaping can reduce this effect.

As discussed in Section 3.3, shaping the leader satellite's trajectory can improve the response of it and the follower satellite. The starting position of the follower satellite dictates the amount of benefit it receives from the leader's shaped trajectory. The farther the follower satellite is from its desired initial position, the smaller the vibration reduction. However, as discussed in Section 3.3.1.2, even if the follower satellite's starting position is far from its desired position, it still has a lower amount of vibration present in the flexible appendage. The separation distance between the two satellites is better for the shaped cases.

For both the straight-line and circular cases studied, using input shaping creates a temporal delay. The size of this delay is directly related to the shaper's duration. However, the unshaped and shaped trajectories can be aligned for almost all of the maneuver time if the shaped maneuver is started before the unshaped maneuver. The details for this can be found in Sections 2.3.3, 3.4, and 3.5.

Shaping circular trajectories leads to shaped trajectories with radii that are smaller than the desired circular radius. The amount the radius is shortened is related to the shaper's duration. The amount the radius is shortened is small, and it is possible to generate a shaped trajectory with an effective radius equal to the original desired radius. This is done by slightly enlarging the formation's radius and then convolving it with the shaper as discussed in Section 2.3.4.

After examining the effect of shaping on the leader-follower architecture, the following design procedure was developed.

- *Select PD gains to provide excellent tracking performance.* A balance must be struck between trajectory tracking and high PD gains. Excessively high PD gains may not be

physically realizable. The selection of the PD gains used in the simulations is discussed in Section 2.3.2, and the response of the main satellite body is shown in Figures 17, 18 and 21. The selected gains provide good trajectory tracking for straight-line and circular maneuvers as shown in Figures 46, 47, 65, 75, 80, and 84.

The follower satellite is able to maintain the desired separation distance for the matched starting positions discussed in Section 3.3.1.1, and for unmatched starting positions discussed in Section 3.3.1.2. For the same-orbit maneuvers, the choice of PD gains affects the separation distance of the formation as shown in Figure 66. Increasing the PD gains led to increased system oscillation as shown in Figure 67, but the higher the gains, the better the separation distance between satellites.

For the multi-mode formation using PD gains discussed in Section 3.5, the selection of gains determines the frequency of the closed-loop response. As seen in Figure 99, the maximum separation distance is a function of the controller gain selection. The higher the frequency of the follower satellite (which corresponds to increased K_p gains), the smaller the maximum separation distance.

- *Convolve the leader's desired trajectory with a robust shaper.* The selection of PD gains is paramount to the satellite's tracking, but enhanced separation distance between the satellites can be obtained by utilizing trajectory shaping. Section 3.3.1 discusses the straight-line maneuvers, and Figure 55 shows the improvement in the separation distance. The effect of trajectory shaping on the circular maneuvers is discussed in Sections 3.3.2-3.3.5.

  The benefits of using robust shapers are discussed in Sections 1.6.2 and 1.6.3. The ZVD and EI shapers are more insensitive to changes in the system's natural frequency or damping ratio. Shaping the leader satellite's trajectory with a ZVD shaper improves the response of the flexible appendage. This can be seen by examining Figures 53, 54, 58, 59, 68, 69, 71, 76, 77, 81 and 82. Using trajectory shaping also improves the separation distance for both the straight-line and circular trajectories. This effect can be seen by examining Figures 55, 70, 72, 97, 99-104, and 107. For

formations where the distance between the satellites is very small, using a robust shaper can provide a measure of collision avoidance as discussed in Section 3.4. The collision avoidance properties of the ZVD shaper can be seen by studying the minimum separation distance between the spacecraft shown in Figure 100.

- *When temporal tracking is of paramount importance, start the shaped maneuvers early.* The shaped maneuvers should be started one-half the shaper's duration early. Section 2.3.3 shows that when a command is convolved with a shaper, a time delay is introduced. Table 9 compares the time lag for the unshaped and shaped cases. For the leader-follower architecture, shaping the leader's trajectory introduces a delay. However, as discussed in Sections 3.3.1.1 and 3.3.1.2, the delay can be almost completely eliminated for straight-line maneuvers by starting the shaped maneuvers early.

  When the straight-line trajectories are started early, the trajectories will be aligned for all time after the duration of the shaper. Initially the slope of the shaped trajectory is smaller than the unshaped slope. This results from the convolution process. After a time equal to the shaper's duration has passed, the unshaped and shaped trajectories will have the same slope. This can be seen by examining Figure 50. For circular trajectories, the delay cannot be completely eliminated, but it can be significantly reduced. This can be seen by examining Figures 73 and 74. As discussed in 3.5, multi-mode formations can also benefit by starting the shaped maneuvers early. This can be seen in Figure 95.

- *Start the follower satellite as close to its designated initial position as possible.* Ensuring that the follower satellite starts as close to its designated starting position increases the vibration reduction benefits it receives from the leader's shaped trajectory. The importance of the follower spacecraft's starting position is discussed in Sections 3.3.1.2 and 3.4. For formations with identical spacecraft, the follower satellite receives the maximum possible vibration reduction. This can be seen by comparing Figures 61 and 63. For formations where the flexibility comes from the controller gains, the relationship between the initial starting position and maximum separation distance can

be seen by examining Figures 101-104.

- *For circular maneuvers, increase the desired radius before shaping.* In Section 2.3.4, it was shown that applying shaping to a circular trajectory will cause a decrease in the radius. The shaped circular trajectory will have a slightly smaller radius than the original circular trajectory. Tables 6 and 7 show that the reduction in the radius depends on the shaper used in the convolution. The decrease is directly related to the duration of the shaper. The more robust the shaper, the longer the shaper's duration. This is shown by comparing (9) to (13) and is discussed in Section 1.6.2.

- *For largely spaced multi-mode formations, use a multi-mode shaper.* For formations that contain multiple vibration frequencies, multi-mode shapers can provide superior vibration reduction for all modes of vibration. This is especially true when the modes in the formation are far apart. Two cases of multi-mode formations were examined in Sections 3.4 and 3.5. If the leader satellite's trajectory is convolved with a shaper designed only to eliminate one mode of vibration, the beneficial vibration reduction the follower satellite receives decreases as seen in Figure 111. If an average frequency shaper is used, then the leader's vibration response is changed as seen in Figure 112. If a multi-mode shaper is used, then both the leader and follower satellites have superior vibration reduction. This can be seen by examining Figures 111 and 113.

- *For closely spaced multi-mode formations, use a robust shaper.* The preceding guideline discussed what to do if the formation has largely spaced modes. If the modes are closely spaced, then a multi-mode shaper may not be needed. Sections 3.4 and 3.5 discuss the multi-mode scenarios. As the frequency separation between the formation modes decreases, the responses of the ZVD, average frequency and multi-mode shaped responses begin to converge. This effect can be seen in Figure 111. Therefore, when the modes are closely spaced, it is unnecessary to use a multi-mode shaper. A robust shaper such as the ZVD or EI may be sufficient. Although a multi-mode shaper will reduce the vibration, it has a longer shaper duration. This can be seen by comparing the amplitudes and time locations of the ZVD shaper described by (72) and the

multi-mode ZVD shaper described by (73). Keeping the shaper's duration as short as possible ensures that the time delay introduced into the system is as small as possible. For circular trajectories, the shorter the shaper's duration, the smaller the change in the radius of the formation.

7.1.2 Virtual Structure Architecture

Section 4.6 addresses maneuvers where the satellites' trajectories are generated by commanding a single step change (for both straight-line and circular maneuvers). For these maneuvers, the unshaped and shaped trajectories cannot be aligned temporally. In addition to the temporal differences, spatial differences exist for these types of trajectories. Although the shaped trajectories differ from the unshaped trajectories, the satellites following the shaped trajectories have superior vibration reduction for both the main body of the satellite and the flexible appendage. If the formation structure must be maintained, then the trajectories should not be generated by a single step change.

For maneuvers where the satellites' trajectories are not generated by one step change, but are generated from multiple small steps, the temporal differences between the unshaped and shaped trajectories can be lessened as discussed in Section 4.7.3.2. Temporal alignment between the unshaped and shaped maneuvers is accomplished by starting the shaped maneuvers before the unshaped maneuvers. The spatial differences between the unshaped and shaped trajectories is small. Input shaping these circular trajectories shortens the radius, but the shortening is constant throughout the entire maneuver. It is possible to eliminate the shortening effect by enlarging the desired radius as discussed in Section 2.3.4.

When the satellites in the formation have identical flexible modes, then each satellite can be treated as an isolated system and studied. This is because input shaping affects all of the trajectories the same. There is no difference between implementing the shaping at the supervisor or local level as discussed in Section 4.8. For systems that do not have identical flexible modes, it matters where the input shaping occurs. When the frequency of the shapers differs significantly, then the structure of the formation can be affected. This scenario is discussed in Section 4.9.

When utilizing input shaping in combination with a virtual-structure formation flying architecture the following design procedure should be used:

- *Select PD gains to provide excellent tracking performance.* A balance must be struck between trajectory tracking of the spacecraft and high PD gains. Excessively high PD gains may not be physically realizable. The selection of the PD gains used for each of the spacecraft was discussed in Section 2.3.2 and the responses were shown in Figures 17, 18 and 21.

  For the virtual-structure architecture, the selection of the formation PD gains is critical. The response of the formation states determines the satellites' desired trajectories. Section 4.7 discusses how to select the PD gains for the virtual-structure architecture. The effect of the PD gain selection on the formation state response is shown in Figure 120. For this architecture, the PD gains play an important role in determining the tracking error of the formation.

- *Convolve the satellites' desired trajectories with a robust shaper.* Utilize trajectory shaping for improved system performance. In addition to reducing the vibration of the flexible appendages, trajectory shaping also reduces the tracking error of the satellites. This is discussed in Section 4.5.1 and can be seen by comparing Figures 134 and 135.

  For all of the cases examined, trajectory shaping significantly reduces the vibration of the flexible appendage and is discussed in Sections 4.5.1-4.9. The vibration reduction of the flexible appendage can be seen by examining Figures 137, 138, 143-145, and 151-154. For straight-line maneuvers, Figures 137 and 138 show the vibration reduction of the flexible appendage. In addition to straight-line motions, trajectory shaping can be used for different rotation maneuvers as seen in Figure 145, and for different formation radii as seen in Figures 153 and 154.

  For multi-mode formations, it is important to shape for all satellite frequencies. Figure 158 shows the effect when one of the satellite frequencies is not accounted for. As seen from the figure, the vibration of the satellite is only slightly reduced. This is

because the shaper was not designed to eliminate the frequency of the this satellite. It was designed to eliminate the frequency of the other satellites in the formation. When ZV or ZVD shapers are used, the amplitude of the shaped response will never exceed the amplitude of the unshaped response.

- *For circular maneuvers, increase the desired radius before shaping.* In Section 2.3.4, it was shown that applying shaping to a circular trajectory will cause a decrease in the radius. The shaped circular trajectory will have a slightly smaller radius than the original circular trajectory. Tables 6 and 7 show that the reduction in the radius depends on the shaper used in the convolution. The decrease is directly related to the duration of the shaper. The more robust the shaper the longer the shaper's duration.

- *When temporal tracking is of paramount importance, generate the satellites' desired trajectories using small step changes.* Satellite trajectories generated by large single step changes should not be used. The desired trajectories of the satellites in this architecture are generated from the convergence of the formation states. When the formation states are given a single step change in position or rotation as discussed in Sections 4.7 and 4.7.3.1, it is impossible to align the trajectories in time. This can be seen by examining Figures 132 and 133. When the formation states are given a series of small step changes, it is possible to reduce the mismatch in temporal alignment as discussed in Section 4.7.3.2.

- *When temporal tracking is of paramount importance, start the shaped maneuvers early.* It is possible to align the trajectories generated from multiple small step changes as discussed in Section 2.3.3 and 4.7.3.2. In order to align the trajectories, the shaped maneuvers must be started $\frac{1}{2}$ the shaper's duration early. The more robust the shaper, the longer its duration and the earlier the shaped maneuver must be started. Motions that are generated from single large step changes cannot be temporally aligned as discussed in Sections 4.6.2 and 4.6.3.

- *For largely spaced multi-mode formations, use a supervisor level multi-mode shaper.* As discussed in Section 4.9, multi-mode shapers should be used when the spacecraft

in the formation have a wide range in frequencies. The benefit of using a multi-mode shaper over a ZV or ZVD shaper is evident by examining Figures 160, 161 and 167. In all of these figures, the best vibration suppression for largely spaced modes occurs when utilizing the multi-mode ZVD shaper. There are two places to integrate the trajectory shaping into the virtual-structure architecture: at the supervisor level, or at the local satellite level. The advantages and disadvantages of each are discussed in Sections 4.9.1 and 4.9.2.

When the formation maneuvers are generated from single step changes as discussed in Section 4.9.1.1, the multi-mode shaper has a large effect on the formation radius. This effect can be seen in Figure 163. When the shaping is performed at the supervisor level, each trajectory is affected the same way. Each trajectory has the same reduction in radius at the same time. When the shaping is completed at the local level as discussed in Section 4.9.2.1, the effect on each trajectory is not the same. This is evident by examining Figures 170 and 171. If the frequencies of the spacecraft are largely spaced and shaping is implemented at the local level, then the formation will not maintain its desired shape.

For trajectories that are generated from continuous functions or multiple small step changes, the effect of shaping the trajectory is small. This scenario is discussed in Section 4.9.2.2. As seen from Figures 168 and 175, the changes to the radius are much smaller than the trajectories generated by a single step change. Although the effect on the radius is small, the shaping should be completed at the supervisor level for largely spaced modes. This ensures that every trajectory in the formation is changed in the same way. Even though the spacecraft in the formation have different flexible modes, using a multi-mode shaper will not adversely affect the responses of the formation satellites. This can be seen by examining Figures 165 and 166.

- *For closely spaced multi-mode formations, use a supervisor level robust shaper.* For closely spaced modes the differences between shaping at the supervisor level and local level diminish. When the frequencies of the satellites are the same, there is no

difference as discussed in Section 4.9.2.2. This effect can be seen by examining Figures 168, 170, and 174. From Figures 160, 161 and 167 it is clear that as the frequencies of the satellites get closer to each other, the responses of the spacecraft using the multi-mode ZVD, and ZVD shapers approach each other. Therefore, when the modes are closely spaced, a ZVD or EI shaper should be used. As discussed in Sections 1.6.2 and 1.6.3, both the ZVD and EI are robust to changes in natural frequency. However, it is recommended that the shaping always be applied at the supervisor level as discussed in Section 4.9.1. This ensures uniformity in the satellites' desired trajectories.

7.1.3 Flexible Satellite Model

In Chapter 2, a simple, flexible model was developed to capture the dynamics that dominate the satellite's response. In reality, spacecraft are complex bodies that have complicated dynamics. The efficacy of command shaping depends on reasonable estimates of the system's natural frequencies and damping ratios. When using a simplified model, it is important to make sure that the modeled frequency and the actual frequency of the system are close in magnitude. If the frequencies differ significantly, then a more complicated model should be used to accurately capture the dynamics of the system. The frequency of the input shaper is developed from the modeled frequency, so it is imperative that the model's frequency be as close to the actual frequency as possible.

The ZV and ZVD shapers will never cause the system to have a response worse than the corresponding unshaped response. This is an important artifact of using the ZV or ZVD shapers. For example, suppose that one of the satellites in the formation has a large change in the natural frequency as a result of a collision or impact with a micro meteor. The vibration reduction due to input shaping would not be as effective because the shaper is not tuned to the new frequency. It will not be worse than if shaping was not applied to the system. If the frequency change is small and a very robust shaper is used, then the change in the response would also be small.

7.1.4 Combined Input Shaped Pulse Width Modulation

Most spacecraft use thrusters to maneuver. A pulse width modulation (PWM) technique is often used to convert the continuous control signal generated by the satellite's control to a pulse train that is realizable by the thrusters. Therefore, it is important to know what effect combining input shaping with PWM has on the vibration response of a system. In order to investigate this effect, sensitivity curves for a combined shaped, PWM command were developed and discussed in Section 5.3.

The sensitivity curves are a function of the number of PWM cycles used. This is an important parameter since it corresponds to the number of times a thruster is turned on. A thruster cannot be turned on and off an unlimited number of times. In addition, there is also a lower time limit that the thruster must remain on in order to be effective. In order to help determine the minimum number of PWM cycles needed to describe a command, a MATALB tool was developed and is described in Section 5.4. This tool allows the user to input a system's transfer function, tolerable vibration limit and desired shaper. The tool then calculates the lowest number of PWM cycles needed to meet all the requirements and displays the sensitivity curve and system response to a step input.

7.1.5 Formation Flying Experiments

Formation flying experiments were conducted at the Tokyo Institute of Technology. Shaping changes the desired trajectory of the system. The magnitude of the change depends on the formation's architecture and the shape of the original trajectory. However, for circular trajectories, it was experimentally verified that shaping a circular trajectory does not significantly alter the response of the main satellite body. These results are discussed in Section 6.3 and can be seen by comparing Figure 212a and 212b. In addition, utilizing trajectory shaping can save fuel. This effect was experimentally verified and can be seen in Figure 216.

7.2 Extension of This Work

The design procedures developed here give the controls engineer guidance in how to implement trajectory shaping in order to achieve the maximum vibration suppression possible. However, this dissertation cannot cover all of the possible scenarios. Therefore, this section discusses some possible extensions of this work.

This dissertation examined the effect of command shaping on two formation flying architectures, but there are many more types of architectures available. It is postulated that trajectory shaping can be integrated into any of these architectures with good success provided the following conditions are met:

- For architectures where the trajectories of the formation satellites are generated based on the motion of a leader satellite, the trajectory of the leader satellite must be known in advance.
- For architectures where the trajectories of the formation satellites are generated independently, then the trajectories of all the satellites must be known in advance.

When either of these conditions are met, the effect of command shaping on the formation should be very similar to the results discussed in this dissertation. The formation's structure would not be significantly altered provided that the trajectories are not generated by single large step changes.

Fundamentally, the effect of shaping the trajectory wound not be different for these different architectures. The process would be the same with the only difference being in how the trajectories are generated and in how the trajectory tracking is implemented. It is also possible that the trajectory tracking would not be implemented with a simple PD controller. However, command shaping has been shown to work effectively on many types of feedback control systems such as PID and Sliding Mode Control [14].

Some of the available architectures focus on developing an overall control structure for the formation. In [16], a leader-follower structure was used to develop a control algorithm for deciding which role a robot in the formation should have. The role is not set for the duration of the maneuver, but can change depending on the environment and situation. For

this type of formation, input shaping cannot be applied to the trajectories. This is because the trajectories are not generated ahead of time. However, input shaping can still be used to reduce the vibration of the system. This would be done by shaping the control effort determined by each of the robots. Each of the robots would be responsible for shaping their own natural frequency. If the control effort is shaped, then a breakdown in the formation should not occur.

For control architectures that do not focus on generating trajectories, but on rendezvousing or capturing targets [37], command shaping can also be applied to these architectures. However, the method of integrating command shaping for these types of architectures would be different than the trajectory shaping discussed in this dissertation. For this work, command shaping was applied to the desired trajectories, but it can be used on other types of commands. It is possible to shape desired actuator effort, or desired velocity. Shaping either actuator effort, or velocity produces the same results as shaping the trajectory. The system will move with little or no residual vibration, and the transient deflection will be reduced.

For example, in [18], the only trajectory known in advance was the desired trajectory of the formation center. The other vehicles in the formation were not given specific trajectories but rather allowable regions in the workspace. For these types of architectures, it does not seem likely that shaping the desired trajectory of the formation's center would have any effect on the vibration reduction of the vehicles. This architecture is not a leader-follower architecture, so the vehicles are not trying to follow the center, but are only trying to remain in the allowable region. It is possible for the motion of the vehicles to be shaped. The best solution would be to implement a real-time command generator that shapes the actuation forces. This would keep the integrity of the formation architecture and eliminate the vibration.

In [20], a hybrid control algorithm was presented that utilized leader-follower and obstacle avoidance control schemes. It may be possible to extend the leader-follower work presented in this dissertation to the architecture discussed in [20]. The biggest difference between the architectures studied here and the one presented in [20], is that the follower

robots switch control schemes. If the follower robots are in leader-follower mode, they would receive some vibration reduction benefits provided they started near their desired positions. If the robots switched to obstacle avoidance mode, then the dynamics would probably be dominated by the controller and the beneficial effects of shaping the leader's trajectory would possibly be reduced.

Another leader-follower architecture was discussed in [49]. In this architecture, a sliding mode controller was developed for the follower satellite. It has been shown that sliding mode control and input shaping can be used effectively to reduce the vibration in a system [14]. The work completed in this dissertation could be extended to this type of sliding mode control system since the trajectory of the leader satellite would be shaped. It is anticipated that the follower satellite would also receive vibration reduction of any flexible mode, even if the mode is unobservable as is the case discussed in [14].

In the previous chapters, only two dimensional motion was considered. The work presented in the previous chapters can easily be extended to three dimensions without a significant change in the results. First, the simple flexible model must be modified. For the most general case, at least seven state variables would be needed to describe each of the satellite's configurations: six for the general motion and at least one describing the response of the flexible appendage. However, command shaping could still be utilized for the three dimensional case. For the leader-follower and virtual-structure architectures, the results would be similar to the two dimensional case. This is because command shaping can be used to reduce the vibration of any known estimates of the system's frequency. It does not depend on two dimensional or three dimensional motion.

The satellite model developed here is an extremely simple model. If desired, a more complicated model can be used without significantly changing the results. As long as the frequency of the unwanted vibration can be identified, the shaper can be developed in order to eliminate or reduce that mode. If the model has more than one mode, a multi-mode shaper can be used in order to suppress two or more modes. The effect of using a multi-mode shaper was discussed in Chapters 3 and 4. Multi-mode shapers can be used to suppress the vibration of two satellites with different frequencies or two frequencies on a

single satellite.

7.3 Future Work

The work presented in this dissertation is an important first step in determining the effect input shaping has on formation flying control architectures. This area of combining input shaping with formation flying is in its infancy and there are many areas of research that can be explored.

A natural extension of this work would be to investigate how input shaping affects the performance of a leader-follower system that utilizes thruster pulse profiles. For more complicated trajectories, such as the epi-cyclic, it may be possible to increase the beneficial effect of trajectory shaping on the follower satellite by utilizing shaped thruster commands instead of relying solely on shaping the leader's trajectory. If this were implemented, then anytime the satellites moved, they would retain the beneficial effects of input shaping.

During the initialization portion of the maneuver, only step changes in position were used for both the formation frame and the satellites. However, it is possible to utilize smooth trajectories during this part of the maneuver. If smooth trajectories were generated and used, then the effect of input shaping should be examined.

As stated before, only two dimensional motion was examined. For many cases, three dimensional motion is required and should be investigated. In order to study three dimensional motion, a different model must be used.

Another area of study could focus on the effect of perturbations in the formation's properties. For the ZV and ZVD shaped cases, the response of the system will never be worse than the unshaped case. However, if different shapers are used, then the results could be different. Shapers containing negative impulses excite high frequency modes [43, 59, 25]. If a satellite has a change in frequency and it matches the frequency of the excited high mode, its response to the shaped command would be significantly different than the other satellites in the formation.

APPENDIX A

FLEXIBLE SATELLITE EQUATIONS OF MOTION

Figure 228 shows the Free Body Diagrams (FBD) for the flexible satellite model. Figure 228a is the free body diagram for the main satellite body, and Figure 228b is the FBD for the flexible appendage. The flexible appendage is attached to the main satellite body, $m1$, at point P. The connection is modeled as a pin connection.

The forces F_1 and F_2 are fixed with respect to the inertial X and Y directions. The orientation of the m_1 is described by the intertially fixed angle θ. The spring angle deflection is described by the angle ϕ, and is referenced with respect to a body fixed frame attached to m_1. The accelerations of points G, P and G_2 can be found using kinematics. The acceleration of point G is

$$\vec{a_G} = \ddot{x}\vec{I} + \ddot{y}\vec{J}$$

The acceleration of point P is

$$\vec{a_P} = \vec{a_G} + \vec{\alpha} \times \vec{r_{P/G}} + \vec{\omega} \times \vec{\omega} \times \vec{r_{P/G}}$$

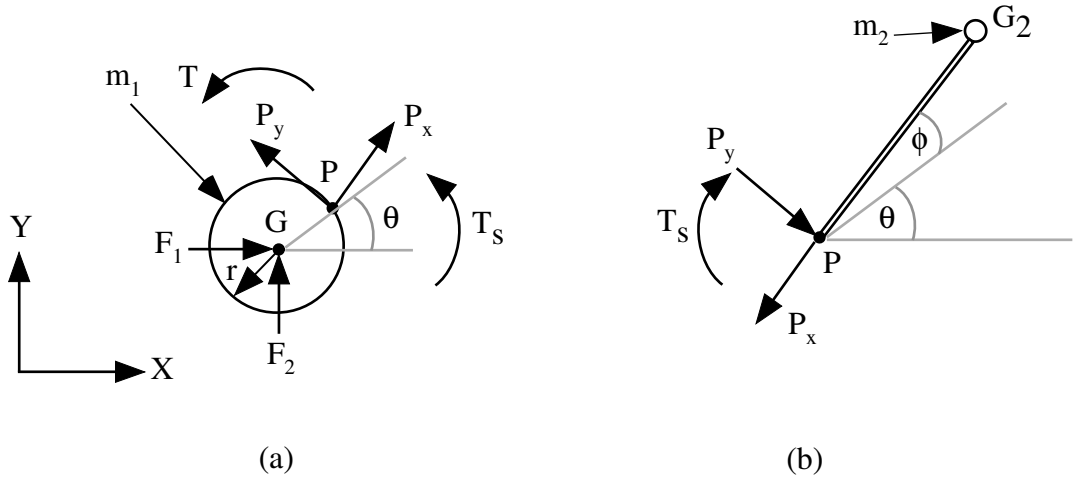

Figure 228: Free Body Diagrams for Flexible Satellite.

where

$$r_{P/G} = r\cos\theta\vec{I} + r\sin\theta\vec{J}$$

so the acceleration of point P is

$$\vec{a_P} = \left(\ddot{x} - r\sin\theta\ddot{\theta} - \dot{\theta}^2 r\cos\theta\right)\vec{I} + \left(\ddot{y} + r\cos\theta\ddot{\theta} - \dot{\theta}^2 r\sin\theta\right)\vec{J}$$

$$\vec{a}_{G_2} = \vec{a_P} + \vec{\alpha}\times\vec{r}_{G_2/P} + \vec{\omega}\times\vec{\omega}\times\vec{r}_{G_2/P}$$

where $\alpha = \ddot{\theta}\vec{K} + \ddot{\phi}\vec{K}$. After simplifying, the acceleration at point G_2 is

$$\begin{aligned}\vec{a}_{G_2} = &\left[\ddot{x} - r\sin\theta\ddot{\theta} - \dot{\theta}^2 r\cos\theta - \left(\ddot{\theta}+\ddot{\phi}\right)L\sin(\theta+\phi) - \left(\dot{\theta}+\dot{\phi}\right)^2 L\cos(\theta+\phi)\right]\vec{I}\\ &+\left[\ddot{y} + r\cos\theta\ddot{\theta} - \dot{\theta}^2 r\sin\theta + \left(\ddot{\theta}+\ddot{\phi}\right)L\cos(\theta+\phi) - \left(\dot{\theta}+\dot{\phi}\right)^2 Lsin(\theta+\phi)\right]\vec{J}\end{aligned} \quad (107)$$

where

$$a_{2x} = \left[\ddot{x} - r\sin\theta\ddot{\theta} - \dot{\theta}^2 r\cos\theta - \left(\ddot{\theta}+\ddot{\phi}\right)L\sin(\theta+\phi) - \left(\dot{\theta}+\dot{\phi}\right)^2 L\cos(\theta+\phi)\right] \quad (108)$$

$$a_{2y} = \left[\ddot{y} + r\cos\theta\ddot{\theta} - \dot{\theta}^2 r\sin\theta + \left(\ddot{\theta}+\ddot{\phi}\right)L\cos(\theta+\phi) - \left(\dot{\theta}+\dot{\phi}\right)^2 Lsin(\theta+\phi)\right] \quad (109)$$

Taking the sum of the forces in X direction for Figure 228a gives:

$$\Sigma F_x = m_1\ddot{x} \quad (110)$$

$$F_1 + P_x\cos(\theta+\phi) - P_y\sin(\theta+\phi) = m_1\ddot{x} \quad (111)$$

Taking the sum of the forces in the Y direction for Figure 228a gives:

$$\Sigma F_y = m_1\ddot{y} \quad (112)$$

$$F_2 + P_x\sin(\theta+\phi) + P_y\cos(\theta+\phi) = m_1\ddot{y} \quad (113)$$

Taking the sum of moments around point G gives:

$$\Sigma M_G = I\ddot{\theta} \quad (114)$$

$$T + T_s + r\cdot P_x\sin\phi + r\cdot P_y\cos\phi = I\ddot{\theta} \quad (115)$$

where I is the moment of inertia for the main satellite body, m_1.

Taking the sum of the forces in the X direction for the flexible appendage gives:

$$\Sigma F_x = m_2 \cdot a_{2x} \tag{116}$$

$$-P_x \cos(\theta + \phi) + P_y \sin(\theta + \phi) = m_2 \cdot a_{2x} \tag{117}$$

where a_{2x} is the x component of the acceleration of point G_2. Taking the sum of the forces in the Y direction for the flexible appendage gives:

$$\Sigma F_y = m_2 \cdot a_{2y} \tag{118}$$

$$-P_y \cos(\theta + \phi) - P_x \sin(\theta + \phi) = m_2 \cdot a_{2y} \tag{119}$$

where a_{2y} is the y component of the acceleration of point G_2.

The reaction forces P_x and P_y are found by simultaneously solving (117) and (119).

$$P_x = -m_2 \cdot a_{2x} \cos(\theta + \phi) - m_2 \cdot a_{2y} \sin(\theta + \phi) \tag{120}$$

$$P_y = m_2 \cdot a_{2x} \sin(\theta + \phi) - m_2 \cdot a_{2y} \cos(\theta + \phi) \tag{121}$$

Substituting (120) and (121) into (111), (113) and (115) gives:

$$F_1 - m_2 \cdot a_{2x} = m_1 \ddot{x} \tag{122}$$

$$F_2 - m_2 \cdot a_{2y} = m_1 \ddot{y} \tag{123}$$

$$T + T_s + r \cdot m_2 \cdot a_{2x} \sin\theta - r \cdot m_2 \cdot a_{2y} \cos\theta = I\ddot{\theta} \tag{124}$$

$$T_s = K\phi \tag{125}$$

For the flexible appendage, taking $\sum M$ about point P yields

$$\sum M_p = \dot{H}_{G_2} + \vec{r}_{P/G_2} \times m_2 \vec{a_{G_2}} \tag{126}$$

but $\dot{H}_{G_2}$ is equal to zero since m_2 is a point mass; therefore,

$$-T_s = \vec{r}_{P/G} \times m_2 \vec{a_{G_2}} \tag{127}$$

where

$$\vec{r}_{G_2/P} = L\left(\cos(\theta + \phi)\,\vec{I} + \sin(\theta + \phi)\,\vec{J}\right) \tag{128}$$

After substituting the acceleration for point G_2 into the moment equation, and after utilizing trigonometric identities, the equation of motion is

$$\ddot{\phi} = \frac{\sin(\theta+\phi)\,\ddot{x} - \cos(\theta+\phi)\,\ddot{y} - (r\cos\theta + L)\,\ddot{\theta} - r\sin\phi\cdot\dot{\phi}^2}{L} - \frac{K\phi}{m_2 L^2} \tag{129}$$

The equations of motion given in (122), (123), (124), and (129) depend on the other generalized coordinates. The expressions can be solved explicitly. The equations can be written in matrix form.

$$A \cdot \begin{bmatrix} \ddot{x} \\ \ddot{y} \\ \ddot{\theta} \\ \ddot{\phi} \end{bmatrix} = B \tag{130}$$

where

$$A = \begin{bmatrix} m_1+m_2 & 0 & -m_2 r\sin\theta - m_2 L\sin(\theta+\phi) & -m_2 L\sin(\theta+\phi) \\ 0 & m_1+m_2 & m_2 L\cos(\theta+\phi) + m_2 r\cos\theta & m_2 L\cos(\theta+\phi) \\ -m_2 r\sin\theta & m_2 r\cos\theta & I + m_2 r^2 + m_2 r\cdot L\cos\theta & m_2 r\cos\theta\cdot L \\ -\frac{\sin(\theta+\phi)}{L} & \frac{\cos(\theta+\phi)}{L} & \frac{r\cos\phi+L}{L} & -1 \end{bmatrix} \tag{131}$$

$$B = \begin{bmatrix} F_1 + m_2 r\cos\phi\cdot\dot{\phi}^2 + (\dot{\theta}+\dot{\theta})^2 L\cos(\theta+\phi)m_2 \\ F_2 + m_2 r\sin\phi\cdot\dot{\phi}^2 + m_2 L\sin(\theta+\phi)(\dot{\theta}+\dot{\phi})^2 \\ T + K\phi + r m_2 L\sin\phi(\dot{\theta}+\dot{\phi})^2 \\ \frac{-K\phi}{m_2 L^2} - \frac{\sin\phi\cdot r\dot{\phi}^2}{L} \end{bmatrix} \tag{132}$$

Assuming that the inverse of A exists, then the equations of motion can be found by computing:

$$\begin{bmatrix} \ddot{x} \\ \ddot{y} \\ \ddot{\theta} \\ \ddot{\phi} \end{bmatrix} = A^{-1}\cdot B \tag{133}$$

A.1 Simplified Satellite Flexible Model

When the mass of the flexible appendage is small compared to the mass of the main satellite body (less than 5%), the model can be further simplified. It is assumed that the reaction

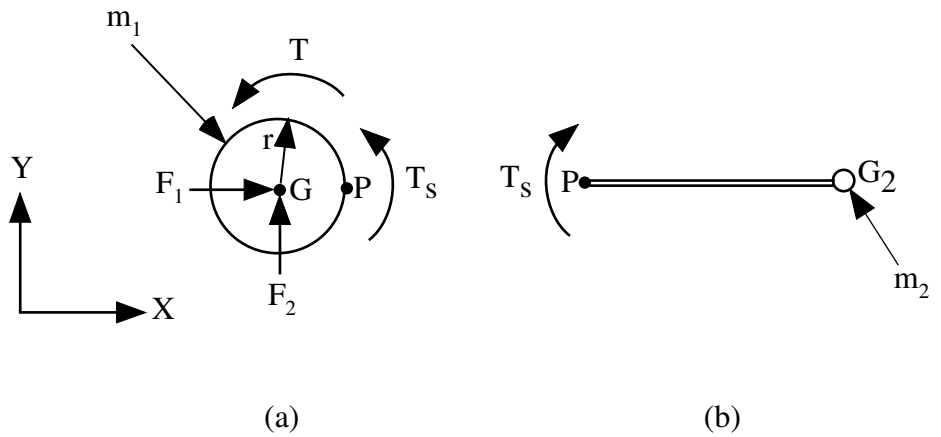

Figure 229: Free Body Diagrams for Simplified Satellite Model.

forces P_x and P_y are small and have little effect on the motion of the main satellite body. Figure 229 shows the FBD for the simplified m_1 and m_2. Taking the sum of forces in the x and y directions yields the following two equations of motion:

$$\ddot{x} = \frac{F_1}{m_1}$$

$$\ddot{y} = \frac{F_2}{m_1}$$

Taking the $\sum M$ about point G yields

$$T + T_s = I\ddot{\theta}$$

where $I = \frac{1}{2}m_1 r^2$ and $T_s = K\phi$. Solving for $\ddot{\theta}$ gives the third equation of motion

$$\ddot{\theta} = \frac{T + K\phi}{I}$$

REFERENCES

[1] "Crosslink," *The Aerospace Corporation http://www.aero.org/publications/crosslink/winter2001/04.html*.

[2] "Emerald," *http://ssdl.stanford.edu/Emerald/mission.html*.

[3] "The hubble space telescope," *National Aeronautics and Space Administration http://hubble.nasa.gove/index/php*.

[4] "Laser interferometer space antenna," *http://lisa.jpl.nasa.gov/*.

[5] "The satellite site," *The Satellite Site http://www.thetech.org/exhibits/online/satellite/*.

[6] "Techsat 21 space missions using satellite clusters," *Air Force Research Laboratory, http://www.vs.afrl.af.mil/Factsheets/techsate21.html*.

[7] "Cloudsat," *http://cloudsat.atmos.colostate.edu/*, 2003.

[8] "Formation flying: The afternoon a-train satellite constellation," NASA Facts FS-2003-1-053-GSFC, Goddard Space Flight Center, March 2003.

[9] Balch, T. and Arkin, R. C., "Behavior-based formation control for multirobot teams," *IEEE Transactions on Robotics and Automation*, vol. 14, no. 6, pp. 926–939, 1998.

[10] Banerjee, A. K., Pedreiro, N., and Singhose, W. E., "Vibration reduction for flexible spacecraft following momentum dumping with/without slewing," *J. of Guidance, Control, and Dynamics*, vol. 24, no. 3, pp. 417–427, 2001.

[11] Bang, H., Park, Y., Han, J., and Hwangbo, H., "Feedback control for slew maneuver using on-off thrusters," *Journal of Guidance, Control and Dynamics*, vol. 22, no. 6, pp. 816–822, 1999.

[12] Beard, R., Lawton, J., and Hadaegh, F., "A coordination architecture for spacecraft formation control," *IEEE Transations on Control Systems Technology*, vol. 9, no. 6, pp. 777–790, 2001.

[13] Ben-Asher, J., Burns, J. A., and Cliff, E. M., "Time-optimal slewing of flexible spacecraft," *J. of Guidance, Control, and Dynamics*, vol. 15, no. 2, pp. 360–367, 1992.

[14] Biediger, E., Lawrence, J., and Singhose, W., "Improving trajectory tracking for systems with unobservable modes using command generation," in *American Control Conference*, (Portland, Oregon), 2005.

[15] Campbell, M. E. and Schetter, T., "Formation flying mission for the uw dawgstar satellite," in *Aerospace Conference*, vol. 7, pp. 117–125, 2000.

[16] Chaimowicz, L., Kumar, V., and Campos, M. F., "A paradigm for dynamic coordination of multiple robots," *Autonomous Robots*, vol. 17, pp. 7–21, 2004.

[17] Drapeau, V. and Wang, D., "Verification of a closed-loop shaped-input controller for a five-bar-linkage manipulator," in *Proceedings IEEE International Conference on Robotics and Automation*, (Atlanta, GA), pp. 216–221, 1993.

[18] Dunbar, W. B. and Murray, R. M., "Model predicted control of coordinated multi-vehicle formations," in *41st IEEE Conference on Decision and Control*, (Las Vegas, Nevada), pp. 4631–4636, 2002.

[19] Feddema, J. T., Lewis, C., and Schoenwald, D. A., "Decentralized control of cooperative robotic vehicles: Theory and application," *IEEE Transactions on Robotics and Automation*, vol. 18, no. 5, pp. 852–864, 2002.

[20] Fierro, R., Das, A., Kumar, V., and Ostrowski, J., "Hybrid control of formations of robots," in *IEEE International Conference on Robotics and Automation*, (Seoul, Korea), pp. 157–162, 2001.

[21] Folta, D. C., Newman, L. K., and Gardner, T., "Foundations of formation flying for mission to planet earth and new millennium," in *AIAA/AAS Astrodynamics Conference*, (San Diego, CA), pp. 656–666, 1996.

[22] Fourcade, J., "Mission analysis and orbit control of interferometric wheel formation flying," in *18th International Symposium on Space Flight Dynamics*, (Munich, Germany), 2004.

[23] Frakes, D., Conrad, C., Healy, T., Monaco, J., Smith, M., Fogel, M., Sharma, S., and Yoganathan, A., "Application of an adaptive control grid interpolation technique to morphological vascular reconstruction," in *IEEE Transactions on Biomedical Engineering*, 2003.

[24] Frakes, D. and Singhose, W., "Geometrically constrained optical flow-based tracking for the extraction of kinematic data from video," in *Fifth International Symposium on Computer Methods in Biomechanics and Biomedical Engineering*, (Rome, Italy), 2001.

[25] Grosser, K., Fortgang, J., and Singhose, W., "Limiting high mode vibration and rise time in flexible telerobotic arms," in *Conf. on Systemics, Cybernetics, and Informatics*, (Orlando, FL), 2000.

[26] Gurfil, P., Idan, M., and Kasdin, N. J., "Adaptive neural control of deep-space formation flying," *Journal of Guidance, Control and Dynamics*, vol. 26, no. 3, pp. 491–501, 2003.

[27] Horowitz, P. and Hill, W., *The Art of Electronics*. New York: Cambridge University Press, second ed., 1999.

[28] Kapila, V., Sparks, A. G., Buffington, J. m., and Yan, Q., "Spacecraft formation flying: Dynamics and control," *Journal of Guidance, Control and Dynamics*, vol. 23, no. 3, pp. 561–563, 2000.

[29] Kapila, V., Tzes, A., and Yan, Q., "Closed-loop input shaping for flexible structures using time-delay control," *Transactions of the ASME Journal of Dynamic Systems, Measurement and Control*, vol. 122, pp. 454–460, 2000.

[30] Kenison, M. and Singhose, W., "Concurrent design of input shaping and proportional puls derivative feedback control," *J. of Dynamic Sys., Measurement, and Control*, vol. 124, no. 3, pp. 398–405, 2002.

[31] Kim, Y., Mesbahi, M., and Hadaegh, F. Y., "Dual-spacecraft formation flyin in deep space: Optimal collision-free reconfigurations," *Journal of Guidance, Control and Dynamics*, vol. 26, no. 2, pp. 375–379, 2003.

[32] King, L. B., parker, G. G., Deshmukh, S., and Chong, J.-H., "Study of inter-spacecraft coulomb forces and implications for formation flying," *Journal of Propulsion and Power*, vol. 19, no. 3, pp. 497–505, 2003.

[33] Li, F. and Bainum, P., "Rapid reorientation maneuvers of experimental spacecraft with a pendulum appendage," *Journal of Guidance, Control and Dynamics*, vol. 21, no. 1, pp. 164–171, 1998.

[34] Liu, Q. and Wie, B., "Robust time-optimal control of uncertain flexible spacecraft," *J. of Guidance, Control, and Dynamics*, vol. 15, no. 3, pp. 597–604, 1992.

[35] Magee, D. and Book, W. J., "Optimal filtering to minimize the elastic behavior in serial link manipulators," in *American Control Conference*, (Philadelphia, PA), pp. 2637–2642, 1998.

[36] Manikonda, V., Arambel, P., Gopinathan, M., Mehra, R., and Hadaegh, F., "A model predictive control-based approach for spacecraft formation keeping and attitude control," in *American Control Conference*, (San Diego, CA), pp. 4258–4262, 1999.

[37] Marshall, J., Broucke, M. E., and Francis, B. A., "Formations of vehicles in cyclic pursuit," *IEEE Transactions on Automatic Control*, vol. 49, no. 11, pp. 1963–1974, 2004.

[38] Matunaga, S., Mori, O., Tsurumi, S., and Okada, H., "Robot satellite cluster system and its ground experiment system," in *51st International Astronautical Congress*, (Rio de Janeiro, Brazil), pp. 1–6, 2000.

[39] Mesbahi, M. and Hadaegh, F., "Formation flying control of multiple spacecraft via graphs, matrix inequalities, and switching," *Journal of Guidance, Control and Dynamics*, vol. 24, no. 2, pp. 369–377, 2001.

[40] Middour, J. W., "Along track formationkeeping for satellites with low eccentricity," *The Journal of the Astronautical Sciences*, vol. 41, no. 1, pp. 19–33, 1993.

[41] Nakasuka, S., Aoki, T., Ikeda, I., and Tsuda, Y., ""furoshiki satellite" - a large membrane structure as a novel space system," *Acta Astronautica*, vol. 48, no. 5-12, pp. 461–468, 2001.

[42] Ooten, E. and Singhose, W., "Command generation with sliding mode control for flexible systems," in *Sixth Int. Workshop on Advanced Motion Control*, (Nagoya, Japan), 2000.

[43] Pao, L. and Singhose, W., "Unity magnitude input shapers and their relation to time-optimal control," in *IFAC World Congress*, (San Francisco, CA), pp. 385–390, 1996.

[44] Parman, S. and Koguchi, H., "Controlling the attitude maneuvers of flexible spacecraft by using time-optimal/fuel-efficient shaped inputs," *Journal of Sound and Vibration*, vol. 221, no. 4, pp. 545–565, 1999.

[45] Pollini, L., Giulietti, F., and Innocenti, M., "Robustness to communication failures within formation flight," in *American Control Conference*, (Anchorage, AK), pp. 2860–2866, 2002.

[46] Queiroz, M. S. d., Kapila, V., and Yan, Q., "Adaptive nonlinear control of multiple spacecraft formation flying," *Journal of Guidance, Control and Dynamics*, vol. 23, no. 3, pp. 385–390, 2000.

[47] Ren, W. and Beard, R. W., "A decentralized scheme for spacecraft formation flying via the virtual structure approach," in *American Control Conference*, (Denver, CO), pp. 1746–1751, 2003.

[48] Robertson, A., Inalhan, G., and How, J., "Formation control strategies for a separated spacecraft interferometer," in *American Control Conference*, (San Diego, CA), pp. 4142–4147, 1999.

[49] Sanchez, J. and Fierro, R., "Sliding mode control for robot formations," in *IEEE International Symposium on Intelligent Control*, (Houston, Texas), pp. 438–443, 2003.

[50] Schaub, H. and Alfriend, K., "Hybrid cartesian and orbit element feedback law for formation flying spacecraft," *Journal of Guidance, Control and Dynamics*, vol. 25, no. 2, pp. 387–393, 2002.

[51] Singer, N. C. and Seering, W. P., "Preshaping command inputs to reduce system vibration," *Journal of Dynamics, Systems, Measurement and Control*, vol. 112, no. March, pp. 76–82, 1990.

[52] Singhose, W., Biediger, E., Chen, Y.-H., and Mills, B., "Reference command shaping using specified-negative-amplitude input shapers for vibration reduction," *J. of Dynamic Sys., Measurement, and Control*, vol. 126, no. 1, pp. 210–214, 2004.

[53] Singhose, W., Biediger, E., Matunaga, S., and Okada, H., "Control of flexible satellites using analytic on-off thruster commands," in *AIAA Guidance, Navigation, and Control*, (Austin, Texas.), 2003.

[54] Singhose, W., Bohlke, K., and Seering, W., "Fuel-efficient pulse command profiles for flexible spacecraft," *AIAA Journal of Guidance, Control, and Dynamics*, vol. 19, no. 4, pp. 954–960, 1996.

[55] Singhose, W., Derezinski, S., and Singer, N., "Extra-insensitive input shapers for controlling flexible spacecraft," *AIAA J. of Guidance, Control, and Dynamics*, vol. 19, no. 2, pp. 385–91, 1996.

[56] Singhose, W., Mills, B., and Seering, W., "Closed-form methods for generating on-off commands for undamped flexible structures," *AIAA J. of Guidance, Control, and Dynamics*, vol. 22, no. 2, 1999.

[57] Singhose, W. and Pao, L., "Slewing multimode flexible spacecraft with zero derivative robustness constraints," *J. of Guidance, Control, and Dynamics*, vol. 20, no. 1, pp. 204–206, 1997.

[58] Singhose, W., Seering, W., and Singer, N., "Residual vibration reduction using vector diagrams to generate shaped inputs," *Journal of Mechanical Design*, vol. 116, no. June, pp. 654–659, 1994.

[59] Singhose, W., Singer, N., and Seering, W., "Time-optimal negative input shapers," *J. of Dynamic Systems, Measurement, and Control*, vol. 119, no. June, pp. 198–205, 1997.

[60] Singhose, W. E., "Slewing flexible spacecraft with deflection-limiting input shaping," *J. of Guidance, Control, and Dynamics*, vol. 20, no. 2, pp. 291–298, 1997.

[61] Singhose, W. E., Crain, E. A., and Seering, W. P., "Convolved and simultaneous two-mode input shapers," *IEE Control Theory and Applications*, no. Nov., pp. 515–520, 1997.

[62] Singhose, W. E. and Pao, L., "A comparison of input shaping and time-optimal flexible -body control," *Control Engineering Practice*, vol. 5, no. 4, pp. 459–467, 1997.

[63] Singhose, W. E. and Singer, N., "Effects of input shaping on two-dimensional trajectory following," *IEEE Transations on Robotics and Automation*, vol. 12, no. 6, pp. 881–887, 1996.

[64] Singhose, W. E., Singh, T., and Seering, W., "On-off control with specified fuel usage," *J. of Dynamic Sys., Measurement, and Control*, vol. 121, pp. 206–212, 1999.

[65] Smith, O. J. M., *Feedback Control Systems*. New York: McGraw-Hill Book Co., Inc., 1958.

[66] Smith, O. J. M., "Posicast control of damped oscillatory systems," *Proceedings of the IRE*, vol. 45, no. September, pp. 1249–1255, 1957.

[67] Staehlin, U. and Singh, T., "Design of closed-loop input shaping controllers," in *American Control Conference*, (Denver, CO), pp. 5167–5172, 2003.

[68] Suk, J., Kim, Y., and Bang, H., "Experimental evaluation of the toque-shaping method for slew maneuver of flexible space structures," *Journal of Guidance, Control and Dynamics*, vol. 21, no. 6, pp. 817–822, 1998.

[69] Tillerson, M. and How, J., "Advanced guidance algorithms for spacecraft formation-keeping," in *American Control Conference*, (Anchorage, AK), pp. 2830–2835, 2002.

[70] Tillerson, M. and How, J. P., "Formation flying control in eccentric orbits," in *AIAA Guidance, Navigation, and Control Conference and Exhibit*, (Montreal, Canada), 2001.

[71] Tsuda, Y. and Nakasuka, S., "Impulsive optimal guidance algorithm for formation flying spacecraft," in *23rd International Symposium of Space Technology and Science*, (Matsue, Japan), pp. 917–923, 2002.

[72] Veres, S., Gabriel, S., Mayne, D., and Rogers, E., "Analysis of formation flying control of a pair of nanosatellites," *Journal of Guidance, Control and Dynamics*, vol. 25, no. 5, pp. 971–974, 2002.

[73] Zethocha, P., Self, L., Wainwight, R., Burns, R., Brito, M., and Surka, D., "Commanding and controlling satellite clusters," *IEEE Intelligent Systems*, vol. 15, no. 6, pp. 8–13, 2000.

[74] Zuo, K., Drapeau, V., and Wang, D., "Closed loop shaped-input strategies for flexible robots," *International Journal of Robotics Research*, vol. 14, no. 5, pp. 510–529, 1995.